School of Chemical and Petroleum Engineering

Department of Chemical Engineering

Photocatalytic Degradation of Organic Compounds using Carbon Based Composite Catalysts

Guanliang Zhou

THIS THESIS IS PRESENTED FOR THE DEGREE OF

Doctor of Philosophy

Of

Curtin University

February 2013

Declaration

To the best of my knowledge and belief this thesis contains no material previously published by any other person except where due acknowledgement has been made. This thesis contains no material which has been accepted for the award of any other degree or diploma in any university.

Signature: ..... Date: 20.June.2013

Guanliang Zhou

I dedicate this thesis to

my parents, Yang Gao and Mingxiang Zhou,

my wife, Lu Wang, for their constant support and unconditional love.

I love you all dearly.

Acknowledgement

I would like to express my heartfelt gratitude to Professor Shaobin Wang for his continuous support of my PhD study and research. I could not have asked for a better role model, inspirational, supportive, and patient. Without his warm encouragement and thoughtful guidance, I had no chance to complete this thesis. I am also thankful for the excellent example he has provided as a successful scientist and professor, and it has been an honour to be one of his students.

I owe my deep gratitude to my co-supervisor Professor Shaomin Liu and Professor Ming Ang, whose kindness, as well as their academic experience, has been invaluable to me. The laboratory demonstrating job offered by Professor Shaomin Liu was a great help for my finance, and wonderful chance for me to improve my English skills and knowledge.

I am also grateful to Professor Moses Tade being head of the department and my thesis chairman, who always encouraged me and praised my work, supported me morally and financially with great pleasure.

My sincere gratitude must go to Dr. Hongqi Sun who helped me to make everything possible during my postgraduate years, and this thesis would certainly not have existed without him. He was not only the greatest advisor but also my dear friend and elder brother.

I am also thankful to my colleagues and friends, Dr. Hussein, Eddy and Xiaohui Feng who have been always ready to help me for my research without return, given me trainings on various equipment and software.

To all of laboratory technical staffs, Karen Hanes, Jason Write, Ann Carrol, Xiao Hua, and Roshanak Doroushi, I am grateful for welcoming me as a friend and for their great and valuable help to develop the ideas in my research.

I am also thankful to those undergraduate and postgraduate students who have worked with me on this research.

I also would like to thank my parents who gave birth to me at the first place and encouraged and supported me, both emotionally and financially throughout my degree. I would not have made my research this far without them. In particular, the patience and understanding shown by my mum and dad during the honours year is greatly appreciated.

And last, but not the least, I would like to thank my beloved wife, Lu Wang, who gave up her excellent opportunity of career and accompanied me here with her great patience and unconditionally love. I truly thank Lu for sticking by my side, even when I was irritable and depressed. I must say that I married the best person out of there for me.

Publications by author

Hongqi Sun, Guanliang Zhou, Shizhen Liu, H. Ming Ang, Moses O Tade, Shaobin Wang, "Nano-Fe^0 Encapsulated in Microcarbon Spheres: Synthesis, Characterization, and Environmental Applications", ACS APPLIED MATERIALS & INTERFACES, 2012, 4(11): p. 6235-6241.

Hongqi Sun, Shizhen Liu, Guanliang Zhou, H. Ming Ang, Moses O Tade, Shaobin Wang, "Reduced Graphene Oxide for Catalytic Oxidation of Aqueous Organic Pollutants", ACS APPLIED MATERIALS & INTERFACES , 2012, 4(10): p. 5466-5471.

Guanliang Zhou, Hongqi Sun, Shaobin Wang, H. Ming Ang, Moses O Tade, "Titanate supported cobalt catalysts for photochemical oxidation of phenol under visible light irradiations", SEPARATION AND PURIFICATION TECHNOLOGY, 2011, 80(3): p. 626-634.

Guanliang Zhou, Huyong Tian, Hongqi Sun, Shaobin Wang, C.Edward Buckley, "Synthesis of carbon xerogels at varying sol-gel pHs, dye adsorption and chemical regeneration", CHEMICAL ENGINEERING JOURNAL, 2011, 171(3): p. 1399-1405.

Contents

Abstract

In recent decades, the applications of advanced oxidation processes (AOPs) for organic pollutants treatment in wastewater have been thoroughly investigated. These techniques base on chemical destruction and give a complete solution to the problem of wastewater containing toxic organics. Among these processes, semiconductor-based photocatalytic process has been employed as a low-cost, environmentally friendly and sustainable technique to purify water/wastewater. Meanwhile, chemical oxidation process is also considered as an effective remediation technique to reduce the concentrations of targeted toxic organics in wastewater to acceptable levels.

The aim of this work is emphasizing the role of new synthesized catalysts in advanced oxidation process for wastewater treatment. The key conclusion of this thesis is that novel photocatalysts being capable to degrade organics in aqueous phase at room temperature were successfully synthesized and the investigation of “green cobalt based catalysts” for degradation of organic pollutants via advanced oxidation processes was achieved. Various types of catalysts were synthesized with hydrothermal carbonization method or wet impregnation method, and used for degradation of phenol in aqueous phase with UV-vis and visible light irradiation. Titanates: $ZnTiO_3$, $FeTiO_3$ and $Bi_4Ti_3O_{12}$ were modified by coating cobalt (Co) to prepare photocatalysts. Microcarbon spheres were also synthesized by hydrothermal method, and used to support TiO_2 (C-TiO_2), nanoscaled zerovalent iron (nano-Fe^0@CS), cobalt (micro-CS@Co) and graphitic carbon nitride (C-g-CN). All of these catalyst materials were tested for phenol degradation. Some of these synthesized catalysts were also examined for activating peroxymonosulfate (PMS, Oxone) for the decomposition of phenol.

1

Chapter 1: Introduction

1.1. Motivation

The modern society continues to produce and discharge wastewater, which contains a wide range of hazardous organic compounds such as pharmaceutical, surfactants, flame retardants, plasticizers, steroides, and other trace organics. In recent decades, 80% of human diseases have been related to wastewater, and 1.2 million people die of using contaminated water every year in developing countries [1-4]. Organic pollutants in wastewater therefore have become an extremely serious issue to human beings.

There are two major sources of organic compounds in wastewater: i) natural organic matter (NOM), including humus, microbial secretions, dissolution of plant tissue, and animal waste, and ii) synthesized organic compounds (SOCs), present in industrial wastewater, domestic sewage, pesticides, and the byproducts of the traditional drinking water treatment processes. Among the numerous organic compounds, SOCs have been identified as the major contributors to water pollution. Most of SOCs are recalcitrant pollutants and can cause bioaccumulation, deformity, cancer, and genic mutation. Some SOCs are non or low toxic, however, they can still be harmful. With the enrichment of organic compounds in water/wastewater and the distinguishing feature of organic matter transformation, the concentration of total hazardous SOCs would become much higher, and has been proven as the main potential source of above diseases [5]. The large numbers of synthesized organic compounds are from a wide range of sources, such as industry, agriculture, and households, which may enter water and wastewater systems. The U.S Environmental Protection Agency (EPA) identified over 400 hazardous synthesized organic compounds in waters and wastewaters. Moreover, US EPA and World Health Organizations (WHO) have also identified some types of SOCs as precedent-controlled harmful pollutants, such aspolychlorinated biphenyls (PCBs), di-(2-ethyhexyl)-phthalate (DEHP), polycyclic aromatic hydrocarbons (PAHs), tetrachloroethane, dibutyl phthalate (DBP), tolune, benzene,

acetone, dimethylphenol and phenol, etc.

Most of organics in wastewater are toxic, and resistant to be degraded by natural environment. The adverse effects on human being and natural environment caused by persistent organic pollutants (POPs) are irreversible. Irrigation with wastewater makes it worse. WHO indicates that in developing countries, irrigation with wastewater, which is heavily contaminated by organic compounds, have produced much more health damage cases, including enlargement of the liver, cancers and raised rates of congenital malformation rates, compared to the areas where wastewater is not used for irrigation [6].

A number of techniques have been proven effective in removal of SOCs from wastewater, such as coagulation, membrane separation, electrochemical process, and adsorption [7]. However, limitations usually appear in terms of economic issues, efficiency, and potential secondary pollution problems. Recently, advanced oxidation processes (AOPs), which refer to a set of chemical treatment processes by oxidation, have been extensively investigated as a promising technique for environmental remediation. AOPs include UV photolysis, photocatalysis, supercritical water oxidation, chemical oxidation process, and so on. Therefore, this research focused on the preparation of highly efficient, and environmentally friendly catalyst materials for degradation of SOCs.

1.1.1. Degradation of organic pollutants via photocatalysis

In recent decades, semiconductor-based photocatalytic process has been employed as a low-cost, environmentally friendly and sustainable technique to purify water/wastewater containing SOCs. Various pure and modified photocatalysts have been introduced to wastewater treatment. However, commercially available photocatalysts, such as TiO_2, have

barriers in practical application: i) low photocatalytic efficiency at low level pollution; ii) complicated recovery after use; iii) aggregation of particles in suspension; and iv) requirement of UV light and/or high intensity radiation which may cause health issues. Therefore, new photocatalysts whiach can be used under visible light or low intensity radiation are highly desirable.

1.1.2. Degradation of organic pollutants via chemical oxidation

Chemical oxidation is considered as an effective remediation technique to reduce the concentrations of targeted toxic organics in wastewater to acceptable levels. This technique introduces strong chemical oxidizers to break down the molecules of various SOCs which are resistant to other techniques and natural degradation.

Permanganate, Fenton's reagents, persulfate, and ozone are four types of typical oxidants which are commonly used in water treatment industries. They are efficient and cost-effective, however, would pose serious hazards to operators as strong oxidizing agents. Furthermore, common catalysts used with these oxidants, such as cobalt oxide and ferrous iron salts, are usually resistant to be separated from treated water, and cause secondary pollution as heavy metal compounds. The hazards of oxidizing agents can be controlled via series of standards: test ozone level in the air, store oxidants properly, do not have skin contact [8, 9], and consequently, how to develop efficient and environmentally friendly catalysts for chemical oxidation process has shown a great potential.

1.1.3. Development of novel nanomaterials for environmental catalysis

Recent developments in nanotechnologies have opened up new directions to make the synthesis of novel nanomaterials more feasible and less harmful. Nanosized photocatalysts

possess promising properties from the particle size in the region of transition between the molecular and the bulk phases [10]. As the size of the semiconductor particle is below a critical diameter, the spatial confinement of the charge carries within a potential well [11], which means bands split into discrete electronic states in the valence and conduction bands very well. Thus one of the main advantages in applications of nano-semiconductor materials is the increase in the band gap energy with the decreasing particle size [12]. Some types of semiconductors are considered as ideal photocatalysts which are stable, inexpensive, non-toxic and highly photoactive. These semiconductors include TiO_2, WO_3, $SrTiO_3$, α -Fe_2O_3, and ZnO [12, 13].

Depositing or incorporating metal ions or metal oxides into nanosized catalysts can not only improve their performance of organic removal, but also increase the stabilities of these catalysts. Thus modified nanomaterials can be developed as highly effective and environmentally friendly catalysts. Heterogeneous cobalt catalysts have been widely investigated [14, 15] to restrict the discharge of cobalt ions to avoid secondary pollution. Further, the sulphate radicals produced by cobalt catalysis has been proven highly effectively in oxidation of organic compounds [16, 17]. Nanomaterials are supposed as good support materials due to the unique structures and large surface areas. Hence, activation of peroxymonosulfate by novel nanomaterial supported Co catalsysts is promising environmental method for oxidation of organic compounds in wastewater.

1.2. Objectives of thesis

This study aims at the development of novel carbon spheres based catalysts for degradation of organic compounds in wastewater and the specific objectives are:

i. To synthesize novel photocatalysts being capable to degrade organics in aqueous

phase at room temperature.

ii. To synthesize and develop modified photocatalysts for photochemical degradation of organics in aqueous phase.

iii. To develop photocatalyst supported Co catalysts, and evaluate the photocatalytic activities of the newly synthesized materials with UV-vis light irradiation at room temperature.

iv. To investigate novel catalysts for degradation of organic pollutants via advanced oxidation processes.

1.3. Thesis organization

Chapter one mainly introduced the major techniques for removal of organic pollutants in wastewater and briefly presented the overall adverse health effects on human beings caused by synthesized organic pollutants in wastewater. Two main techniques: photocatalysis and chemical oxidation were described and compared.

Chapter two provided a comprehensive literature review on pollutant removal techniques, particularly on advanced oxidation processes (AOPs), novel photocatalytic materials, novel micro/nano-support material selection, and sources and health effects of main types of synthesized organic pollutants in wastewater. The advantages and disadvantages of multi-AOPs were discussed in details. The main objectives of this literature review were: to (1) select “green” techniques of high efficiency and low cost for degradation of organic pollutants in wastewater; (2) select suitable novel environmentally friendly semiconductor materials for removal of organics; (3) select suitable support materials to synthesize and optimize catalysts.

Chapter three presented synthesis, characterization, photocatalytic and photochemical oxidation properties of cobalt coated $ZnTiO_3$, $FeTiO_3$ and $Bi_4Ti_3O_{12}$ photocatalysts. This chapter highlighted the possibilities of three titanates and cobalt doped titanates as efficient photocatalysts, and also discussed the effects of cobalt loading on phenol removal with the applications of peroxymonosulfate (PMS) or peroxydisulfate (PDS) on synthesized cobalt coated titanates. The stability studies of homemade photocatalysts were investigated in this chapter as well.

Chapter four described the synthesis of nanoscaled zero-valent iron encapsulated in microcarbon spheres. The optimum synthesis conditions were discussed. In this chapter, synthesized catalysts were also demonstrated as an effective material in activating PMS for the oxidation of phenol.

Chapter five showed research efforts on synthesis, characterization and chemical oxidation activities of microcarbon spheres supported cobalt catalysts. This chapter described the effects of preparation condition on phenol degradation with PMS and stabilities of the microcarbon spheres supported cobalt catalysts.

Chapter six investigated the synthesis of graphitic carbon nitride and microcarbon spheres coated graphitic carbon nitride. Synthesis methods, characterization and photocatalytic decomposition of phenol under visible and UV light irradiation were presented in this chapter.

Chapter seven studied the synthesis and photocatalytic properties of microcarbon spheres supported commercial P25 TiO_2. Photocatalytic activities of the photocatalysts in phenol degradation were examined under UV and visible light irradiation and compared with

commercial photocatalyst of P25 TiO_2.

Chapter eight summarized the overall thesis and discussed the performance of all the materials which were synthesized during the research work for organic degradation. The final part of this chapter was devoted to the possible suggestions and future work.

1.3. References

1. Focazio, M.J., et al., *A national reconnaissance for pharmaceuticals and other organic wastewater contaminants in the United States - II) Untreated drinking water sources.* Science of the Total Environment, 2008. **402**(2-3): p. 201-216.

2. Halling-Sorensen, B., G. Sengelov, and J. Tjornelund, *Toxicity of tetracyclines and tetracycline degradation products to environmentally relevant bacteria, including selected tetracycline-resistant bacteria.* Archives of Environmental Contamination and Toxicology, 2002. **42**(3): p. 263-271.

3. Daughton, C.G. and T.A. Ternes, *Pharmaceuticals and personal care products in the environment: Agents of subtle change?* Environmental Health Perspectives, 1999. **107**: p. 907-938.

4. Hignite, C. and D.L. Azarnoff, *DRUGS AND DRUG METABOLITES AS ENVIRONMENTAL CONTAMINANTS - CHLOROPHENOXYISOBUTYRATE AND SALICYLIC-ACID IN SEWAGE WATER EFFLUENT.* Life Sciences, 1977. **20**(2): p. 337-341.

5. Bhattacharyya, K.G. and A. Sharma, *Kinetics and thermodynamics of Methylene Blue adsorption on Neem (Azadirachta indica) leaf powder.* Dyes and Pigments, 2005. **65**(1): p. 51-59.

6. Hamdaoui, O., *Batch study of liquid-phase adsorption of methylene blue using cedar sawdust and crushed brick.* Journal of Hazardous Materials, 2006. **135**(1-3): p. 264-273.

7. Weng, C.H. and Y.F. Pan, *Adsorption characteristics of methylene blue from aqueous solution by sludge ash.* Colloids and Surfaces a-Physicochemical and

Engineering Aspects, 2006. **274**(1-3): p. 154-162.

8. Yuan, *Etiological Study of High Stomach Cancer Incidence Among Residents in Wastewater Irrigated Areas, Environmental Protection Science, 1993, 19(1):70-73, in: World Resources Institute, A guide to the global environment: environmental change and human health, New York.* Oxford University Press, 1993: p. 122.

9. Huling, S.G., Bruce E. Pivetz *In-Situ Chemical Oxidation.* Engineering Issue of EPA (USA Environmental Protection Agency) (United States Environmental Protection Agency), 2006.

10. Bahnemann, D.W., *ULTRASMALL METAL-OXIDE PARTICLES - PREPARATION, PHOTOPHYSICAL CHARACTERIZATION, AND PHOTOCATALYTIC PROPERTIES.* Israel Journal of Chemistry, 1993. **33**(1): p. 115-136.

11. Sato, T., et al., *Photocatalytic properties of layered hydrous titanium oxide CdS-ZnS nanocomposites incorporating CdS-ZnS into the interlayer.* Journal of Chemical Technology and Biotechnology, 1996. **67**(4): p. 339-344.

12. Beydoun, D., et al., *Role of nanoparticles in photocatalysis.* Journal of Nanoparticle Research, 1999. **1**(4): p. 439-458.

13. Cozzoli, P.D., et al., *Role of metal nanoparticles in TiO2/Ag nanocomposite-based microheterogeneous photocatalysis.* Journal of Physical Chemistry B, 2004. **108**(28): p. 9623-9630.

14. Anipsitakis, G.P., E. Stathatos, and D.D. Dionysiou, *Heterogeneous activation of oxone using Co3O4.* Journal of Physical Chemistry B, 2005. **109**(27): p. 13052-13055.

15. Yang, Q.J., et al., *Heterogeneous activation of peroxymonosulfate by supported cobalt catalysts for the degradation of 2,4-dichlorophenol in water: The effect of support, cobalt precursor, and UV radiation.* Applied Catalysis B-Environmental, 2008. **77**(3-4): p. 300-307.

16. Anipsitakis, G.P. and D.D. Dionysiou, *Degradation of organic contaminants in water with sulfate radicals generated by the conjunction of peroxymonosulfate with cobalt.* Environmental Science & Technology, 2003. **37**(20): p. 4790-4797.

17. Shukla, P.R., et al., *Activated carbon supported cobalt catalysts for advanced oxidation of organic contaminants in aqueous solution.* Applied Catalysis B: Environmental, 2010. **100**(3–4): p. 529-534.

2

Chapter 2: Literature Review

2.1. Introduction

Organic compounds in wastewater represent a serious problem to public health. The synthesized organic compounds (SOCs), such as polychlorinated biphenyls (PCBs), di-(2-ethyhexyl)-phthalate (DEHP), polycyclic aromatic hydrocarbons (PAHs), tetrachloroethane, dibutyl phthalate (DBP), toluene, benzene, acetone, dimethylphenol and phenol, in wastewater discharged by chemical industries have attracted particular concerns. In recent decades, great efforts have been made to control, reduce, and rectify these types of toxic pollutants in wastewater. Limiting the toxic sources used in industries, recycling the wastes and terminal products, improving productive processes, and controlling the waste treatment processes from both production stages and disposal stages are conventional strategies, and have been widely employed to treat the toxic organic compounds harmlessly, efficiently, and thoroughly [1, 2].

However, available techniques still have barriers when treating large amount and multi-types of SOCs in wastewater. Traditional methods such as solvent extraction, activated carbon adsorption, and chemical oxidation often suffer from serious drawbacks including high cost or formation of hazardous by-products [1, 2]. For example, activated carbon adsorption involves phase transfer of pollutants without decomposition, which induces another pollution problem [3]. The new techniques such as biodegradation, photodegradation, and bioaccumulation are environmentally friendly and cost effective; however, the time-consuming and critical operation conditions, such as proper pH and temperature, restrict the wide applications in industries. For instance, in MITI-I-test which is designed to quickly estimate the rate of biodegradation, 60% to 70% of phenol in wastewater is reduced after four days, and 85% is reduced after 14 days by using the traditional methods such as solvent extraction and activated carbon adsorption [4, 5].

Despite these defects, photodegradation by semiconductor mediated photo catalysis still appears more attractive than others because of its ability to decompose a wide range of organic and inorganic pollutants at room temperature and pressure, without generation of harmful by-products. The most commonly used photocatalysts are TiO_2, ZnO, ZrO_2, CdS, and SnO_2 [6, 7]. However, the limitations of photodegradation are also present: TiO_2 is the most popular photocatalyst, but it can only be activated by UV light irradiation [8, 9] which is harmful and high energy consumption, while ZnO, ZrO_2, CdS, and SnO_2 are easy to be decomposed into unexpected by-products during photo catalysis processes. Meanwhile, purification of the wastewater by destroying the organic contaminants can also been done by another traditional technique: chemical oxidation. It is a very effective method that aims at mineralization of SOCs to carbon dioxide, water and nontoxic inorganics, or at least, at their transformations into harmless products. Nevertheless, formation of hazardous by-products, and toxic metal leaching are the two main issues which cannot be ignored [10-12]. Therefore, integration of the two techniques mentioned above will provide the complete solutions for SOCs treatment processes. Furthermore, overcoming the limitations of photocatalysis and chemical oxidation, and applying their significant efficiency for organics removal make development of novel catalysts highly desirable.

2.2. Synthesized organic compounds and Sources

Most of toxic organic compounds are not intentionally produced. However, they are released during a wide range of industrial processes and products degradation, such as monosodium glutamate industry (MSG), metal processing, paper-mill, production of technical formulations of chlorinated compounds, agricultural sludge treatment processes, applications of detergents, and plastic industries [13-16]. The details of major SOCs and

their sources are as follows:

Polychlorinated Biphenyls (PCBs): Polychlorinated biphenyls (PCBs) are synthetic organic chemicals, and are mainly used as dielectric and coolant fluid in many areas [17]. For example, PCBs are filled in power transformers and capacitors by manufactures of electrical equipment to provide fireproof insulation between coils or plates conducting electricity [18, 19], and used as heating and cooling agent in various chemical, food, synthetic resin industry, and preheating agent of the fuel oil of vessels, central heating systems, and panel heaters [20].

PCBs have been detected in virtually all environmental media: indoor and outdoor, surface and ground water, soil, and food with the garbage cremation and discharge of wastewater [17]. PCBs are very stable organic compounds with a long life (8 to 10 years) and hardly decompose in natural environment [21]. Research indicates that PCBs can be adsorbed by soils and therefore accumulate in sewage sludge. The highly substituted (high chlorine content) PCBs are the main representatives potentially present in sewage sludge, while the amount is just 35% of the total technical PCBs [17, 22]. Though PCBs are insoluble in water, they readily penetrate skin of organisms such as fishes and mammals in polluted water, and enrich in organs [21].

Polycyclic Aromatic Hydrocarbons (PAHs): Polycyclic aromatic hydrocarbons (PAHs) are potent atmospheric pollutants. The main sources of PAHs are combustion from transportation and commercial processes, such as food preparation sources and waste incineration [23]. However, nowadays because PAHs dyes are widely used, about 0.7 million tons of PAHs dyes are produced every year, and 10-15% of these PAHs dyes are discharged into water [15, 24-26]. The emission of PAHs from wastewater comes into

atmosphere and directly contacts with operators in wastewater treatment plants (WWTPs) [27, 28]. Therefore, properly treating PAHs in wastewater before the emission is a significant option which does get enough attention.

Di-2(ethy-hexyl)-phthalate (DEHP): DEHP is a wildly used plasticizer in cosmetics, building materials, automobiles, and polyvinyl chloride (PVC) products [29], such as intravenous tubing and bags, catheters, nasogastric tubes, dialysis bags and tubing, blood bags and transfusion tubing, and air tubes, all of which are medical devices [30, 31]. DEHP can be adsorbed from food and water, and it is found regularly in municipal wastewater, especially the wastewater produced during the synthetic processes of PVC industry. Furthermore, because of its lipophilic properties, it also concentrates in sewage sludge.

Surfactants: Surfactants are organic chemicals that reduce surface tension in water and other liquids. There are four major commercial and industrial surfactants: anionic surfactants, such as liner athylbenzene sulphonates (LAS); cationic surfactants, such as amine compounds; non-ionic surfactants, such as fatty acid alkanolamides; and amphoteric surfactants, such as betaines [32]. They are commonly found in soaps, laundry detergents, dish washing liquids, and shampoos. Anionic and non-ionic surfactants are soluble in water, and toxic for water organisms [33, 34].

Polychlorinated Dibenzo-p-dioxins and Dibenzofurans (PCDD/Fs): PCDD/Fs are already assigned with toxic equivalency factor (TEF) values by the WHO (World Health Organization). PCDD/Fs and other undesired chlorinated species are inadvertently produced during many industrial processes, including bleaching (papermaking and textiles), brineprocessing (metal recovery), and chlorination (pesticide and chemical production) [35, 36]. People ingest PCDD/Fs from food, specifically through the consumption of fish and

meat of which organisms are on the top of food chain [37, 38], and this is due to the enrichment of PCDD/Fs in water bodies.

Phenolic compounds: Phenolics are produced in a large scale, about 7 billion kilograms every year in the world now. Phenol and its chemical derivatives are very important raw and intermediate materials in various synthetic processes [39], including polycarbonates, epoxies, Bakelite, nylon, detergents, herbicides, resin paint, dying, textile wood, pulp mill, and pharmaceutical drugs [40-42]. Because of their toxicity and extensive use, phenol and phenolic compounds are ubiquitous pollutants which are released to natural water bodies and wastewater systems from the industrial processes mentioned above. In addition, phenol is also found in vehicle emissions, and smoke from cigarettes, bonfires and bush fire.

In summary, all of major SOCs reviewed in this section are classes of aromatic organic compounds. They have similar physical, chemical properties and toxicities. These SOCs are ubiquitous and can hardly be decomposed by natural processes; furthermore, they enrich in organisms which may be turned into food for human beings. Among these major pollutants, phenol is a classic benzene derivative and has the simplest member of the phenolic chemical. Phenol is produced naturally, synthesized artificially, and applied widely. Due to phenol's stability, refractory, and high level in productions and wastewater, it is an ideal and logical model for wastewater treatment studies.

2.3. Health issues associated with synthesized organic compounds in wastewater

SOCs usually have a long life and enrich in organisms (especially aquatic life) and then are served as part of food to human who are at the top of food chain. Dermal contact is another

common way of exposure to these toxic compounds. Long term exposure of SOCs can cause harmful effects on the central nervous system and heart, such as dysrhythmia and coma, and also may cause kidney disease, liver disease, skin rashes, itching, burning, eye irritation, skin and fingernail pigmentation changes, immune system disease, headaches, dizziness, depression, memory loss, possible cancer, and development effects [43].

Phenol, one of the major SOCs included in most of substances and wastewaters, is degraded rapidly in air (half-life of approximately 15 hours), but persistant in water for longer period [44, 45]. It is associated to cardiovascular disease, serious gastrointestinal damage, severe skin damage, muscle twitching [43-45]. Furthermore, phenol can also remain in human breast milk, and cause vomiting and lethargy of children. Some birth defects have been observed in animals due to females exposure to phenol during pregnancy [45]. Estimated lethal oral doses of phenol in adults vary widely, from 1 g (14 mg/kg, assuming an adult body weight of 70 kg) to as much as 65 g (930 mg/kg, assuming an adult body weight of 70 kg) [46-48]. Therefore, the control and removal of organic pollutants in wastewater are imperative for environment and public health.

2.4. Synthesized Organic Compounds Treatment Techniques

Water pollution from SOCs is a severe environmental problem to the whole world. A range of techniques, such as sedimentation-flocculation [49], coagulation [50], adsorption or reverse osmosis [51], have been introduced to remove SOCs in wastewater. Although all methods are proven effective for certain compounds, lack of non-selectivity to most of SOCs is the limitation of these techniques. For example, activated carbon cannot remove large number of organic pollutants at the level of few ppb [52, 53]. Sedimentation-flocculation is effective to remove the organic solids in wastewater, but

toxic organic compounds (e.g. PCB) are remained in sludge leading to secondary pollution [54]. Generally, physical processes only transfer pollutants from one phase (liquid) to another (solid), and will not completely decompose toxics. These techniques cost high price for production and regeneration, and are dependent on temperature, concentration, physical and chemical properties of target organic pollutants, and surface area [55-57]. There are two elements to judge if any technology suitable or not for use in industry: technical feasibility and economic feasibility [58]. Comparing with other techniques, advanced oxidation process (AOP) is particularly suitable for cleaning biologically toxic, non-degradable compounds and organic pollutants in wastewater [59]. This method based on chemical destruction gives complete solution to the problem of SOCs.

2.5. Advanced Oxidation Process (AOP)

Advanced oxidation processes (AOPs) are those processes based on destruction of organics in water and wastewater by production and utilization of active radicals [60-62]. Hydroxyl radicals are extremely reactive to attack organic species rapidly and non-specifically with rate constants usually in the order of 10^6-10^9 $M^{-1}s^{-1}$ [64]. AOP also offers optional ways for production and utilization of radicals, thus allowing a better compliance with the specific treatment requirements. AOPs theoretically do not produce any new hazardous substances into treated water. Details of AOPs are as follows.

2.5.1. Fenton processes

Fenton processes are classically reactive systems containing solutions of hydrogen peroxide and iron catalysts, which were discovered in the last century. Fenton's reagent was used as an analytical reagent at the beginning [63], but nowadays, it has been developed by a significant number of investigations for its application in wastewater treatment processes.

It has been proven that Fenton's reagent is effective in destroying toxic organic compounds in wastewater, such as trichloroethylene (TCE), tetrachloroethylene (PCE) and phenol.

In Fenton processes [64], ferrous iron (II) is oxidized by hydrogen peroxide to ferric iron (III):

$$Fe^{2+} + H_2O_2 \rightarrow Fe^{3+} + OH^- + OH^\bullet \quad (2\text{-}1)$$

In this way, producing hydroxyl radicals is simple and effective. It does require neither special apparatus nor reactants. The hydroxyl radical generated by Fenton's reagent is a powerful, non-selective oxidant. This oxidative system has been investigated by a large number of studies due to the fact that iron is a very abundant and non-toxic element and hydrogen peroxide is easy to handle and environmentally friendly.

Furthermore, in the condition of a proper value of pH (2.7-2.8), the reduction of Fe^{3+} to Fe^{2+} occurs [65]:

$$Fe^{3+} + H_2O_2 \rightarrow H^+ + Fe^-OOH^{2+} \quad (2\text{-}2)$$

$$Fe^-OOH^{2+} \rightarrow HO_2^\bullet + Fe^{2+} \quad (2\text{-}3)$$

Where, iron is used as a catalyst.

A lot of studies have developed different catalytic Fenton reaction and reagents [66-70]. For instance, due to the large specific surface area, carbon nanotubes (CNTs) are used as supports in synthesis of catalysts applied in Fenton reaction [68, 71, 72]. In one example [71], multi-walled carbon nanotube (MWCNTs) supported Fe_2O_3 catalysts were synthesized and used in degradation of phenol by heterogeneous Fenton reaction. The results indicated that phenol degradation performance of Fe_2O_3/MWCNTs is improved as compared with bare F_2O_3. Several studies have also suggested that activated carbon (AC) supported Fe is effective in organic compound degradation [73, 74], due to the excellent

properties in mechanical strength and porous structures of AC [75, 76]. As a new type of carbon materials, graphene has a perfect two-dimensional cycle plane structure and can be an excellent support material [77]. Guo et al. prepared Fe nanoparticles@graphene by the reduction of Fe^{3+} and graphene oxide (GO) in one step using $NaBH_4$ solution, and found that Fe nanoparticles@graphene showed a high catalytic activity in liquid phase [78]. Therefore, carbon materials including carbon nanotubes, activated carbon, carbon black, graphite, carbon nano-fibers, and nano-carbon spheres have aroused great attention as catalyst supports for Fenton processes.

Meanwhile, heterogeneous Fenton-like systems using iron supported catalysts, such as zero-valent iron (ZVI or Fe^0), goethite (α-FeOOH), Fe_3O_4, and Fe^0/Fe_3O_4, have recently developed [79-83]. For instance, zero-valent iron (ZVI or Fe^0) has been paid great attention as an inexpensive and environmentally friendly strong reductant [66, 67]. Besides, ZVI in oxygen-containing water can facilitate the degradation of toxic organic compounds, such as phenol [68]. The reactions can be described generally as follow:

$$Fe^0 \rightarrow Fe^{2+} + 2e^- \quad (2\text{-}4)$$

$$organics + ne^- \rightarrow X + H_2O \quad (2\text{-}5)$$

Xu & Wang's study indicated that nanoparticulate zero-valent iron has significant efficience for degradation of 4-chloro-3-methyl phenol in heterogeneous Fenton-like system at initial pH 6.1 [83]. However, only a few oxidations of organic pollutants using ZVI have been conducted, because the activity of this process not only depends on the ZVI, but also on the presence of dissolved oxygen (DO) [76-78].

To sum up, Fenton processes are classic and effective. Suitable oxidants introduced into reaction systems can significantly improve their selectivity and efficiency. Furthermore, due to the environmentally friendly properties, Fenton processes are valuable for

degradation of organic pollutants in wastewater.

2.5.2. Photo-Fenton process

Photo-Fenton process is one of the photochemical processes (see **2.5.3**). It is an efficient route for degradation of various organics, and has already been successfully used for wastewater treatment [84]. This technique produces large amount of hydroxyl radicals by photo reduction of $Fe(OH)^{2+}$, and Fe(II) by photolysis of Fe(III) [85] (Figure 2.1 [86]):

$$Fe(OH)^{2+} + h\nu \rightarrow Fe^{2+} + \bullet OH \qquad (2\text{-}6)$$

$$R(CO_2) - Fe(III) + h\nu \rightarrow R(\bullet CO_2) + Fe(II) \rightarrow \bullet R + CO_2 \qquad (2\text{-}7)$$

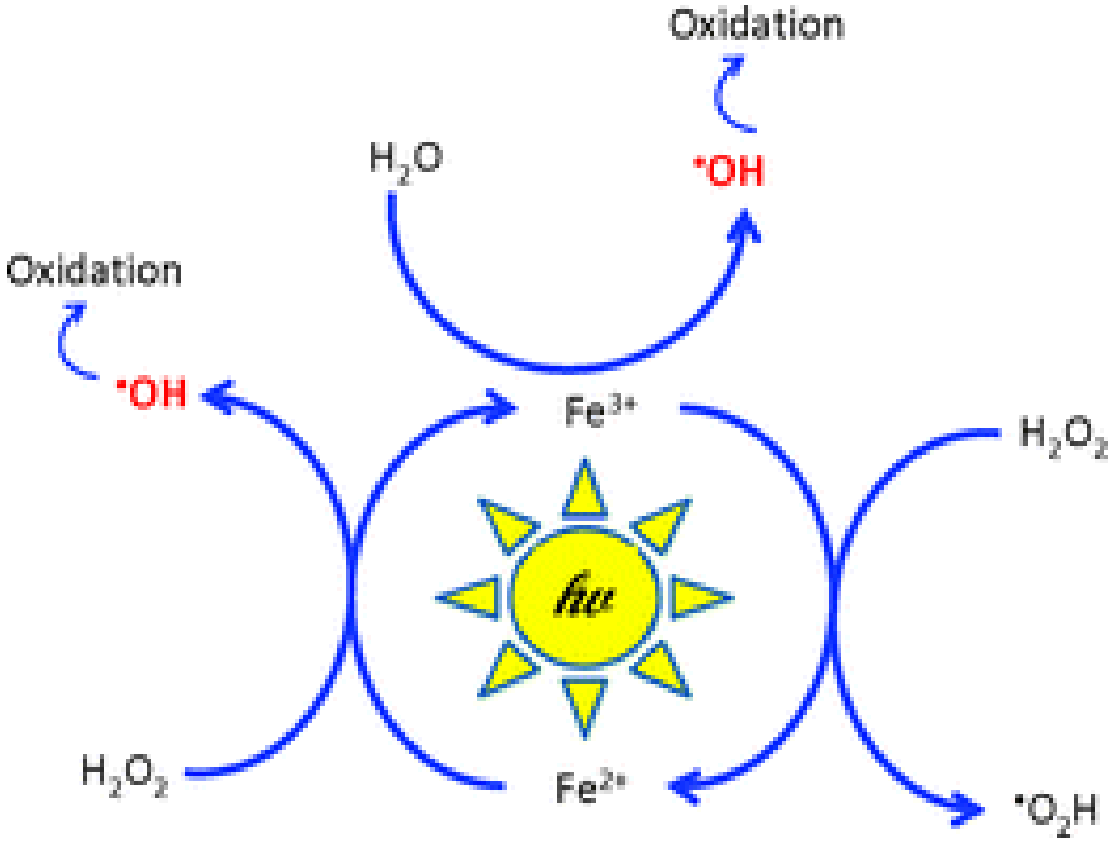

Figure 2.1 Mechanism of photo-Fenton process

However, this process has several disadvantages in practical applications: high iron concentration remained [87], large amount of manpower are required to remove sludge, complex before treatment processes, and catalysts recycling [88]. To overcome these limitations, more efficient heterogeneous iron species catalysts were investigated, such as oxides on different supporters including silica [89], activated carbon [90], clays [91, 92], fly ash [93]. The applications of these materials make photo-Fenton processes more feasible at a wider range of initial pH values. But recovery of catalyst after treatment is still tough due to the instability of these mixed oxides catalysts. Furthermore, better supporting materials, utilizing solar to replace UV light and the potential applicability of iron sludge require more studies.

Besides, Fenton processes are also coupled with ultrasonic irradiation process (Fenton/US) to remove resistant organic substances. Fenton/US has been proven more effective than normal Fenton process [94-96]. The principle reactions are as shown below [65]:

$$H_2O_2 + Fe^{2+} \rightarrow Fe^{-}OOH^{2+} \quad (2\text{-}8)$$

$$Fe^{-}OOH^{2+} +))) \rightarrow Fe^{2+}(isolated) + HO_2^{\bullet} \quad (2\text{-}9)$$

$$H_2O_2 + Fe^{2+}(isolated) \rightarrow OH^{\bullet} + OH^{-} + Fe^{3+} \quad (2\text{-}10)$$

Where "))) " means ultrasonic irradiation.

However, considering the high cost of Fenton/US, healthy effects on operators, high inlet pressures, and high operating temperature, Fenton/US is not suitable for wide application in wastewater treatment industry at present.

2.5.3. Oxidation in sulfate radical systems

To improve the zero-valent iron (ZVI or Fe^0) system, persulfate (peroxydisulfate, PDS,

$S_2O_8^{2-}$) was used in Fenton-like systems in some studies [97-99]. PDS is a strong oxidant ($E^0(S_2O_8^{2-})$=2.01V), but kinetically slow in degradation of most organic compounds [99, 100]. Further, when persulfate anion is activated chemically or thermally, it generates the intermediate sulfate radical ($SO_4^{\cdot-}$) (E^0=2.6V) which is stronger than persulfate anion [98]. The produced sulfate radicals should be more effective than persulfate anion in organic compound degradation. On the other hand, sulfate radical ($SO_4^{\cdot-}$) has been proven more stable than hydroxyl radical by Huang, et al. [101]. The generation reaction of sulfate radical activated by Fe^{2+} is shown as below:

$$S_2O_8^{2-} + Fe^{2+} \rightarrow SO_4^{\bullet-} + SO_4^{-} + Fe^{3+} \quad (2\text{-}11)$$

Cobalt/peroxymonosulfate (Co/PMS) has also demonstrated significant results in oxidation of organic compounds by using Fenton-like process [102-104]. The sulfate radical is activated from peroxymonosulfate by cobalt and can be applied for the decomposition of organics [105]:

$$Co^{2+} + HSO_5^{-} \rightarrow Co^{3+} + SO_4^{\bullet-} + OH^{-} \quad (2\text{-}12)$$

However, according to some researches, Co/PMS is only effective in oxidation of specific organics, such as 2,4-dichlorophenol, atrazine and naphthalene [105-109]. Moreover, the leaching of cobalt ions in water is the major issue of cobalt-based catalysts, because the discharge of cobalt in water causes the secondary pollution and several health problems. Hence, novel heterogeneous cobalt catalysts are highly demanded. Few studies showed the positive results of heterogeneous Co^{2+} based catalysts for organic compound degradation in sulfate radical systems [102, 110-112]. Employing extra materials, such as Al_2O_3, SiO_2, TiO_2, to cobalt catalysts is one of the novel photochemical oxidation methods. Since UV light irradiation used in Yang et al.'s study is harmful and high energy is required [112],

semiconductors with visible light activity can be promising supports for cobalt catalysts. Therefore, novel support materials for cobalt catalysts are important for Co/PMS systems or photochemical oxidation systems. Pradeep et al. investigated the activated carbon supported cobalt catalysts (Co/AC), and found Co/AC exhibited high activity in oxidation of phenol and less Co leaching from Co/AC solid phase [113]. This study proved that appropriate carbon materials could be novel supports to restrict the discharge of cobalt in water, and also enhance the adsorption capacity of catalysts due to its large surface area.

2.5.4. Photocatalysis

2.5.4.1. Photocatalysis mechanism

Heterogeneous photocatalysis are promising AOP techniques for wastewater treatment which have also been successfully used to deal with other environmental problems, such as indoor air pollutions [114-116]. Utilization of sun light in photocatalysis can decompose organic pollutants to CO_2 and water by an effectively and environmentally friendly manner. In recent years, heterogeneous photocatalysis has been studied for degradation of organic pollutants via UV irradiation. Efficient photocatalysts are solids that harmoniously combine good chemical and photoelectronic properties: (1) absorption of efficient photons; (2) generation of electron-hole pairs; (3) separation of electron-hole pairs with minimum of recombination. Various n-type semiconductor metal oxides, such as TiO_2, ZnO, ZnS, WO_3, etc., have been investigated for photocatalytic oxidation of organic pollutants in wastewater. These most common semiconductor materials applied as photocatalysts are summarized in Table 2.1.

Table 2.1 List of band gap energy and absorption threshold of various semiconductor photocatalysts

Semiconductor	Band Gap Energy (eV)	Wavelength Sensitivity (nm)
TiO_2 (anatase)	3.2	388
TiO_2 (rutile)	3.0	413
ZnO	3.2	388
ZnS	3.6	344
Fe_2O_3	2.3	539
$SrTiO_3$	3.2	388
WO_3	2.8	443
$SrTiO_3$	3.2	388

Photocatalytic process starts with the irradiation of a semiconductor material by light with sufficient energy. The electron (e^-)/hole (h^*) pairs are generated in the conduction band (CB) and valence band (VB), respectively, and then migrate to the surface of the semiconductor where they are involved in the development of redox reactions. The holes (h^*) react with hydroxyl anions and H_2O molecules to generate hydroxyl radicals. The excited electrons react with oxygen molecules, leading to the formation of the superoxide radical anion, peroxide radicals and H_2O_2 molecules at the same time. These reactive oxygen species contribute to renew the radical attack mechanisms [117-119]:

$$TiO_2 + h\nu \rightarrow e^- + h^+ \quad (2\text{-}13)$$

$$TiO_2(h^+) + H_2O_{ad} \rightarrow TiO_2 + HO^{\bullet}_{ad} + H^+ \quad (2\text{-}14)$$

$$TiO_2(h^+) + HO_{ad} \rightarrow TiO_2 + HO^{\bullet}_{ad} \quad (2\text{-}15)$$

$$TiO_2(h^+) + RX_{ad} \rightarrow TiO_2 + RX^{\bullet+}_{ad} \quad (2\text{-}16)$$

Or

$$RX_{ad} + H_2O + O_2 \rightarrow \frac{h\nu}{TiO_2} \rightarrow H_2O + CO_2 + Mineral.Acid. \quad (2\text{-}17)$$

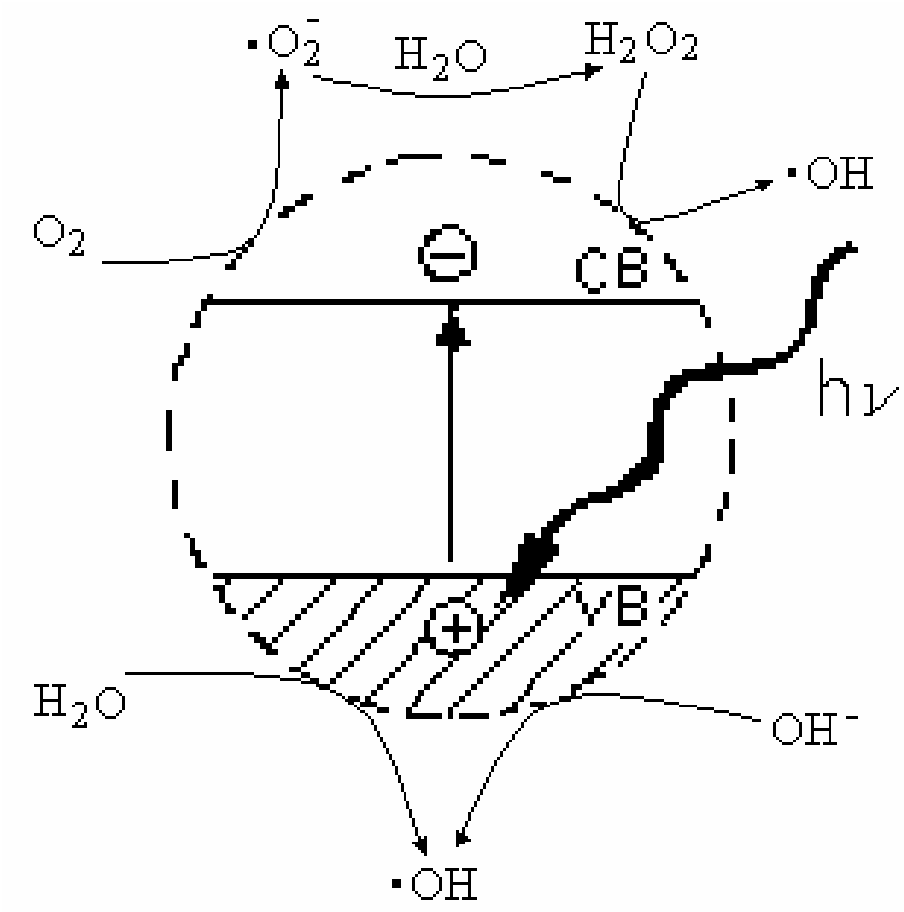

Figure 2.2 Mechanism of photocatalysis process

One of the most important aspects of environmental photocatalysis is the selection of photoactive materials. ZnO and TiO_2 are close to being ideal photocatalysts (Table 2.1), due to their relatively low prices, and ability to provide photo-generated holes with high oxidizing power which contributes to their wide band gap energy [120, 121]. Moreover, for more effective utilization of sunlight, in which visible light represents about 42% of spectrum energy, visible light responsive photocatalysts have been extensively investigated.

2.5.4.2. Heterogeneous ZnO photocatalysis

The semiconductor ZnO has been widely used as a photocatalyst for hosting a series of reductive and oxidative reaction on the surface, such as phenol degradation. ZnO has a few advantages over TiO_2: higher quantum efficiency and catalytic efficiency [122-124]. Further, ZnO photocatalysts have also been found to be effective for degradation of polymers and polymer composites [125]. When the photon energy brightened on the surface of ZnO is bigger than or equal to the band gap of ZnO (E_g=3.2 eV), e^- will be activated to the empty conduction band, as shown in Figure 2.3 [126]. The photo excitation leaves as a sequence of an unfilled valence band, which in turn produces the electron-hole pair (e^- - h^+). The presence of $h_{VB}{}^+$ and $e_{CB}{}^-$ illustrates the surface trapped conduction-band hole and valence-band electron. The charge carriers are connected with the surface of photocatalysts and do not recombine immediately after photo excitation [127]. Then the recombination of photoexcited electron and valence band hole takes place in nanosecond with delivery of energy. Hence, the existence of electron scavengers is of great importance for delaying the recombination and processing photocatalysis successfully. The presence of oxygen also prolongs the recombination of electron-hole pairs, at the same time producing the superoxides radicals ($O_2^{\bullet -}$). The superoxides radicals ($O_2^{\bullet -}$) could further combine with $HO_2\cdot$ and H^+ to produce H_2O_2. The presence of both dissolved oxygen and water molecules is essential because it leads to the occurrence of the entire photocatalytic reactions. In the

absence of water molecules, the highly active hydroxyl radicals cannot be produced and the degradation of organic materials will stop. The procedures of oxidative and reductive reactions taking place on the surface of ZnO are represented as below [128]:

Photo-excitation of ZnO: $ZnO + hv \rightarrow e^- + h^+$ (2-18)

Formation of H_2O_2: $O_2^- \cdot + HO_2 \cdot + H^+ \rightarrow H_2O_2 + O_2$ (2-19)

Charge-carrier trapping of e^-: $e_{CB}^- \rightarrow e_{TB}^-$ (2-20)

Charge-carrier trapping of h^+: $h_{VB}^+ \rightarrow h_{TB}^+$ (2-21)

Electron-hole recombination: $e^- + h^+ \rightarrow heat$ (2-22)

Photoexcited e^-: $e^- + O_2 \rightarrow O_2 \cdot^-$ (2-23)

Oxidation of OH_{ads}: $h^+ + \cdot OH_{ads}^- \rightarrow \cdot OH_{ads}$ (2-24)

Photo-degradation by OH·: $R_1 - H + OH \cdot \rightarrow R_2 \cdot + H_2O$ (2-25)

Degradation of phenol: $OH_{ads} + Phenol \rightarrow CO_2 + H_2O$ (2-26)

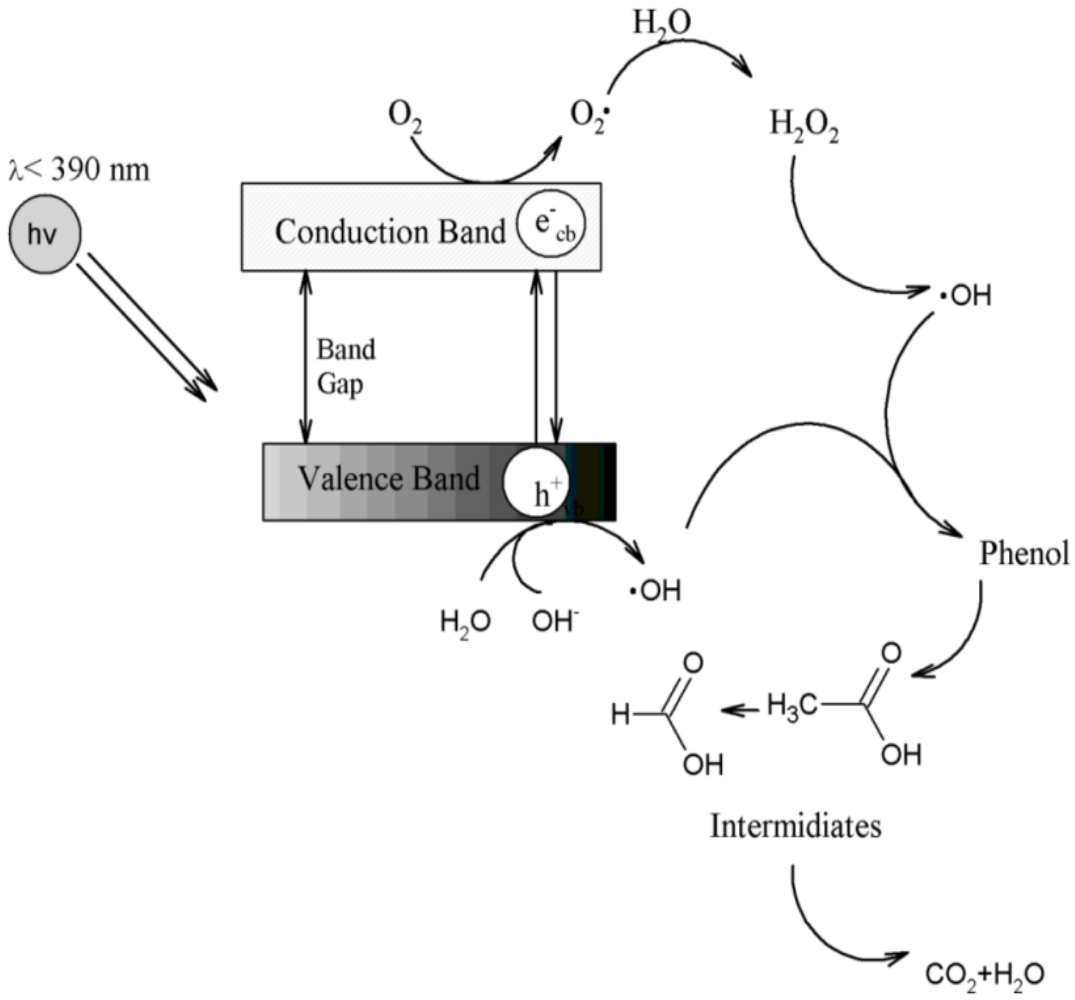

Figure 2.3 Mechanism of photocatalytic oxidation of phenol

Since the electron-hole of photocatalysts could be recombined with the discharge of energy in the form of heat/light, oxygen has been used as an electron receiver in the photocatalytic reaction. In order to reduce the combination of electron-hole and increase the residence time of electron-hole, other efficient electron acceptors have been applied to compare with oxygen. Hence, other oxidizing agents (e.g. H_2O_2, persulfate or peroxymonosulfate) have been found to significantly increase the degradation rate of organic chemicals due to their capacity of electron capture and the generation of other radicals [129].

In the case of hydrogen peroxide, the addition of small amount of oxidizing agents H_2O_2 could enhance the generation of radicals OH·. Because ZnO and TiO_2 have the similar

properties, researches based on TiO_2 are also possible to be applied on ZnO photocatalysts. According to Doong and Chang [130], the application of catalyst TiO_2 using an oxidizing agent H_2O_2 in the presence of UV has enhanced the degradation rate of pesticide compared with UV/TiO_2. Elmolla and Chaudhuri [131] also illustrated that enhancement of degradation of amoxicillin, ampicillin and cloxacillin antibiotics in aqueous solution was obtained by TiO_2 photocatalysis under H_2O_2/UV. Considering persulfate (PDS) and peroxymonosulfate (PMS) as oxidants, some researchers have also found that the combination of PDS or PMS with photocatalysts in the presence of UV illumination enhanced the photo degradation of pollutants. Malato et. al. [132] found that the additional oxidants $S_2O_8^{2-}$ strongly increased the degradation rate of photocatalysts on organic pollutants. Do et al. [128, 133] also reported that a single addition of PMS/Co(II) could degrade around fifty percent of maximum amount of diesel while only about 30% of diesel could be conversed by using the same amount of Co(II). Therefore, introducing strong oxidants such as PMS and PDS can enhance photocatalytic processes for organic pollutant degradation.

Another way for the generation of radicals is that the pollutants behave as sensitizers when they absorb the visible light. The photo-generated electrons from the pollutants are transferred to the semiconductors. The mechanism follows the steps as shown below [128]:

$$\text{Pollutant} + h\nu \rightarrow \text{Pollutant}^* \rightarrow \text{Pollutant}^+ + e^- \quad (2\text{-}27)$$

$$ZnO + e^- \rightarrow ZnO^{\bullet -} \quad (2\text{-}28)$$

$$ZnO^{\bullet -} + O_2 \rightarrow ZnO + O_2^{\bullet -} \quad (2\text{-}29)$$

$$O_2^{\bullet -} + 2H_2O + e^- \rightarrow 2H_2O_2 \quad (2\text{-}30)$$

$$H_2O_2 + e^- \rightarrow OH\cdot + OH^- \quad (2\text{-}31)$$

It shows that the light was absorbed by the pollutants to generate the active pollutant* molecules. Then the active pollutant* molecules transfer the electron to the conduction

band of ZnO as shown in equations above, where the hole is trapped by the oxygen to form $O_2^{\bullet -}$. Finally, the hydroxyl radicals are produced by the reaction of H_2O_2 and e^-

2.5.4.3. Heterogeneous TiO_2 photocatalysis

Titanium dioxide (E_g=3.2eV) as a heterogeneous photocatalyst is widely applied for organic degradation since 1970s. The mechanism is that if the light with photon energy higher or equal to the band gap energy of TiO_2, the electron-hole pairs will be produced when the TiO_2 particle is irradiated. The photonic excitation leaves behind an empty unfilled valence band, and thus creating the electron-hole pair [134].

However, after so many years studies, either ZnO or TiO_2 or other popular photocatalysts such as WO_3 and SnO_2, have the similar disadvantages: (1) large band gap, often necessitating near UV light (λ < 400 nm) to induce electron photoexcitation; (2) instability in aqueous medium, leading to photocatalyst decomposition; (3) high electron-hole recombination rates. For example: ZnO shows photo-corrosion effect that makes ZnO self-deactivate by forming Zn^{2+} ions when reacting with photo-generated holes in water, then will be dissolved into solution [135-137]. Therefore, photocatalysts which are photo-stable, feasible under visible light, and more efficient are required. Heterogeneous photocatalytic oxidation using visible light photocatalysts is considered as a highly attractive technology. Doping of a foreign element (Cr, V, Fe, Mn, Co, Ni, etc.) into TiO_2 or ZnO photocatalysts have been studies for a long time. Most of doped photocatalysts can be used in photodegradation of organics in wastewater under visible light due to the formation of a localized narrow band in the forbidden band of semiconductor photocatalysts. Studies indicated that metal ion dopants into the TiO_2 particles can influence the performance of photocatalyst by the effects on the dynamics of electron: hole recombination and interfacial charge transfer [138, 139]. The largest enhancement of photocatalytic activity through doping was found in

nanosized TiO_2 particles, in which the dopants are located within 1-2 nm of the surface, and the high surface areas result in the high visible light activity of the photocatalysts [138, 139]. Moreover, according to recent studies [102, 111, 112, 140], few heterogeneous Co^{2+}-based photocatalysts with Co supported on silica or titania have been proven effective in organic compounds degradation. It has been found that doped titanates appear to be sensitive to both UV light and visible light in some studies [110, 141]. Inorganic materials, such as silica, carbon nanotubes, activated carbon, carbon aerogels, etc are also applied in extensive investigations of visible light photocatalysts [142-145].

Carbon nanotubes/TiO_2

Titanium dioxide can be employed as a photocatalyst for the successful decontamination of pollutants in both liquid and gas phases [146]. Nevertheless, there is a serious issue that TiO_2 cannot be activated by UV which occupies less than 5% of the total solar irradiance at the earth's surface because of its large band gap of 3.2eV. It was reported that modification of TiO_2 could make it absorb visible light and improve the efficient utilization of sunlight [147]. Because of conducting electrons, high surface area and high adsorption capacity, the carbon nanotubes are good supports for modification of TiO_2 samples [146]. CNT/TiO_2 composite materials increase the rate of photo-catalytic oxidation of pollutants due to the conductive structure. The CNT scaffolds might facilitate the separation of the photo-generated electron/hole pairs at the CNT–TiO_2 interface, leading to the faster rates of photo-catalytic oxidation [148, 149]. There are a range of different methods for preparation of heterogeneous CNT/TiO_2 such as mechanically mixing TiO_2 and CNT, sol–gel synthesis of TiO_2 in the presence of CNT, electro-spinning method, electrophoretic deposition, and chemical vapor deposition [150, 151]. Sol–gel route and complete heat treatment at high temperatures are widely used because of the exposure of bare CNT surfaces and consequent random aggregation of TiO_2 onto the CNT surfaces [152].

Graphene oxide/TiO_2

The UV-assisted photocatalytic reduction of graphene oxide with TiO_2 without high temperature annealing has been well developed [153]. Graphene can act as an electron transfer channel, and reduce the recombination of the photo-generated [154]. Graphene has been widely applied to prepare TiO_2-based materials. Moreover, the surface properties of graphene could be adjusted via chemical modification, which facilitates its use in composite materials. Thus, the combination of TiO_2 and graphene is a promising strategy to simultaneously possess excellent adsorptivity, transparency, conductivity, and controllability, which could facilitate effective photo-degradation of pollutants [155]. Molecular grafting that incorporates carbon into a TiO_2 matrix by chemically exfoliated graphene is wildly used. It was also found that the implanted graphene provided additional transport pathways for photo-induced carriers, leading to an increase in photocurrent. Graphene with a high specific surface area and dispersion ability is very difficult to prepare, therefore improving the dispersion of graphene in the matrix is critical to its successful application in photoanodes. A sonochemical method was used to homogeneously embed TiO_2 nanoparticles into graphene oxide (GO) nanosheets without functionalizing the surface with a surfactant. Graphene–TiO_2 composite (GR–TiO_2) was obtained by chemical reduction. The photocatalytic properties of the obtained GR–TiO_2 composites were investigated by measuring the photo-degradation of methylene blue under UV-light, and showed a high photocatalytic performance on the obtained composites [156].

Carbon doped TiO_2

It is now commonly recognized that visible-light absorption does not always result in visible-light photocatalytic activity, and the key to enhance the photocatalytic activity is to effectively combine the photon absorption, bulk diffusion, and surface transfer of

photo-induced charge carriers in the photocatalyst. When dopants and defects are introduced, additional extrinsic electronic levels can be located in the energy band gap of TiO_2. It has been demonstrated that carbon doping can dramatically improve the absorption and photocatalytic activity of TiO_2 in the visible-light region [157]. Owing to the doped C atoms, carbon /TiO_2 have a particular oxidation state. Among various anionic dopants, the modification with carbon has been reported to be a promising way to extend the absorbance of TiO_2 into visible light [158]. The carbon dopant has been described either as an anion that replaces oxygen substitutionally in the lattice or as a cation that occupies an interstitial lattice site. The formal oxidation state of carbon dopants ranges from -4 (as carbides with Ti–C bond) to +4 (as carbonates with C–O bond). Ti–C bond was formed at conditions like flame pyrolysis of Ti metal sheet, annealing of TiC powders, and ion-assisted electron beam evaporation. On the other hand, C–O bond (carbonate) was often observed at conditions like sol–gel processes with carbon precursors and high temperature reactions of TiO_2 with carbon precursors. Although carbon is a ubiquitous impurity, the addition of external carbon precursors such as glucose was essentially needed to make C-TiO_2 in all reported cases [157].

There are several methods for preparation of carbon-doped TiO_2. Researchers prepared carbon-doped TiO_2 by oxidizing titanium sheet in a natural gas flame and obtained water-splitting efficiency of 8.35% with a visible light absorption shifted from 414 to 535 nm [154]. However, this method did not compensate the different spectral photon flux distribution when comparing the overall intensity of the experimental light source with that of standard solar illumination. The other way is to prepare photoelectrode by the hydrolysis of titanium tetrachloride with carbon-containing bases [157]. However, the prepared film had no obvious spectrum extension to the visible light. Compared with these two ways, the best way is to prepare mesoporous carbon-doped TiO_2 at low temperature using glucose and

amorphous TiO_2 as the carbon and TiO_2 sources, respectively [158]. Moreover, it was reported that the reduction of glucose and crystallization of TiO_2 as well as the carbon doping could take place at the same time under hydrothermal treatment at 160ºC [154] [158].

2.5.5. Other AOPs

Besides Fenton, Fenton-like, and photocatalysis processes, there are some other AOP techniques which are studied and applied in organic wastewater treatment, such as ozonation, UV/O_3, H_2O_2, UV/H_2O_2, $UV/H_2O_2/O_3$, O_3/H_2O_2 [58].

Ozone is a strong oxidant (E^0=2.07V), and can oxidize a large number of organic compounds that mainly include multiple bonds (e.g. C=C, C=N, and N=N) [159]. Ozonation process is a pathway that directly reacts with all organic pollutants in wastewater at various rates at same time. Ozonation process also has an indirect way which generates hydroxyl radicals that also reacts with organic targets [160]:

$$O_3 + OH^- \rightarrow HO_2^- + O_2 \quad (2\text{-}32)$$

$$O_3 + HO_2^- \rightarrow HO_2^{\bullet} + O_3^{\bullet -} \quad (2\text{-}33)$$

However, it is difficult for ozone to react rapidly with singly bonded functionality (e.g. C-C, C-O, and O-H) [159]. Hydrogen peroxide (H_2O_2) is another strong oxidant, and has already been widelyutilized in industry. 50% of H_2O_2 is required in wastewater treatment processes, because low concentration hydrogen peroxide lead to low reaction rate. Meanwhile, high concentration H_2O_2 (more than 50%) is dangerous for operators due to the detonable byproducts released during reactions [161]. In O_3/H_2O_2 process, ozone reacts with hydrogen peroxide to generate hydroxyl radicals. The hydroxyl radicals in turn oxidize target organics [162]:

$$2O_3 + H_2O_2 \rightarrow 2OH\bullet + 3O_2 \quad (2\text{-}34)$$

UV/H_2O_2 is a great potential AOP technique due to the wide acceptance and application of UV as effective disinfectant [163, 164]. This process is irradiating the organic wastewater containing H_2O_2 with UV light (<280nm) [119, 165]:

$$H_2O_2 + h\nu \rightarrow 2OH\bullet \quad (2\text{-}35)$$

Nevertheless, UV/H_2O_2 was proven insufficient for degradation of specific organics like trihalomethanes, halo-acetic acids in drinking water [119]. Furthermore, combining UV irradiation and ozone is another way to enhance oxidation power for organic compounds degradation. The mechanism of this UV/O_3 based AOP is [166, 167]:

$$O_3 + H_2O + h\nu \rightarrow 2OH\bullet + O_2 \quad (2\text{-}36)$$

But, neither UV/H_2O_2 nor UV/O_3 may be practical to be used in wastewater treatment plants because of their high energy cost.

There is another combined AOP of $UV/H_2O_2/O_3$ which is similar to UV/H_2O_2 and UV/O_3. The principle reaction is [168]:

$$O_3 + H_2O_2 + H_2O + h\nu \rightarrow 4OH\bullet + O_2 \quad (2\text{-}37)$$

The rate constants of AOPs for gradation of phenol and reactive azo dye are summarized in Table 2.2.

Table 2.2 Rate constants of AOPs for degradation of phenol and reactive azo dye

AOPs	Rate constants (*k*)	References
***Part A**: <u>For phenol</u>*		
UV (254nm)	0.0021 min^{-1}	[169]
US (300kHz)	0.0008 min^{-1}	[169]
O_3 (2mg/L)	0.0279 min^{-1}	[169]
US+UV	0.005 min^{-1}	[169]
US+O_3	0.0326 min^{-1}	[169]
UV+O_3	0.0869 min^{-1}	[169]
US+UV+O_3	0.1793 min^{-1}	[169]
US+H_2O_2+CuO	0.0149 min^{-1}	[170]
Fenton	0.0106 min^{-1}	[171]
SonoFenton	0.058 min^{-1}	[171]
UV+H_2O_2	0.0524 min^{-1}	[172]
Photocatalysis	0.433 ppm min^{-1}	[173]
***Part B**: <u>For reactive azo dye</u>*		
UV (254nm)	No degradation	
US (300kHz)	0.00175	[174]
O_3 (2mg/L)	0.01108	[174]
US+UV	0.0055	[174]
US+O_3	0.01674	[174]
UV+O_3	0.02064	[174]
US+UV+O_3	0.02171	[174]
US+H_2O_2	0.0032	[175]
UV+H_2O_2	0.0124	[175]
Photocatalysis	0.0207	[176]

Therefore, among various advanced oxidation processes, photocatalysis is a significant technique for degradation of organics pollutants, due to its high efficiency and low-cost. Meanwhile, because of high efficiency and non-selectivity for various organic compounds in wastewater, chemical oxidation and photochemical oxidation do also have development potential.

Although oxidants like O_3 and H_2O_2 have a wide selective range of organic pollutants, the

oxidizing reactions present much lower rate of degradation and higher operation requirements comparing with free radicals [175]. Therefore, these techniques mentioned above (section **2.5.5**) will not be applied in this study.

2.6. Development of Photocatalyst Materials

Photocatalysis has attracted attention since last century, due to its extremely high oxidizing power and the abilities of oxidation and decomposition of organic pollutants. Simple metal oxide materials, such as TiO_2 and ZnO, have been proven active, but cannot effectively utilize visible light. Considering the issues of cost and environment, the requirements of development of green photocatalysts should be: (1) doping some element into conventional photocatalysts with wide band gaps, such as TiO_2 to form a donor level above a valence band; (2) making a solid solution to control the band structure; (3) employing some element to create a new valence band [177-179]; (4) improving response to green energy (solar, visible light). Doping is an effective method to enhance the visible light activities of TiO_2 (or the other well-known materials, such as ZnO, ZnS and WO_3). Doping TiO_2 with elements, such as Fe [180, 181], Pt [181], and Ag [182], Co [183], was successful in organic degradation under visible light. Moreover, carbon materials, such as carbon aerogel [157], activated carbon [184], carbon nanotube [148, 149], graphene oxide [155], etc., were used for preparation of modified TiO_2.

Besides those well-known photocatalysts, other materials such as titanates ($ZnTiO_3$, $FeTiO_3$, $Bi_4Ti_3O_{12}$, etc.), have also been previously used as photocatalysts, luminescent, lasing materials, solar cells, dielectrics, microwave, and gas sensors [185-187]. These titanates are promising photocatalysts with narrow band gap and photocatalytic activity under visible light; however, they are not employed in organic treatments. Further, introducing new

elements into these titanates may be one potential way to enhance their photocatalytic activities under visible light. On the other hand, developing new photocatalysts is considered as a challenging and promising way to meet the requirements of environmental protection. In recent years, non-metal materials with photocatalytic properties, such as graphene, graphene oxide (GO), graphitic carbon nitride (g-C_3N_4), and carbon spheres, or their doping products are very attractive for researchers. For instance, Lu, et al. investigated the photocatalytic properties of g-C_3N_4/TiO_2, and found g-C_3N_4/TiO_2 displayed good visible light activity for degradation of rhodamine B [188]. Few studies applied g-C_3N_4 in degradation of resisted organic pollutants, such as phenol. However, it is still a promising material worth further investigations.

2.7. Development of catalyst Materials for Sulfate Radicals System

Metal-free materials, such as activated carbon, multiwall carbon nanotube and carbon-xerogel, are proven to be able to positively restrict the leaching of Co^{2+} and enhance the organic compounds degradation capacities of cobalt catalysts in sulfate radicals system [113, 189, 190]. However, the critical requirements (e.g. high temperature) of synthesis process are their major limitations. Micro-carbon sphere materials have become very attractive due to their unique spherical shape with a diameter of approximately 1 to 40μm, high density and high strength [191]. Simple synthesis process (hydrothermal method at 160 to 230^{o}C) and inexpensive raw material (glucose) are the extra advantages of micro-carbon sphere materials [191-193]. Researchers were barely using micor-carbon as catalyst supporting materials. However, due to the unique properties of structures, low cost synthesis process, and non-toxic characteristic, micro-carbon sphere materials have significantly development potentials as support materials for cobalt catalysts in sulfate radicals systems.

2.7. Conclusions

Industrial processes, productions, and human activities emit a huge amount of toxic organic pollutants. Polychlorinated biphenyls (PCBs), di-(2-ethyhexyl)-phthalate (DEHP), polycyclic aromatic hydrocarbons (PAHs), tetrachloroethane, dibutyl phthalate (DBP), tolune, benzene, acetone, dimethylphenol and phenol are identified by EPA and WHO as precedent-controlled harmful pollutants. Various physical and chemical techniques have been applied for removal of toxic organic compounds in wastewater, but, there is not a complete solution for these environmental problems yet. Among these techniques, photocatalysis and chemical oxidation using suitable catalysts have been proven as efficient and cost-effective methods to completely remove or mineralize SOCs. However, the catalysts still need to be improved.

Primary objectives of this literature review were to find suitable techniques for organic compound degradation, and promising catalyst materials for efficient degradation under visible light irradiation. According to vast literatures, the following points were identified:

(1) Phenol is an ideal and logical model for wastewater treatment studies, due to its stability, refractory, and high level in productions and wastewater.
(2) Titanates, such as $ZnTiO_3$, $FeTiO_3$, and $Bi_4Ti_3O_{12}$, have a narrow band gap and photocatalytic activity under visible light. If suitable element is introduced to them, these titanates should be more effective for organics degradation via photocatalysis or photochemical oxidation.
(3) Nanoscaled zero-valent iron and cobalt have been proven highly effective for decomposing organics via Fenton reaction. However, only a few studies of oxidation of organic pollutants using ZVI were conducted, and hydrolytic cobalt caused

second pollution. Therefore, appropriate support materials (e.g. carbon sphere) and strong oxidants (e.g. PDS and PMS) are proposed to improve ZVI or cobalt contained catalysts for organic degradation.

(4) As a non-metal material, g-C_3N_4 has photocatalytic activity, but has not been used in degradation of resistant organic compounds under UV/visible light irradiation. It would be of great interest to develop metal-free photocatalyst materials for phenol removal.

2.8. References

1. Brown, V.M., D.H.M. Jordan, and B.A. Tiller, *The effect of temperature on the acute toxicity of phenol to rainbow trout in hard water.* Water Research, 1967. **1**(8–9): p. 587-594.

2. Takeda, N. and K. Teranishi, *Generation of superoxide anion radical from atmospheric organic matter.* Bulletin of Environmental Contamination and Toxicology, 1988. **40**(5): p. 678-682.

3. Pardeshi, S.K. and A.B. Patil, *A simple route for photocatalytic degradation of phenol in aqueous zinc oxide suspension using solar energy.* Solar Energy, 2008. **82**(8): p. 700-705.

4. MITI, *Biodegradation and bioaccumulation data of existing chemicals based on the CSCL. Japan. Chemical Products Safety Division, Basic Industries Bureau MITI. Hrsg. CITI.* Japan Chemical Industry Ecology-Toxicology and Information Cente, 1992: p. 14 – 19.

5. Urano, K. and Z. Kato, *A METHOD TO CLASSIFY BIODEGRADABILITIES OF ORGANIC-COMPOUNDS.* Journal of Hazardous Materials, 1986. **13**(2): p. 135-145.

6. Brezova, V.S., A., *Spin Trap Study of Hydroxyl Radicals Formed in the Photocatalytic System TiO2-Water-p-Cresol-Oxygen.* Journal of Catalysis, 1994. **147**(1): p. 156-162.

7. Vione, D., et al., *Degradation of phenol and benzoic acid in the presence of a*

TiO2-based heterogeneous photocatalyst. Applied Catalysis B-Environmental, 2005. **58**(1-2): p. 79-88.

8. H. Gerischer, A.H., *Photocatalytic oxidation of organic molecules at TiO_2 particles by sunlight in aerated water.* Electrochem. Soc., 1992. **139**: p. 113-118.

9. Linsebigler, A.L., G. Lu, and J.T. Yates, *Photocatalysis on TiO2 Surfaces: Principles, Mechanisms, and Selected Results.* Chemical Reviews, 1995. **95**(3): p. 735-758.

10. Fedorak, P.M. and S.E. Hrudey, *Anaerobic treatment of phenolic coal conversion wastewater in semicontinuous cultures.* Water Research, 1986. **20**(1): p. 113-122.

11. M., R.T.a.J., *Dissolved organics in tannery wastewater and their alteration by a combined anaerobic and aerobic treatment.* Water Research, 1997. **31**: p. 1035-1046.

12. Pratt, R.B.J.R., *Toxic effects of chemicals on microorganisms.* Water Environment Research 1992. **64**(4): p. 632-641.

13. Eljarrat, E., J. Caixach, and J. Rivera, *Effects of sewage sludges contaminated with polychlorinated dibenzo-p-dioxins, dibenzofurans, and biphenyls on agricultural soils.* Environmental Science & Technology, 1997. **31**(10): p. 2765-2771.

14. Langenkamp, H., Part, P., Erhardt, W., Pruoes, A. , *Organic contaminants in sewage sludge for agricultural use.* European Commission, Joint Research Centre Institute for Environment and Sustainability Soil and Waste Unit, 2001.

15. Singh, S., et al., *Wastewater from monosodium glutamate industry as a low cost fertilizer source for corn (Zea mays L.).* Biomass & Bioenergy, 2011. **35**(9): p. 4001-4007.

16. Yang, Q., et al., *Treatment of wastewater from a monosodium glutamate manufacturing plant using successive yeast and activated sludge systems.* Process Biochemistry, 2005. **40**(7): p. 2483-2488.

17. Chemicals, U., *Guidelines for the Identification of PCBs and Materials Containing*

PCBs. United Nations Environment Programme. 2007.

18. Broadhurst, M.C., *Use and replaceability of polychlorinated biphenyls.* Envir. Hlth Perspect, 1972. **2**: p. 81-102.

19. H.L., H., *Chlorinated biphenyl and related compounds.* Kirk-Othmer Encyclopedia of Chemical Technology, 2nd edn, 1964. **5**(289-297).

20. *Brand names of PCBs — What are PCBs?* Japan Offspring Fund / Center for Marine Environmental Studies (CMES), Ehime University, Japan, 2003.

21. *Identifying PCB-Containing Capacitors.* Australian and New Zealand Environment and Conservation Council (ANZECC), 1997: p. 4–5.

22. M, V.d.B., *Toxic Equivalency Factors (TEFs) for PCBs, PCDDs, PCDFs for Humans and Wildlife.* Environ Health Perspect, 1998. **106**(12): p. 775–792.

23. Fetzer, J.C., *The Chemistry and Analysis of the Large Polycyclic Aromatic Hydrocarbons.* Polycyclic Aromatic Compounds (New York: Wiley) 2000. **27**(2).

24. Poon, C.S., Q. Huang, and P.C. Fung, *Degradation kinetics of cuprophenyl yellow RL by UV/H2O2/ultrasonication (US) process in aqueous solution.* Chemosphere, 1999. **38**(5): p. 1005-1014.

25. Guivarch, E., et al., *Degradation of azo dyes in water by Electro-Fenton process.* Environmental Chemistry Letters, 2003. **1**(1): p. 38-44.

26. Singh, P., K. Mondal, and A. Sharma, *Reusable electrospun mesoporous ZnO nanofiber mats for photocatalytic degradation of polycyclic aromatic hydrocarbon dyes in wastewater.* Journal of Colloid and Interface Science, (0).

27. Nisbet ICT, L.P., *Toxic equivalency factors (TEFs) for polycyclic aromatic-hydrocarbons (PAHs).* Regul Toxicol Pharm 1992. **16**(3): p. 290–300.

28. S., O., *Assessment of polycyclic aromatic hydrocarbons (PAHs) in soil of a Natural Reserve (Isola delle Femmine) (Italy) located in front of a plant for the production of cement.* J Hazard Mater 2010. **173**(1-3): p. 358–680.

29. K. Choi, H.J., J.L. Campbell Jr., R.A. Clewell, M.E. Andersen, H.J. Clewell III, *In vitro metabolism of di(2-ethylhexyl) phthalate (DEHP) by various tissues and cytochrome P450s of human and rat.* Toxicology in Vitro, 2012. **26**: p. 315–322.

30. *Agency for Toxic Substances and Disease Registry (ATSDR), 2002. Toxicological profile for di(2-ethyhexyl) phthalate (DEHP).* Available at: http:// www.atsdr.cdc.gov/toxprofiles/tp9.html.

31. *Food and Drug Administration (FDA), 2001. Safety assessment of di(2-ethylhexyl) phthalate (DEHP) released from PVC medical devices.* Available at: http://www.fda.gov/downloads/MedicalDevices/DeviceRegulationandGuidance/GuidanceDocuments/ UCM080457.pdf. Center for Devices and Radiological Health, US Food and Drug Administration, Rockville, MD.

32. CCME, *Canadian Water Quality Guidelines, prepared by the Task Force on Water Quality Guidelines of the Canadian Council of Ministers of the Environment.* Eco-Health Branch, Ottawa, Ontario, Canada, 1992.

33. Whitehouse, P., Wilkinson, M., Fawell, J. and Sutton, A, *Proposed Environmental Quality Standards for Nonylphenol in Water.* Report for the Environment Agency R&D Technical Report 1998: p. 42.

34. Whitehouse, P., Young, W., Fawell, J., Sutton, A. and Wilkinson, M, *Proposed Environmental Quality Standards for Octylphenol in Water.* Report for the Environment Agency R&D Technical Report, 1998: p. 59.

35. G. Choudhary, L.K., C. Rappe, *Chlorinated Dioxinsand Dibenzofurans in the Total Environment.* Butterworth Publishers, 1983.

36. R. Peterson, E.M., *Chemical Treatment of Dioxin Residues from Wastewater Processing.* Chemosphere, 1992. **25**(7-10): p. 1565-1568.

37. A.K. Liem, P.F., C. Rappe, *Exposure of populations to dioxins and related compounds.* Food Additives and Contaminants, 2000. **17**: p. 241-259.

38. Schecter A, C.P., Boggess K, Stanley J, Päpke O, Olson J, Silver A, Schmitz M, *Intake of dioxins and related compounds from food in the U.S. population.* J Toxicol

Environ Health A, 2001. **63**(1).

39. Zazo, J.A., et al., *Catalytic wet peroxide oxidation of phenol with a Fe/active carbon catalyst.* Applied Catalysis B-Environmental, 2006. **65**(3-4): p. 261-268.

40. Mukherjee, D., et al., *Biological significance of 14C phenol accumulation in different organs of a murrel, Channa punctatus, and the common carp, Cyprinus carpio.* Biomedical and environmental sciences : BES, 1990. **3**(3): p. 337-42.

41. Mukherjee, D., et al., *IMPAIRMENT OF STEROIDOGENESIS AND REPRODUCTION IN SEXUALLY MATURE CYPRINUS-CARPIO BY PHENOL AND SULFIDE UNDER LABORATORY CONDITIONS.* Aquatic Toxicology, 1991. **21**(1-2): p. 29-40.

42. Fleeger, J.W., K.R. Carman, and R.M. Nisbet, *Indirect effects of contaminants in aquatic ecosystems.* Science of the Total Environment, 2003. **317**(1-3): p. 207-233.

43. Paustenbach, D., et al., *A recommended occupational exposure limit for formaldehyde based on irritation.* Journal of Toxicology and Environmental Health, 1997. **50**(3): p. 217-263.

44. Munoz-de-Toro, M., et al., *Perinatal exposure to bisphenol-A alters peripubertal mammary gland development in mice.* Endocrinology, 2005. **146**(9): p. 4138-4147.

45. *U.S Department of Health and Human Services, Toxicological Profile for Phenol.* 2008: p. 4-87.

46. Deichmann, W.B.K.M., *Phenols and phenolic compounds. In: Clayton, GD, Clayton, FE (Eds.).* Patty's industrial hygiene and toxicology 1981: p. 2567-2627.

47. Bruce, R.M., J. Santodonato, and M.W. Neal, *SUMMARY REVIEW OF THE HEALTH-EFFECTS ASSOCIATED WITH PHENOL.* Toxicology and Industrial Health, 1987. **3**(4): p. 535-568.

48. McCall, I.C., et al., *Effects of phenol on barrier function of a human intestinal epithelial cell line correlate with altered tight junction protein localization.* Toxicology and Applied Pharmacology, 2009. **241**(1): p. 61-70.

49. Shen, Y.H., *Removal of phenol from water by adsorption-flocculation using*

organobentonite. Water Research, 2002. **36**(5): p. 1107-1114.

50. Ndabigengesere, A. and K.S. Narasiah, *Quality of water treated by coagulation using Moringa oleifera seeds.* Water Research, 1998. **32**(3): p. 781-791.

51. Sun, L., E.M. Perdue, and J.F. McCarthy, *USING REVERSE-OSMOSIS TO OBTAIN ORGANIC-MATTER FROM SURFACE AND GROUND WATERS.* Water Research, 1995. **29**(6): p. 1471-1477.

52. Li, D. and M. Ma, *Nanoporous polymers: New nanosponge absorbent media.* Filtration & Separation, 1999. **36**(10): p. 26-28.

53. Allabashi, R., et al., *Removal of some organic pollutants in water employing ceramic membranes impregnated with cross-linked silylated dendritic and cyclodextrin polymers.* Water Research, 2007. **41**(2): p. 476-486.

54. Guo, L., et al., *Levels and distributions of polychlorinated biphenyls in sewage sludge of urban wastewater treatment plants.* Journal of Environmental Sciences-China, 2009. **21**(4): p. 468-473.

55. Ozturk, B. and D. Yilmaz, *Absorptive removal of volatile organic compounds from flue gas streams.* Process Safety and Environmental Protection, 2006. **84**(B5): p. 391-398.

56. Li, R., et al., *Reduction of VOC emissions by a membrane-based gas absorption process.* Journal of Environmental Sciences-China, 2009. **21**(8): p. 1096-1102.

57. Song, Y.H., et al., *Effects of adsorption and temperature on a nonthermal plasma process for removing VOCs.* Journal of Electrostatics, 2002. **55**(2): p. 189-201.

58. Mahamuni, N.N. and Y.G. Adewuyi, *Advanced oxidation processes (AOPs) involving ultrasound for waste water treatment: A review with emphasis on cost estimation.* Ultrasonics Sonochemistry, 2010. **17**(6): p. 990-1003.

59. Brillas, E., et al., *Aniline mineralization by AOP's: anodic oxidation, photocatalysis, electro-Fenton and photoelectro-Fenton processes.* Applied Catalysis B-Environmental, 1998. **16**(1): p. 31-42.

60. W.H. Glaze, e.a., *Ozone-Hydrogen peroxide system for control of organics in municipal water supplies, in: Proc. 2nd Int. Conf. On the Role of Ozone in Water and Wastewater Treatment.* Tek Tran Intern., Ltd., Edmonton, Alberta, 1987: p. 233.

61. Esplugas, S., et al., *Comparison of different advanced oxidation processes for phenol degradation.* Water Research, 2002. **36**(4): p. 1034-1042.

62. Parsons, S., *Advanced Oxidation Processes for Water and Wastewater Treatment.* IWA Publishing, London, 2004.

63. H.J.H., F., *Oxidation of tartaric acid in presence of iron.* J. Chem. Soc., Trans. , 1894. **65**(65): p. 899–911.

64. Walling, C. and A. Goosen, *MECHANISM OF FERRIC ION CATALYZED DECOMPOSITION OF HYDROGEN-PEROXIDE - EFFECT OF ORGANIC SUBSTRATES.* Journal of the American Chemical Society, 1973. **95**(9): p. 2987-2991.

65. Neppolian, B., et al., *Sonolytic degradation of methyl tert-butyl ether: the role of coupled fenton process and persulphate ion.* Water Research, 2002. **36**(19): p. 4699-4708.

66. Li, X.Q., D.W. Elliott, and W.X. Zhang, *Zero-valent iron nanoparticles for abatement of environmental pollutants: Materials and engineering aspects.* Critical Reviews in Solid State and Materials Sciences, 2006. **31**(4): p. 111-122.

67. Noubactep, C., *A critical review on the process of contaminant removal in Fe-0-H2O systems.* Environmental Technology, 2008. **29**(8): p. 909-920.

68. Shimizu, A., et al., *Phenol removal using zero-valent iron powder in the presence of dissolved oxygen: Roles of decomposition by the Fenton reaction and adsorption/precipitation.* Journal of Hazardous Materials, 2012. **201**: p. 60-67.

69. Kallel, M., et al., *Removal of organic load and phenolic compounds from olive mill wastewater by Fenton oxidation with zero-valent iron.* Chemical Engineering Journal, 2009. **150**(2-3): p. 391-395.

70. Zhao, J.Y., et al., *Enhanced oxidation of 4-chlorophenol using sulfate radicals*

generated from zero-valent iron and peroxydisulfate at ambient temperature. Separation and Purification Technology, 2010. **71**(3): p. 302-307.

71. Garcia, J., et al., *Carbon nanotube supported ruthenium catalysts for the treatment of high strength wastewater with aniline using wet air oxidation.* Carbon, 2006. **44**(12): p. 2384-2391.

72. Liao, Q., J. Sun, and L. Gao, *Degradation of phenol by heterogeneous Fenton reaction using multi-walled carbon nanotube supported Fe(2)O(3) Catalysts.* Colloids and Surfaces a-Physicochemical and Engineering Aspects, 2009. **345**(1-3): p. 95-100.

73. Martinez, F., et al., *Influence of preoxidizing treatments on the preparation of iron-containing activated carbons for catalytic wet peroxide oxidation of phenol.* Journal of Chemical Technology and Biotechnology, 2012. **87**(7): p. 880-886.

74. Ramirez, J.H., et al., *Azo-dye Orange II degradation by heterogeneous Fenton-like reaction using carbon-Fe catalysts.* Applied Catalysis B-Environmental, 2007. **75**(3-4): p. 312-323.

75. Pignatello, J.J., E. Oliveros, and A. MacKay, *Advanced oxidation processes for organic contaminant destruction based on the Fenton reaction and related chemistry.* Critical Reviews in Environmental Science and Technology, 2006. **36**(1): p. 1-84.

76. Ahumada, E., et al., *Catalytic oxidation of Fe(II) by activated carbon in the presence of oxygen. Effect of the surface oxidation degree on the catalytic activity.* Carbon, 2002. **40**(15): p. 2827-2834.

77. Ghosh, T., et al., *The characteristic study and sonocatalytic performance of CdSe-graphene as catalyst in the degradation of azo dyes in aqueous solution under dark conditions.* Ultrasonics Sonochemistry, 2013. **20**(2): p. 768-76.

78. Guo, J., et al., *Synthesis of Fe nanoparticles@graphene composites for environmental applications.* Journal of Hazardous Materials, 2012. **225**: p. 63-73.

79. Zhou, T., et al., *Oxidation of 4-chlorophenol in a heterogeneous zero valent iron/H2O2 Fenton-like system: Kinetic, pathway and effect factors.* Separation and

Purification Technology, 2008. **62**(3): p. 551-558.

80. de la Plata, G.B.O., O.M. Alfano, and A.E. Cassano, *Decomposition of 2-chlorophenol employing goethite as Fenton catalyst. I. Proposal of a feasible, combined reaction scheme of heterogeneous and homogeneous reactions.* Applied Catalysis B-Environmental, 2010. **95**(1-2): p. 1-13.

81. Zhang, S.X., et al., *Superparamagnetic Fe3O4 nanoparticles as catalysts for the catalytic oxidation of phenolic and aniline compounds.* Journal of Hazardous Materials, 2009. **167**(1-3): p. 560-566.

82. Costa, R.C.C., et al., *Highly active heterogeneous Fenton-like systems based on Fe-0/Fe3O4 composites prepared by controlled reduction of iron oxides.* Applied Catalysis B-Environmental, 2008. **83**(1-2): p. 131-139.

83. Xu, L.J. and J.L. Wang, *A heterogeneous Fenton-like system with nanoparticulate zero-valent iron for removal of 4-chloro-3-methyl phenol.* Journal of Hazardous Materials, 2011. **186**(1): p. 256-264.

84. Flox, C., et al., *Electro-Fenton and photoelectro-Fenton degradation of indigo carmine in acidic aqueous medium.* Applied Catalysis B-Environmental, 2006. **67**(1-2): p. 93-104.

85. Ting, W.P., M.C. Lu, and Y.H. Huang, *The reactor design and comparison of Fenton, electro-Fenton and photoelectro-Fenton processes for mineralization of benzene sulfonic acid (BSA).* Journal of Hazardous Materials, 2008. **156**(1-3): p. 421-427.

86. Melgoza, D., A. Hernandez-Ramirez, and J.M. Peralta-Hernandez, *Comparative efficiencies of the decolourisation of Methylene Blue using Fenton's and photo-Fenton's reactions.* Photochemical & Photobiological Sciences, 2009. **8**(5): p. 596-599.

87. Li, D., et al., *Accelerated photobleaching of Orange II on novel (H(5)FeW(12)O(40)10H(2)O)/silica structured fabrics.* Water Research, 2004. **38**(16): p. 3541-3550.

88. Gonzalez-Bahamon, L.F., et al., *Photo-Fenton degradation of resorcinol mediated*

by catalysts based on iron species supported on polymers. Journal of Photochemistry and Photobiology a-Chemistry, 2011. **217**(1): p. 201-206.

89. Hanna, K., T. Kone, and G. Medjahdi, *Synthesis of the mixed oxides of iron and quartz and their catalytic activities for the Fenton-like oxidation.* Catalysis Communications, 2008. **9**(5): p. 955-959.

90. Nishimura, T., et al., *Synthesis of metastable rare-earth-iron mixed oxide with the hexagonal crystal structure.* Journal of Solid State Chemistry, 2013. **197**: p. 402-407.

91. Guo, X.L., et al., *Preparation of decolorizing ceramsites for printing and dyeing wastewater with acid and base treated clay.* Applied Clay Science, 2008. **40**(1-4): p. 20-26.

92. Ramirez, J.H., et al., *Fenton-like oxidation of Orange II solutions using heterogeneous catalysts based on saponite clay.* Applied Catalysis B-Environmental, 2007. **71**(1-2): p. 44-56.

93. Becelic-Tomin, M.R., et al., *DEGRADATION OF INDUSTRIAL AZO DYE IN AQUEOUS SOLUTION BY HETEROGENEOUS FENTON PROCESS (FLY ASH/H2O2).* Hemijska Industrija, 2012. **66**(4): p. 485-494.

94. Bremner, D.H., et al., *Mineralisation of 2,4-dichlorophenoxyacetic acid by acoustic or hydrodynamic cavitation in conjunction with the advanced Fenton process.* Ultrasonics Sonochemistry, 2008. **15**(4): p. 416-419.

95. Ozdemir, C., et al., *Color Removal from Synthetic Textile Wastewater by Sono-Fenton Process.* Clean-Soil Air Water, 2011. **39**(1): p. 60-67.

96. Chen, B., et al., *Degradation of azo dye direct sky blue 5B by sonication combined with zero-valent iron.* Ultrasonics Sonochemistry, 2011. **18**(5): p. 1091-1096.

97. Do, S.H., Y.J. Kwon, and S.H. Kong, *Effect of metal oxides on the reactivity of persulfate/Fe(II) in the remediation of diesel-contaminated soil and sand.* Journal of Hazardous Materials, 2010. **182**(1-3): p. 933-936.

98. Yen, C.H., et al., *Application of persulfate to remediate petroleum*

hydrocarbon-contaminated soil: Feasibility and comparison with common oxidants. Journal of Hazardous Materials, 2011. **186**(2-3): p. 2097-2102.

99. Usman, M., et al., *Application of magnetite catalyzed chemical oxidation (Fenton-like and persulfate) for the remediation of oil hydrocarbon contamination.* Fuel, 2012. **96**(1): p. 270-276.

100. Osgerby, I.T., *ISCO technology overview: Do you really understand the chemistry?* Contaminated Soils, Sediments and Water Volume 10: Successes and Challenges, ed. E.J. Calabrese, P.T. Kostecki, and J. Dragun. 2006, New York: Springer. 287-308.

101. Huang, K.C., R.A. Couttenye, and G.E. Hoag, *Kinetics of heat-assisted persulfate oxidation of methyl tert-butyl ether (MTBE).* Chemosphere, 2002. **49**(4): p. 413-420.

102. Chan, K.H. and W. Chu, *Degradation of atrazine by cobalt-mediated activation of peroxymonosulfate: Different cobalt counteranions in homogenous process and cobalt oxide catalysts in photolytic heterogeneous process.* Water Research, 2009. **43**(9): p. 2513-2521.

103. Anipsitakis, G.P., D.D. Dionysiou, and M.A. Gonzalez, *Cobalt-mediated activation of peroxymonosulfate and sulfate radical attack on phenolic compounds. Implications of chloride ions.* Environmental Science & Technology, 2006. **40**(3): p. 1000-1007.

104. Ling, S.K., S.B. Wang, and Y.L. Peng, *Oxidative degradation of dyes in water using Co2+/H2O2 and Co2+/peroxymonosulfate.* Journal of Hazardous Materials, 2010. **178**(1-3): p. 385-389.

105. Bandala, E.R., et al., *Degradation of 2,4-dichlorophenoxyacetic acid (2,4-D) using cobalt-peroxymonosulfate in Fenton-like process.* Journal of Photochemistry and Photobiology a-Chemistry, 2007. **186**(2-3): p. 357-363.

106. Anipsitakis, G.P. and D.D. Dionysiou, *Transition metal/UV-based advanced oxidation technologies for water decontamination.* Applied Catalysis B-Environmental, 2004. **54**(3): p. 155-163.

107. Anipsitakis, G.P. and D.D. Dionysiou, *Radical generation by the interaction of transition metals with common oxidants.* Environmental Science & Technology, 2004. **38**(13): p. 3705-3712.

108. Anipsitakis, G.P. and D.D. Dionysiou, *Degradation of organic contaminants in water with sulfate radicals generated by the conjunction of peroxymonosulfate with cobalt.* Environmental Science & Technology, 2003. **37**(20): p. 4790-4797.

109. Anipsitakis, G.P. and D.D. Dionysiou, *Degradation of organic contaminants in water and wastewater with transition metal-catalyzed chemical oxidation.* Abstracts of Papers of the American Chemical Society, 2002. **223**: p. U529-U529.

110. Chen, X.Y., et al., *Performance of nano-Co3O4/peroxymonosulfate system: Kinetics and mechanism study using Acid Orange 7 as a model compound.* Applied Catalysis B-Environmental, 2008. **80**(1-2): p. 116-121.

111. Yang, Q.J., H. Choi, and D.D. Dionysiou, *Nanocrystalline cobalt oxide immobilized on titanium dioxide nanoparticles for the heterogeneous activation of peroxymonosulfate.* Applied Catalysis B-Environmental, 2007. **74**(1-2): p. 170-178.

112. Yang, Q.J., et al., *Heterogeneous activation of peroxymonosulfate by supported cobalt catalysts for the degradation of 2,4-dichlorophenol in water: The effect of support, cobalt precursor, and UV radiation.* Applied Catalysis B-Environmental, 2008. **77**(3-4): p. 300-307.

113. Shukla, P.R., et al., *Activated carbon supported cobalt catalysts for advanced oxidation of organic contaminants in aqueous solution.* Applied Catalysis B: Environmental, 2010. **100**(3–4): p. 529-534.

114. Fujishima, A., X.T. Zhang, and D.A. Tryk, *TiO2 photocatalysis and related surface phenomena.* Surface Science Reports, 2008. **63**(12): p. 515-582.

115. Hashimoto, K., H. Irie, and A. Fujishima, *TiO2 photocatalysis: A historical overview and future prospects.* Japanese Journal of Applied Physics Part 1-Regular Papers Brief Communications & Review Papers, 2005. **44**(12): p. 8269-8285.

116. Choi, D.Y., J.Y. Park, and J.W. Lee, *Adsorption and photocatalysis of spherical TiO2 particles prepared by hydrothermal reaction.* Materials Letters, 2012. **89**: p.212-215.

117. Adewuyi, Y.G., *Sonochemistry in environmental remediation. 1. Combinative and hybrid sonophotochemical oxidation processes for the treatment of pollutants inwater.* Environmental Science & Technology, 2005. **39**(10): p. 3409-3420.

118. Adewuyi, Y.G., *Sonochemistry in environmental remediation. 2. Heterogeneous sonophotocatalytic oxidation processes for the treatment of pollutants in water.* Environmental Science & Technology, 2005. **39**(22): p. 8557-8570.

119. Legrini, O., E. Oliveros, and A.M. Braun, *PHOTOCHEMICAL PROCESSES FOR WATER-TREATMENT.* Chemical Reviews, 1993. **93**(2): p. 671-698.

120. Jing, L.Q., et al., *Deactivation and regeneration of ZnO and TiO2 nanoparticles in the gas phase photocatalytic oxidation of n-C7H16 or SO2.* Applied Catalysis a-General, 2004. **275**(1-2): p. 49-54.

121. Chen, H.H., C.E. Nanayakkara, and V.H. Grassian, *Titanium Dioxide Photocatalysis in Atmospheric Chemistry.* Chemical Reviews, 2012. **112**(11): p. 5919-5948.

122. Hoffmann, M.R., et al., *ENVIRONMENTAL APPLICATIONS OF SEMICONDUCTOR PHOTOCATALYSIS.* Chemical Reviews, 1995. **95**(1): p. 69-96.

123. Sakthivel, S., et al., *Photocatalytic degradation of leather dye over ZnO catalyst supported on alumina and glass surfaces.* Water Science and Technology, 2001. **44**(5): p. 211-218.

124. Bhatkhande, D.S., V.G. Pangarkar, and A. Beenackers, *Photocatalytic degradation for environmental applications - a review.* Journal of Chemical Technology and Biotechnology, 2002. **77**(1): p. 102-116.

125. Chakrabarti, S., et al., *Degradation mechanism and kinetic model for photocatalytic oxidation of PVC-ZnO composite film in presence of a sensitizing dye and UV radiation.* Journal of Hazardous Materials, 2008. **154**(1-3): p. 230-236.

126. Behnajady, M.A., N. Modirshahla, and R. Hamzavi, *Kinetic study on photocatalytic degradation of CI Acid Yellow 23 by ZnO photocatalyst.* Journal of Hazardous Materials, 2006. **133**(1-3): p. 226-232.

127. Furube, A., et al., *Direct observation of a picosecond charge separation process in photoexcited platinum-loaded TiO2 particles by femtosecond diffuse reflectance spectroscopy.* Chemical Physics Letters, 2001. **336**(5-6): p. 424-430.

128. Konstantinou, I.K. and T.A. Albanis, *TiO2-assisted photocatalytic degradation of azo dyes in aqueous solution: kinetic and mechanistic investigations - A review.* Applied Catalysis B-Environmental, 2004. **49**(1): p. 1-14.

129. Martin, S.T., A.T. Lee, and M.R. Hoffmann, *CHEMICAL MECHANISM OF INORGANIC OXIDANTS IN THE TIO2/UV PROCESS - INCREASED RATES OF DEGRADATION OF CHLORINATED HYDROCARBONS.* Environmental Science & Technology, 1995. **29**(10): p. 2567-2573.

130. Doong, R.A. and W.H. Chang, *Photoassisted titanium dioxide mediated degradation of organophosphorus pesticides by hydrogen peroxide.* Journal of Photochemistry and Photobiology a-Chemistry, 1997. **107**(1-3): p. 239-244.

131. Elmolla, E.S. and M. Chaudhuri, *Photocatalytic degradation of amoxicillin, ampicillin and cloxacillin antibiotics in aqueous solution using UV/TiO(2) and UV/H(2)O(2)/TiO(2) photocatalysis.* Desalination, 2010. **252**(1-3): p. 46-52.

132. Malato, S., et al., *Optimising solar photocatalytic mineralisation of pesticides by adding inorganic oxidising species; application to the recycling of pesticide containers.* Applied Catalysis B-Environmental, 2000. **28**(3-4): p. 163-174.

133. Do, S.H., et al., *Application of a peroxymonosulfate/cobalt (PMS/Co(II)) system to treat diesel-contaminated soil.* Chemosphere, 2009. **77**(8): p. 1127-1131.

134. Chong, M.N., et al., *Recent developments in photocatalytic water treatment technology: A review.* Water Research, 2010. **44**(10): p. 2997-3027.

135. Neppolian, B., H. Jung, and H. Choi, *Photocatalytic degradation of 4-chlorophenol using TiO2 and Pt-TiO2 nanoparticles prepared by sol-gel method.* Journal of Advanced Oxidation Technologies, 2007. **10**(2): p. 369-374.

136. Comparelli, R., et al., *UV-induced photocatalytic degradation of azo dyes by organic-capped ZnO nanocrystals immobilized onto substrates.* Applied Catalysis B-Environmental, 2005. **60**(1-2): p. 1-11.

137. Serpone, N., et al., *EXPLOITING THE INTERPARTICLE ELECTRON-TRANSFER PROCESS IN THE PHOTOCATALYZED OXIDATION OF PHENOL, 2-CHLOROPHENOL AND PENTACHLOROPHENOL - CHEMICAL EVIDENCE FOR ELECTRON AND HOLE TRANSFER BETWEEN COUPLED SEMICONDUCTORS.* Journal of Photochemistry and Photobiology a-Chemistry, 1995. **85**(3): p. 247-255.

138. Beydoun, D., et al., *Role of nanoparticles in photocatalysis.* Journal of Nanoparticle Research, 1999. **1**(4): p. 439-458.

139. Choi, W.Y., A. Termin, and M.R. Hoffmann, *THE ROLE OF METAL-ION DOPANTS IN QUANTUM-SIZED TIO2 - CORRELATION BETWEEN PHOTOREACTIVITY AND CHARGE-CARRIER RECOMBINATION DYNAMICS.* Journal of Physical Chemistry, 1994. **98**(51): p. 13669-13679.

140. Anipsitakis, G.P., E. Stathatos, and D.D. Dionysiou, *Heterogeneous activation of oxone using Co3O4.* Journal of Physical Chemistry B, 2005. **109**(27): p. 13052-13055.

141. Li, B.Y., et al., *Synthesis and Characterization of Fe-N-S-tri-Doped TiO2 Photocatalyst and Its Enhanced Visible Light Photocatalytic Activity.* Advances in Materials Science and Engineering, 2012.

142. Salvetat-Delmotte, J.P. and A. Rubio, *Mechanical properties of carbon nanotubes: a fiber digest for beginners.* Carbon, 2002. **40**(10): p. 1729-1734.

143. Saito, T., K. Matsushige, and K. Tanaka, *Chemical treatment and modification of multi-walled carbon nanotubes.* Physica B-Condensed Matter, 2002. **323**(1-4): p. 280-283.

144. Matos, J., J. Laine, and J.M. Herrmann, *Effect of the type of activated carbons on the photocatalytic degradation of aqueous organic pollutants by UV-irradiated titania.* Journal of Catalysis, 2001. **200**(1): p. 10-20.

145. Melechko, A.V., et al., *Control of carbon nanostructure: From nanofiber toward nanotube and back.* Journal of Applied Physics, 2007. **102**(7).

146. Chen, L.C., et al., *Enhanced visible light-induced photoelectrocatalytic degradation of phenol by carbon nanotube-doped TiO2 electrodes.* Electrochimica Acta, 2009. **54**(15): p. 3884-3891.

147. Lin, X.X., et al., *Carbon-doped mesoporous TiO2 film and its photocatalytic activity.* Microporous and Mesoporous Materials, 2011. **142**(1): p. 276-281.

148. Chen, M.L., F.J. Zhang, and W.C. Oh, *Synthesis, characterization, and photocatalytic analysis of CNT/TiO2 composites derived from MWCNTs and titanium sources.* New Carbon Materials, 2009. **24**(2): p. 159-166.

149. O´scik, J., *Adsorption.* Ellis Horwood, Chichester, PWN, Warsaw, 1982.

150. Zhang, K., et al., *Comparison of catalytic activities for photocatalytic and sonocatalytic degradation of methylene blue in present of anatase TiO2-CNT catalysts.* Ultrasonics Sonochemistry, 2011. **18**(3): p. 765-772.

151. Kim, S.R., M.K. Parvez, and M. Chhowalla, *UV-reduction of graphene oxide and its application as an interfacial layer to reduce the back-transport reactions in dye-sensitized solar cells.* Chemical Physics Letters, 2009. **483**(1-3): p. 124-127.

152. Yoo, D.H., et al., *Enhanced photocatalytic activity of graphene oxide decorated on TiO2 films under UV and visible irradiation.* Current Applied Physics, 2011. **11**(3): p. 805-808.

153. Nguyen-Phan, T.D., et al., *The role of graphene oxide content on the adsorption-enhanced photocatalysis of titanium dioxide/graphene oxide composites.* Chemical Engineering Journal, 2011. **170**(1): p. 226-232.

154. Guo, J.J., et al., *Sonochemical synthesis of TiO2 nanoparticles on graphene for use as photocatalyst.* Ultrasonics Sonochemistry, 2011. **18**(5): p. 1082-1090.

155. Li, H.Y., et al., *Synthesis of highly efficient C-doped TiO2 photocatalyst and its photo-generated charge-transfer properties.* Journal of Colloid and Interface Science, 2011. **354**(1): p. 175-180.

156. Wu, Y.M., et al., *Properties of carbon and iron modified TiO2 photocatalyst synthesized at low temperature and photodegradation of acid orange 7 under visible light.* Applied Surface Science, 2010. **256**(13): p. 4260-4268.

157. Park, Y., et al., *Carbon-doped TiO2 photocatalyst synthesized without using an external carbon precursor and the visible light activity.* Applied Catalysis B-Environmental, 2009. **91**(1-2): p. 355-361.

158. Ren, W.J., et al., *Low temperature preparation and visible light photocatalytic activity of mesoporous carbon-doped crystalline TiO2.* Applied Catalysis B-Environmental, 2007. **69**(3-4): p. 138-144.

159. Gogate, P.R. and A.B. Pandit, *A review of imperative technologies for wastewater treatment I: oxidation technologies at ambient conditions.* Advances in Environmental Research, 2004. **8**(3-4): p. 501-551.

160. Beltrtan, F.J., *Ozone Reaction Kinetics for Water and Waste Water Systems.* Lewis Publishers, CRC Press, Boca Raton, Florida, USA, 2003.

161. Arslan, I. and I.A. Balcioglu, *Degradation of Remazol Black B dye and its simulated dyebath wastewater by advanced oxidation processes in heterogeneous and homogeneous media.* Coloration Technology, 2001. **117**(1): p. 38-42.

162. Glaze, W.H. and J.W. Kang, *ADVANCED OXIDATION PROCESSES - DESCRIPTION OF A KINETIC-MODEL FOR THE OXIDATION OF HAZARDOUS MATERIALS IN AQUEOUS-MEDIA WITH OZONE AND HYDROGEN-PEROXIDE IN A SEMIBATCH REACTOR.* Industrial & Engineering Chemistry Research, 1989. **28**(11): p. 1573-1580.

163. Buxton, G.V., et al., *CRITICAL-REVIEW OF RATE CONSTANTS FOR REACTIONS OF HYDRATED ELECTRONS, HYDROGEN-ATOMS AND HYDROXYL RADICALS (.OH/.O-) IN AQUEOUS-SOLUTION.* Journal of Physical and Chemical Reference Data, 1988. **17**(2): p. 513-886.

164. Toor, R. and M. Mohseni, *UV-H2O2 based AOP and its integration with biological activated carbon treatment for DBP reduction in drinking water.* Chemosphere, 2007. **66**(11): p. 2087-2095.

165. Prousek, J., *Advanced oxidation processes for water treatment. Photochemical processes.* Chemicke Listy, 1996. **90**(5): p. 307-315.

166. Glaze, W.H., J.W. Kang, and D.H. Chapin, *THE CHEMISTRY OF WATER-TREATMENT PROCESSES INVOLVING OZONE, HYDROGEN-PEROXIDE AND ULTRAVIOLET-RADIATION.* Ozone-Science & Engineering, 1987. **9**(4): p. 335-352.

167. Peyton, G.R. and W.H. Glaze, *DESTRUCTION OF POLLUTANTS IN WATER WITH OZONE IN COMBINATION WITH ULTRAVIOLET-RADIATION .3. PHOTOLYSIS OF AQUEOUS OZONE.* Environmental Science & Technology, 1988. **22**(7): p. 761-767.

168. Mokrini, A., D. Ousse, and E. Esplugas, *Oxidation of aromatic compounds with UV radiation/ozone/hydrogen peroxide.* Water Science and Technology, 1997. **35**(4): p. 95-102.

169. Kidak, R. and N.H. Ince, *Catalysis of advanced oxidation reactions by ultrasound: A case study with phenol.* Journal of Hazardous Materials, 2007. **146**(3): p. 630-635.

170. Drijvers, D., H. van Langenhove, and M. Beckers, *Decomposition of phenol and trichloroethylene by the ultrasound/H2O2/CuO process.* Water Research, 1999. **33**(5): p. 1187-1194.

171. Entezari, M.H., C. Petrier, and P. Devidal, *Sonochemical degradation of phenol in water: a comparison of classical equipment with a new cylindrical reactor.* Ultrasonics Sonochemistry, 2003. **10**(2): p. 103-108.

172. Primo, O., et al., *Mathematical modelling of phenol photooxidation: Kinetics of the process toxicity.* Chemical Engineering Journal, 2007. **134**(1-3): p. 23-28.

173. Chen, Y.C. and P. Smirniotis, *Enhancement of photocatalytic degradation of phenol and chlorophenols by ultrasound.* Industrial & Engineering Chemistry Research, 2002. **41**(24): p. 5958-5965.

174. Tezcanli-Guyer, G. and N.H. Ince, *Individual and combined effects of ultrasound, ozone and UV irradiation: a case study with textile dyes.* Ultrasonics, 2004.

42(1-9): p. 603-609.

175. Fung, P.C., K.M. Sin, and S.M. Tsui, *Decolorisation and degradation kinetics of reactive dye wastewater by a UV/ultrasonic/peroxide system.* Journal of the Society of Dyers and Colourists, 2000. **116**(5-6): p. 170-173.

176. An, T.C., et al., *Decolourization and COD removal from reactive dye-containing wastewater using sonophotocatalytic technology.* Journal of Chemical Technology and Biotechnology, 2003. **78**(11): p. 1142-1148.

177. Kudo, A., *Photocatalyst materials for water splitting.* Catalysis Surveys from Asia, 2003. **7**(1): p. 31-38.

178. Kudo, A. and Y. Miseki, *Heterogeneous photocatalyst materials for water splitting.* Chemical Society Reviews, 2009. **38**(1): p. 253-278.

179. Kudo, A., *Development of photocatalyst materials for water splitting.* International Journal of Hydrogen Energy, 2006. **31**(2): p. 197-202.

180. Cui, L.F., et al., *Synthesis and visible light photocatalysis of Fe-doped TiO2 mesoporous layers deposited on hollow glass microbeads.* Journal of Solid State Chemistry, 2009. **182**(10): p. 2785-2790.

181. Morikawa, T., et al., *Visible-light-induced photocatalytic oxidation of carboxylic acids and aldehydes over N-doped TiO2 loaded with Fe, Cu or Pt.* Applied Catalysis B-Environmental, 2008. **83**(1-2): p. 56-62.

182. Iliev, V., et al., *Photocatalytic properties of TiO2 modified with platinum and silver nanoparticles in the degradation of oxalic acid in aqueous solution.* Applied Catalysis B-Environmental, 2006. **63**(3-4): p. 266-271.

183. Srinivasan, S.S., et al., *Synergistic effects of sulfation and co-doping on the visible light photocatalysis of TiO2.* Journal of Alloys and Compounds, 2006. **424**(1-2): p. 322-326.

184. Zhang, W., L.D. Zou, and L.Z. Wang, *A novel charge-driven self-assembly method to prepare visible-light sensitive TiO2/activatecl carbon composites for dissolved organic compound removal.* Chemical Engineering Journal, 2011. **168**(1): p. 485-492.

185. Yu, Y.H. and M. Xia, *Preparation and characterization of ZnTiO3 powders by sol-gel process.* Materials Letters, 2012. **77**: p. 10-12.

186. Pal, J. and P. Chauhan, *Study of physical properties of cobalt oxide (Co3O4) nanocrystals.* Materials Characterization, 2010. **61**(5): p. 575-579.

187. Wei, W., Y. Dai, and B.B. Huang, *First-Principles Characterization of Bi-based Photocatalysts: Bi12TiO20, Bi2Ti2O7, and Bi4Ti3O12.* Journal of Physical Chemistry C, 2009. **113**(14): p. 5658-5663.

188. Lu, X.F., Q.L. Wang, and D.L. Cui, *Preparation and Photocatalytic Properties of g-C3N4/TiO2 Hybrid Composite.* Journal of Materials Science & Technology, 2010. **26**(10): p. 925-930.

189. Sun, H.Q., et al., *Preparation of cobalt/carbon-xerogel for heterogeneous oxidation of phenol.* Catalysis Today, 2012. **186**(1): p. 63-68.

190. Wang, Q., et al., *Removal of cobalt from aqueous solution by magnetic multiwalled carbon nanotube/iron oxide composites.* Chemical Engineering Journal, 2011. **174**(1): p. 126-133.

191. Mi, Y.Z., et al., *Synthesis of carbon micro-spheres by a glucose hydrothermal method.* Materials Letters, 2008. **62**(8-9): p. 1194-1196.

192. Sevilla, M. and A.B. Fuertes, *Chemical and Structural Properties of Carbonaceous Products Obtained by Hydrothermal Carbonization of Saccharides.* Chemistry-a European Journal, 2009. **15**(16): p. 4195-4203.

193. Sun, X.M. and Y.D. Li, *Colloidal carbon spheres and their core/shell structures with noble-metal nanoparticles.* Angewandte Chemie-International Edition, 2004. **43**(5): p. 597-601.

3

Chapter 3: Titanate supported cobalt catalysts for photochemical oxidation of phenol under visible light irradiations

Abstract

Three metal titanates, $ZnTiO_3$ (Zn), $FeTiO_3$ (Fe) and $Bi_4Ti_3O_{12}$ (Bi), were employed to prepare supported cobalt catalysts for photocatalytic and photochemical oxidation of phenol with peroxymonosulfate (PMS) or peroxydisulfate (PDS) under visible light irradiations. It was found that the oxidation efficiencies varied greatly due to the different photochemical behaviours of various supports. Using PMS, both Co(5%)/Zn and Co(3%)/Bi achieved complete degradation of phenol in 120 min, as compared to 66.9% of phenol removal over Co(5%)/Fe in 150 min. However, those catalysts were found to be not efficient in activation of PDS, in which the best catalyst, Co(5%)/Bi, only provided 66.9% of phenol degradation in 150 min. The effects of the supports were from the varying photophysical properties and their interactions with loaded Co_3O_4. The stability of Co(5%)/Zn with PMS was further investigated and it was found that the activity remained at 85.4% phenol degradation in the fourth run.

3.1. Introduction

Recently, advanced oxidation processes (AOPs) have been proposed to be an effective strategy for waste water treatment. Compared with conventional methods such as adsorption, filtration, and membrane separation, which mostly transfer the pollution from one phase (liquid) to another (solid), however, AOPs manage to completely destroy organic

molecules to CO_2 and H_2O [1]. That would become more promising when treating high toxic pollutants such as phenol and chlorophenols, which are comparatively more refractory to natural degradation. Therefore, much attention has been paid to AOPs in both academia and industry [2-4].

In general, the active radicals, which are used to attack C-C and C-H bonds in organics, would be produced by external drivers such as ozone (ozonolysis), UV irradiations (photolysis/photocatalysis), and chemical oxidants, etc. Ozonolysis and photolysis, despite of high efficiency, require high energy and critical operation conditions, failing to treat refractory compounds [5]. Photocatalysis has shown its effective and non-selective decomposition to many kinds of pollutants; however, it is still suffering from lower quantum efficiency, especially in visible light region [6-8]. The addition of oxidants can be alternative to UV irradiations to provide extra active radicals. For instance, Fenton (Fe^{2+}/H_2O_2) and Fenton-like (Fe^{3+}/H_2O_2) reactions could provide powerful hydroxyl radicals for complete oxidation of organics. However, such homogeneous process is limited by the acidic requirement (pH 2–4), high amount of sludge in the coagulation and loss of Fe ions [9].

More recently, sulfate radicals have been suggested to be a substitution to the hydroxyl radicals for overcoming the limitation of Fenton reaction [10, 11]. The sulfate radicals can be generated by the activation of sulfate-based oxidants (PMS, $2KHSO_5 \cdot KHSO_4 \cdot K_2SO_4$ and PDS, $K_2S_2O_8$) using heat, UV radiation and/or transition metal ions, such as cobalt, iron, and silver. Homogeneous reactions using Co ions to activate PMS were proven to be of high efficiency for oxidation of organic compounds. But, the loss of cobalt from homogeneous processes leads to a priority of metal pollutant, which may cause several health problems such as asthma, pneumonia and other lung problems [12]. Many

investigations have been made on developing heterogeneous oxidation systems as a commercially feasible trial. Yang et al. [13] reported that Co_3O_4 immobilized on TiO_2 (Degussa P25) would show a higher activity and stability in oxidation of 2,4-dichlorophenol. The effects of supports, Al_2O_3, SiO_2 and TiO_2, on the activity of supported Co were investigated, and they found that cobalt-support interaction would play a significant role in determining the activity, stability, and photochemical behaviour of the supported Co samples [14]. More recently, Zhang et al. [15] reported that MgO supported Co could serve as an efficient catalyst for activation of PMS to oxidize organic dyes. By combining adsorption and oxidation, Co loaded onto an activated carbon showed enhanced phenol removal and high reusability in heterogeneous reactions [16]. Cobalt exchanged zeolites (ZSM-5, zeolite-A, and zeolite-X) were also prepared and tested for the heterogeneous oxidation of phenol by activation of PMS [5].

It was known that UV would further enhance the efficiency of Co/PMS system [6, 14, 17], therefore, it is of an interest to investigate loading Co onto photo-responsive materials which may induce synergistic effects under UV or visible light irradiation. Titanate, such as $ZnTiO_3$, $FeTiO_3$, and $Bi_4Ti_3O_{12}$, have been proposed as photocatalysts, luminescent, lasing materials, solar cells, dielectrics, microwave, and gas sensors [18-20]. In this chapter, three titanate materials were employed as Co supports, and their performances in photooxidation of phenol by activation of PMS or PDS under visible light were investigated.

3.2. Experimental

3.2.1. Materials

Powdered zinc titanate ($ZnTiO_3$), iron (II) titanate ($FeTiO_3$), and bismuth (III) titanate

($Bi_4Ti_3O_{12}$), were purchased from Sigma-Aldrich and used as supports. Cobalt (II) nitrate hexahydrate ($Co(NO_3)_2•6H_2O$) from Sigma was used as a Co precursor. Peroxymonosulfate (PMS) and peroxydisulfate (PDS) obtained from Aldrich were used as oxidants. Pure methanol was used as a quenching reagent to stop the reaction in the sample bottles before high performance liquid chromatography (HPLC) analysis. Phenol from Aldrich was used to prepare model pollutant solutions.

3.2.2. Preparation of titanate supported cobalt catalysts

Supported cobalt samples were prepared by a wet impregnation method [16]. In a typical process, a fixed amount of titanates ($ZnTiO_3$, $FeTiO_3$ and $Bi_4Ti_3O_{12}$) was added into cobalt nitrate solution and the obtained suspension was stirred for 24 h, and then evaporated whilst stirring at 50 ^oC. The precipitate was recovered and calcined in air at 500 ^oC for 6 h with a heating rate of 2.5^oC/min. The obtained powders were ground thoroughly and labelled as Co(X%)/Zn, Co(X%)/Fe, or Co(X%)/Bi, where X% represents cobalt weight loading on $ZnTiO_3$, $FeTiO_3$ and $Bi_4Ti_3O_{12}$. In this study, the X values were set at 1, 3, and 5, respectively.

3.2.3. Characterization of catalysts

The crystalline structure of various samples was analyzed using powder X-ray diffraction (XRD). The spectra were obtained on a Bruker D8-Advance X-ray diffractometer with Cu Kα radiation (λ = 1.5418 Å), at accelerating voltage and current of 40 kV and 40 mA, respectively. UV-visible diffuse reflectance spectroscopy (DRS) was recorded on a Jasco V-570 equipped with an integrating sphere, in which $BaSO_4$ was used as a reference material. Scanning electron microscopy (SEM), performed on a Zeiss Neon 40EsB FIBSEM, was used to evaluate the morphology, size and textural information of the

samples. The integrated EDS and elemental mapping (cobalt) were applied to analyze the dispersion of cobalt in the samples.

3.2.4. Photochemical oxidation of phenol

The aqueous oxidation of phenol was carried out in a 1-L of Pyrex double-jacket reactor. A water bath connected with a pump was used to maintain the reaction temperature at 30 ± 0.5 ^{o}C, and a magnetic stirrer was used to maintain the catalyst or oxidant dispersed uniformly in reaction solutions. At a typical run, 0.1 g of catalyst (0.5 g/L) was added into 200 mL of 25 ppm phenol solution, and 30 min later, 0.4 g of PDS or PMS (2 g/L) was added into the stirred solution. The light irradiation was immediately switched on after the addition of the oxidants. The irradiations were supplied by a MSR 575/2 metal halide lamp (575 W, Philips). A UV Lee filter was equipped with the lamp to block UV radiation under 380 nm. The UV intensity ($315 < \lambda < 400$ nm) was measured to be 60 $\mu W/cm^2$, and the visible light intensity ($\lambda > 400$ nm) was 84 mW/cm^2. At set time intervals, 1 mL solution was withdrawn by a syringe and filtered by 0.25 μm Millipore film into HPLC vials which were filled with 0.5 mL of methanol to quench the oxidation reactions. The concentration of phenol was analyzed using a Varian HPLC with a UV detector set at $\lambda = 270$ nm. A C–18 column was used to separate the organics while the mobile phase of 30% CH_3CN and 70% water was flowing through the column at a flowrate of 1.5 mL/min.

Reusability of a catalyst was investigated by monitoring the phenol degradation at certain time using recovered Co(5%)/Zn in different runs. After each run, the catalyst was collected by filtration, rinsed with plenty of ultra-pure water, and then dried at 80 ^{o}C in an oven overnight. The reaction volume and the oxidant amount were decreased according to actual catalyst amount collected.

3.3. Results and discussion

3.3.1. Characterization of supported Co samples

Fig. 3.1 shows XRD patterns of the supports and supported Co catalysts. Fig. 3.1 (A) indicates that the support of $ZnTiO_3$ was of hexagonal structure, and the peaks assigned to rutile TiO_2 were also observed. [21] For the supported sample (curve b), no significant change was found, suggesting no cobalt oxide detectable in XRD profiles. This is possibly due to lower percentage of 5 wt%, and good dispersion of fine Co_3O_4 crystallites. Yang et al. [13] observed XRD peaks of Co_3O_4 and $CoTiO_3$ in TiO_2 supported Co samples, but in their case, Co/Ti was above 0.1. In previous studies, Co_2O_3 peaks were found in Co/activated-carbon samples [16], however, no cobalt oxides were found in cobalt exchanged zeolite samples [5]. Zhang et al. [15] reported that the XRD peaks of Co_3O_4 (5 wt%, same as the present study) were found in the samples of Co/Al_2O_3, Co/SBA-15, and Co/ZnO, but could not be observed in Co/TiO_2-P25, Co/ZrO, and Co/MgO. Fig. 3.1 (B) shows a clear difference between support of $FeTiO_3$ and Co(5%)/Fe. The support of $FeTiO_3$ suggests an ilmenite crystal structure, with the impurity of rutile TiO_2 phase. After loading of Co, the crystal phase was transformed to be $Fe_2Ti_3O_9$, named as H239 [19]. Similar to Co(5%)/Zn, no cobalt oxide signals were found in the XRD pattern of Co(5%)/Fe. No phase transition was found in Co(5%)/Bi, as shown in Fig. 3.1 (C), and neither the peaks of cobalt oxide were found.

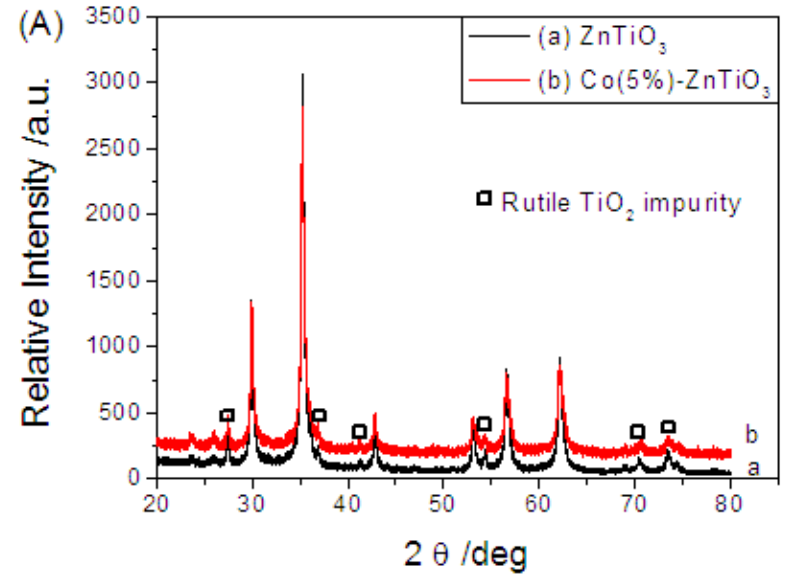
(A)
Relative Intensity /a.u.
3500
3000
2500
2000
1500
1000
500
0
20
30
40
50
60
70
80
2 θ /deg
(a) ZnTiO3
(b) Co(5%)-ZnTiO3
Rutile TiO2 impurity
b
a

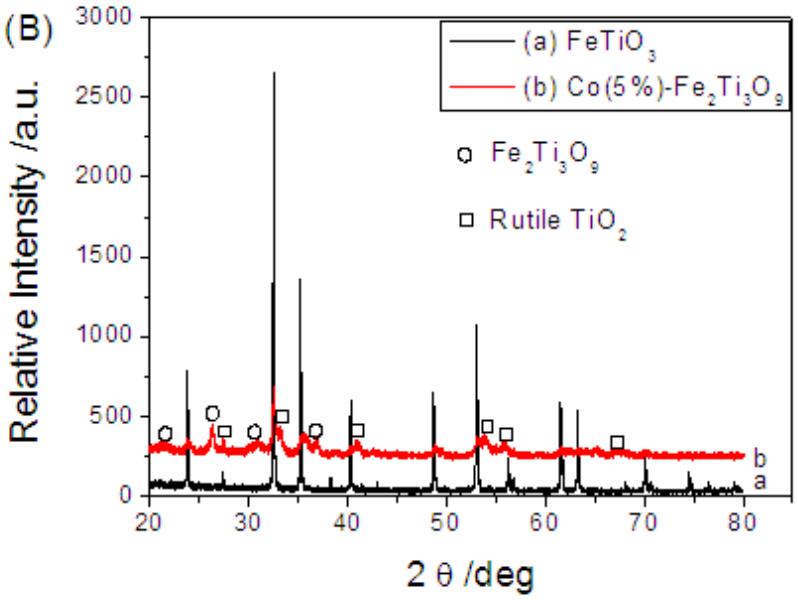
(B)
Relative Intensity /a.u.
3000
2500
2000
1500
1000
500
0
20
30
40
50
60
70
80
2 θ /deg
(a) FeTiO3
(b) Co(5%)-Fe2Ti3O9
Fe2Ti3O9
Rutile TiO2
b
a

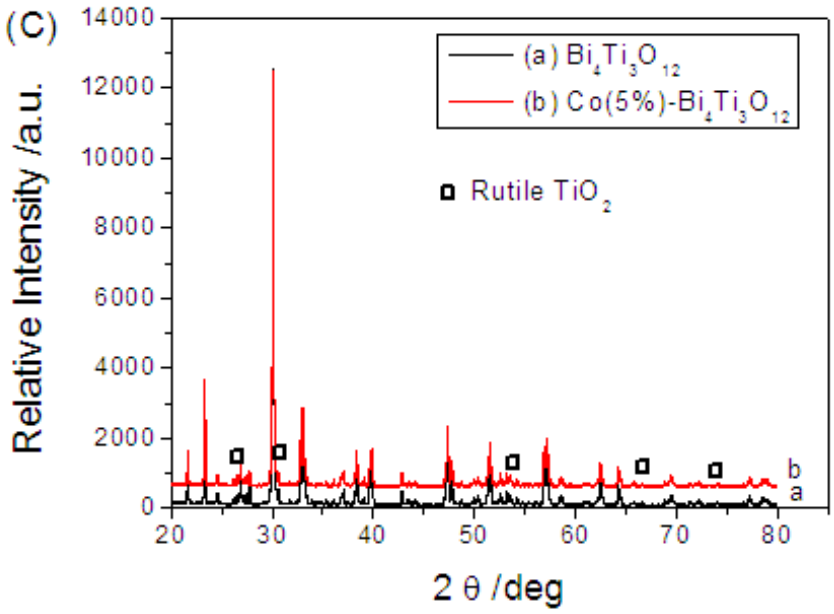

Figure 3.1 XRD patterns of titanates and the supported samples

Fig. 3.2 displays the optical properties of various supports and their supported samples. Fig. 3.2 (A) indicates that $ZnTiO_3$ has an absorption threshold of 418 nm. Loading of Co would result in a significant red-shift. With increasing the Co loading from 1 to 3 wt%, the absorption edge would be extended from 508.2 to 708.6 nm. Further increase in the Co loading to 5 wt%, two extra peaks were found at 449 and 737 nm, which were assigned to the signals of Co_3O_4 [22]. The former peak was attributed to the $O^{2-} \rightarrow Co^{2+}$ charge transfer process, and the latter one was arose from $O^{2-} \rightarrow Co^{3+}$ charge transfer process [22]. The band gap energies of the materials can be estimated by the following equation.

$$(\alpha h\nu)^n = B(h\nu - Eg) \quad (3\text{-}1)$$

Where $h\nu$ is the photon energy, α is the absorption coefficient which can be obtained from the scattering and reflectance spectra according to the Kubelka-Munk theory, B is a constant relative to the material and n is a value that depends on the nature of transition: 2 for a direct allowed transition, 3/2 for direct forbidden transition, and 1/2 for indirect

allowed transition. The $(\alpha h\nu)^n$ (n = 1/2) versus $h\nu$ extrapolated to α = 0 represents the absorption band gap energy [18]. Fig. 3.2(B) shows the estimations of the band gap energies of $ZnTiO_3$ and supported catalysts. It was found that pure $ZnTiO_3$ possesses a band gap of 2.96 eV and with increased Co, the band gap energies decreased to be 2.44, 1.75 and 1.42 eV at 1, 3 and 5% loading of Co, respectively. Fig. 3.3(C) also shows two peaks at 449 and 737 nm in Co modified $FeTiO_3$, suggesting the presence of Co_3O_4. The band gap of $FeTiO_3$ was reported to be 2.58 – 2.90 eV, however, no characteristic peak was observed, due to the intervalence charge transfer between Fe^{2+} and Ti^{4+} ($Fe^{2+} + Ti^{4+} \rightarrow Fe^{3+} + Ti^{3+}$) in $FeTiO_3$ [23]. It is noteworthy that the optical difference from Co loading was also partly due to the crystal phase transition from ilmenite to H239. Fig. 3.2(D) shows the absorption spectra of $Bi_4Ti_3O_{12}$ and its supported Co catalyst. With the estimation by Eq. (1) at n = 2, the band gap energy of $Bi_4Ti_3O_{12}$ was determined to be 3.27 eV, which was very close to the value reported by Pintilie et al. [24] After loading 5 wt% Co onto the support, the band gap energy would decrease to 3.08 eV. Moreover, similar to $ZnTiO_3$ and $FeTiO_3$, the characteristic peaks of Co_3O_4 were observed.

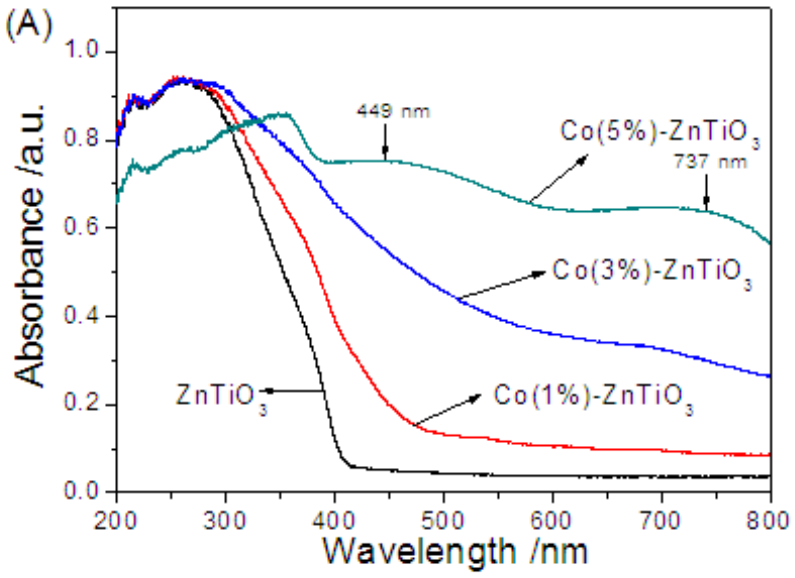

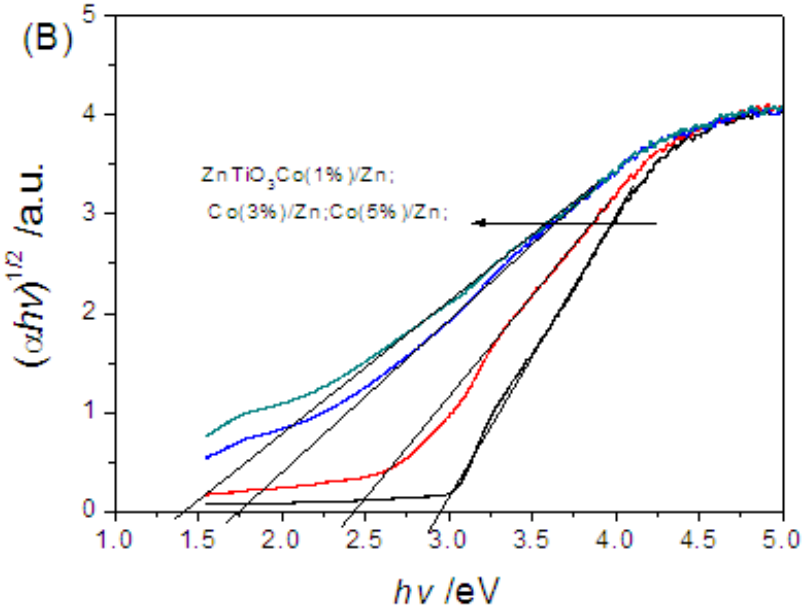
(B)
ZnTiO3Co(1%)/Zn;
Co(3%)/Zn;Co(5%)/Zn;
(αhν)^1/2 /a.u.
hν /eV
0
1
2
3
4
5
1.0
1.5
2.0
2.5
3.0
3.5
4.0
4.5
5.0

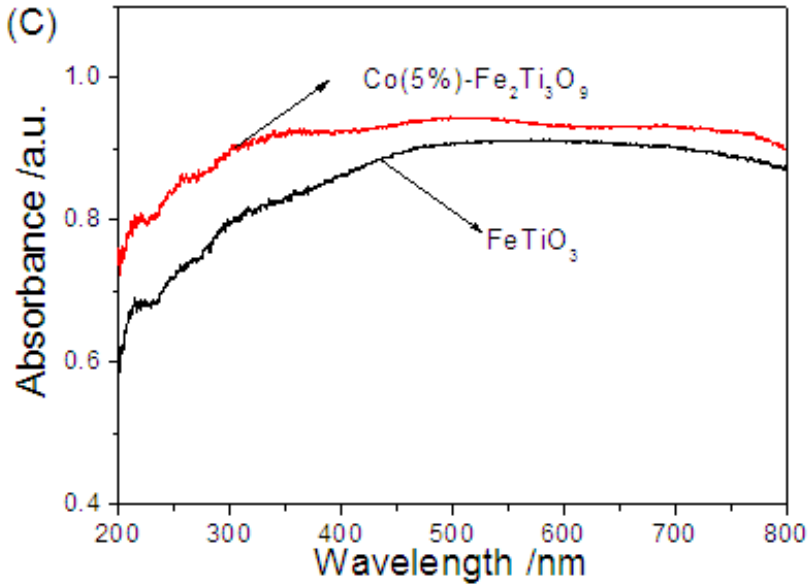
(C)
Co(5%)-Fe2Ti3O9
FeTiO3
Absorbance /a.u.
Wavelength /nm
0.4
0.6
0.8
1.0
200
300
400
500
600
700
800

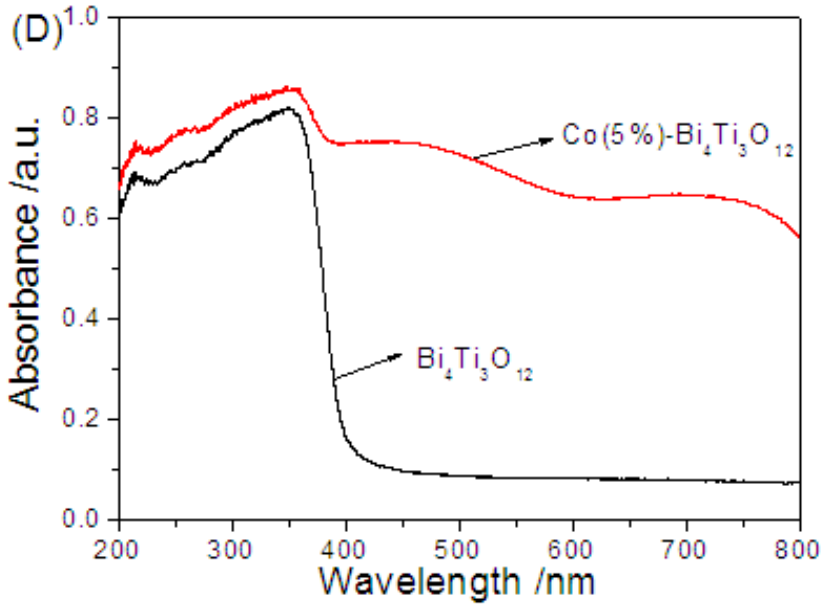

Figure 3.2 UV-visible diffuse reflectance absorption spectra of supports and supported catalysts

Fig. 3.3 presents the SEM images, EDS and Co mapping of the supported Co catalysts. The left of Fig. 3.3(A) shows the SEM image of Co(5%)/Zn, which was aggregation of fine particles < 100 nm. The right part shows the EDS results. Carbon was from the contamination, Zn and Ti from the support, O from both supports and Co_3O_4, Pt from coating, and Co from the supported Co_3O_4. To further confirm the distribution of Co, elemental mapping was conducted, as shown in the insert, and that suggests a good dispersion of Co in the prepared catalyst samples. The particle size of $FeTiO_3$ was larger (Fig. 3.2(B)) at about several microns. From the EDS and Co mapping, it was confirmed the good dispersion of Co in the samples. From Fig. 3.3(C), larger particle size was also found in Co(5%)/Bi. The results suggested that Co_3O_4 would be uniformly dispersed on the surfaces of the three supports.

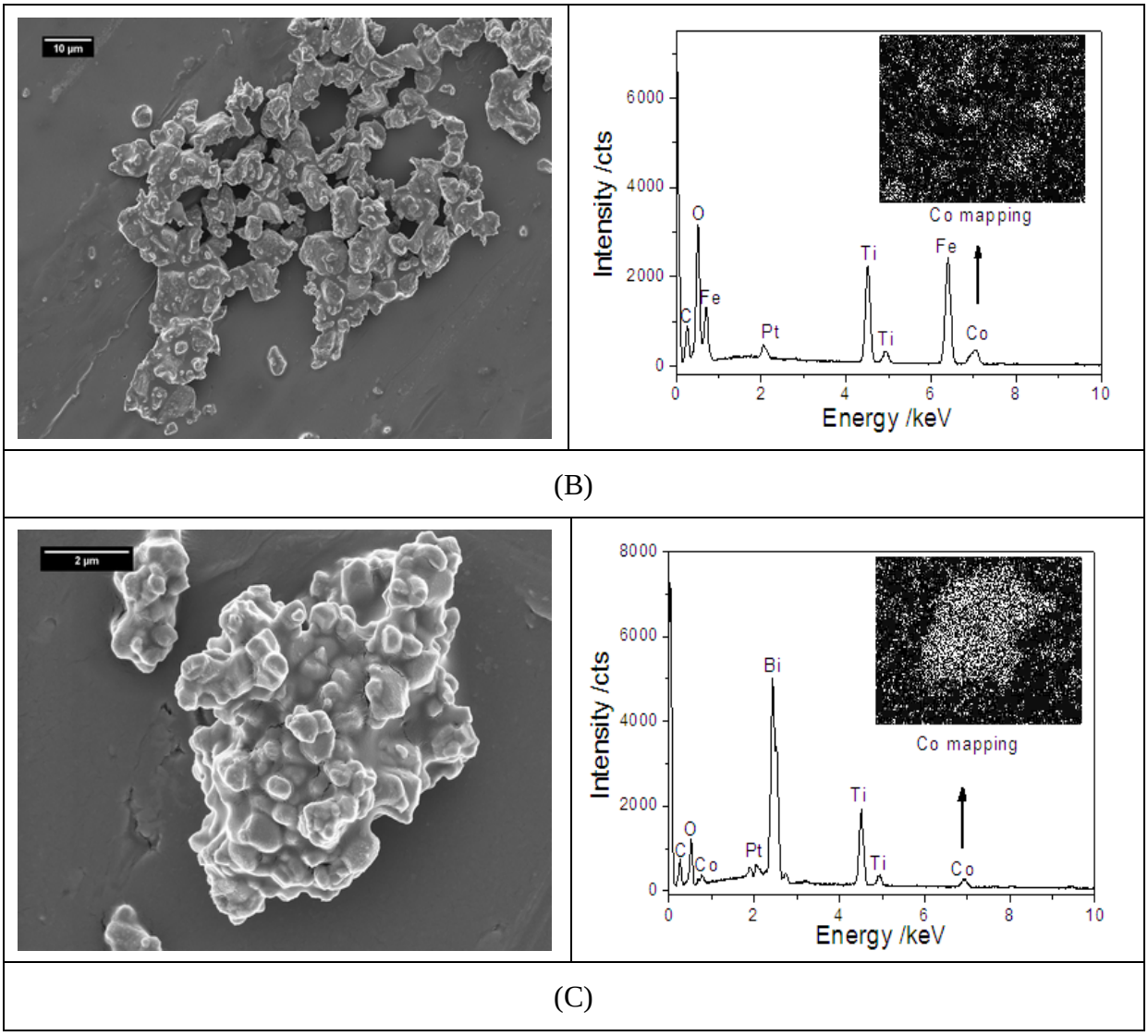

Figure 3.3 SEM images, EDS and Co mapping of Co(5%)/Zn (A), Co(5%)/Fe (B) and Co(5%)/Bi (C)

3.3.2. Photochemical oxidation of phenol

3.3.2.1. Control experiments of oxidation of phenol at various conditions

Preliminary experiments were carried out to test the activation of oxidants by heat or light for phenol degradation. Photocatalytic degradation of phenol using Degussa P25 was also

shown to visualize the experimental condition with light irradiation. Fig. 3.4 shows 17.1, 11.5, 38.4, 30.4, and 47.8% of phenol removals within heat activation of PDS and PMS, light activation of PDS and PMS, and photocatalysis over P25, respectively, in 150 min. PDS and PMS would be activated by heat, irradiation, or metal ions, as shown below.

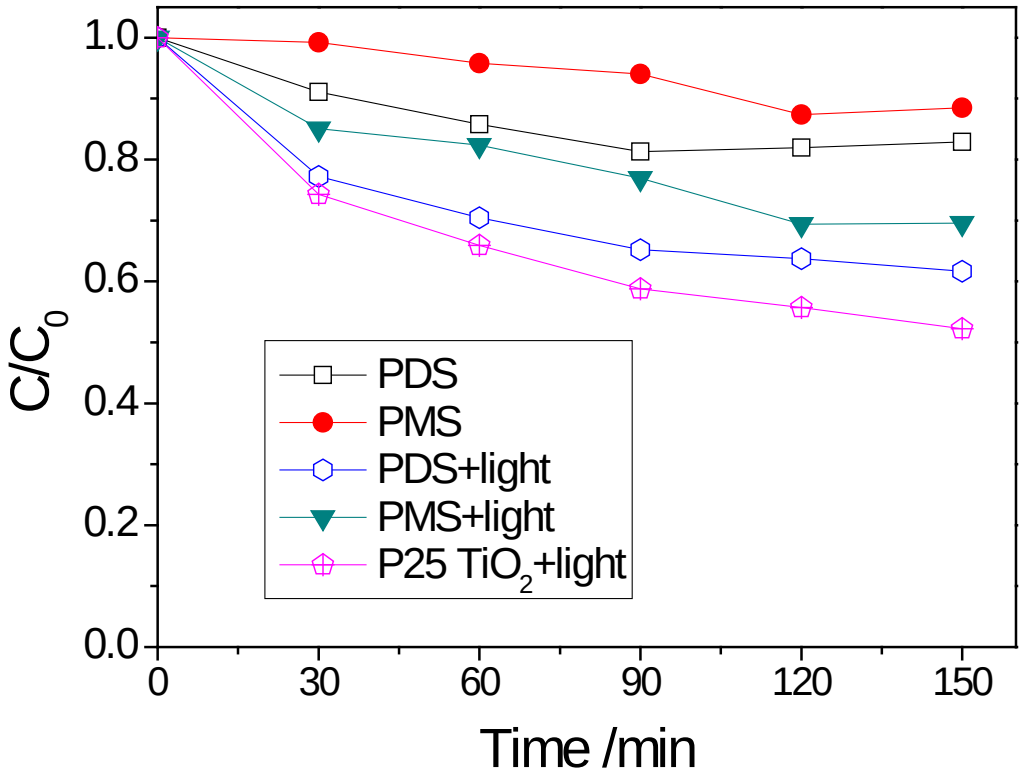

Figure 3.4 Oxidation of phenol via peroxymonosulfate (PMS); peroxydisulfate (PDS); P25 TiO_2 at various conditions. [Phenol: 25 ppm; Temperature: 30^{o}C; Oxidants dosage: 2 g/L]

PMS reactions with heat, metal ions or irradiation [5, 6],

$$M^{n+} + HSO_5^- \rightarrow M^{(n+1)+} + SO_4^{\bullet -} + OH^- \quad (3\text{-}2)$$

$$HSO_5^- + h\nu \rightarrow SO_4^{\bullet -} + OH^{\bullet} \quad (3\text{-}3)$$

$HSO_5^- + heat \rightarrow SO_4^{\bullet-} + OH^{\bullet}$ (3-4)

$HSO_5^- + e^- \rightarrow SO_4^{\bullet-} + OH^-$ (3-5)

PDS reactions with heat, metal ions or irradiation [6, 17],

$M^{n+} + S_2O_8^{2-} \rightarrow M^{(n+1)+} + SO_4^{\bullet-} + SO_4^{2-}$ (3-6)

$S_2O_8^{2-} + h\nu \rightarrow 2SO_4^{\bullet-}$ (3-7)

$S_2O_8^{2-} + heat \rightarrow 2SO_4^{\bullet-}$ (3-8)

$S_2O_8^{2-} + e^- \rightarrow SO_4^{\bullet-} + SO_4^{2-}$ (3-9)

The photocatalysis over P25 follows another reaction as follows. [25]

$TiO_2 + h\nu \rightarrow h_{vb}^+ + e_{cb}^-$ (3-10)

Thus, it was found that only little amount of phenol (< 40%) was removed in 150 min if no catalyst was used to activate oxidants.

3.3.2.2. Oxidation of phenol using PMS activated by supports and supported Co catalysts

Fig. 3.5 shows phenol degradation efficiencies by photocatalysis and photochemical oxidation using $ZnTiO_3$ and supported Co catalysts. It was found that $ZnTiO_3$ only showed minor photocatalytic activity, providing 10.1% phenol degradation in 150 min. Loading Co would decrease the photocatalytic efficiency, resulting in 4.8, 6.1, and 6.9% phenol removals in 150 min over Co(1%)/Zn, Co(3%)/Zn, and Co(5%)/Zn, respectively. The photocatalysis of phenol on $ZnTiO_3$ would be promoted by addition of PMS, achieving 62.8 % phenol degradation in 150 min, which was higher than the numerical sum of photocatalysis of $ZnTiO_3$ and photochemical oxidation of PMS/irradiation. Loading Co onto $ZnTiO_3$ would significantly enhance the efficiencies of phenol degradation, and 100% of phenol removal was made in 150 min over Co(1%)/Zn. At increased Co loading, the activity was increased, and the reaction time of complete decomposition of phenol was reduced to be 120 min. Yang et al. [14] systematically studied the photocatalysis and

photochemical oxidation of 2,4-dichlorophenol over TiO_2 supported Co. They found that the photocatalytic activity would be decreased with Co loading, but the photochemical oxidation efficiency (with PMS) would increase with increasing Co loading. However, they did not mention if TiO_2 would further activate PMS under irradiation to promote the photochemical efficiency. In our case, it was discovered that $ZnTiO_3$ would activate the irradiation/PMS system, and Co loading would further promote the reaction rate.

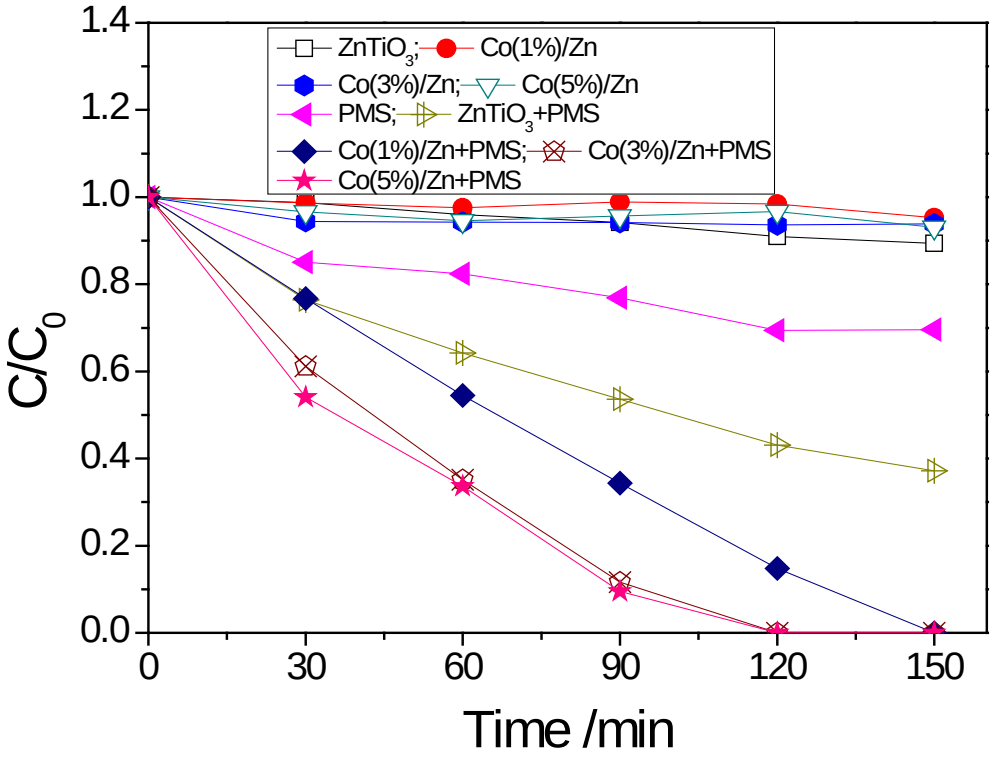

Figure 3.5 Photocatalytic and/or photochemical oxidation of phenol by $ZnTiO_3$ and its supported Co catalysts under visible light irradiations.

Fig. 3.6 shows the degradation of phenol using $FeTiO_3$ and supported Co catalysts with addition of PMS. The support showed minor photocatalysis, removing 3.9% of phenol in 150 min. Different from $ZnTiO_3$, loading Co on $FeTiO_3$ would slightly enhance the

photocatalytic activity of $FeTiO_3$, and the phenol degradation became 6.4, 6.9 and 11.6% at 1, 3 and 5% Co loading, respectively. Few studies have been conducted using $FeTiO_3$ as a photocatalyst. Kim et al. [26] found that pure $FeTiO_3$ showed minor activity, but the heterojunction of $FeTiO_3/TiO_2$ would greatly enhance the photocatalytic activity. From XRD it was found that the crystal structure of $FeTiO_3$ was transformed to $Fe_2Ti_3O_9$ after Co loading, which might form heterojunction with Co_3O_4 and then become a photocatalyst. It was also found that $FeTiO_3$ would inhibit the light activation of PMS, resulting in a lower efficiency. That would be attributed to its colour in black and broad light absorption, as shown in Fig. 3.2(C), such characteristics prevented PMS adsorbing light. Moreover, the conversion of $Fe^{2+} \rightarrow Fe^{3+}$ would also consume the active radicals, leading to lower oxidation efficiency. Loading Co onto $FeTiO_3$ would greatly increase the oxidation efficiency, which was gradually enhanced at increased Co loading. However, $FeTiO_3$ showed less effective than $ZnTiO_3$. Only 66.9% phenol removal was made in 150 min by Co(5%)/Fe, much inferior to 100% phenol removal in 120 min over Co(5%)/Zn.

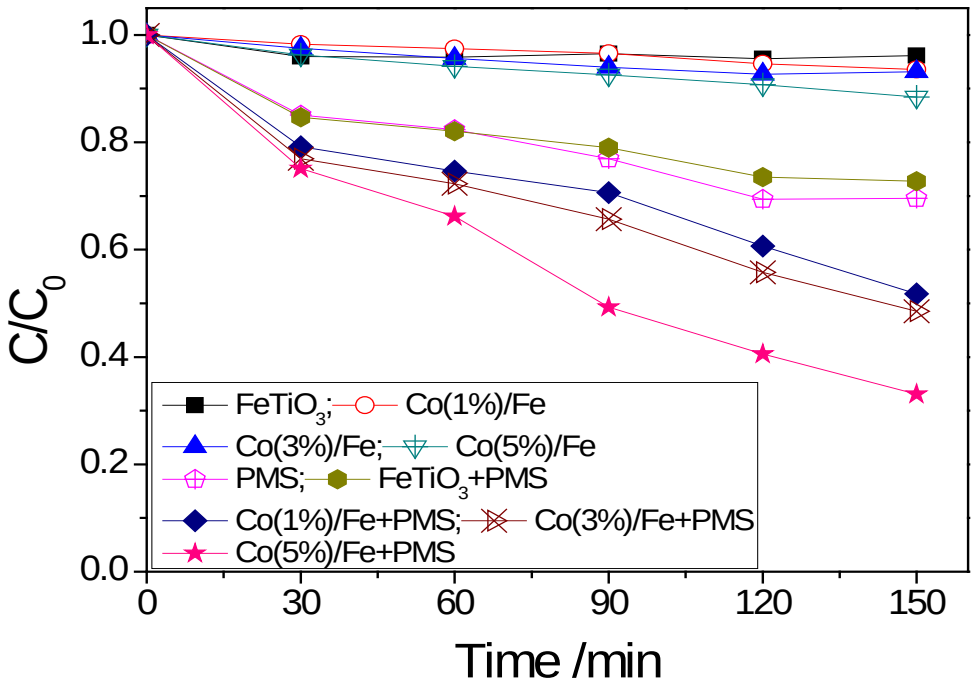

Figure 3.6 Photocatalytic and/or photochemical oxidation of phenol by $FeTiO_3$ and its supported Co catalysts under visible light irradiations.

Fig. 3.7 shows the oxidation performances of $Bi_4Ti_3O_{12}$ and its supported Co catalysts. The pure $Bi_4Ti_3O_7$ could decompose 10.1% of phenol in 150 min in photocatalysis, which was the same as $ZnTiO_3$ and higher than that on $FeTiO_3$. Yao et al. [27] reported that $Bi_4Ti_3O_{12}$ was an effective photocatalyst. The bond angle of Ti-O-Ti in $Bi_4Ti_3O_{12}$ forming an intra-electric field would promote the separation of photoinduced electron-hole pairs. However, once cobalt was loaded onto $Bi_4O_3Ti_{12}$, the photocatalytic activity was completely lost. This photocatalytic behaviour was similar to $ZnTiO_3$ as shown before. It was also found that the degradation rate was maintained unchanged after addition of the support into PMS/light system. Supported Co catalysts would further activate PMS/irradiation system and 3 wt% Co loading was found to be the optimum, providing complete destruction of phenol in 120 min, which was comparable to the activity on

Co(5%)/Zn.

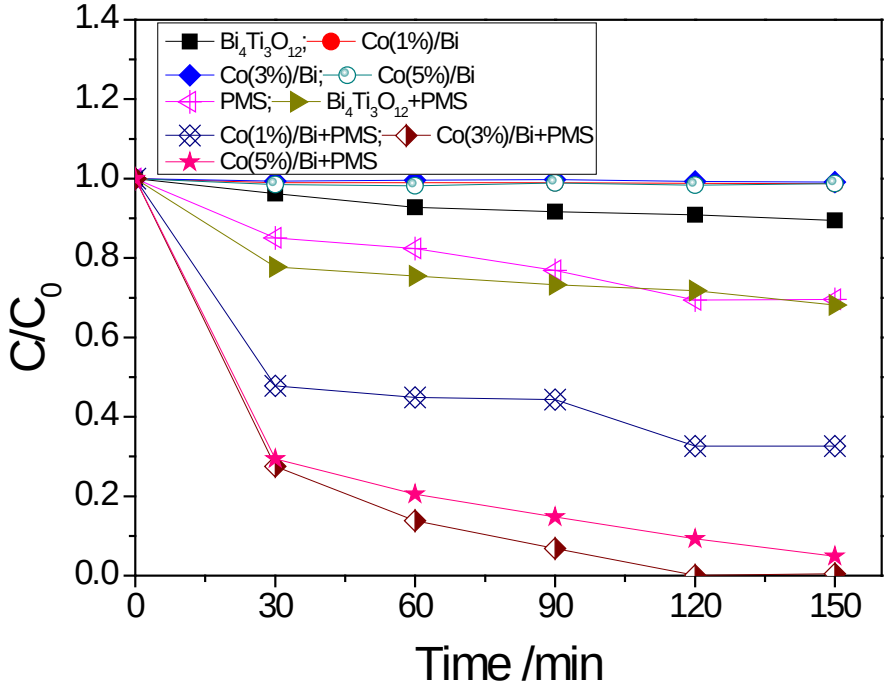

Figure 3.7 Photocatalytic and/or photochemical oxidation of phenol by $Bi_4Ti_3O_{12}$ and its supported Co catalysts under visible light irradiations.

The photocatalysis was not found to be efficient over the three supports and the supported catalysts. The main contribution to phenol removal was attributed to the photochemical oxidation with PMS. However, the supports exhibited great influence on the degradation efficiency of the supported catalysts. A pseudo first order kinetics for photochemical oxidation of phenol was employed in the systems to compare different efficiencies of the investigated reactions.

$$\ln C/C_0 = kt \qquad (3\text{-}11)$$

Where k is the apparent first order rate constant of phenol degradation, C is the constant concentration of phenol during reaction, C_0 is the initial concentration, and t is the reaction

time. Table 3.1 lists the apparent reaction rate constants and regression coefficients of the reactions. For the supports themselves, $FeTiO_3$ was found to inhibit the UV activation of PMS, $Bi_4Ti_3O_{12}$ showed slight enhance, and $ZnTiO_3$ would significantly promote the photochemical oxidation of phenol. Loading Co onto the supports would greatly enhance the activity of photochemical oxidation. $Bi_4Ti_3O_{12}$ as a support provided the best activity, and $FeTiO_3$ was not effective to be a good support. Zhang et al. [15] suggested that the supports of Co would significantly influence the activities of a supported catalyst in activation of PMS. They found that MgO was the best in their case, and the activities followed the order of MgO > ZnO > P25 > ZrO_2 > Al_2O_3 > SBA-15. They proposed that the differences in efficiencies were attributed to the surface hydroxyl species which might favour the formation of $CoOH^+$ intermediate accelerating the generation of sulphate radicals from PMS. In the present study, we focused on the photochemical behaviours of various photosensitive catalysts. The worst activity of $FeTiO_3$ supported catalysts was firstly attributed to the broad absorption from UV to visible light. Secondly, the photocatalytic activity would be lower in the activation of PMS. It was known that, as shown in Eq. (3-11), the photocatalysis of $FeTiO_3$ can produce e^-_{CB}, which may react with surface hydroxyl species [25],

$$e^-_{CB}+CoOH^+ \rightarrow CoOH^\bullet \quad (3\text{-}12)$$

resulting in lower production of $CoOH^+$. Although $OH^\bullet$ itself is an active radical and ready for decomposing organics, it has lower oxidation activity than the sulphate radical due to its low oxidation potential of 1.7eV [5].

However, we cannot conclude that the photocatalysts are not good supports for Co materials. Yang et al. [14] suggested the best efficiency of Co/TiO_2 in photochemical activation of PMS. A number of parameters including band positions of the support and cobalt oxide, surface radicals, multiple-activation (heat, UV, Co, and e^-) of PMS, would

interact together to determine the photochemical behaviours of the supported Co catalysts.

Table 3.1 Comparison of the efficiencies of photochemical oxidation of phenol by PMS

Reactions	Apparent rate constant /min^{-1}	Regression coefficient (R^2)
PMS+light	0.00286	0.89
$ZnTiO_3$+light+PMS	0.00704	0.99
Co(1%)/Zn+light+PMS	0.01285	0.94
Co(3%)/Zn+light+PMS	0.01864	0.98
Co(5%)/Zn+light+PMS	0.02064	0.99
$FeTiO_3$+light+PMS	0.00255	0.81
Co(1%)/Fe+light+PMS	0.00440	0.93
Co(3%)/Fe+light+PMS	0.00504	0.94
Co(5%)/Fe+light+PMS	0.00758	0.99
$Bi_4Ti_3O_{12}$+light+PMS	0.00317	0.57
Co(1%)/Bi+light+PMS	0.01077	0.72
Co(3%)/Bi+light+PMS	0.03880	0.99
Co(5%)/Bi+light+PMS	0.03200	0.96

3.3.2.3. Oxidation of phenol using PDS activated by various supported catalysts

The performances of the supports and supported catalysts in photochemical oxidation of phenol using PDS were also investigated. Fig. 3.8 shows the photochemical efficiencies of $ZnTiO_3$ and supported Co activating PDS in degradation of phenol. The system of $ZnTiO_3$/irradiation/PDS showed the most efficient degradation in this investigation and 45.6% of phenol removal was obtained. This degradation was not comparable to those systems with PMS. The supported Co catalysts showed less activity compared to the pure $ZnTiO_3$ and the efficiencies were even lower than light activation of PDS.

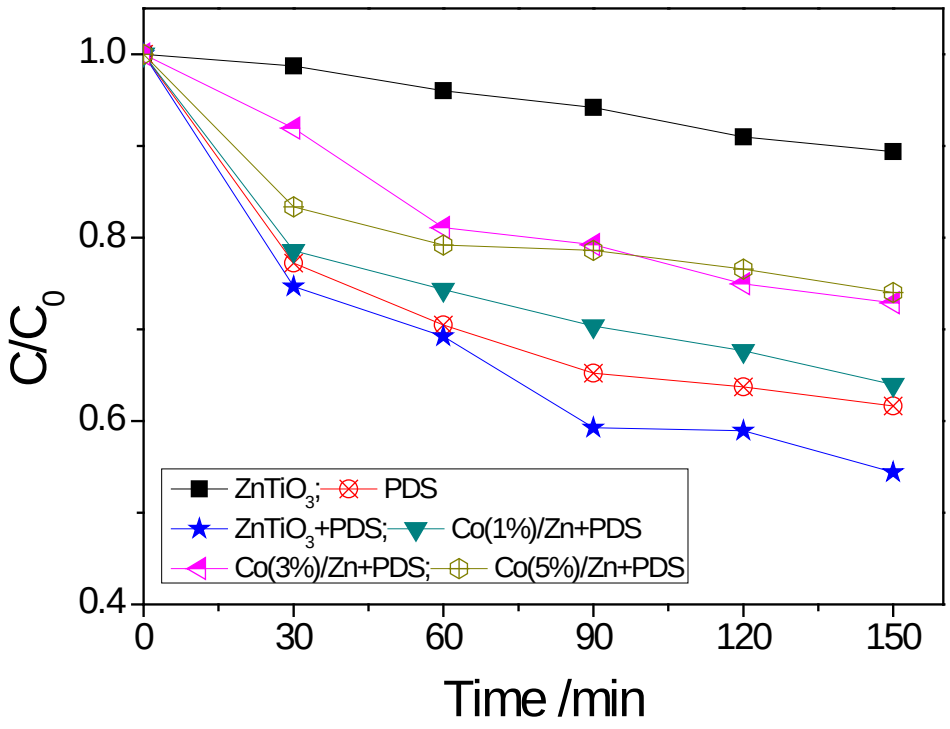

Figure 3.8 Photocatalytic and/or photochemical oxidation of phenol by $ZnTiO_3$ and its supported Co catalysts with PDS under visible light irradiations.

Fig. 3.9 shows the performances of $FeTiO_3$ and its supported Co catalysts in photochemical oxidation of phenol with PDS. It was observed that addition of $FeTiO_3$ into PDS/irradiation system would almost diminish the light activation of PDS. After loading Co on the support, the activity of phenol degradation would be gradually recovered. At 5% Co loading, the activity could reach 45.2% of phenol removal in 150 min, better than PDS/irradiation in degradation of phenol.

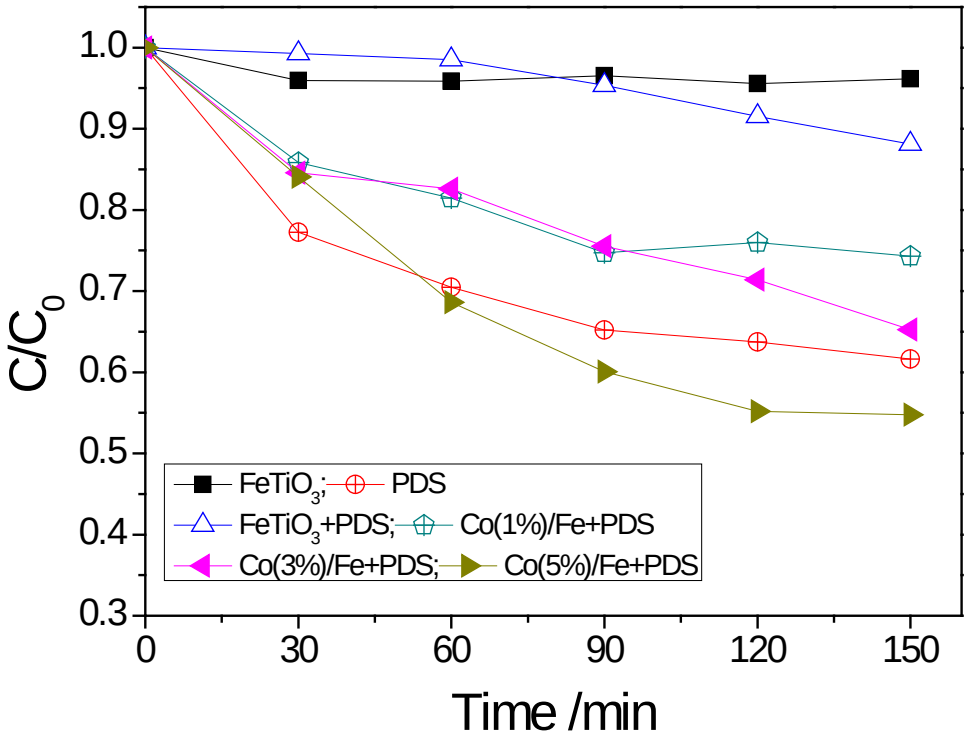

Figure 3.9 Photocatalytic and/or photochemical oxidation of phenol by $FeTiO_3$ and its supported Co catalysts with PDS under visible light irradiations.

Fig. 3.10 shows that $Bi_4Ti_3O_{12}$ hardly influenced the irradiation/PDS system, suggesting no reactions between $Bi_4Ti_3O_{12}$ and PDS. The supported Co would increase the degradation rate of phenol and 66.9% of phenol degradation was achieved in 150 min, suggesting better performance of $Bi_4Ti_3O_{12}$ being as an support than either $FeTiO_3$ or $ZnTiO_3$.

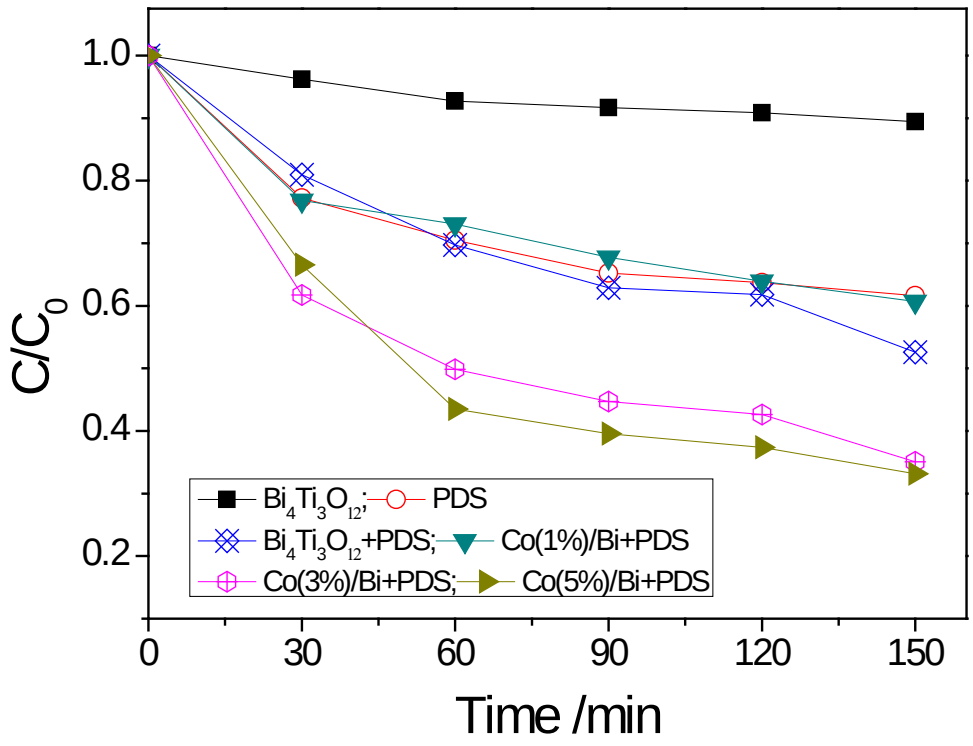

Figure 3.10 Photocatalytic and/or photochemical oxidation of phenol by $Bi_4Ti_3O_{12}$ and its supported Co catalysts with PDS under visible light irradiations.

Shukla et al. [28] previously reported that ZnO would promote the degradation efficiency of phenol in PDS/UV-visible, higher than that of TiO_2. This was attributed to the varying photophysical properties of ZnO and TiO_2. The photochemical behaviours of various supports in activation of PDS indicated that $ZnTiO_3$ would activate PDS, while $FeTiO_3$ would quench the light activation of PDS, and that $Bi_4Ti_3O_{12}$ would only slightly influence the PDS activation. The loading of Co_3O_4 also posed different effects on the supports: it would gradually increase the photoactivity over $FeTiO_3$ and $Bi_4Ti_3O_{12}$ at increased Co loading, but inhibit the activity of $ZnTiO_3$.

3.3.2.4. Reusability of Co(5%)/Zn in PMS reaction

Fig. 3.11 shows the reusability of Co(5%)/Zn in photochemical oxidation of phenol with PMS. It was found that the $ZnTiO_3$ supported Co showed good stability and maintained the activity at 96.0, 87.6 and 85.4% in the second, third and fourth runs, respectively. Previous studies of supported cobalt catalysts for activation of PMS have indicated varying stability of the catalysts. Chu et al. [29] reported that the reusability of the supported cobalt depended on the supports. Co/Zeolite showed poor stability and degradation efficiency of monuron only remained 30% at the second run after UV regeneration. Zhang et al. [15] tested Co/MgO for dye decomposition and found that the activity of the catalyst dropped slightly in three runs. Compared to our previous studies, the stability of Co(5%)/Zn was less than Co/activated- carbon [16], but slightly higher than Co/ZSM-5 [5]. That suggested that $ZnTiO_3$ supported Co can be a stable catalyst for phenol removal by photochemical oxidation.

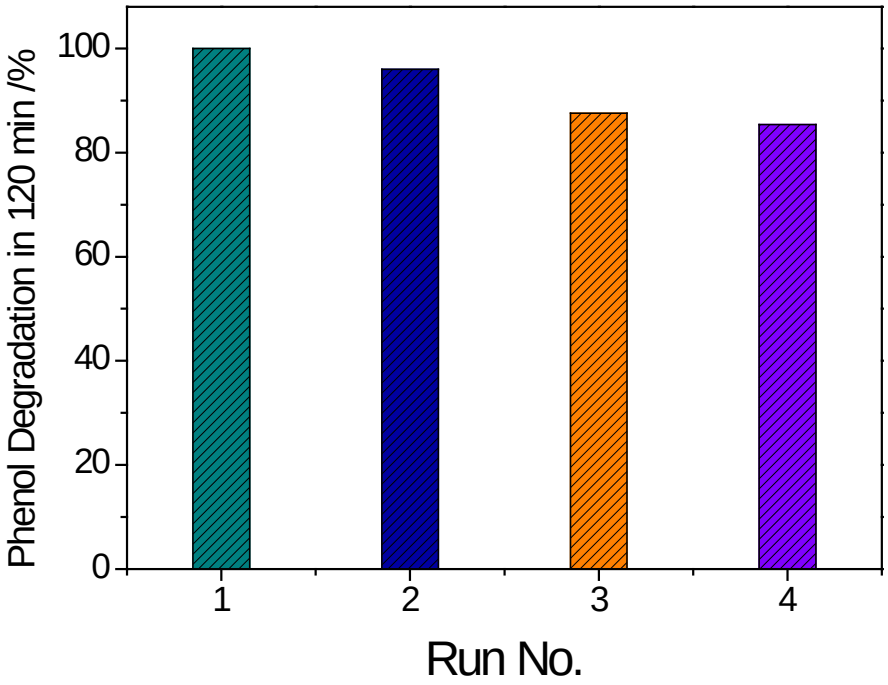

Figure 3.11 Reusability of Co(5%)/Zn in photochemical oxidation of phenol with PMS.

3.3.2.5. Mechanism of synergistic effects

PMS was known to undergo degradation upon UV ($\lambda < 260$ nm) and PDS would be also activated under UV ($200 < \lambda < 310$ nm) [6]. In this investigation, UV at wavelength shorter than 280 nm was not detectable, and UV between 315 to 400 nm was detected to be 60 $\mu W/cm^2$, thus the UV activation of PMS and PDS was minimised. However, PDS can be activated by longer wavelength light, it showed higher phenol degradation efficiency than PMS, which was confirmed in Fig. 3.4. When catalysts participate in the reactions, a complicated process of electron transfer would occur. Fig. 3.12 illustrates the band edges of cobalt oxide and supports, as well as the redox potentials of PMS and PDS oxidants [10, 30, 31]. As shown in Eq. (3-10), a semiconductor is activated by light, an electron-hole pair will be produced with e^- jumping to conduction band (CB) and h^+ left at valence band (VB). All the VB and CB levels of the supports are higher than those of Co_3O_4, making it thermodynamically possible to transfer charges to Co_3O_4. The activation of PMS or PDS would mostly take place on the surface of Co_3O_4, the activated sulphate radicals will be influenced by the photogenerated charges [28].

$$SO_4^{\bullet-} + e^- \rightarrow SO_4^{2-} \quad (3\text{-}13)$$

$$SO_4^{2-} + h^+ \rightarrow SO_4^{\bullet-} \quad (3\text{-}14)$$

Eq. (3-13) would be detrimental to the oxidation efficiency, and Eq. (3-14) would improve the degradation rate. In other words, a lower CB edge and higher VB edge of a support would favour the improvement of phenol degradation efficiency. This is well accordance with the experimental results, which showed the efficiencies in an order of Co (X%)/Bi > Co (X%)/Zn > Co (X%)/Fe with PMS.

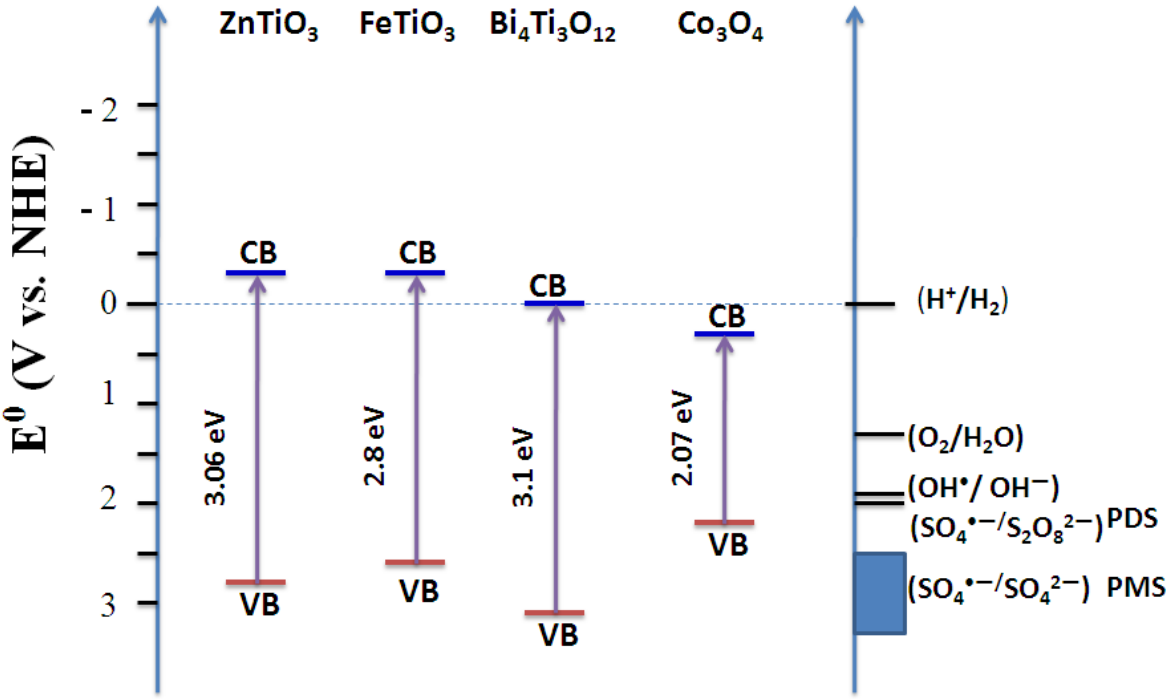

Figure 3.12 Conduction and valence band positions of cobalt oxide and the supports compared to redox potentials of several active radicals

On the other hand, the instinct feature of supports would also affect the photochemical oxidation reactions with PMS and light irradiations, which presents as $ZnTiO_3$ > $Bi_4Ti_3O_{12}$ > $FeTiO_3$. Due to lower photocatalytic efficiencies, those effects from the supports were not strong enough to be dominant in the overall photochemical oxidation with PMS.

However, in the reactions containing PDS, the supports were found to play more crucial role in determination of the overall efficiencies. $ZnTiO_3$ improved the efficiency of PDS/light system, and the loading of Co would gradually decrease the efficiency. $FeTiO_3$ would quench the activation of PDS by light, possibly due to the conversion of $Fe^{2+} \rightarrow Fe^{3+}$, which consumed the active sulphate radicals. After the loading of cobalt, $FeTiO_3$ was

transformed to be $Fe_2Ti_3O_9$, as shown in Fig. 3.1(B). The loaded cobalt would regenerate the oxidation efficiency without the conversion of $Fe^{2+} \rightarrow Fe^{3+}$. Similar to $ZnTiO_3$, $Bi_4Ti_3O_{12}$ would slightly increase the phenol removal in PDS/light system. However, loading cobalt would further improve the oxidation efficiency.

3.4. Conclusions

Cobalt supported on titanates, $ZnTiO_3$, $FeTiO_3$ and $Bi_4Ti_3O_{12}$, were proven as efficient catalysts for photochemical oxidation of phenol by activation of PMS and PDS. The cobalt was suggested to be in the form of Co_3O_4, which would strongly influence the photocatalysis and photochemical behaviours in activation of sulphate oxidants of PMS and PDS. Co_3O_4 decreased the photocatalytic activity of $ZnTiO_3$ and $Bi_4Ti_3O_{12}$, but enhanced the activity of $FeTiO_3$. Generally, loading of Co_3O_4 would promote the photochemical efficiency in phenol removal by activation of PMS, in which $Bi_4Ti_3O_{12}$ supported catalysts showed the best activities. Although the efficiencies of the titanate supported Co in activation of PDS were not as high as PMS, $Bi_4Ti_3O_{12}$ supported catalysts still provided the best activity. $ZnTiO_3$ supported Co was selected to check the reusability and the results showed that this catalyst was stable in multiple runs of phenol degradation with PMS.

3.5. References

1. S. Wang, *A comparative study of Fenton and Fenton-like reaction kinetics in decolourisation of wastewater*. Dyes and Pigments, 2008.**76**: p. 714-720.

2. I. Arslan, I. A. Balcioglu, D. W. Bahnemann, H*eterogeneous photocatalytic treatment of simulated dyehouse effluents using novel TiO_2-photocatalysts*. Applied Catalysis B-Environmental, 2000. **26**: p. 193-206.

3. S. Esplugas, J. Gimenez, S. Contreras, E. Pascual, M. Rodriguez, *Comparison of different advanced oxidation processes for phenol degradation*. Water Research, 2002. **36**: p. 1034-1042.

4. V. Kavitha, K. Palanivelu, *The role of ferrous ion in Fenton and photo-Fenton processes for the degradation of phenol*. Chemosphere, 2004. **55**: p. 1235-1243.

5. P. Shukla, S. B. Wang, K. Singh, H. M. Ang, M. O. Tade, *Cobalt exchanged zeolites for heterogeneous catalytic oxidation of phenol in the presence of peroxymonosulphate*. Applied Catalysis B-Environmental, 2010. **99**: p. 163-169.

6. P. Shukla, I. Fatimah, S. Wang, H. M. Ang, O. Tade Moses, *Photocatalytic generation of sulphate and hydroxyl radicals using zinc oxide under low-power UV to oxidise phenolic contaminants in wastewater.* Catalysis Today, 2010. **157**: p. 410-414.

7. H. Q. Sun, Y. Bai, H. J. Liu, W. Q. Jin, N. P. Xu, *Photocatalytic decomposition of 4-chlorophenol over an efficient N-doped TiO_2 under sunlight irradiation.* Journal of Photochemistry and Photobiology A-Chemistry, 2009. **201**: p:15-22.

8. H. Q. Sun, Y. Bai, H. J. Liu, W. Q. Jin, N. P. Xu, G. J. Chen, B. Q. Xu, *Mechanism of nitrogen-concentration dependence on pH value: Experimental and theoretical studies on nitrogen-doped TiO_2*. Journal of Physical Chemistry C, 2008. **112**: p. 13304-13309.

9. P. Shukla, S. Wang, H. Sun, H.-M. Ang, M. Tade, *Adsorption and heterogeneous advanced oxidation of phenolic contaminants using Fe loaded mesoporous SBA-15 and H_2O_2*. Chemical Engineering Journal, 2010. **164**: p. 255-260.

10. G. P. Anipsitakis, D. D. Dionysiou, *Degradation of organic contaminants in water with sulfate radicals generated by the conjunction of peroxymonosulfate with cobalt*. Environmental Science & Technology, 2003. **37**: p. 4790-4797.

11. G. P. Anipsitakis, D. D. Dionysiou, M. A. Gonzalez, *Cobalt-mediated activation of peroxymonosulfate and sulfate radical attack on phenolic compounds. Implications of chloride ions*. Environmental Science & Technology, 2006. **40**: p. 1000-1007.

12. D. Lison, *Human toxicity of cobalt-containing dust and experimental studies on the mechanism of interstitial lung disease (hard metal disease)*. Critical Reviews in Toxicology, 1996. **26**: p. 585-616.

13. Q. J. Yang, H. Choi, D. D. Dionysiou, *Nanocrystalline cobalt oxide immobilized on*

titanium dioxide nanoparticles for the heterogeneous activation of peroxymonosulfate. Applied Catalysis B-Environmental, 2007. **74**: p. 170-178.

14. Q. J. Yang, H. Choi, Y. J. Chen, D. D. Dionysiou, *Heterogeneous activation of peroxymonosulfate by supported cobalt catalysts for the degradation of 2,4-dichlorophenol in water: The effect of support, cobalt precursor, and UV radiation*. Applied Catalysis B-Environmental, 2008. **77**: p. 300-307.

15. W. Zhang, H. L. Tay, S. S. Lim, Y. S. Wang, Z. Y. Zhong, R. Xu, *Supported cobalt oxide on MgO: Highly efficient catalysts for degradation of organic dyes in dilute solutions*. Applied Catalysis B-Environmental, 2010. **95**: p. 93-99.

16. P. R. Shukla, S. Wang, H. Sun, H. M. Ang, M. Tade, *Activated carbon supported cobalt catalysts for advanced oxidation of organic contaminants in aqueous solution*. Applied Catalysis B: Environmental, 2010. **100**: p. 529-534.

17. G. P. Anipsitakis, D. D. Dionysiou, *Transition metal/UV-based advanced oxidation technologies for water decontamination*. Applied Catalysis B-Environmental, 2004. **54**: p. 155-163.

18. J. Z. Kong, A. D. Li, H. F. Zhai, H. Li, Q. Y. Yan, J. Ma, D. Wu, *Preparation, characterization and photocatalytic properties of $ZnTiO_3$ powders*. Journal of Hazardous Materials, 2009. **171**: p. 918-923.

19. X. Fu, Y. Wang, F. Wei, *Phase Transitions and Reaction Mechanism of Ilmenite Oxidation*. Metallurgical and Materials Transactions A, 2010. **41**: p. 1338-1348.

20. W. Wei, Y. Dai, B. B. Huang, *First-Principles Characterization of Bi-based Photocatalysts: $Bi_{12}TiO_{20}$, $Bi_2Ti_2O_7$, and $Bi_4Ti_3O_{12}$*. Journal of Physical Chemistry C, 2009. **113**: p. 5658-5663.

21. L. L. Zhao, F. Q. Liu, X. W. Wang, Z. Y. Zhang, J. F. Yan, *Preparation and characterizations of $ZnTiO_3$ powders by sol-gel process*. Journal of Sol-Gel Science and Technology, 2005. **33**: p. 103-106.

22. J. Pal, P. Chauhan, *Study of physical properties of cobalt oxide (Co_3O_4) nanocrystals*. Materials Characterization, **61**: p. 575-579

23. B. Gao, Y. J. Kim, A. K. Chakraborty, W. I. Lee, *Efficient decomposition of organic compounds with $FeTiO_3/TiO_2$ heterojunction under visible light irradiation*. Applied Catalysis B-Environmental, 2008. **83**: p. 202-207.

24. L. Pintilie, I. Pintilie, *Ferroelectrics: new wide-gap materials for UV detection*. Materials Science and Engineering B-Solid State Materials for Advanced Technology, 2001. **80**: p. 388-391.

25. M. R. Hoffmann, S. T. Martin, W. Y. Choi, D. W. Bahnemann, *Environmental applications of semiconductor photocatalysis*. Chemical Reviews, 1995. **95**: p. 69-96.

26. Y. J. Kim, B. Gao, S. Y. Han, M. H. Jung, A. K. Chakraborty, T. Ko, C. Lee, W. I. Lee, *Heterojunction of $FeTiO_3$ Nanodisc and TiO_2 Nanoparticle for a Novel Visible Light Photocatalyst*. Journal of Physical Chemistry C, 2009. **113**: p.19179-19184.

27. W. F. Yao, X. H. Xu, H. Wang, J. T. Zhou, X. N. Yang, Y. Zhang, S. X. Shang, B. B. Huang, P*hotocatalytic property of perovskite bismuth titanate*. Applied Catalysis B-Environmental, 2004. **52**: p. 109-116.

28. P. R. Shukla, S. B. Wang, H. M. Ang, M. O. Tade, *Photocatalytic oxidation of phenolic compounds using zinc oxide and sulphate radicals under artificial solar light*. Separation and Purification Technology, 2010. **70**: p. 338-344.

29. W. Chu, W. K. Choy, C. Y. Kwan, *Selection of supported cobalt substrates in the presence of oxone for the oxidation of monuron*. Journal of Agricultural and Food Chemistry, 2007. **55**: p. 5708-5713.

30. Y. Xu, M. A. A. Schoonen, *The absolute energy positions of conduction and valence bands of selected semiconducting minerals*. American Mineralogist, 2000. **85**: p. 543-556.

31. J. Fernandez, P. Maruthamuthu, A. Renken, J. Kiwi, *Bleaching and photobleaching of Orange II within seconds by the oxone/Co^{2+} reagent in Fenton-like processes*. Applied Catalysis B-Environmental, 2004. **49**: p. 207-215.

4

Chapter 4: Nano-Fe^0 Encapsulated in Microcarbon Spheres: Synthesis, Characterization, and Environmental Applications

Abstract

Nanoscaled zerovalent iron (ZVI) encapsulated in carbon spheres (nano-Fe^0@CS) were prepared via a hydrothermal carbonization method, using glucose and iron(III) nitrate as precursors. The properties of the nano-Fe^0@CS were investigated by X-ray diffraction (XRD), thermogravimetric analysis-differential scanning calorimetry (TGA-DSC), Fourier transform infrared spectroscopy (FTIR), scanning electron microscopy (SEM), transmission electron microscopy (TEM), and nitrogen adsorption/desorption isotherms. Nano-Fe^0@CS was demonstrated, for the first time, as an effective material in activating Oxone (peroxymonosulfate, PMS) for the oxidation of organic pollutants. It was found that the efficiency of nano-Fe^0@CS was higher than ZVI particles, iron ions, iron oxides, and a cobalt oxide. The mechanism of the high performance was discussed. The structure of the nano-Fe^0@CS leads to not only high efficiency in the activation of PMS, but also good stability. This study extended the application of ZVI from reductive destruction of organics to oxidative degradation of organics by providing a green material for environmental remediation due to its good stability in the processes of organics degradation.

4.1. Introduction

Iron is a low-cost, naturally abundant, and environmentally friendly material that has been widely applied in remediation of various contaminants in water [1, 2] or soil [3]. There were extensive studies of zerovalent iron (ZVI) for use in the decontamination of halogenated organics [3, 4] as well as applications as nitro aromatic compounds [5], dyes [6], pesticides [7], nitrates [1], and heavy metals [8, 9]. In these applications, ZVI was exclusively used as a strong reductant, and relative reactions can be described as shown below [1, 5, 10].

$$Fe^0 + RX + H^+ \rightarrow RH + Fe^{2+} + X^- \quad (4\text{-}1)$$

$$3Fe^0 + ArNO_2 + 6H^+ \rightarrow ArNO_2 + 3Fe^{2+} + 2H_2O \quad (4\text{-}2)$$

$$TiO_2(h^+) + HO_{ad} \rightarrow TiO_2 + HO^{\bullet}_{ad} \quad (4\text{-}3)$$

$$2Fe^0 + 3Pb^{3+} + 4H_2O \rightarrow +3Pb^0 + 2FeOOH + 6H^+ \quad (4\text{-}4)$$

However, the reduction performance of ZVI fails to facilitate the degradations of those organics that cannot directly receive electrons, such as phenol [11, 12]. To overcome the barrier of contaminant dependence, it is highly desirable to develop oxidation reactions using ZVI [13]. Compared to the extensive investigations of reactive reduction, only a few oxidations of organic pollutants using ZVI have been conducted. The oxidation was generally initiated by the reactivity of ZVI with dissolved oxygen [13, 14], hydrogenperoxide [15-17], or persulfate [18-22]. The former two oxidations proceed in the following mechanism [14].

$$Fe^0 + O_2 + 2H^+ \rightarrow Fe^{2+} + H_2O_2 \quad (4\text{-}5)$$

$$Fe^{2+} + H_2O_2 \rightarrow Fe^{3+} + HO\cdot + OH^- \quad (4\text{-}6)$$

The activation of persulfate (peroxydisulfate, PDS) for oxidation of organic pollutants can be obtained via the following reactions [19, 21, 22]:

To the best of our knowledge, there is no study using ZVI to activate peroxymonosulfate (PMS, commercially known as Oxone; $2KHSO_5 \cdot KHSO_4 \cdot K_2SO_4$), although a ferrous PMS system has been reported [23].

$$Fe^0 + O_2 + 2H_2O \rightarrow 2Fe^{2+} + 4OH^- \quad (4\text{-}7)$$

$$Fe^{2+} + S_2O_8 \rightarrow SO_4^{-\bullet} + SO_4^- + Fe^{3+} \quad (4\text{-}8)$$

Recently, it was found that nanoscale ZVI can show a higher activity in reduction reactions, when compared to conventional microscale ZVI particles [1, 4, 10]. Nanoscaled Fe^0 generally offers high surface-area-to-volume ratios, high specific surface area, and high surface reactivity. But it favors strong aggregation into microscale particles, because of high surface energy and intrinsic magnetic interaction [24]. Thus, many materials have been employed as supports for nano-Fe^0 for a better Fe distribution, including polystyrene resin [25], alumina [26], bentonite [27], kaolinite [28], zeolite [29], carbon black [30], activated carbon [31], carbon nanotubes [32], and carbon spheres [33]. Most of supported Fe^0 was prepared by a liquid-phase reduction method using borohydride salt [25-29, 31, 32]. However, the N_2 atmosphere, vacuum operation, high cost of borohydride, and the production of large volume of hydrogen make such a process complex and cost-intensive. Furthermore, without calcination, the mechanical stability of nano-Fe^0 on supports would be an additional issue that might influence the dispersion and mechanical strength of ZVI. Hoch et al. reported that ZVI nanoparticles could be prepared by the reduction of carbon black, which was also used as a support material, under Ar flow at a calcination of above 600 °C [30]. In supported nano- Fe^0, nanoparticles are exposed on the surface of the supports. Another concern of nano-Fe^0 is the

stability in air [23, 30, 34]. Encapsulation of nano-Fe^0 into porous carbon spheres was suggested to be a promising way for enhancement of transportation, suspension, and stability of nanoscaled ZVI without significantly sacrificing activity [3, 19, 35].

In this chapter, nanoscaled Fe^0 (ca. 10 nm) encapsulated in microscale carbon spheres (6−8 μm) was synthesized via an in situ formation from a glucose-induced hydrocarbonization, followed by a self-reduction. For the first time, the activation of PMS using nanoscaled ZVI for the oxidation of phenol solutions was discovered. Supported cobalt/PMS were extensively investigated in our previous studies [11, 12, 36-38], while cobalt is recognized as a priority pollutant that may cause many health issues [36]. The proposed nano-ZVI/PMS system exhibits superiority in the prevention of metal leaching.

4.2. Experimental

4.2.1. Fabrication of Nano-Fe^0@Microcarbon Spheres

The nano-Fe^0@CS materials were prepared via a green chemistry route without using any toxic compounds. Scheme 4.1 shows the formation process of the material. In a typical synthesis, 7.24g of D-glucose (99.5%, Sigma) and 4.62g of iron (III) nitrate nonahydrate (98%, Sigma−Aldrich) were dissolved in 80 mL of ultrapure water, and the mixture was then stirred for 4 h. The mixed solution was then transferred into a Teflon-lined autoclave (120mL) and treated in an oven at 180°C for 18h. After cooling to room temperature, the obtained black suspension was filtered and washed by ethanol/water for three cycles. The precipitate was dried in an oven at 80°C, and the obtained sample was labelled as Fe^x@CS-f. The dried sample was further annealed in N_2 atmosphere in a tubular furnace at 350, 550, or 750°C for 2h, and the samples were denoted as Fe^x@CS-350, Fe^0@CS-550, and Fe^0@CS-750,

respectively.

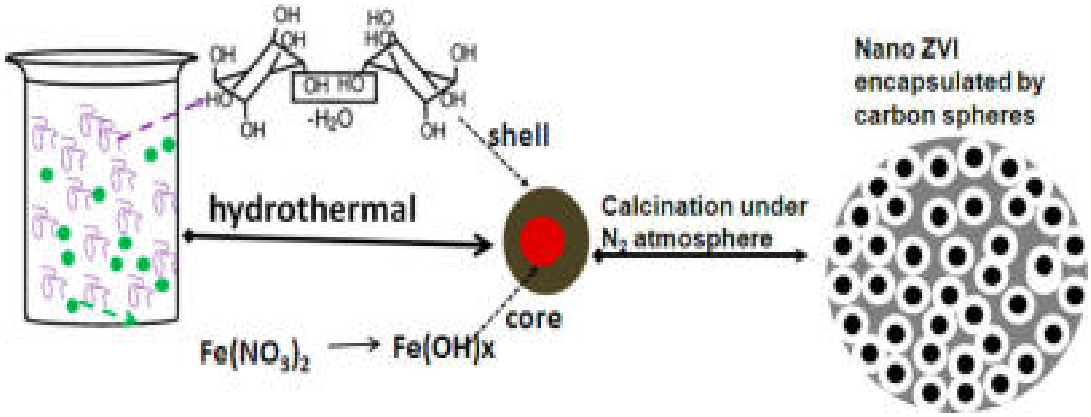

Scheme 4.1 Fabrication of Nano- Fe^0@Microcarbon Spheres

Unsupported nanoscaled Fe^0 particles were prepared by reduction of Fe_3O_4 nanopowder (<50 nm, Aldrich) under 10% H_2 in Ar at 550 °C for 6 h. The obtained ZVI aggregated into 2−5 μm particles. The prepared sample was marked as HR-Fe^0. A commercial iron powder (45−150 μm, Chem Supply), denoted as commercial Fe^0, was used as a reference material. Iron oxide (Fe_2O_3) and cobalt oxide (Co_3O_4) were obtained via the thermal decomposition of iron (III) nitrate and cobalt (II) nitrate, respectively.

4.2.2. Materials Characterization

The crystalline structure of samples was analyzed by powder X-ray diffraction (XRD) using a Bruker D8-Avance X-ray diffractometer with Cu Kα radiation (λ = 1.5418 Å). The iron content and thermal stability of Fe^x@CS and reference materials were investigated using thermogravimetric analysis−differential scanning calorimetry (TGA-DSC) in argon or air on a Mettler-Toledo Stare system. Fourier transform infrared (FTIR) spectra were acquired from a Bruker instrument, using an ATR mode. Scanning electron microscopy (SEM), energy-dispersive spectroscopy (EDS), and iron elemental mapping, performed on a Zeiss

Neon 40EsB FIBSEM, were used to evaluate the morphology, size, and texture information of the samples. Transmission electron microscopy (TEM) was applied, using a JEOL 2011 TEM instrument. The Brunauer-Emmett-Teller (BET) surface area and pore size distribution were evaluated by nitrogen sorption at -196 ℃, using a Quantachrome Autosorb AS-1 system. The samples were evaporated under vacuum at 200 ℃ for 4h prior to the adsorption measurements.

4.2.3. Adsorption and Catalytic Oxidation

Oxidation of phenol solutions using ZVI with sulfate radicals was performed in a 1-L double-jacket reactor. The reaction temperature was maintained at 30℃, using recycling water driven by a pump. In a typical run, 0.1 g of material was added into 200 mL of 20 ppm phenol solution. After stirring for 10 min, 0.4 g of Oxone was added into the mixed solution to start the reaction. At a set time interval, 1 mL of solution was withdrawn by a syringe and filtered through a Millipore film. The filtered solution was then injected into a vial, which was filled with 0.5mL of methanol as a quenching reagent. Unsupported ZVI reaction was performed using an equivalent iron loading in Fe^0@CS-550 at 0.115 g/L. Homogeneous iron/PMS system for phenol degradation was carried out using Fe (II) or Fe (III) ion solutions. In recycled experiments, used catalyst was collected by filtration, washed by water, and dried at 80 ℃ in air for reuse.

Adsorption experiments were carried out in a manner similar to the oxidation reactions, without the addition of oxidants and a quenching reagent.

The concentration of phenol solution was analyzed by a high performance liquid chromatography (HPLC, Varian) with a UV detector set at λ = 270nm. A C-18 column was

used to separate the organics while the mobile phase, with a flow rate of 1.0 mL/min, was composed of 20% CH_3CN and 80% water.

4.3. Results and Discussion

4.3.1. Characterization of Nano- Fe0@CS

Figure 4.1 shows X-ray diffraction (XRD) patterns of three different samples containing zero-valent iron, nano-Fe^0@CS-550, HR-Fe^0, and commercial Fe^0 particles. The latter two samples showed a pure α-Fe with a body-centered cubic (bcc) crystalline structure, with Fe(110) at 2θ = 44.7° and Fe(200) at 2θ = 64.9°. No peaks assigned to iron oxides were observed [39]. The intensities of the peaks on HR-Fe^0 were much stronger than those of commercial Fe^0 particles. In the pattern of nano-Fe^0@CS-550, besides the peaks of Fe^0, a peak at 26.3° was observed, which was due to the (100) face of graphitic carbon [30]. Another weak peak at 35.6° was possibly due to the (311) face of Fe_3O_4 [30, 39]. XRD patterns of Fe^x@CS-f and Fe^x@CS-350 did not have peaks that could be assigned to ZVI.

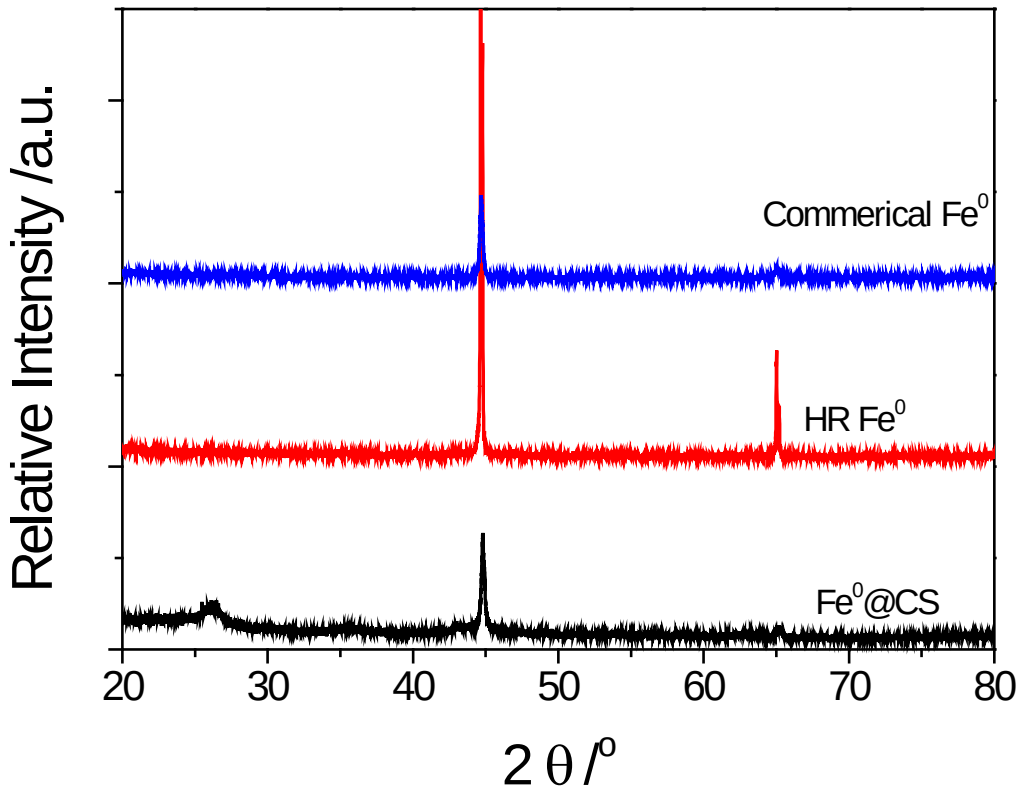

Figure 4.1 XRD patterns of nano Fe^0@CS-550, HR Fe^0, and commercial Fe^0.

Figure 4.2 displays TGA profiles of Fe^x@CS-f and ZVI samples in Ar or air. Figure 4.2A shows the phase transformation of iron species and the desorption performance, under an argon atmosphere, of the fresh sample of Fe^x@CS-f. Below 100 °C, only adsorbed water or ethanol was removed. Above 100°C, three endothermic peaks were observed, at 167, 381, and 521°C, respectively. The first peak arose from the transformation of amorphous $Fe(OH)_3$ to FeOOH [40], which was also indicated by XRD results. Fe^x@CS-f and Fe^x@CS-350 did not show any iron (oxide) peaks. The second endothermic peak at 381 °C was attributed to the transformation of FeOOH (or Fe_2O_3) to Fe_3O_4, and the peak at 521°C was from the reduction of Fe_3O_4 to Fe^0 [41]. Figure 4.2B shows the combustion performance of Fe^x@CS-f. Exothermic peaks from 200°C to 450°C were from the decomposition and combustion of

organics and amorphous carbon. Weight loss was determined to be stabilized at 15.0% after 444°C, indicating the complete combustion of carbon and oxidation of iron with a final product of Fe_2O_3. The elemental iron loading on Fe^x@CS-f was then calculated to be 10.5%. The elemental iron loadings in Fe^x@CS-350, Fe^0@CS-550, and Fe^0@CS-750 were determined based on their TGA profiles to be 14.2%, 22.9%, and 28.6%, respectively.

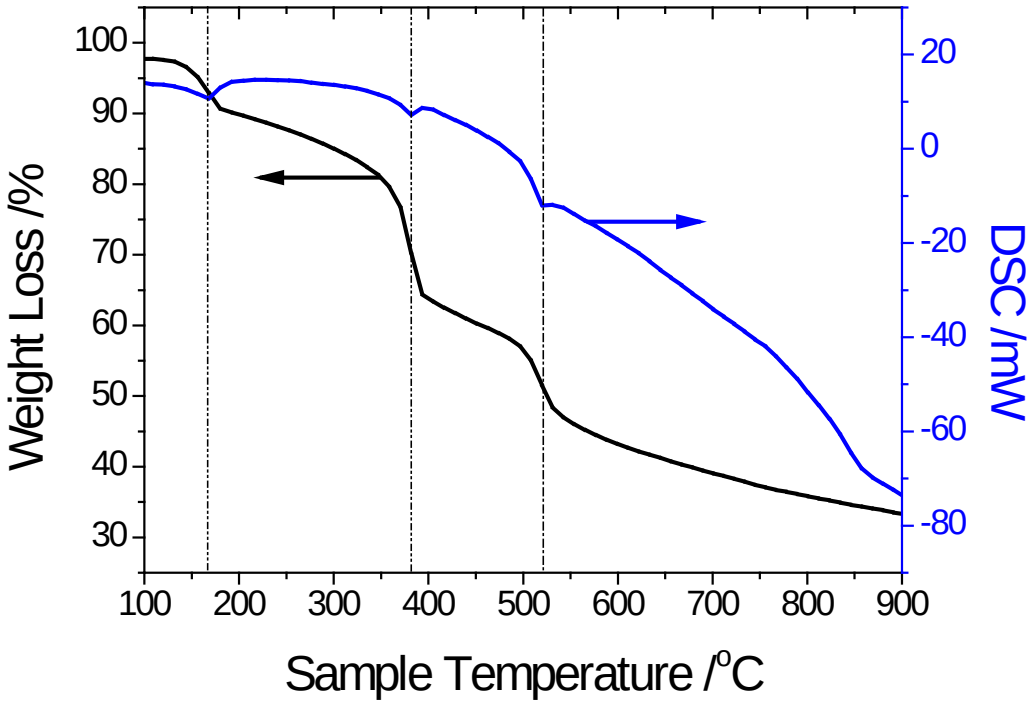

(A)

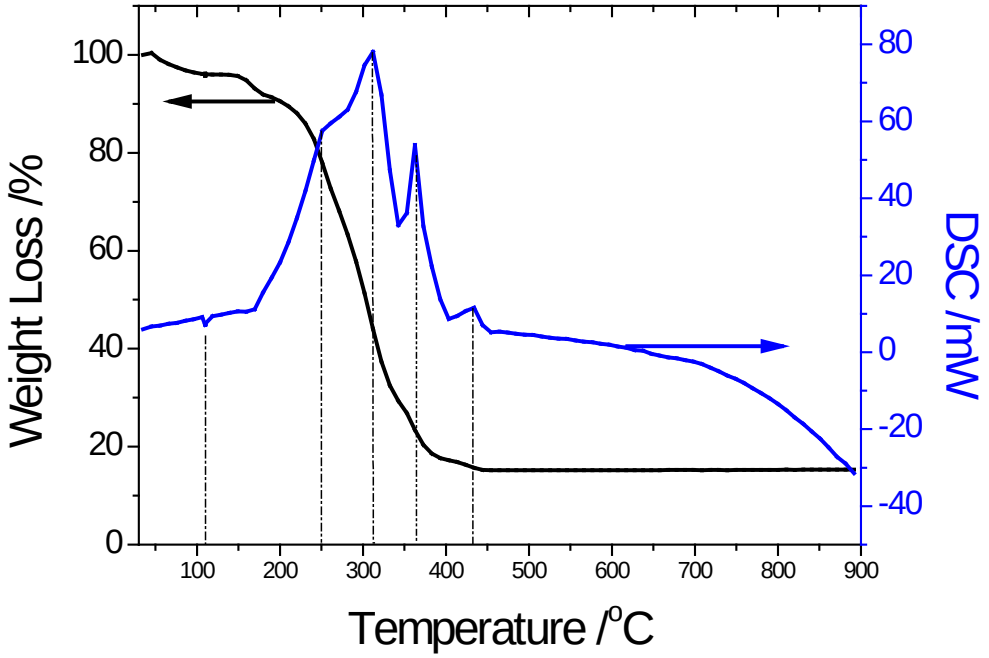

(B)

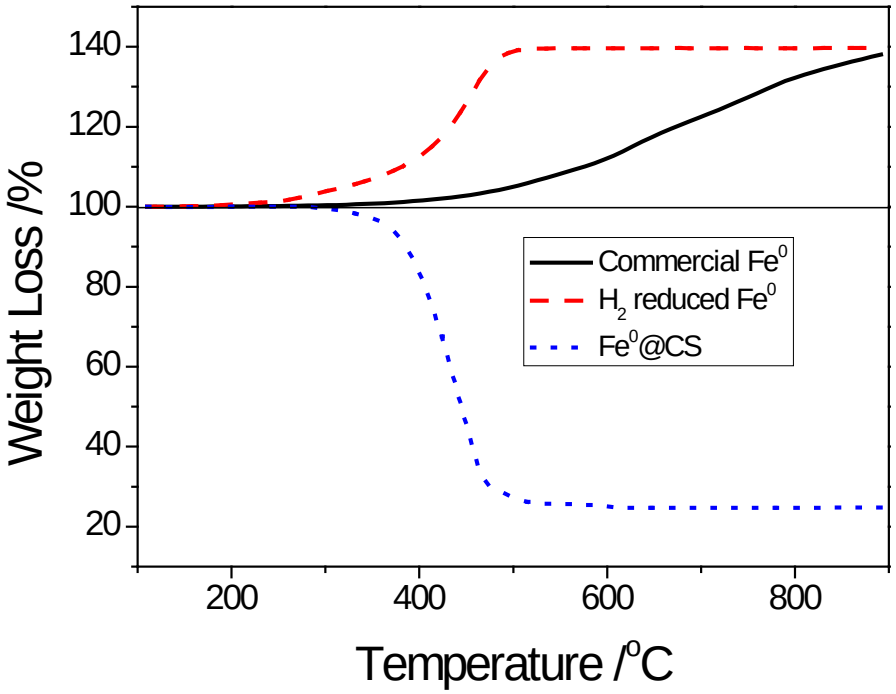

(C)

Figure 4.2 TGA profiles of Fe^{x}@CS-f under (A) argon and (B) air, and (C) TGA comparison

of three ZVI samples under air.

Figure 4.2C shows the weight changes of commercial Fe^0 powders, HR- Fe^0, and nano-Fe^0@CS-550. Weight increases of the first two samples were observed, indicating the oxidation of ZVI to iron oxides. Weight increase on commercial Fe0 started at 284.9°C, while it started at 181.4°C on HR-Fe^0. It suggested that the smaller size of ZVI is more easily oxidized in air. It was interesting to see that the weight remained unchanged on Fe^0@CS until the temperature reached 296.2°C, suggesting a better stability of Fe^0 on Fe^0@CS.

Figure 4.3 shows FTIR spectra of prepared iron@CS samples annealed at different temperatures. The fresh sample of Fe^x@ CS-f without calcination presented many organic functional groups. The band at 1685cm^{-1} was attributed to C=O vibrations, and the peak of 1598cm^{-1} was assigned to C=C vibrations. The band at 1019 cm^{-1} possibly arose from C−O stretching vibration, 1309cm^{-1} was from O−H bonding vibration, and 1360cm^{-1} indicated the presence of O−C=O. The band at 797cm^{-1} was due to aromatic C−H out-of-plane bending vibrations, while the band at 2998cm^{-1} was from stretching vibrations of aliphatic C−H. The band at 3329 corresponded to stretching vibrations of O−H. The results suggested that dehydration and aromatization occurred during the hydrothermal carbonization of glucose [42]. Calcination at 350°C significantly reduced the intensities of the bands, indicating a further carbonization of the carbon spheres under N_2 atmosphere. In the spectrum of Fe^x@CS-350, two new bands at 877 and 743cm^{-1} were observed, indicating the formation of FeOOH [43]. Calcination at 550 °C under N_2 would remove most of the organic groups, while the band at 1598cm^{-1} assigned to C=C vibrations was still clear.

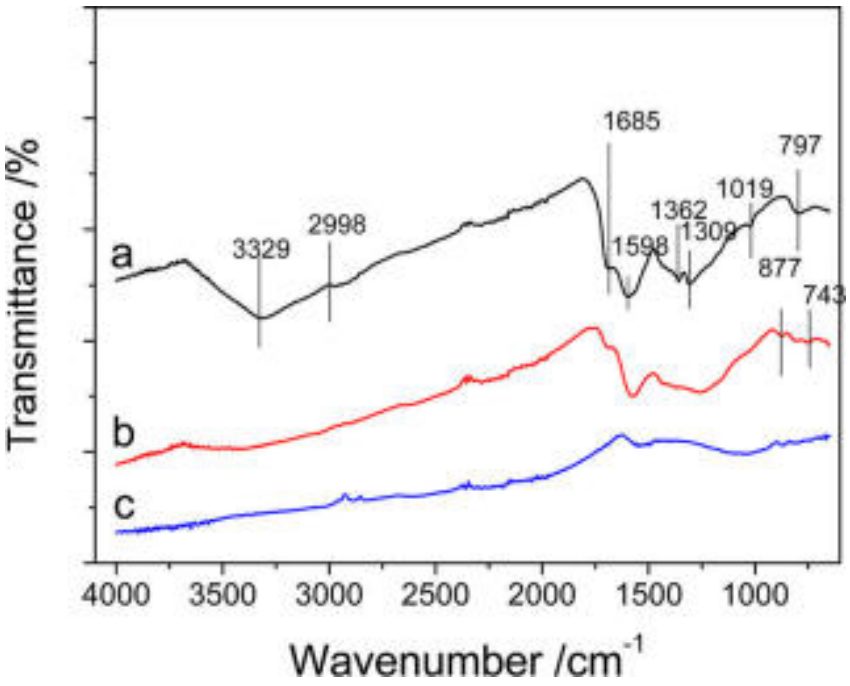

Figure 4.3 Fourier transform infrared (FTIR) spectra of Fe^{x}@CS-f (spectrum a), Fe^{x}@CS-350 (spectrum b), and Fe^{0}@CS-550 (spectrum c).

Figure 4.4 shows SEM images of Fe^{x}@CS-f, Fe^{x}@CS-350, Fe^{0}@CS-550, and Fe^{0}@CS-750. It was found that the prepared iron−carbon composites showed typical microspherical morphology. It is noted that the size of the carbon sphere is dramatically dependent on the synthesis conditions, such as glucose concentration, temperature and hydrothermal time [42]. In this study, a certain glucose concentration and hydrothermal condition were applied, and uniform carbon nanospheres can be obtained at the nanoscale level. The addition of an iron precursor significantly increased the size of carbon spheres, compared to bare spheres.

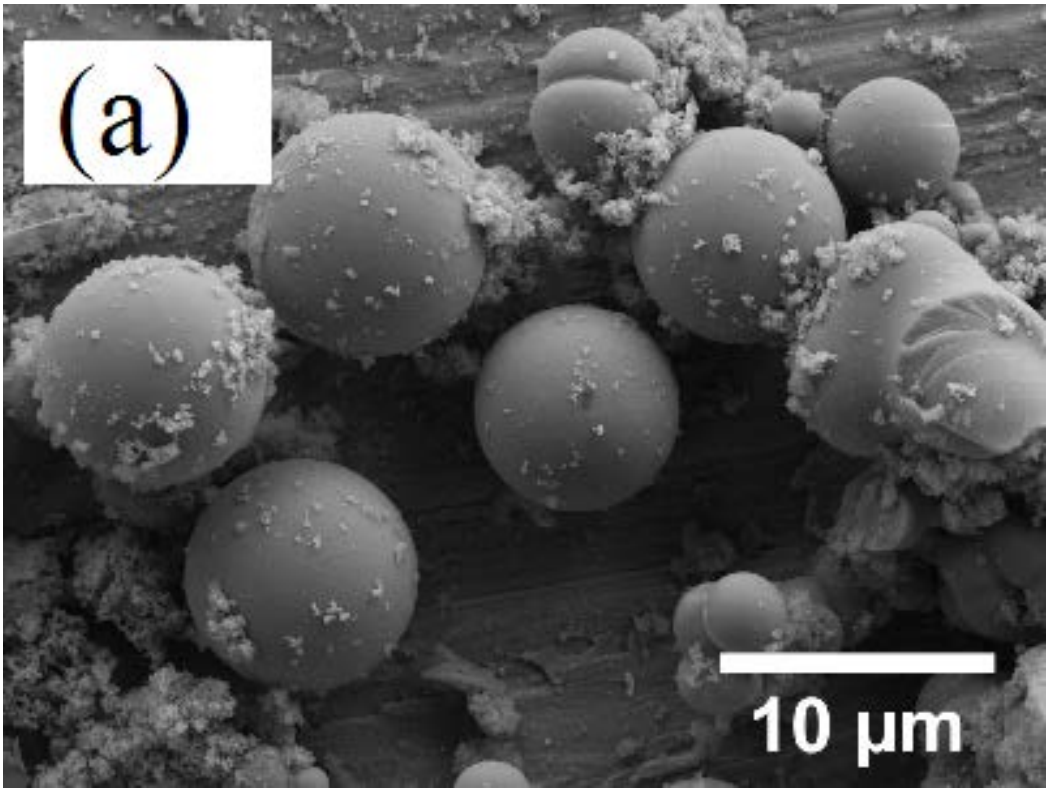
(a)
10 µm

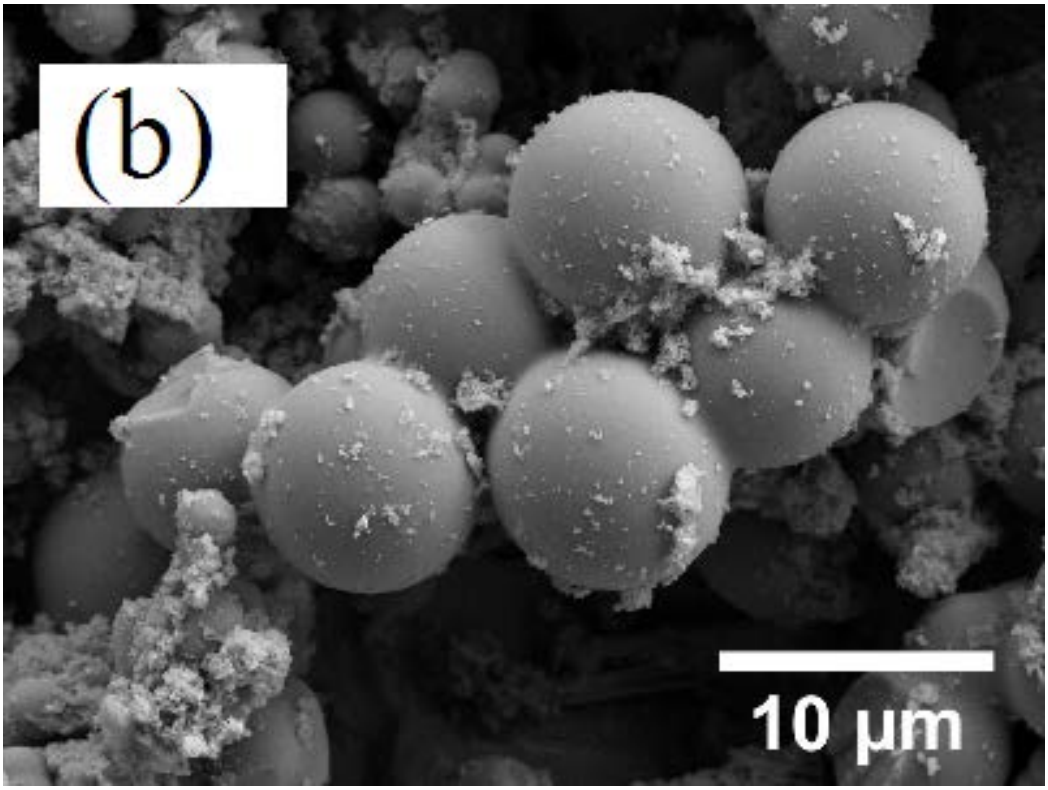
(b)
10 µm

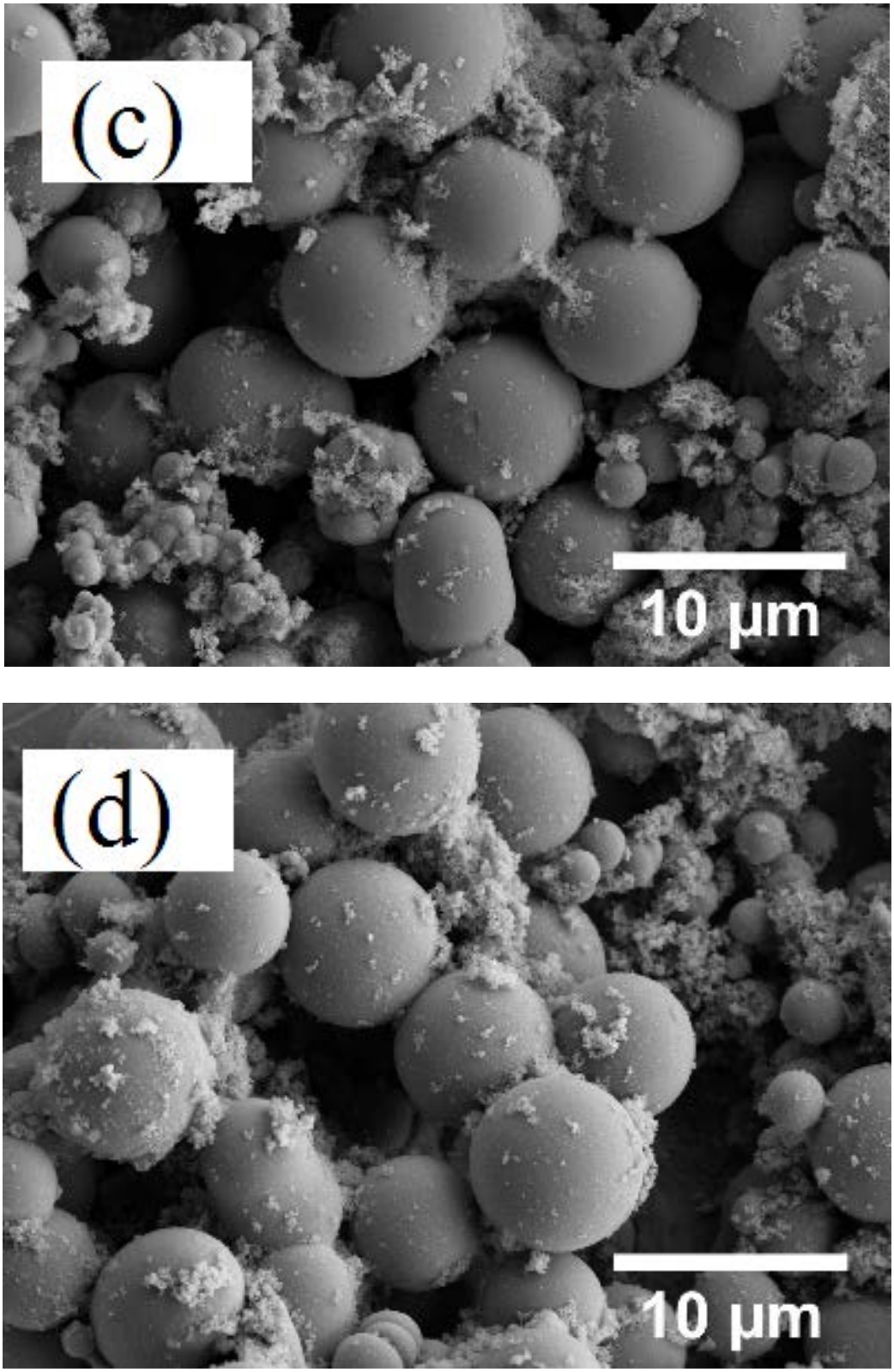

Figure 4.4 Scanning electron microscopy (SEM) images of (a) Fe^{x}@ CS-f, (b) Fe^{x}@CS-350, (c) Fe^{0}@CS-550, and (d) Fe^{0}@CS-750.

As a catalyst, microscale particles would be beneficial to easy separation. In this study, the size of the carbon sphere was ~6−8μm. Besides the microspheres, some fine particles (50−200nm) were found to attach to large spheres. Similar observation was reported by Yu et al [44]. In their study, Fe_xO_y was encapsulated in carbon spheres ca. 6μm in size. Individual energy-dispersive X-ray spectroscopy (EDS) analysis focusing on large spheres (0.23 at.% Fe) and fine particles (0.32 at.% Fe) showed similar iron atomic contents in Fe^0@CS-550. The detected Fe loading was much lower than that from TGA, indicating that iron was encapsulated into carbon. It was also found that calcination did not influence the spherical morphology. However, high-resolution SEM focusing on the surface of spheres showed that a porous structure was developed during calcination.

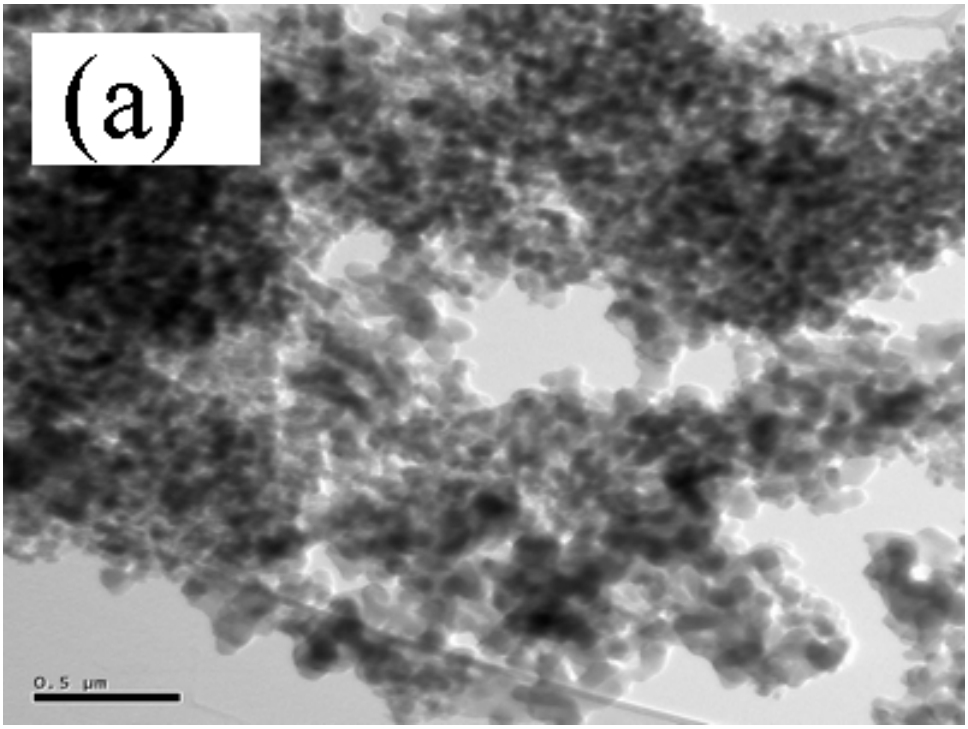

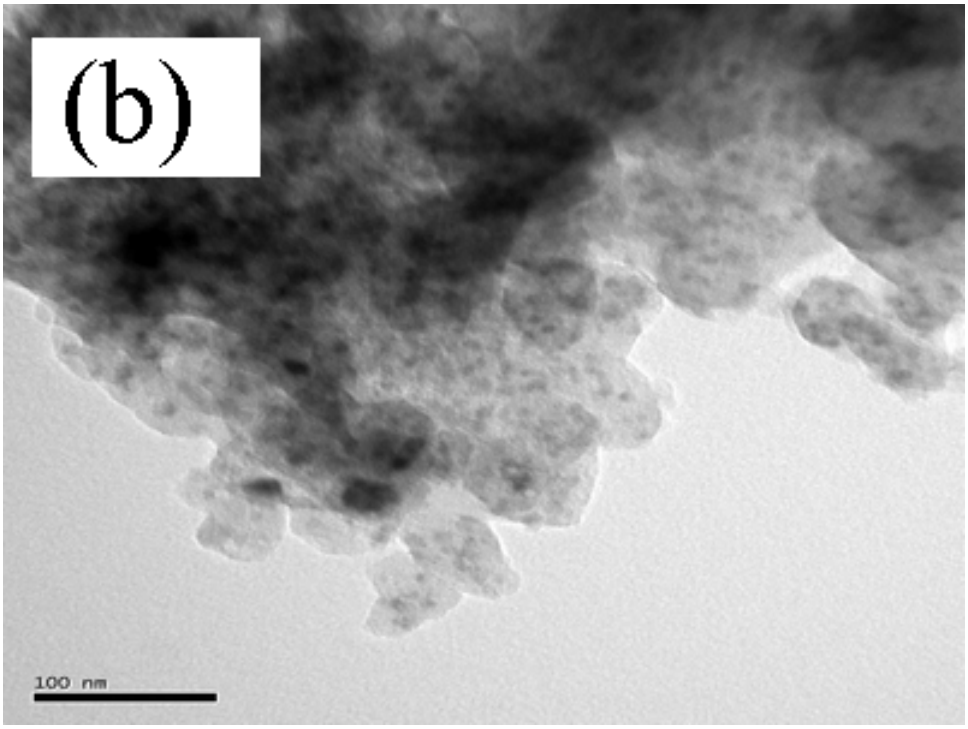

Figure 4.5 TEM images of (a) Fe^{x}@CS-f and (b) Fe^{0}@CS-550.

Figure 4.5 shows TEM images of Fe^{x}@CS-f and Fe^{0}@CS-550. For analysis, the samples were thoroughly ground to crush the large spheres into fine particles. It was seen that the large carbon spheres were aggregated by many nanoscale carbon particles (50−200nm). The nanoscale carbon showed a core/shell-like structure, in which the core of ZVI was ~5−10nm in diameter. Therefore, the nanoscale ZVI was evenly distributed and encapsulated within the spherelike carbon. The size of ZVI supported by polystyrene resins was found to be 5−20nm, whereas Fe loadings were 4−14.5wt %.25 The size of ZVI supported by kaolinite was characterized to be 44.3nm at a Fe loading of 20wt %.28 In NaY zeolite supported ZVI, the size was determined to be 50−100nm at a Fe loading of 1.8wt %.29 In ZVI supported by activated carbon, at a Fe loading of 8.2wt %, the iron particles showed a needle-like morphology, with dimensions of 30−500nm × 1000−2000nm. It was recalled that, in this study, the Fe loading was 22.9wt % in Fe^{0}@CS- 550. At such a high Fe content, Fe^{0} was still confined to be a very tiny size (5−10nm). Compared to other supported ZVI, which was

distributed at the surface of supports, the formation of smaller-sized Fe^0 in our samples was attributed to the three-dimensional (3D) distribution of in-situ-formed carbon spheres. In the hydrothermal carbonization processes, a great variety of glucose reactions would take place and result in a complex mixture of organic compounds. At an increasing temperature, some aromatic compounds and oligosaccharides would form and then lead to a short single burst of nucleation. The nuclei then grew up uniformly and isotropically by diffusion of solutes toward the particle surfaces [42, 45]. Once iron nitrate was introduced, the nuclei of Fe_xO_y would first appear. Then, Fe_xO_y would act as the nuclei for the subsequent formation of carbon spheres, because of the Coulombic interaction with the surface functional groups on carbon colloids. The produced Fe_xO_y -in-C nano-rods would then be self-assembled to Fe_xO_y@C spheres via further intermolecular dehydration [35]. Therefore, large spheres and a homogeneous distribution of iron were fabricated [44].

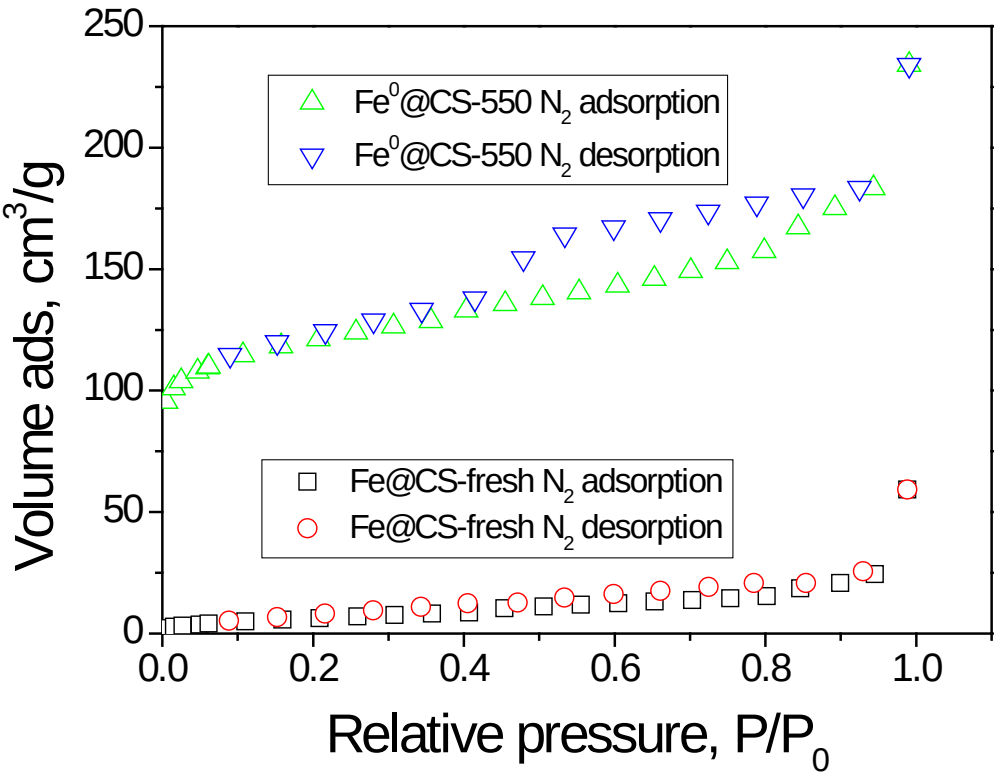

(A)

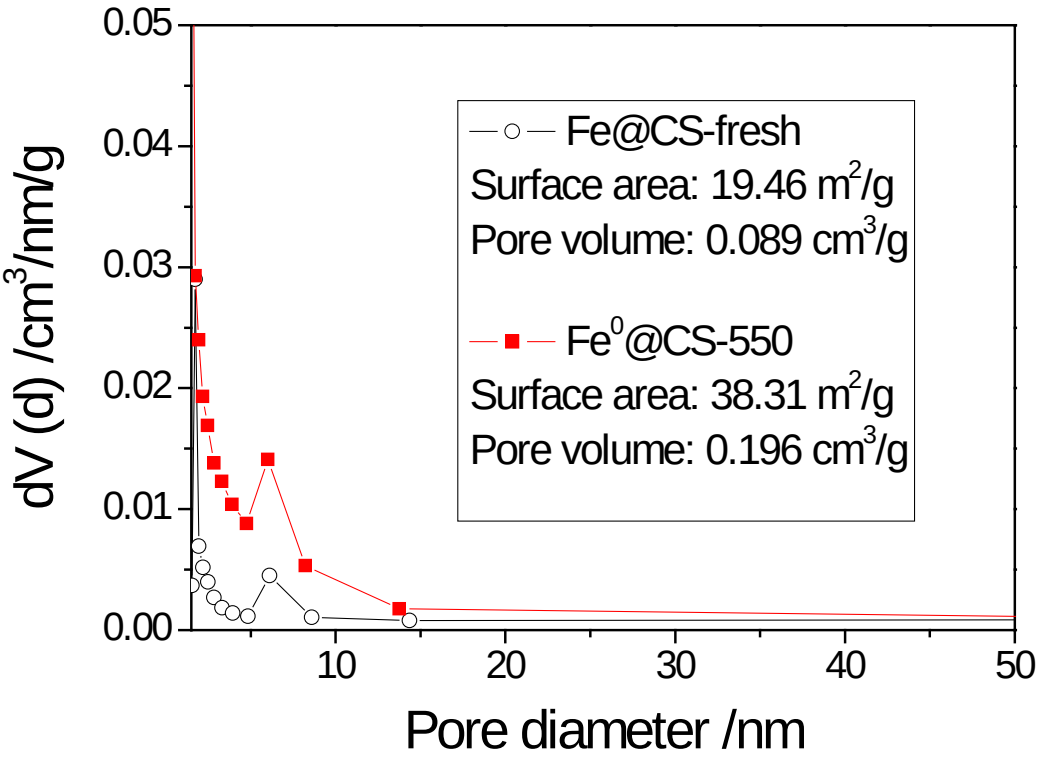

(B)

Figure 4.6 (A) N_2 adsorption/desorption isotherms of Fe^x@CS-f and Fe^x@CS-550 and (B) their pore size distributions.

Figure 4.6 shows N_2 adsorption/desorption isotherms of Fe^x@CS-f and Fe^0@CS-550 and pore size distributions. The specific surface area (S_{BET}) of Fe^x@CS-f was calculated to be 24.1m^2/g. After calcination at 550°C, the S_{BET} value of Fe0@CS-550 was significantly enhanced to be 414.4m^2/g. The specific surface area was higher than that of ZVI supported by carbon black (130m^2/g) [30], and also higher than another ZVI supported by carbon spheres (221m^2/g), which was activated at 1000 °C [33]. Referring to the International Union of Pure Applied Chemistry (IUPAC) classification, the adsorption isotherms of the samples were type IV and exhibited a type H_2 hysteresis loop. A hysteresis loop at p/p_0 = 0.4−0.9 was observed on Fe^0@CS-550, indicating the presence of a mesoporous structure [46, 47]. The pore volumes of Fe^x@CS-f and Fe^0@CS- 550 were 0.040 and 0.284cm^3/g, respectively. The size

of their pores was similar centered at 6−7nm. The increased pore volume and BET surface area after calcination were ascribed to the desorption of organic substances and partial oxidation of carbon by Fe_xO_y. The calcination would first desorb organic compounds and surface groups from the in situ formation of carbon spheres. Higher temperature led to the reduction reactions of Fe_xO_y, and carbon around iron oxide was oxidized to CO_2. Such reactions might act as activation processes for producing mesoporous pores in the carbon spheres.

4.3.2. Adsorption and Activation Performance of Nano-Fe^0@CS

Figure 4.7 shows the adsorption performances of iron (oxide)@CS, acquired from same procedure to oxidation without the addition of Oxone. The samples of Fe^x@CS-f and Fe^x@CS-350 only presented a minor adsorption of phenol, giving 6% of phenol adsorption at 20ppm in 60min. The low adsorption was due to the small S_{BET} value and pore volume. Calcination under N_2 would lead to further carbonization of the carbon spheres and desorption of the organic species, thereby resulted in a larger specific surface area. The reduction between iron oxide and carbon for the formation of ZVI would also enlarge the pore volume of the carbon spheres. As a result, Fe^0@CS-550 showed a phenol adsorption of 21%, while Fe^0@ CS-750 gave 30% phenol adsorption under the same conditions.

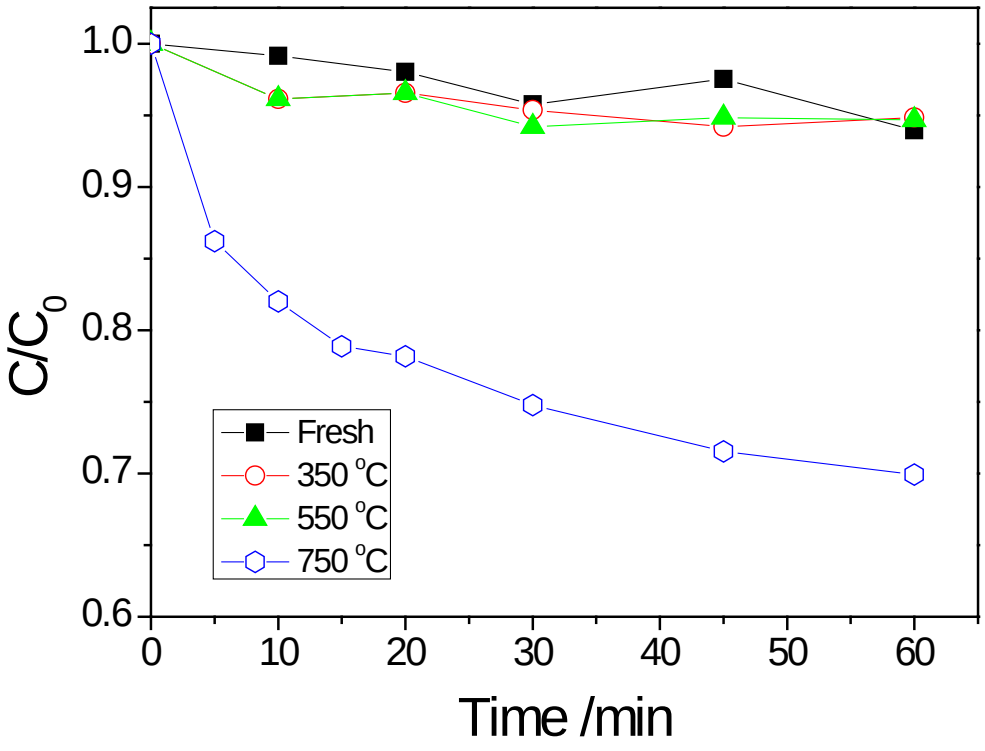

Figure 4.7 Adsorption of phenol on iron@CS at different calcination temperatures.

[Conditions: phenol amount, 20 ppm; temperature, 30°C; catalyst concentration, 0.5 g/L.]

Figure 4.8 shows the oxidation of phenol solutions using iron/carbon annealed at different temperatures. Fe^{x}@CS-f was able to degrade 34.8% of phenol at 60 min, while Fe^{x}@CS-350 only removed 8.1% of phenol at the same time. As shown by TGA, the iron species in Fe^{x}@CS-f was iron(III) hydroxide, then the phenol oxidation was possibly due to the activation of PMS by Fe(III). Calcination at 350 °C might convert iron(III) hydroxide to be FeOOH or Fe_2O_3, resulting in a lower degradation rate. When the calcination temperature reached 520 °C or above, iron oxides would be reduced by carbon to ZVI. Therefore, Fe^{0}@CS-550 and Fe^{0}@CS-750 showed similar activity in the degradation of phenol with PMS. Both samples were able to completely decompose phenol in 15 min.

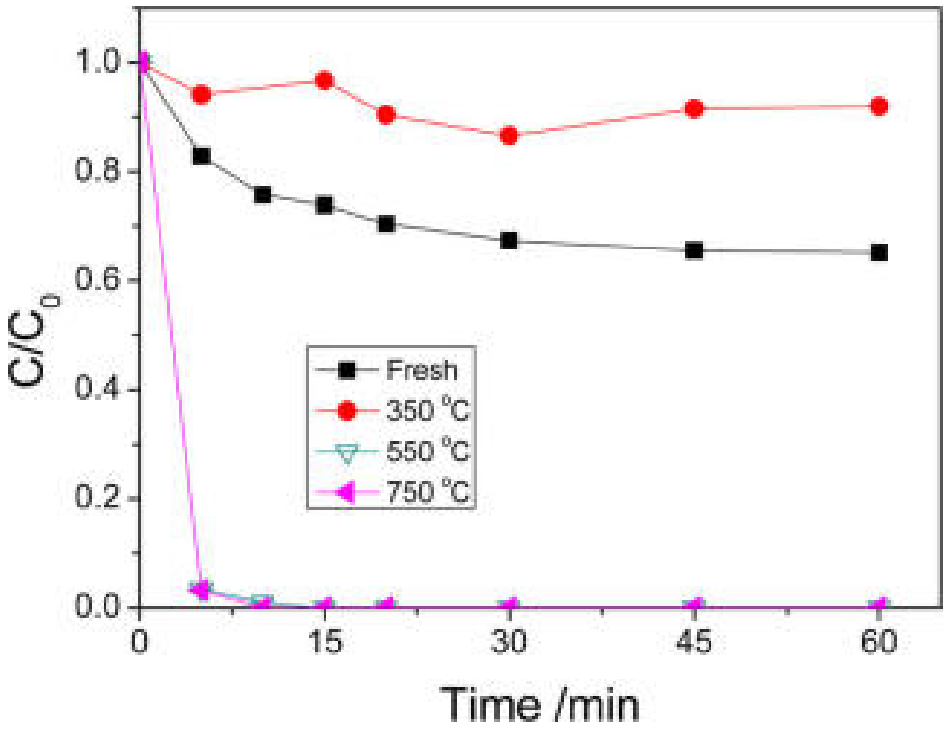

Figure 4.8 Effect of calcination temperature on the activity of oxidation of phenol with PMS. [Conditions: phenol amount, 20ppm; temperature, 30°C; PMS concentration, 2g/L; catalyst concentration, 0.5g/L.]

Figure 4.9 shows the performance of different ZVI materials in the activation of PMS for phenol degradation. Without a ZVI material, PMS was not able to degrade phenol by itself. At 90min, the degradation efficiencies on commercial Fe0, HR-Fe^0, and Fe^0@CS-550 were 15.8%, 54.6%, and 86.9%, respectively. The results strongly suggested that nanoscale ZVI can provide a faster activity in the oxidation of phenol: the smaller the size, the better the activity.

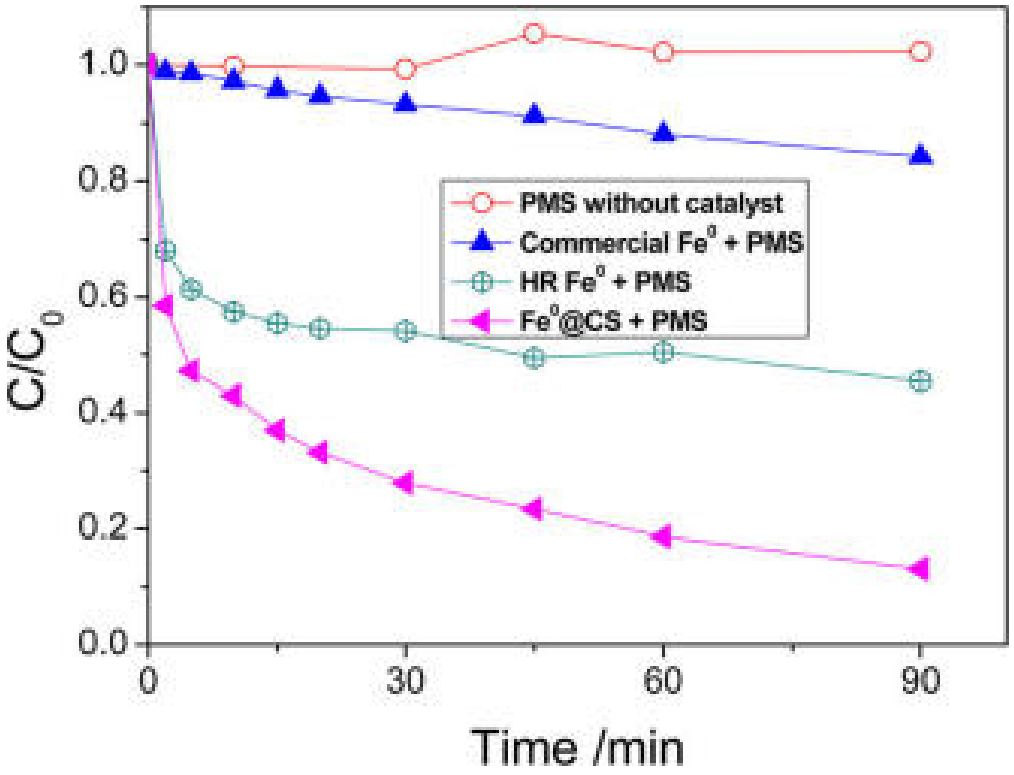

Figure 4.9 Degradation of phenol using different ZVI materials with PMS. [Conditions: phenol amount, 20ppm; temperature, 25°C; PMS concentration, 0.5g/L; catalyst concentration, 0.5g/L of Fe^0@CS-550, and 0.115g/L of HR-Fe^0 and commercial Fe^0.]

Figure 4.10 further compares the activities of various materials in homogeneous or heterogeneous activation of PMS for the oxidation of phenol. It was seen that iron oxides (Fe_2O_3 or Fe_3O_4) could only show minor activity, providing a phenol conversion of <10% after 90min of reaction. In homogeneous reaction, Fe(II) showed 25.3% phenol degradation after 90min, while Fe(III) produced 51.1% phenol degradation.

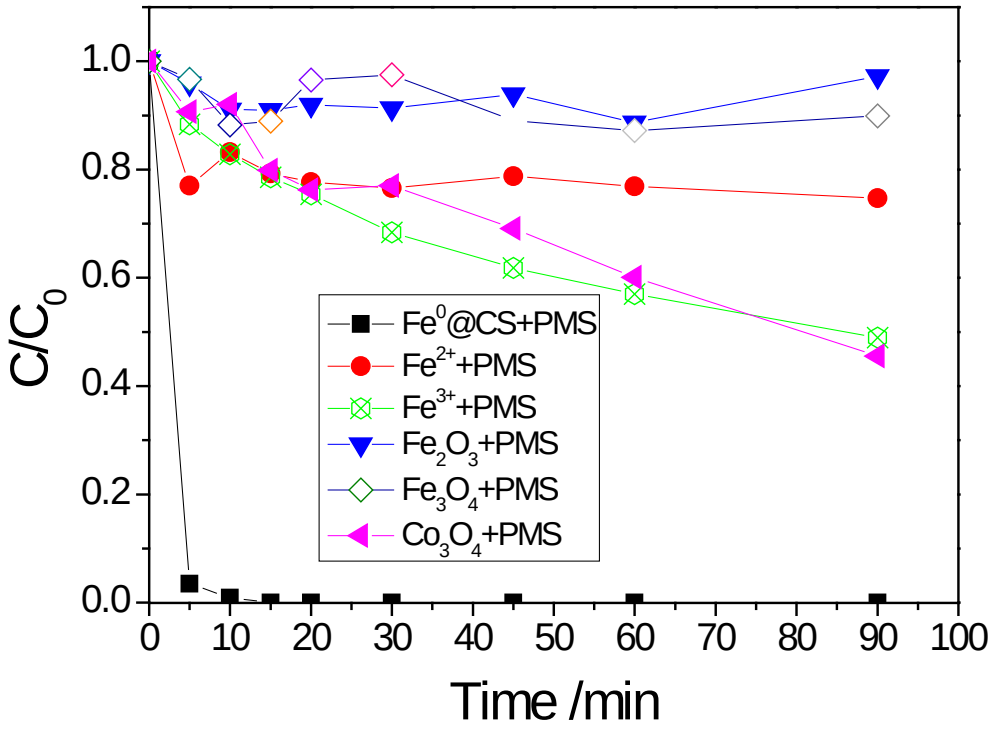

Figure 4.10 Degradation of phenol solutions using various catalysts. [Conditions: phenol amount, 20ppm; temperature, 30°C; PMS concentration, 2g/L; catalyst concentration, 0.5g/L of Fe^0@CS-550, Fe_2O_3, Fe_3O_4, and Co_3O_4, and 0.05M of Fe(II) and Fe(III).]

Cobalt oxide (Co_3O_4) has been widely used to activate PMS, and, so far, it has shown the best activity [12, 36, 37, 48]. In this study, Co_3O_4 that was prepared via the thermal decomposition of cobalt(II) nitrate was also tested and it produced 54.5% phenol removal after 90min, which was comparable to that of Fe(III). Among all the materials, Fe^0@CS-550 displayed the best performance in the activation of PMS for phenol degradation. It achieved complete phenol removal within 15min.

In the reaction of HR-Fe^0 with PMS, it was found that Fe powders were completely dissolved during the reaction. It was interesting to evaluate the reusability of Fe^0@CS-550 as well as its

stability. It was found that the activity rapidly decreased after second and third runs, providing 31.7% and 13.4% phenol removal, respectively. The reduction in phenol degradation was possibly due to Fe^0 conversion to Fe(II)/Fe(III) in reaction. The corrosion processes led to decreased amounts of effective catalyst in the recovered material. Without the support of carbon spheres, the efficiency after the second run would be zero, because all of the ZVI was dissolved. Therefore, Fe^0@CS-550 showed a better performance in reusability for potential application than bare ZVI, because of the remaining activity after second and third runs. Moreover, after the first run, the collected reaction solution was fed with phenol and PMS again at the same concentrations as in the first run, but it only showed 2% phenol removal, suggesting that dissolved Fe ions were ineffective for phenol oxidation.

The high activity and the stability of nano-Fe^0@CS in the activation of PMS were due to the nature of ZVI and the unique structure. ZVI may provide a higher efficiency in activating PMS than Fe(II), as shown in eq 4-9:

$$Fe^0 + 2HSO_5^- \rightarrow Fe^{2+} + SO_4^{-\bullet} + 2OH^- \quad (4\text{-}9)$$

In this case, the concentration of sulfate radicals produced by ZVI are 3 times higher than that of Fe(II) per mole. This is the reason why ZVI shows a higher activity than Fe ions and oxides. The mechanism of higher activity of nano-Fe^0@CS than unsupported ZVI would be ascribed to the porous structure of carbon spheres and the core/shell structure of Fe@carbon. First, the encapsulation of carbon would play a significant role in the controllable release of Fe(II) ions. Second, the porous structure and the large SBET value would attract phenol molecules from the homogeneous solution to the surface of carbon spheres. Therefore, the $SO4^{-\bullet}$ produced would prefer to oxidize phenol, rather than be quenched by Fe(II). The

carbon shell would also prevent the fast corrosion of iron as bare nano ZVI.

4.4. Conclusion

Nanoscaled zerovalent iron (ZVI) encapsulated in carbon spheres (nano-Fe^0@CS) was fabricated using a green chemistry route. The structure of Fe^0@CS consisted of carbon spheres (6−8μm) composed of fine carbon particles (50−200nm) encapsulating nanosized ZVI (5−10nm). The iron/carbon hybrids annealed at 550°C showed a porous structure with high specific surface area and pore volume. The carbon facilitated a good Fe dispersion by an in situ reduction and increased the stability of nanoscaled ZVI. Fe^0@CS showed an efficient activity in producing oxidative radicals from PMS, thus leading to a superior performance in degradation of phenol to homogeneous iron/PMS and cobalt oxide/PMS. The higher activity of Fe^0@CS was attributed to the nature of ZVI and the unique structure. The core of the design was to fabricate a porous structure for attracting substrates, and to controllably release Fe ions to avoid the quenching of active radicals. Therefore, nano-Fe^0@CS-550 has been demonstrated to be a promising material for environmental remediation.

4.5. References

1. *Ryu, A., et al.,* Reduction of highly concentrated nitrate using nanoscale zero-valent iron: Effects of aggregation and catalyst on reactivity. *Applied Catalysis B-Environmental, 2011. 105(1-2): p. 128-135.*

2. *Shi, Z., J.T. Nurmi, and P.G. Tratnyek,* Effects of Nano Zero-Valent Iron on Oxidation-Reduction Potential. *Environmental Science & Technology, 2011. 45(4): p. 1586-1592.*

3. *Zhang, M., et al.,* Degradation of soil-sorbed trichloroethylene by stabilized zero valent iron nanoparticles: Effects of sorption, surfactants, and natural organic matter. *Water Research, 2011. 45(7): p. 2401-2414.*

4. *Song, H. and E.R. Carraway,* Reduction of chlorinated ethanes by nanosized zero-valent iron: Kinetics, pathways, and effects of reaction conditions. *Environmental Science & Technology, 2005. 39(16): p. 6237-6245.*

5. *Bandstra, J.Z., et al.,* Reduction of 2,4,6-trinitrotoluene by iron metal: Kinetic controls on product distributions in batch experiments. *Environmental Science & Technology, 2005. 39(1): p. 230-238.*

6. *Nam, S. and P.G. Tratnyek,* Reduction of azo dyes with zero-valent iron. *Water Research, 2000. 34(6): p. 1837-1845.*

7. *Keum, Y.S. and Q.X. Li,* Reduction of nitroaromatic pesticides with zero-valent iron. *Chemosphere, 2004. 54(3): p. 255-263.*

8. *Ponder, S.M., J.G. Darab, and T.E. Mallouk,* Remediation of Cr(VI) and Pb(II) aqueous solutions using supported, nanoscale zero-valent iron. *Environmental Science & Technology, 2000. 34(12): p. 2564-2569.*

9. *Yoon, I.-H., et al.,* Reduction and adsorption mechanisms of selenate by zero-valent iron and related iron corrosion. *Applied Catalysis B-Environmental, 2011. 104(1-2): p. 185-192.*

10. *Joo, S.H., A.J. Feitz, and T.D. Waite,* Oxidative degradation of the carbothioate herbicide, molinate, using nanoscale zero-valent iron. *Environmental Science & Technology, 2004. 38(7): p. 2242-2247.*

11. *Shukla, P., et al.,* Nanosized Co3O4/SiO2 for heterogeneous oxidation of phenolic contaminants in waste water. *Separation and Purification Technology, 2011. 77(2): p. 230-236.*

12. *Shukla, P.R., et al.,* Activated carbon supported cobalt catalysts for advanced oxidation of organic contaminants in aqueous solution. *Applied Catalysis B-Environmental, 2010. 100(3-4): p. 529-534.*

13. *Kim, D.-h., J. Kim, and W. Choi,* Effect of magnetic field on the zero valent iron induced oxidation reaction. *Journal of Hazardous Materials, 2011. 192(2): p. 928-931.*

14. *Lee, C., C.R. Keenan, and D.L. Sedlak,* Polyoxometalate-enhanced oxidation of organic compounds by nanoparticulate zero-valent iron and ferrous ion in the presence of oxygen. *Environmental Science & Technology, 2008. 42(13): p. 4921-4926.*

15. *Kallel, M., et al.,* Olive mill wastewater degradation by Fenton oxidation with zero-valent iron and hydrogen peroxide. *Journal of Hazardous Materials, 2009. 163(2-3): p. 550-554.*

16. *Zhou, T., et al.,* Oxidation of 4-chlorophenol in a heterogeneous zero valent iron/H2O2 Fenton-like system: Kinetic, pathway and effect factors. *Separation and Purification Technology, 2008. 62(3): p. 551-558.*

17. *Boussahel, R., et al.,* Degradation of obsolete DDT by Fenton oxidation with zero-valent iron. *Desalination, 2007. 206(1-3): p. 369-372.*

18. *Kusic, H., et al.,* Modeling of iron activated persulfate oxidation treating reactive azo dye in water matrix. *Chemical Engineering Journal, 2011. 172(1): p. 109-121.*

19. *Zhao, J., et al.,* Enhanced oxidation of 4-chlorophenol using sulfate radicals generated from zero-valent iron and peroxydisulfate at ambient temperature. *Separation and Purification Technology, 2010. 71(3): p. 302-307.*

20. *Liang, C. and Y.-y. Guo,* Mass Transfer and Chemical Oxidation of Naphthalene Particles with Zerovalent Iron Activated Persulfate. *Environmental Science & Technology, 2010. 44(21): p. 8203-8208.*

21. *Lee, Y.-C., et al.,* Microwave-hydrothermal decomposition of perfluorooctanoic acid in water by iron-activated persulfate oxidation. *Water Research, 2010. 44(3): p. 886-892.*

22. *Liang, C. and M.-C. Lai,* Trichloroethylene degradation by zero valent iron activated persulfate oxidation. *Environmental Engineering Science, 2008. 25(7): p. 1071-1077.*

23. *Rastogi, A., S.R. Ai-Abed, and D.D. Dionysiou,* Sulfate radical-based ferrous-peroxymonosulfate oxidative system for PCBs degradation in aqueous and sediment systems. *Applied Catalysis B-Environmental, 2009. 85(3-4): p. 171-179.*

24. *Li, Y., et al.,* Enhanced removal of pentachlorophenol by a novel composite: Nanoscale zero valent iron immobilized on organobentonite. *Environmental Pollution, 2011. 159(12): p. 3744-3749.*

25. *Jiang, Z., et al.,* Nitrate reduction using nanosized zero-valent iron supported by polystyrene resins: Role of surface functional groups. *Water Research, 2011. 45(6): p. 2191-2198.*

26. *Karabelli, D., et al.,* Preparation and characterization of alumina-supported iron nanoparticles and its application for the removal of aqueous Cu2+ ions. *Chemical Engineering Journal, 2011. 168(2): p. 979-984.*

27. *Chen, Z.-x., et al.,* Removal of methyl orange from aqueous solution using bentonite-supported nanoscale zero-valent iron. *Journal of Colloid and Interface Science, 2011. 363(2): p. 601-607.*

28. *Zhang, X., et al.,* Kaolinite-supported nanoscale zero-valent iron for removal of Pb2+ from aqueous solution: Reactivity, characterization and mechanism. *Water Research, 2011. 45(11): p. 3481-3488.*

29. *Wang, W., et al.,* Novel NaY zeolite-supported nanoscale zero-valent iron as an efficient heterogeneous Fenton catalyst. *Catalysis Communications, 2010. 11(11): p. 937-941.*

30. *Hoch, L.B., et al.,* Carbothermal synthesis of carbon-supported nanoscale zero-valent iron particles for the remediation of hexavalent chromium. *Environmental Science & Technology, 2008. 42(7): p. 2600-2605.*

31. *Zhu, H., et al.,* Removal of arsenic from water by supported nano zero-valent iron on activated carbon. *Journal of Hazardous Materials, 2009. 172(2-3): p. 1591-1596.*

32. *Lv, X., et al.,* Removal of chromium(VI) from wastewater by nanoscale zero-valent iron particles supported on multiwalled carbon nanotubes. *Chemosphere, 2011. 85(7): p. 1204-1209.*

33. *Sunkara, B., et al.,* Nanoscale Zerovalent Iron Supported on Uniform Carbon Microspheres for the In situ Remediation of Chlorinated Hydrocarbons. *Acs Applied Materials & Interfaces, 2010. 2(10): p. 2854-2862.*

34. *Sohn, K., et al.,* Fe(0) nanoparticles for nitrate reduction: Stability, reactivity, and transformation. *Environmental Science & Technology, 2006. 40(17): p. 5514-5519.*

35. *Liu, H., et al.,* Aggregate Nanostructures of Organic Molecular Materials. *Accounts of Chemical Research, 2010. 43(12): p. 1496-1508.*

36. *Shukla, P., et al.,* Co-SBA-15 for heterogeneous oxidation of phenol with sulfate radical for wastewater treatment. *Catalysis Today, 2011. 175(1): p. 380-385.*

37. *Shukla, P., et al.,* Cobalt exchanged zeolites for heterogeneous catalytic oxidation of phenol in the presence of peroxymonosulphate. *Applied Catalysis B-Environmental, 2010. 99(1-2): p. 163-169.*

38. *Shukla, P., et al.,* Adsorption and heterogeneous advanced oxidation of phenolic contaminants using Fe loaded mesoporous SBA-15 and H2O2. *Chemical Engineering Journal, 2010. 164(1): p. 255-260.*

39. *Crane, R.A., et al.,* Magnetite and zero-valent iron nanoparticles for the remediation of uranium contaminated environmental water. *Water Research, 2011. 45(9): p. 2931-2942.*

40. *Bumajdad, A., S. Ali, and A. Mathew,* Characterization of iron hydroxide/oxide nanoparticles prepared in microemulsions stabilized with cationic/non-ionic surfactant mixtures. *Journal of Colloid and Interface Science, 2011. 355(2): p. 282-292.*

41. *Feyzi, M., M. Irandoust, and A.A. Mirzaei,* Effects of promoters and calcination conditions on the catalytic performance of iron-manganese catalysts for Fischer-Tropsch synthesis. *Fuel Processing Technology, 2011. 92(5): p. 1136-1143.*

42. *Sevilla, M. and A.B. Fuertes,* The production of carbon materials by hydrothermal carbonization of cellulose. *Carbon, 2009. 47(9): p. 2281-2289.*

43. *Zhang, T., et al.,* Surface hydroxyl groups of synthetic alpha-FeOOH in promoting (OH)-O-center dot generation from aqueous ozone: Property and activity relationship. *Applied Catalysis B-Environmental, 2008. 82(1-2): p. 131-137.*

44. *Yu, G., et al.,* FexOy@C Spheres as an Excellent Catalyst for Fischer-Tropsch Synthesis. *Journal of the American Chemical Society, 2010. 132(3): p. 935-+.*

45. *Sun, X.M. and Y.D. Li,* Colloidal carbon spheres and their core/shell structures with noble-metal nanoparticles. *Angewandte Chemie-International Edition, 2004. 43(5): p. 597-601.*

46. *Hardjono, Y., et al.,* Synthesis of Co oxide doped carbon aerogel catalyst and catalytic performance in heterogeneous oxidation of phenol in water. *Chemical Engineering Journal, 2011. 174(1): p. 376-382.*

47. *Zhou, G., et al.,* Synthesis of carbon xerogels at varying sol-gel pHs, dye adsorption and chemical regeneration. *Chemical Engineering Journal, 2011. 171(3): p. 1399-1405.*

48. *Zhou, G., et al.,* Titanate supported cobalt catalysts for photochemical oxidation of phenol under visible light irradiations. *Separation and Purification Technology, 2011. 80(3): p. 626-634.*

5

Chapter 5: Microcarbon sphere supported cobalt catalysts for chemical oxidation of phenol

Abstract

Cobalt nitrate and glucose were employed to prepare microcarbon sphere supported cobalt catalysts (micro-CS@Co) via a hydrothermal carbonization method for chemical oxidation of phenol with peroxymonosulfate (PMS, oxone). The characterization of prepared micro-CS@Co was conducted by means of scanning electron microscopy (SEM), energy-dispersive spectroscopy (EDS), X-ray diffraction (XRD) and nitrogen adsorption/desorption isotherms. micro-CS@Co not only showed high efficiency in activation of PMS, but also offered a good stability. Kinetics were carried out to investigate the effect of oxidant and catalyst amount, temperature on the efficiencies of phenol degradation.

5.1. Introduction

The development of various synthesis industries including polycarbonates, epoxies, Bakelite, nylon, detergents, herbicides, resin paint, dyes, textile wood, pulp mill, and pharmaceutical drugs [1-3], has discharged a large range of toxic organic pollutants into wastewater. Such pollution has caused a severe challenge to the sustainably development of the world. Organic pollutants such as phenol are highly toxic and extremely refractory to degradation by natural environment, and causing potential threats to water systems and general public. Both source control and remediation technology are highly required. The industries need to manage the manufacturing sections to reduce the pollutants below permissible level in order to avoid harmful effects; meanwhile the techniques need to be developed to remove organic compounds from natural water bodies and wastewater system.

Owing to the complete degradation of organic pollutants in wastewater, advanced oxidation processes (AOPs) have attracted great interests in wastewater treatment. Various AOP techniques such as ozonation, wet air oxidation, thermal destruction, and homogeneous/ heterogeneous oxidation, have been investigated, and proven effective in oxidising organic compounds in wastewater to water and carbon oxide as final products [4-7]. Fenton reaction is a typical AOP technique involving formation of free hydroxyl radicals in the presence of Fe^{2+} ions. The free hydroxyl radicals generated by Fenton's reagent or Fenton like reagent are powerful, non-selective oxidants, and have been successfully employed in industries for decades [8]. Although Fenton reagent or Fenton-like reactions are used in some industrial applications for wastewater treatment, the barriers of these techniques are experienced: i) requirement of low pH; ii) quenching of hydroxyl radical by carbonate species present in system; iii) production of precipitate [9-13]. The cobalt activating peroxymonosulfate (PMS, oxone) to produce sulphate radicals for oxidation of organic pollutants demonstrated

significant results in many recent studies [9, 14-16]. The activation reactions proceed as follows [9, 10, 17]:

$$Co^{2+} + HSO_5^- \rightarrow Co^{3+} + SO_4^{\bullet -} + OH^- \quad (5\text{-}1)$$

$$Co^{3+} + HSO_5^- \rightarrow Co^{2+} + SO_5^{\bullet -} + H^+ \quad (5\text{-}2)$$

However, the oxidation process involving the utilization of oxone and cobalt ion has several problems as well. The major one is that cobalt ions are toxic and leading to health issues. So, new types of heterogeneous cobalt based catalysts are highly demanded to avoid cobalt being discharged in water, and to improve the oxidation efficiency via support materials. Recently, cobalt catalysts supported by novel carbon materials, such as carbon nanofibers [18, 19], carbon nanotubes [20], and multi-walled carbon tubes [21], and micro/nano carbon spheres [20, 22] were prepared and investigated in oxidation reactions.

In this chapter, microcarbon sphere supported cobalt catalysts were prepared for advanced oxidation of phenol utilizing oxone. It was found that the supported cobalt catalysts showed high activity in phenol oxidation reactions and remained stable in multi-run tests.

5.2. Experimental

5.2.1. Materials

D-glucose (99.5%) was purchased from Sigma. **Cobalt (II) nitrate hexahydrate** ($Co(NO_3)_2 \cdot 6H_2O$) from Sigma was used as a Co precursor. **PMS** (oxone, peroxymonosulfate) was obtained from Aldrich, and used as an oxidant. **Pure methanol** was from Chem Supply. **Phenol** was obtained from Aldrich, and used to prepare pollutant solution. **Urea** (NH_2CONH_2) was purchased from Sigma-Aldrich.

5.2.2. Preparation of micro-CS@Co

Micorcarbon supported cobalt catalysts were prepared by a hydrothermal method [24, 25]. In a typical synthesis, 2.97 g of cobalt (II) nitrate hexahydrate, 7.24 g of D-glucose and 1.20 g of urea were dissolved in 80 mL of ultrapure water. The mixture was stirred for 6 h. Then the mixed solution was transferred into a 120 mL Teflon-lined autoclave. The reactor was put in an oven and heated at 180 ^{o}C for 18h. Then the reactor was naturally cooled down to room temperature. The obtained black precipitate was filtrated and washed with methanol twice and water three times. The precipitate was then dried in an oven at 70 ^{o}C in the air. Later, the dry samples were calcined in the air at 300 , 400, or 500 ^{o}C for 2 h in a crucible with a cover and at a heating rate of 5 ºC/min. Final samples were denoted as micro-CS@Co-300^{o}C, 2h, Air; micro-CS@Co-400^{o}C, 2h, Air; and micro-CS@Co-500^{o}C, 2h, Air, respectively.

5.2.3. Characterization of catalysts

The crystalline structures of microcarbon sphere supported catalysts were analyzed by powder X-ray diffraction (XRD). The spectra were obtained on a Germany Burker D8-Advance X-ray diffractometer with Cu Kα radiation (λ=1.5418Å). Scanning electron microscopy (SEM), energy-dispersive spectroscopy (EDS), and cobalt elemental mapping, performed on a Zeiss Neon 40EsB FIBSEM, were used to evaluate the morphology, size, and texture information of the samples. The Brunauer− Emmett−Teller (BET) surface area and pore size distribution were evaluated by nitrogen sorption at −196 °C, using a Quantachrome Autosorb AS-1 system. The samples were evaporated under vacuum at 200 °C for 4 h prior to the adsorption measurements.

5.2.4. Chemical oxidation of phenol

Oxidation of phenol was carried out in a 1 L of Pyrex double-jacket reactor. A water bath and pump were used to maintain the reaction temperature at 30^{o}C. 0.25 g of micro-CS@Co catalyst was added into 200mL of 20 ppm phenol solution, and the mixture was stirred for 5 min. Then 0.4 g of PMS was added into mixed solution to start the oxidation reaction. At each set time interval, 1mL solution was withdrawn by a 5 mL syringe and filtrated by a 0.25 μm Millipore film into a vial, which was filled with 0.5 mL of pure methanol as a quenching reagent. In stability tests, used catalysts were filtrated and washed by water twice, and then dried in an oven at 70 ^{o}C in the air. The concentrations of phenol solution samples were analyzed by a Varian high performance liquid chromatography (HPLC) with a UV detector set at λ=270 nm. 30% CH_3CN and 70% ultrapure water were combined as mobile phase at a flow rate of 1 mL/min. All experiments employing used catalysts were run in the same reaction conditions as mentioned above.

5.3. Results and discussion

5.3.1. Characterization of micro-CS@Co

Figure 5.1 XRD patterns of carbon sphere and micro-CS@Co-raw 8h

Figure 5.1 shows XRD patterns of two synthesized samples: carbon sphere and micro-CS@Co-raw, which was not calcined in the air. Further, these two catalysts were used as reference samples. Micro-CS@Co-raw and pure carbon sphere did not show any Co crystalline structure peak. The fluctuation between 20 and 30^{o} showed typical diffractions of carbon material [23]. However, in comparison of carbon sphere and micro-CS@Co-raw, the difference of two lines showed that cobalt (II) nitrate might transform to intermediate products.

Figure 5.2 XRD patterns of carbon sphere, micro-CS@Co-raw, and micro-CS@Co, 300^{o}C, 2h, Air.

Figure 5.2 shows that micro-CS@Co, 300^{o}C, 2h, Air did not have peaks that could be assigned to Co_3O_4. It was reported that the decomposition of the Co-B amorphous alloy can occur with the heat treatment above 300 ^{o}C [24]. However, in Figure 5.2, no peaks corresponding to metallic cobalt was detected with the decomposition of Co-B which might be caused by the small amount of formed metallic cobalt [25]. This is also probably because the cobalt particles on this catalyst are too small to be detected by XRD (<4 nm) [3, 4]. Therefore, it might show that cobalt (II) nitrate turned into cobalt (III) hydroxide or cobalt (II) hydroxide as precipitate after the hydrothermal reaction [3]. The calcination at 300 ^{o}C for 2 h could not convert cobalt (III) hydroxide to Co_3O_4.

Figure 5.3 XRD patterns of carbon sphere, micro-CS@Co-raw, and micro-CS@Co, 400^{o}C, 2h, Air.

Figure 5.3 indicates that the support material of microcarbon sphere presented as amorphous phase, but a minor peak at 36.4^{o} was observed and attributed to the presence of crystalline Co_3O_4 [26]. Another extremely weak peak at 38.1^{o} can be ascribed to the phase of cobalt (III) hydroxide or cobalt (II) hydroxide [3]. The presence of trace quantity of cobalt was also confirmed by EDS analysis, which was discussed later in this section.

Figure 5.4 XRD patterns of carbon sphere, micro-CS@Co-raw, and micro-CS@Co, 500^{o}C, 2h, Air.

Figure 5.5 XRD patterns of micro-CS@Co, 300^{o}C, 2h, Air, micro-CS@Co, 400^{o}C, 2h, Air, and micro-CS@Co, 500^{o}C, 2h, Air.

Figure 5.4 shows that micro-CS@Co, 500^{o}C, 2h, Air showed distinct peaks of Co_3O_4 crystallites with Co(220) at 2θ=32.1^{o}, Co(311) at 2θ=37.4^{o}, Co(400) at 2θ=44.6^{o}, Co(511) at 2θ=59.8^{o}, and Co(440) at 2θ=67.1^{o} [27]. Furthermore, Figure 5.5 compares three main catalysts: micro-CS@Co, 300^{o}C, 2h, Air, micro-CS@Co, 400^{o}C, 2h, Air, and micro-CS@Co, 500^{o}C, 2h, Air. It was found that at increased calcination temperature, cobalt (II) nitrate turned into Co_3O_4 crystallites.

(A)

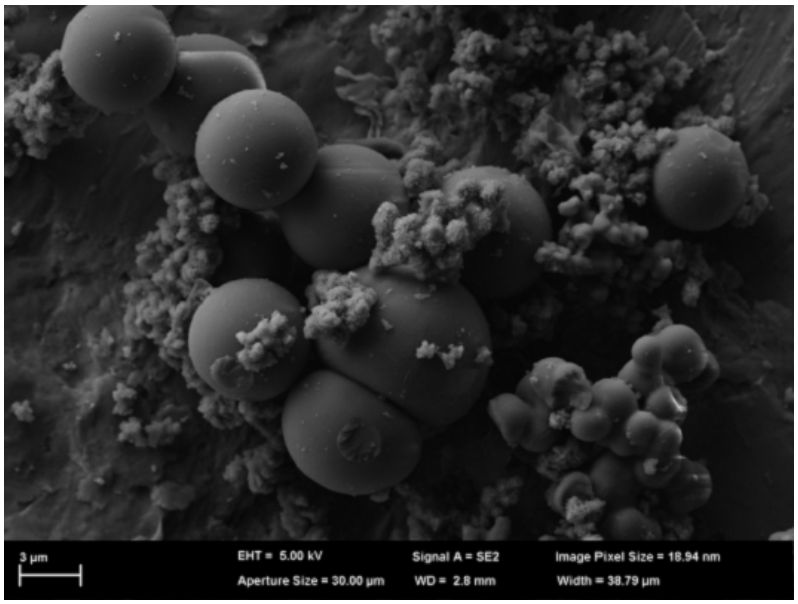

(B)

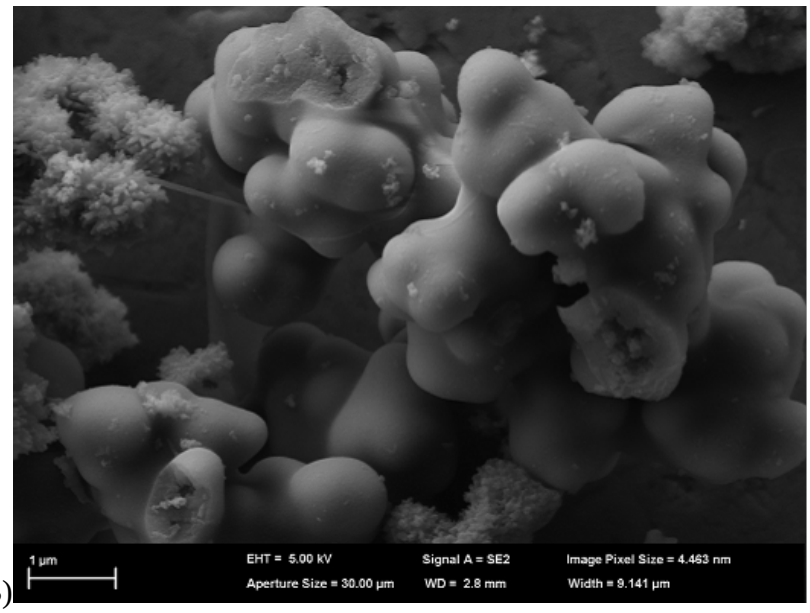

Figure 5.6 SEM images of (A) micro-CS@Co-raw, and (B) cobalt amorphous alloy on microcarbon spheres

Microcarbon spheres were observed (Figure 6.6 A), and cobalt amorphous alloy were showed in Figure 5.6 (B) [25]. Further, Co_3O_4 crystallites were not found in micro-CS@Co, 300^oC, 2h, Air (Figure 6.7). Nevertheless, elemental analysis using the EDS study on micro-CS@Co-raw and micro-CS@Co, 300^oC, 2h, Air suggested the presence of both cobalt and carbon elements.

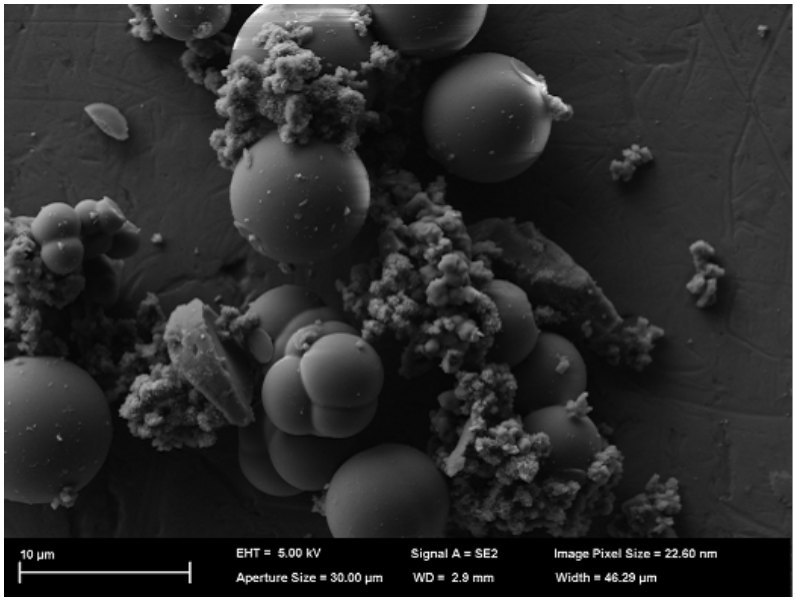

Figure 5.7 SEM images of micro-CS@Co, 300^oC, 2h, Air

Figure 5.7 is similar to Figure 5.6 (A). It proved that the decomposition of the Co-B amorphous alloy is hard to occur with the heat treatment below 300^oC [25].

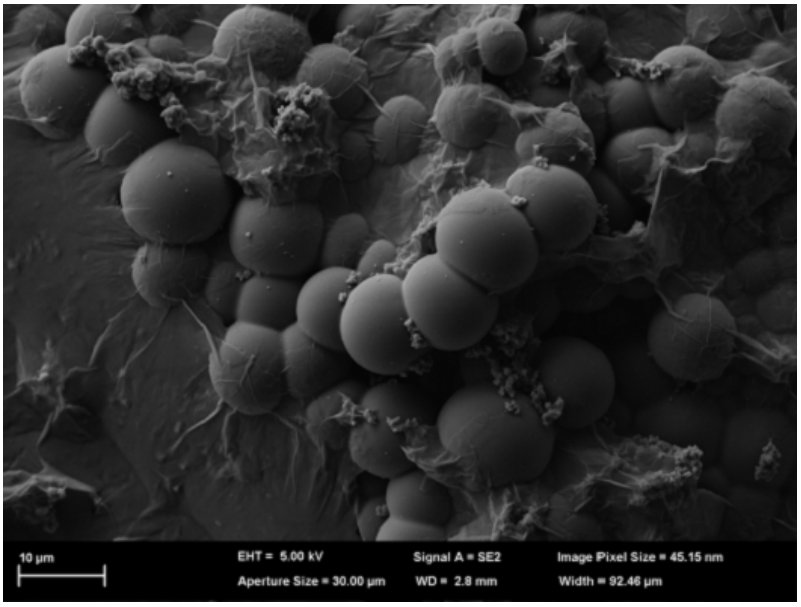

Figure 6.8 SEM images of micro-CS@Co, 400^{o}C, 2h, Air

In Figure 6.7, cobalt (III) hydroxide was hardly found, and few Co_3O_4 crystallites were observed on the surface of carbon spheres. Further, an elemental analysis using EDS study on the particle suggested the presence of both cobalt and carbon elements.

(A)

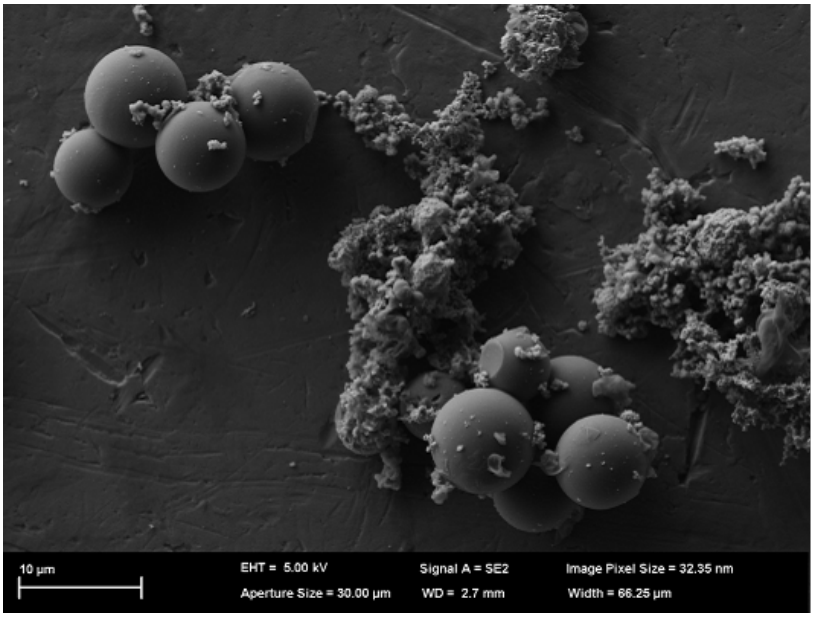

(B) 

Figure 5.9 SEM images of (A) micro-CS@Co, 500^{o}C, 2h, Air, and (B) Co_3O_4 crystallites

Figure 5.9 showed significant Co_3O_4 crystallites, and EDS of micro-CS@Co, 500^{o}C, 2h, Air (Figure 5.12) signified that the finer microcarbon spheres were completely coated by Co_3O_4 crystallites. EDS spectra and SEM images proved that the temperature of calcination was the main factor influencing the production of Co_3O_4 crystallites.

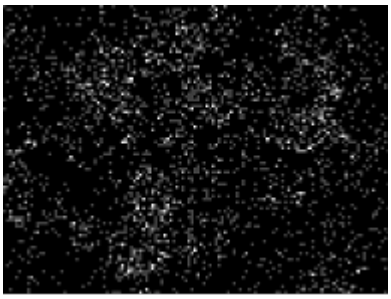

Co mapping

Figure 5.10 EDS spectra of micro-CS@Co-raw

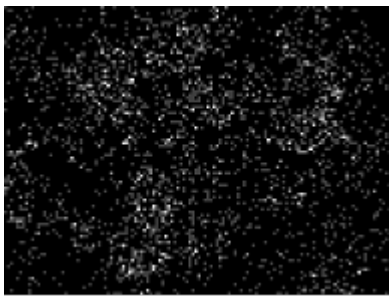

Co mapping

Figure 5.11 EDS spectra of micro-CS@Co, 300^{o}C, 2h, Air

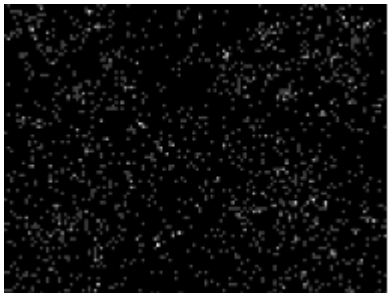

Co mapping

Figure 5.12 EDS spectra of micro-CS@Co, 400^{o}C, 2h, Air

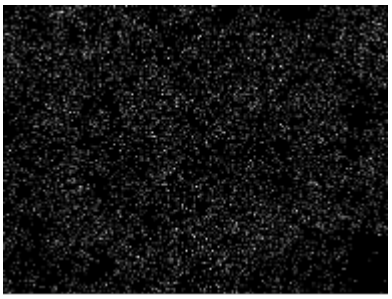

Co mapping

Figure 5.13 EDS spectra of micro-CS@Co, 500^{o}C, 2h, Air

5.3.2. Chemical oxidation of phenol

The performances of PMS and microcarbon sphere supported cobalt catalysts in chemical oxidation of phenol were investigated. Figure 5.14 shows that the micor-CS@Co-no urea added catalyst only removed 10% of phenol within 60 min. It proved that Co_3O_4 crystallites or cobalt amorphous alloy was hard to be synthesized without the employment of urea. Meanwhile, micro-CS@Co-urea catalysts degraded all of phenol at 45 and 15 min respectively. The pure PMS was used as background under the same conditions, and removed 15% phenol at 60 min.

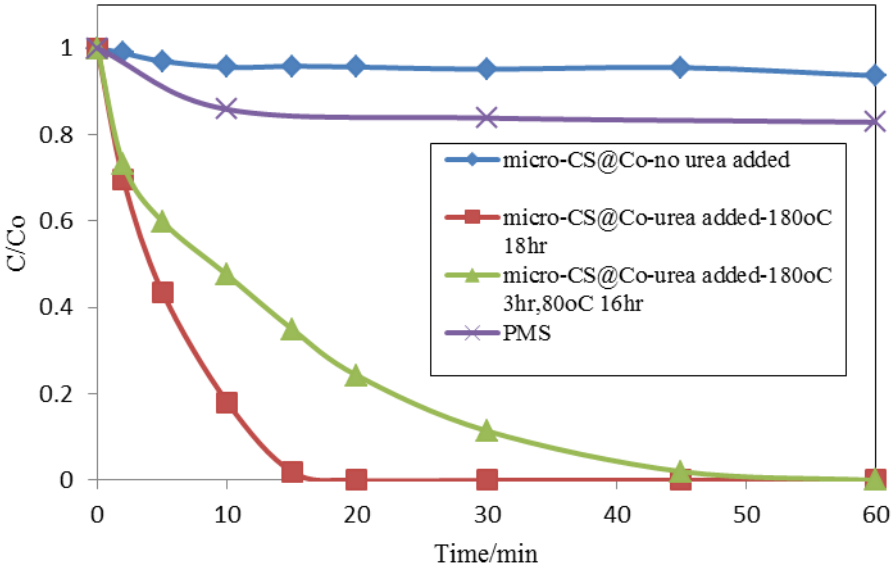

Figure 5.14 Effect of synthesis conditions on the activity of different catalysts in oxidation of phenol with PMS

Therefore, urea acted as an important role in producing cobalt oxides. The mechanism of synthesis of Co_3O_4 crystallites by applying urea is [27]:

$$TiO_2(h^+) + HO_{ad} \rightarrow TiO_2 + HO^{\bullet}_{ad} \quad (5\text{-}3)$$

$$2NH_3 \cdot H_2O \leftrightarrow NH_4^+ + OH^- \quad (5\text{-}4)$$

$$Me^{n+} + OH^- = Me(OH)_n \quad (5\text{-}5)$$

$$xMe(OH)_n + yCO_2 \rightarrow Me_x(OH)_{nx-2y}(CO_3)_y \quad (5\text{-}6)$$

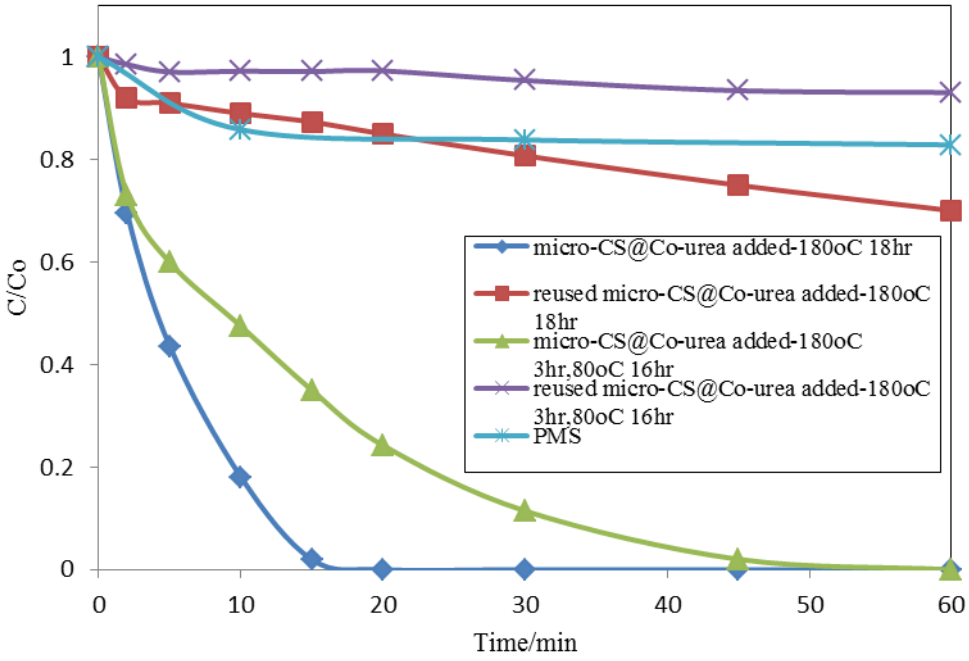

Figure 5.15 Reusabilities of two catalysts synthesized in different conditions for oxidation of phenol with PMS

Figure 5.15 shows the reuse of micro-CS@Co-urea added-180^{o}C, 18hr and micro-CS@Co-urea added-180^{o}C, 3hr-80^{o}C, 16hr for phenol oxidation with PMS. Both of the fresh catalysts were effective in phenol degradation by activation of PMS. These two catalysts degraded all of phenol in the solution at 45 and 15 min, respectively. However, the activities of reused catalysts reduced by 70% and 90%. The results probably proved that

there were no Co_3O_4 crystallites produced after the hydrothermal reaction. $Co(OH)_x$ existed with microcarbon sphere supports, and then lost during the phenol degradation reactions because of the acid solution.

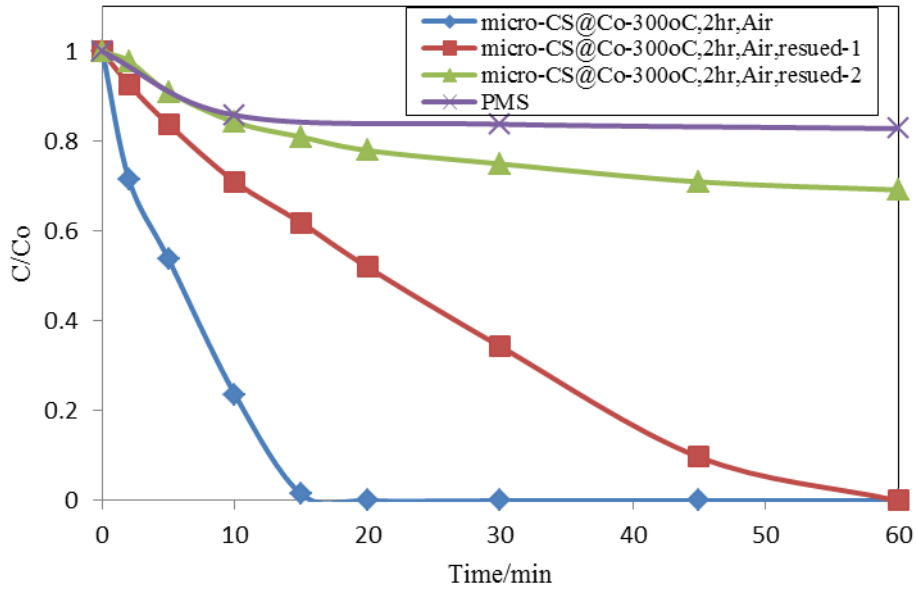

Figure 5.16 Reusabilities of micro-CS@Co, 300°C, 2h, Air for oxidation of phenol with PMS

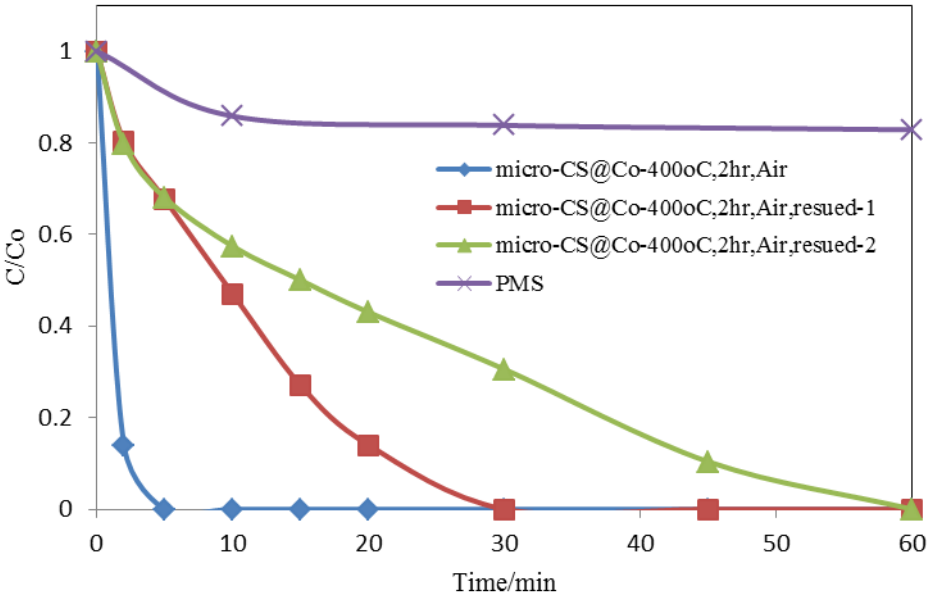

Figure 5.17 Reusabilities of micro-CS@Co, 400°C, 2h, Air for oxidation of phenol with PMS

Figures 5.16-5.18 show that reuse of three main micro-CS@Co catalysts for oxidation of phenol. All of the three catalysts performed significantly effective in degradation of phenol with PMS.

In Chapter 4, nano-Fe^0@CS materials were proven to be high effective catalysts which ended the phenol degradation process at 5min, and cobalt coated microcarbon sphere catalysts: Micro-CS@Co, 300^oC achieved 100% degradation of phenol in 15 min; micro-CS@Co, 400^oC achieved 100% degradation in 5 min; and micro-CS@Co, 500^oC achieved 100% degradation in 10 min.

However, comparing the activities of first and second reusability experiments of all the catalysts, micro-CS@Co, 500^oC was the most stable catalyst, indicating that this catalyst was more environmentally friendly due to the less cobalt leaching in repeated experiments. Further, the results of chemical oxidation reactions with PMS also verified the ratiocination from characterizations: finer microcarbon spheres were completely coated by Co_3O_4 crystallites for micro-CS@Co, 500^oC.

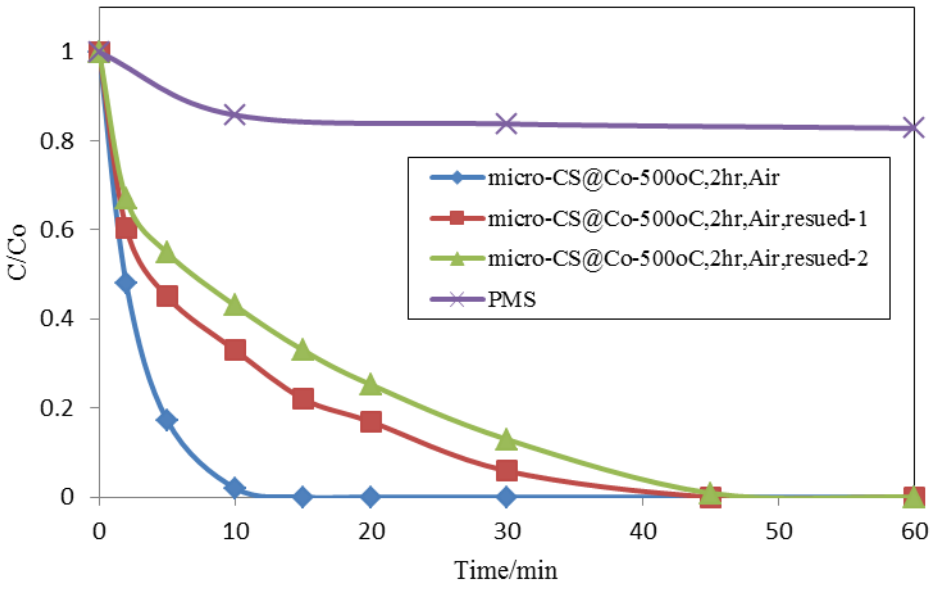

Figure 5.18 Reusabilities of micro-CS@Co, 500^{o}C, 2h, Air for oxidation of phenol with PMS

5.3.3. Kinetic studies of phenol degradation

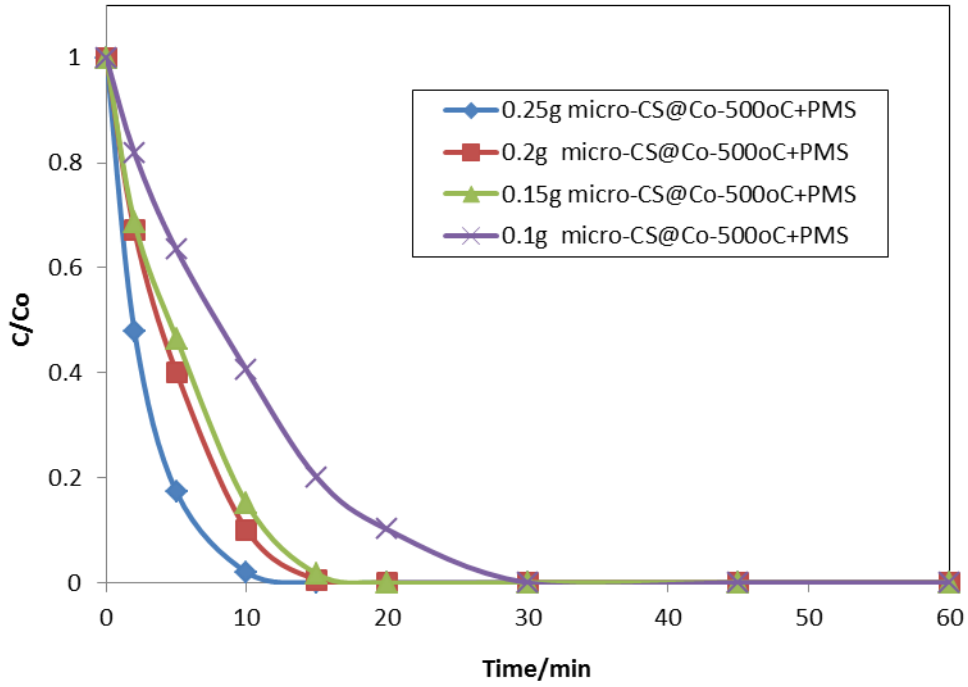

Figure 5.19 Phenol degradation at different catalysts amounts

Figure 5.19 shows the reactions of phenol degradation with different catalyst amounts. Comparatively large amount (0.25g) of micro-CS@Co catalyst was able to degrade 100% of phenol at 10 min, and smaller amount (0.5g and 0.15g) micro-CS@Co catalysts removed all of phenol at 15 min which were very similar to the activity of large amount (0.25g) of catalyst. With the decreasing of dosage of catalyst, the phenol removal efficiency decreased. However, when the catalyst amount was reduced to 0.1g, the removal process was still fast, and ended at 30min.

Figure 5.20 shows the reactions of phenol degradation with different PMS amounts. With utilization of 0.2g/L PMS, the reaction ended at 10 min, and the reaction using 0.15g/L PMS as oxidant stopped at 15 min. Removing all of phenol by using micor-CS@Co catalyst and 1g/L PMS cost 30 min which was same as the reaction by adding 0.5g/L PMS. It is clear that a decrease in utilization of PMS reduced the phenol removal efficiency.

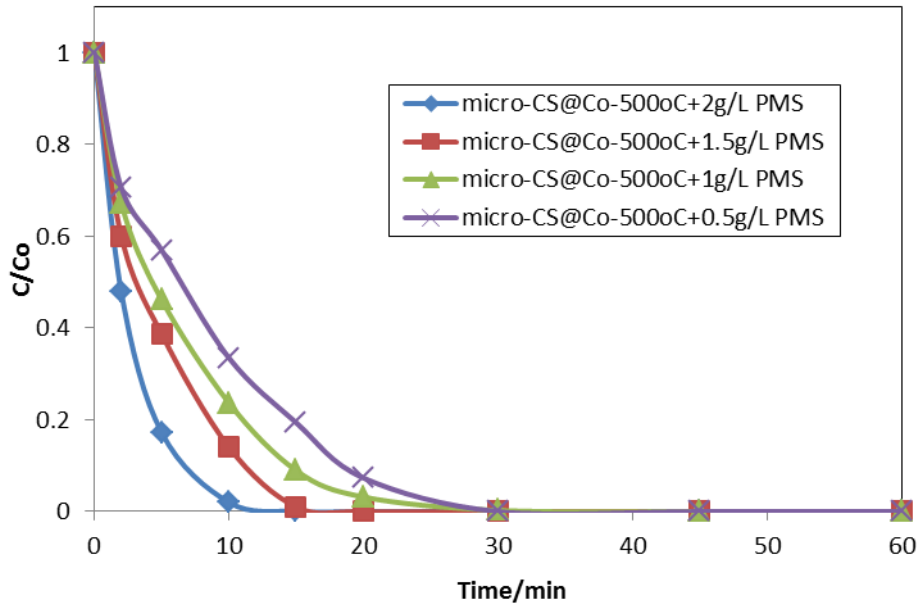

Figure 5.20 Phenol degradation at different oxidant amounts

The reaction temperature would influence the phenol oxidation reaction significantly. Figure 5.21 shows the effect of temperature on removal of phenol using fixed dosages of micro-CS@Co, 500^{o}C, 2h, Air and PMS. It was observed that the reaction rate increased significantly with the rise of temperature. The removal of phenol completed within 5 minutes when the reaction temperatures were 35, 40, 45 ^{o}C. Therefore, 35 ^{o}C is the optimum reaction temperature for this micro-CS@Co-PMS system (V_{phenol}: 200ml, C_{phenol}: 20ppm, $m_{catalyst}$: 0.25g, m_{oxone}: 0.4g). The effect of temperature of reaction is not used to find optimal reaction temperature, but to evaluate the activation energy of the catalyst.

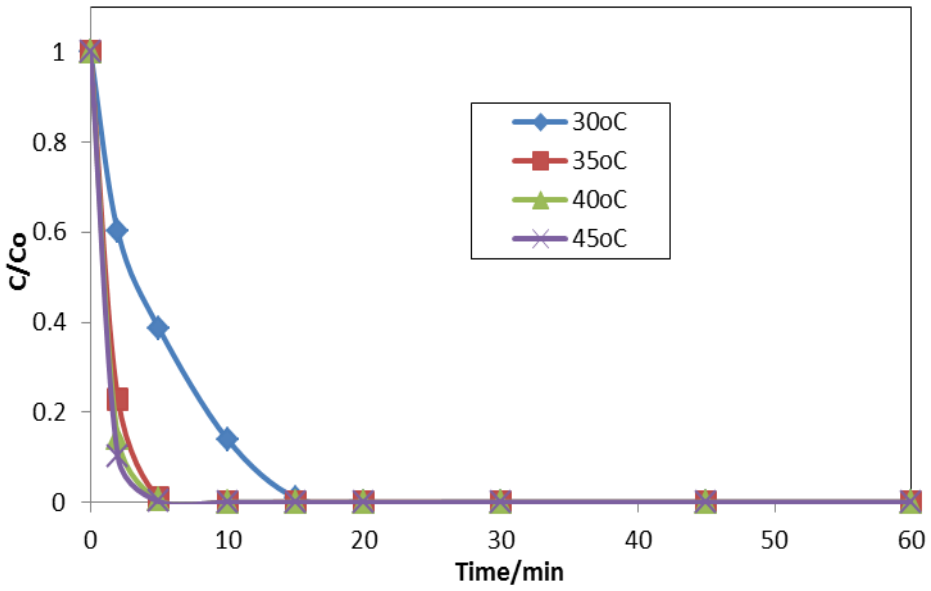

Figure 5.21 Phenol degradation at different temperatures

5.4. Conclusion

Cobalt coated microcarbon sphere catalysts were proven as catalysts with high activity in chemical oxidation of phenol by activation of PMS. Co_3O_4 crystallites were found on the surface of microcarbon. Microcarbon sphere supported cobalt catalysts exhibited high

activity for activation of PMS to produce sulphate radicals for oxidation of phenol. Several factors such as temperature, dosages of catalyst or PMS influenced the degradation of phenol. Although fresh micro-CS@Co, 400^{o}C showed the greatest activity, the micro-CS@Co, 500^{o}C catalyst demonstrated as the most stable and environmentally friendly catalyst by the tests of multiple chemical oxidation experiments.

5.5. References

1. Fleeger, J.W., K.R. Carman, and R.M. Nisbet, *Indirect effects of contaminants in aquatic ecosystems.* Science of the Total Environment, 2003. **317**(1-3): p. 207-233.

2. Mukherjee, D., et al., *Biological significance of 14C phenol accumulation in different organs of a murrel, Channa punctatus, and the common carp, Cyprinus carpio.* Biomedical and environmental sciences : BES, 1990. **3**(3): p. 337-42.

3. Mukherjee, D., et al., *IMPAIRMENT OF STEROIDOGENESIS AND REPRODUCTION IN SEXUALLY MATURE CYPRINUS-CARPIO BY PHENOL AND SULFIDE UNDER LABORATORY CONDITIONS.* Aquatic Toxicology, 1991. **21**(1-2): p. 29-40.

4. Wang, S., *A comparative study of Fenton and Fenton-like reaction kinetics in decolourisation of wastewater.* Dyes and Pigments, 2008. **76**(3): p. 714-720.

5. Wang, Y.B. and C.S. Hong, *Effect of hydrogen peroxide, periodate and persulfate on photocatalysis of 2-chlorobiphenyl in aqueous TiO2 suspensions.* Water Research, 1999. **33**(9): p. 2031-2036.

6. Yang, Q., et al., *Heterogeneous activation of peroxymonosulfate by supported cobalt catalysts for the degradation of 2,4-dichlorophenol in water: The effect of support, cobalt precursor, and UV radiation.* Applied Catalysis B-Environmental, 2008. **77**(3-4): p. 300-307.

7. Agustina, T.E., H.M. Ang, and V.K. Vareek, *A review of synergistic effect of photocatalysis and ozonation on wastewater treatment.* Journal of Photochemistry and Photobiology C-Photochemistry Reviews, 2005. **6**(4): p. 264-273.

8. H.J.H., F., *Oxidation of tartaric acid in presence of iron.* Chem. Soc., Trans. , 1894. **65**(65): p. 899–911.

9. Anipsitakis, G.P. and D.D. Dionysiou, *Degradation of organic contaminants in water with sulfate radicals generated by the conjunction of peroxymonosulfate with cobalt.* Environmental Science & Technology, 2003. **37**(20): p. 4790-4797.

10. Chen, X., et al., *Kinetics of oxidative decolorization and mineralization of Acid Orange 7 by dark and photoassisted Co2+ -catalyzed peroxymono sulfate system.* Chemosphere, 2007. **67**(4): p. 802-808.

11. Madhavan, J., et al., *Kinetic studies on visible light-assisted degradation of acid red 88 in presence of metal-ion coupled oxone reagent.* Applied Catalysis B-Environmental, 2008. **83**(1-2): p. 8-14.

12. Yu, Z.Y., et al., *Detoxification of diluted azo-dyes at biocompatible pH with the oxone/Co2+ reagent in dark and light processes*. Journal of Molecular Catalysis a-Chemical, 2006. **252**(1-2): p. 113-119.

13. Shukla, P., et al., *Cobalt exchanged zeolites for heterogeneous catalytic oxidation of phenol in the presence of peroxymonosulphate.* Applied Catalysis B-Environmental, 2010. **99**(1-2): p. 163-169.

14. Chan, K.H. and W. Chu, *Effect of humic acid on the photolysis of the pesticide atrazine in a surfactant-aided soil-washing system in acidic condition.* Water Research, 2005. **39**(10): p. 2154-2166.

15. Ling, S.K., S. Wang, and Y. Peng, *Oxidative degradation of dyes in water using Co2+/H2O2 and Co2+/peroxymonosulfate.* Journal of Hazardous Materials, 2010. **178**(1-3): p. 385-389.

16. Fernandez, J., et al., *Bleaching and photobleaching of Orange II within seconds by the oxone/Co2+ reagent in Fenton-like processes.* Applied Catalysis B: Environmental, 2004. **49**(3): p. 207-215.

17. Bandala, E.R., et al., *Degradation of 2,4-dichlorophenoxyacetic acid (2,4-D) using cobalt-peroxymonosulfate in Fenton-like process.* Journal of Photochemistry and Photobiology a-Chemistry, 2007. **186**(2-3): p. 357-363.

18. Bezemer, G.L., et al., *Cobalt particle size effects in the Fischer-Tropsch reaction studied with carbon nanofiber supported catalysts.* Journal of the American Chemical Society, 2006. **128**(12): p. 3956-3964.

19. den Breejen, J.P., et al., *On the Origin of the Cobalt Particle Size Effects in Fischer-Tropsch Catalysis.* Journal of the American Chemical Society, 2009. **131**(20): p. 7197-7203.

20. Xiong, H., et al., *Correlating the preparation and performance of cobalt catalysts supported on carbon nanotubes and carbon spheres in the Fischer-Tropsch synthesis.* Journal of Catalysis, 2011. **278**(1): p. 26-40.

21. Kang, J., et al., *Ruthenium Nanoparticles Supported on Carbon Nanotubes as Efficient Catalysts for Selective Conversion of Synthesis Gas to Diesel Fuel.* Angewandte Chemie-International Edition, 2009. **48**(14): p. 2565-2568.

22. Xiong, H., et al., *Autoreduction and Catalytic Performance of a Cobalt Fischer-Tropsch Synthesis Catalyst Supported on Nitrogen-Doped Carbon Spheres.* Chemcatchem, 2010. **2**(5): p. 514-518.

23. Fu, R.W., et al., *The growth of carbon nanostructures on cobalt-doped carbon aerogels.* Journal of Non-Crystalline Solids, 2003. **318**(3): p. 223-232.

24. Lee, J., et al., *A structured Co-B catalyst for hydrogen extraction from NaBH4 solution.* Catalysis Today, 2007. **120**(3-4): p. 305-310.

25. Xu, D., et al., *Carbon-supported cobalt catalyst for hydrogen generation from alkaline sodium borohydride solution.* Journal of Power Sources, 2008. **182**(2): p. 616-620.

6

Chapter 6: Photocatalytic degradation of phenol over microcarbon sphere–modified graphitic carbon nitride catalyst

Abstract

The graphitic carbon nitride (g-C_3N_4) was synthesized by directly heating melamine, and it was treated in D-glucose solution using a hydrothermal route to synthesize microcarbon sphere modified graphitic carbon nitride (C-g-C_3N_4) composite photocatalysts. Photocatalytic activity of C-g-C_3N_4 was evaluated by photodegradation of phenol solutions, which has not been successfully degraded phenol. The characterization for C-g-C_3N_4 photocatalyst was conducted by means of scanning electron microscopy (SEM) and X-ray diffraction (XRD). Compared to g-C_3N_4, the C-g-C_3N_4 photocatalyst showed a very high photocatalytic activity in degradation of phenol solutions under UV-visible irradiations.

6.1. Introduction

Highly toxic organic pollutants in wastewater have become one of the top environmental problems nowadays, and also led to the development of advanced oxidation processes (AOPs) for complete decomposition of pollutants. Generally, AOPs are widely used for aqueous phase oxidation by active radicals to decompose pollutants to harmless water, CO_2 and other inorganic acids [1, 2]. Important AOPs include photocatalysis, Fenton and Fenton-like reactions, and ozonation, etc. In recent decades, heterogeneous photocatalysis has been considered as a promising technique for wastewater treatment owing to their low-cost, environmental friendliness and sustainability. Photocatalytic purification not only has a high development potential for treatment of serious environmental pollutants (in water and air) [3, 4], but also provides a new solution of global energy shortage due to the utilization of solar energy.

In heterogeneous photocatalytic reaction, a semiconductor, usually TiO_2 or ZnO, is activated by UV irradiation [2]. This process starts with the irradiation of photocatalyst by light with sufficient energy. The electron (e^-)/hole (h^+) pairs will be produced in the conduction band (CB) and valence band (VB), respectively, and migrate to the surface of the semiconductor where they are involved in redox reactions. The excited electrons react with oxygen molecules and lead to the formation of the superoxide radical anion, peroxide radicals and H_2O_2 molecules at the same time [5-10]:

$$TiO_2 + h\nu \rightarrow e^- + h^+ \quad (6\text{-}1)$$

The holes (h^+) react with hydroxyl anions and H_2O molecules to generate hydroxyl radicals.

$$TiO_2(h^+) + H_2O_{ad} \rightarrow TiO_2 + HO^{\bullet}_{ad} + H^+ \quad (6\text{-}2)$$

$$TiO_2(h^+) + HO_{ad} \rightarrow TiO_2 + HO^{\bullet}_{ad} \quad (6\text{-}3)$$

Nevertheless, limitations of popular photocatalysts, such as TiO_2, restrict their practical applications: i) low photocatalytic efficiency at low pollutant concentrations; ii) complicated recovery after use; iii) aggregation of particles in suspension; iv) demand of UV light and/or high intensity radiation which may cause health issue. Therefore, for wastewater purification, a promising photocatalyst material should have a band gap that absorbs visible light, strong oxidative ability and high stability in a complex waste solution system [11]. Some photocatalysts, such as ZnO, show photo-corrosion effect. In aqueous media, ZnO may self-deactivate by forming ions when reacting with photo-generated holes, and ions are released into solution [12-15], causing second pollution. Recently, Wang el al. reported that a metal-free polymeric photocatalyst, graphitic carbon nitride (g-C_3N_4), had photocatalytic performance for hydrogen or oxygen production via water splitting under visible light irradiation [16]. High thermal and electronic properties make g-C_3N_4 photocatalysts highly attractive for photocatalysis applications. Further, g-C_3N_4 material is recognized to be the most stable allotrope at ambient conditions. Due to the strong covalent bonds between carbon and nitride atoms, g-C_3N_4 photocatalyst shows significant stability whether it is under light irradiation in basic solution (NaOH, pH=14) or acid solution (HCl, pH=0) [11]. Cyanamide, dicyandiamide, and melamine have been used as precursors to synthesize g-CN solid [11, 17, 18]. Compared with melamine, cyanamide and dicyandiamide are expensive and virulent. So, in some studies, melamine has been used to synthesize g-CN by heat treatment in low vacuum system [19, 20], or under high pressure [21], or by directly heating [11, 18].

However, due to the high recombination rate of photogenerated electron-hole pairs of g-C_3N_4, its photocatalytic efficiency in oxidation of organics is low [16]. Many methods have been

proposed to improve the activity, such as doping [18, 22], and coupling g-C_3N_4 with metals [23, 24]. To our knowledge, the synthesis of microcarbon sphere/g-C_3N_4 (C-g-C_3N_4) photocatalyst has never been achieved. In this study, graphitic carbon nitride (g-C_3N_4) was prepared by directly heating melamine, and then it was used to fabricate C-g-C_3N_4 via a hydrothermal method by mixing g-C_3N_4 and D-glucose in solution. Furthermore, the photocatalytic degradation of phenol was investigated.

6.2. Experimental

6.2.1. Materials

Melamine (99.0%) was obtained from Aldrich. D-glucose (99.5%) was purchased from Sigma. Pure methanol (99.9%) was from Chem Supply. Phenol was obtained from Aldrich, and used to prepare pollutant solution.

6.2.2. Preparation of g-C_3N_4

g-C_3N_4 was synthesized by directly heating melamine in semi-closed system [11]. In a typical synthesis, 5 g melamine powder were added into a crucible with a cover, and calcined in the air at 500 ^oC for 2h, 4h, 6h, 8h at a heating rate of 15 ^oC/min, respectively. 10 g melamine powder was also heated in a crucible with same volume and cover in the air for 2h at a heating rate of 15 ^oC/min.

6.2.3. Preparation of C-g-C_3N_4

Microcarbon sphere modified graphitic nitride photocatalysts were prepared by a hydrothermal method using D-glucose and g-C_3N_4 powder [25, 26]. One of the synthesis processes was that 1.81 g g-CN and 7.24 g D-glucose were dissolved in 80 ml ultrapure

water, and the mixture was stirred for 6 h. Then the mixed solution was transferred into a 120 ml Teflon-lined autoclave. The reactor was put in an oven and heated at 150 ^{o}C for 3 h. The reactor was then cooled down to room temperature. The obtained precipitate was filtrated and washed with methanol twice and water three times. After washing, the precipitate was dried in an oven at 70 ^{o}C in the air.

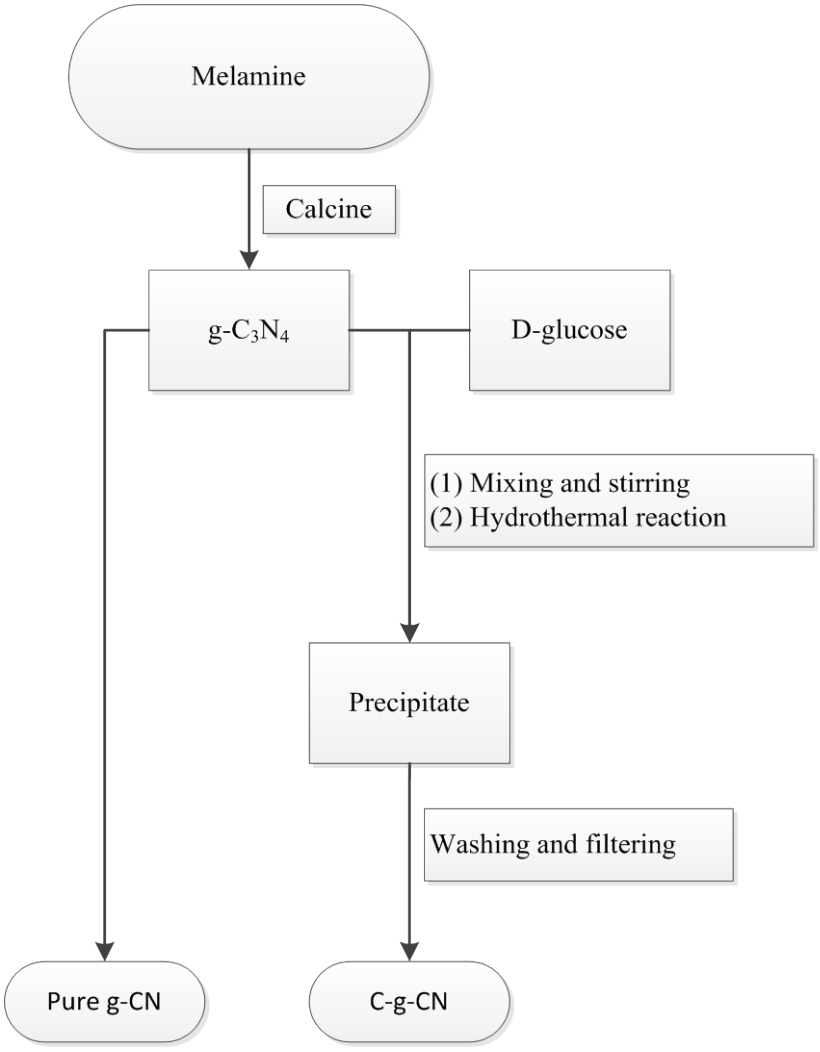

Figure 6.1 Flowchart of the preparation procedure

Synthesized g-C_3N_4 and C-g-C_3N_4 photocatalysts in different reaction conditions are summarized as follows:

Table 6.1 Summary of synthesized photocatalysts

Sample ID	**Melamine (g)**	**D-glucose (g)**	**Calcined temperature in Muffle furnace (°C)**	**Calcined time in Muffle furnace (h)**	**Hydrothermal reaction temperature (°C)**	**Hydrothermal reaction time (h)**
g-C_3N_4-10g	10	N/A	150	2	N/A	N/A
g-C_3N_4-2h	5	N/A	150	2	N/A	N/A
g-C_3N_4-4h	5	N/A	150	4	N/A	N/A
g-C_3N_4-6h	5	N/A	150	6	N/A	N/A
g-C_3N_4-8h	5	N/A	150	8	N/A	N/A
	g-C_3N_4 (g)					
150-1.5h	1.81	7.24	N/A	N/A	150	1.5
150-3h	1.81	7.24	N/A	N/A	150	3
150-6h	1.81	7.24	N/A	N/A	150	6
150-18h	1.81	7.24	N/A	N/A	150	18
135-3h	1.81	7.24	N/A	N/A	135	3
165-3h	1.81	7.24	N/A	N/A	165	3
180-3h	1.81	7.24	N/A	N/A	180	3
180-6h	1.81	7.24	N/A	N/A	180	6

6.2.4. Characterization of photocatalysts

The crystalline structures of pure g-C_3N_4 and microcarbon sphere modified g-C_3N_4 photocatalysts were analyzed by powder X-ray diffraction (XRD). The spectra were obtained on a Germany Burker D8-Advance X-ray diffractometer with Cu Kα radiation (λ=1.5418Å). Scanning electron microscopy (SEM) was used to evaluate the morphology, size, and texture information of the samples.

6.2.5. Photocatalytic and adsorption activity test

The aqueous photocatalytic degradation of phenol was carried out in a 1 L of Pyrex double-jacket reactor. A water bath connected with a pump was used to maintain the reaction temperature at 30^{o}C, and a magnetic stirrer was used to maintain the photocatalyst dispersed uniformly in reaction solutions. In a typical run, 0.2 g of photocatalyst (1.0 g/L) was added into 200 mL of 20 ppm phenol solution and stirred for 30 min, and took the first sample. The light irradiation was immediately switched on after the first sample taking. The irradiations were supplied by a MSR 575/2 metal halide lamp (575 W, Philips). The UV intensity (315 < λ < 400 nm) was measured to be 60 μW/cm^2 and the visible light intensity (λ > 400 nm) was 84 μW/cm^2. At each set time interval, 1 mL solution was withdrawn by a syringe and filtered by a 0.25 μm Millipore film into a HPLC vial. The degradation efficiency (%) can be calculated as:

$$efficiency(\%) = \frac{C_0 - C}{C_0} \times 100\% \quad (6\text{-}4)$$

where C_0 is the initial concentration of phenol, and C is the revised concentration considering phenol degradation on photocatalyst. The concentration of phenol was analyzed on a 380-LC HPLC (Varian, USA) with a UV detector set at λ = 270 nm. A C-18 column was used to separate the organics while the mobile phase of 30% CH_3CN and 70% water was flowing through the column at a flow rate of 1.5

mL/min. The adsorption test was carried out in the same system as photocatalysis reaction except without lamp on.

6.3. Results and discussion

6.3.1. Characterization of g-CN and C-g-CN

Figure 6.2 XRD pattern of graphitic carbon nitride (g-C_3N_4)

Figure 6.2 shows a typical XRD pattern of graphitic carbon nitride (g-C_3N_4-2h). The strongest sharp reflection peak at the position of 27.5^o (d=0.336nm) matches the predicted XRD data of g-C_3N_4 in previous work [11, 28]. The small peak is indexed at 13.1^o (d=0.676 nm).

Figure 6.3 XRD patterns of g-CN-2h and 135-3h

Figure 6.4 XRD patterns of g-CN-2h, 150-3h and 150-6h

Figure 6.3 and Figure 6.4 show the XRD patterns of g-C_3N_4-2h, 135-3h, 150-3h and 150-6h. With microcarbon spheres employed, the strong peak of g-C_3N_4 did not change, but the minor peak at 13.1^o was weaker with increase of the temperature and reaction time of hydrothermal process.

Figure 6.5 XRD patterns of g-C_3N_4-2h and 165-3h

In Figure 6.5, XRD patterns of g-C_3N_4-2h and 165-3h show the similar results compared with Figure 6.3 and Figure 6.4. However, in Figure 6.6, XRD patterns of g-C_3N_4-2h, 180-3h and 180-6h indicate that with the increase of hydrothermal reaction time at 180^{o}C, the minor peak of g-CN at 13.1^o was hard to be observed, and the major peak at 27.5^o became narrower and shaper. The XRD patterns of g-C_3N_4 and C-g-C_3N_4 catalysts did not have other discernible diffraction peak, which means microcarbon spheres did not exhibit diffraction peaks corresponding to g-C_3N_4. This is possibly because the prepared microcarbon spheres were amorphous and did not have a crystalline phase. Therefore, SEM was employed to evaluate the morphology, size, and texture information of synthesized photocatalysts.

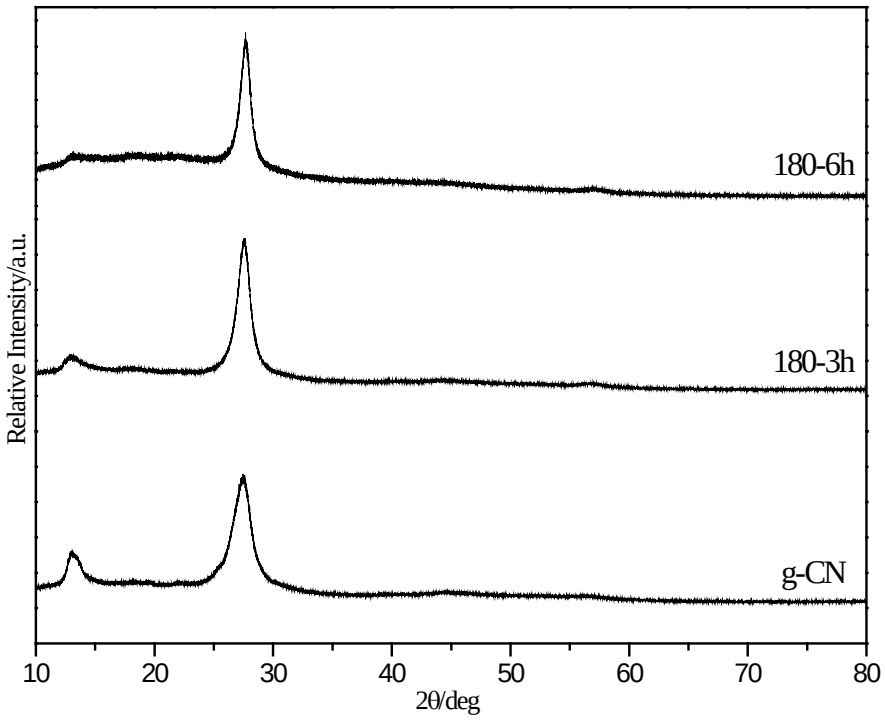

Figure 6.6 XRD patterns of g-CN-2h, 180-3h and 180-6h

Figure 6.7(A) shows clear, crisp edges and rodlike structures. High magnification of g-C_3N_4-2h reveals a morphology that appears to be microcrystalline powders (Figure 6.7(B)) which is accordant with the results from previous study [28].

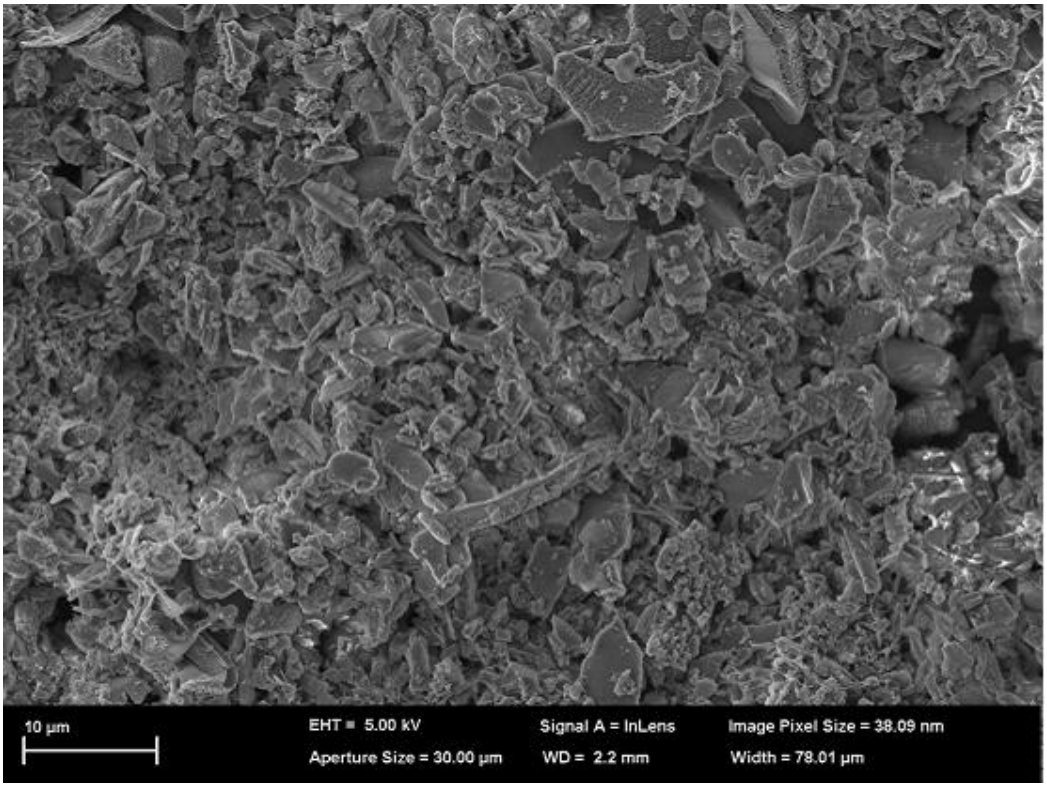

(A)

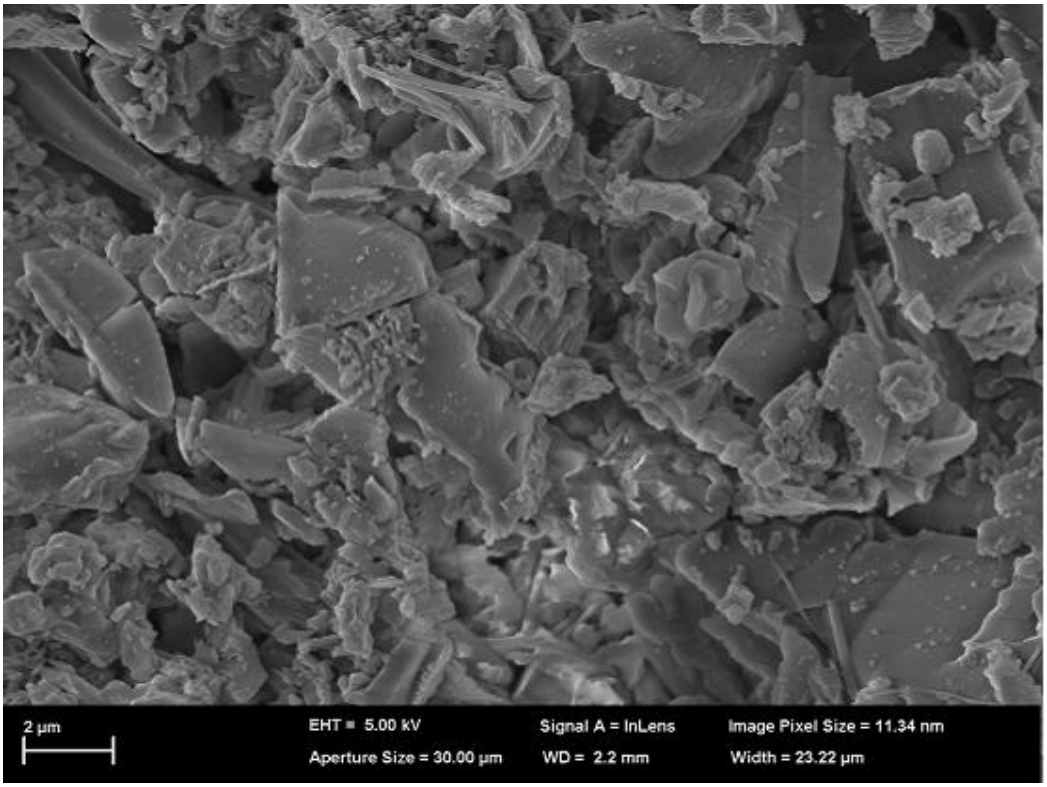

(B)

Figure 6.7 SEM images of pure graphitic carbon nitride (g-CN-2h)

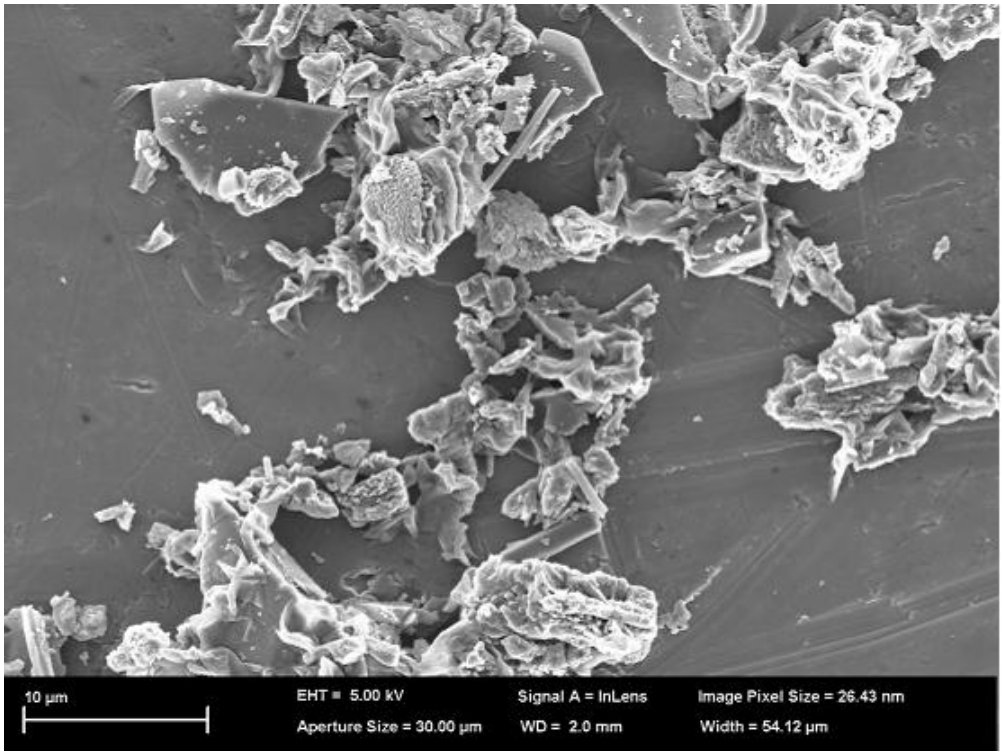

(A)

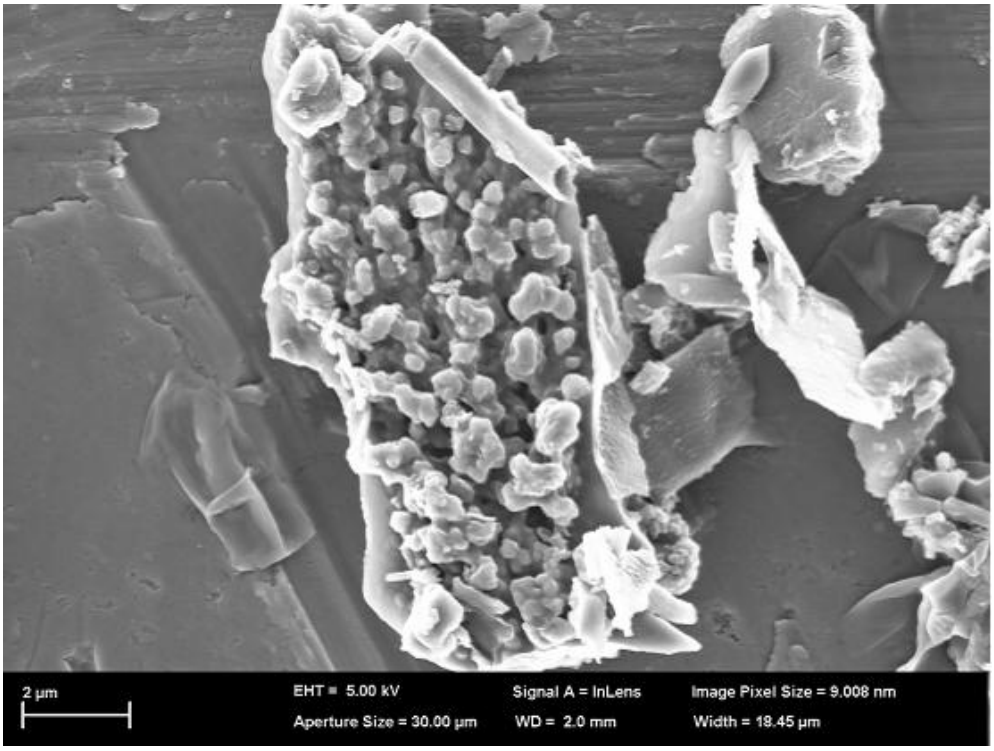

(B)

Figure 6.8 SEM images of C-g-CN (150-3h)

The size of carbon spheres is dramatically dependent on the synthesis conditions, such as precursor concentration, temperature, and hydrothermal reaction time [29]. Figure 6.8 and 6.9 indicate that with increasing hydrothermal reaction time, the

carbon spheres were produced and coated on g-C_3N_4-2h (Figure 6.9). While no carbon spheres were observed in Figure 6.8. However, in the hydrothermal conditions of low temperature (150^oC) and short reaction time (3h), the morphology of g-C_3N_4 was changed (Figure 6.8(B)). Parts of the crisp edges and laminated structure of g-C_3N_4 were reformed to rodlike structures.

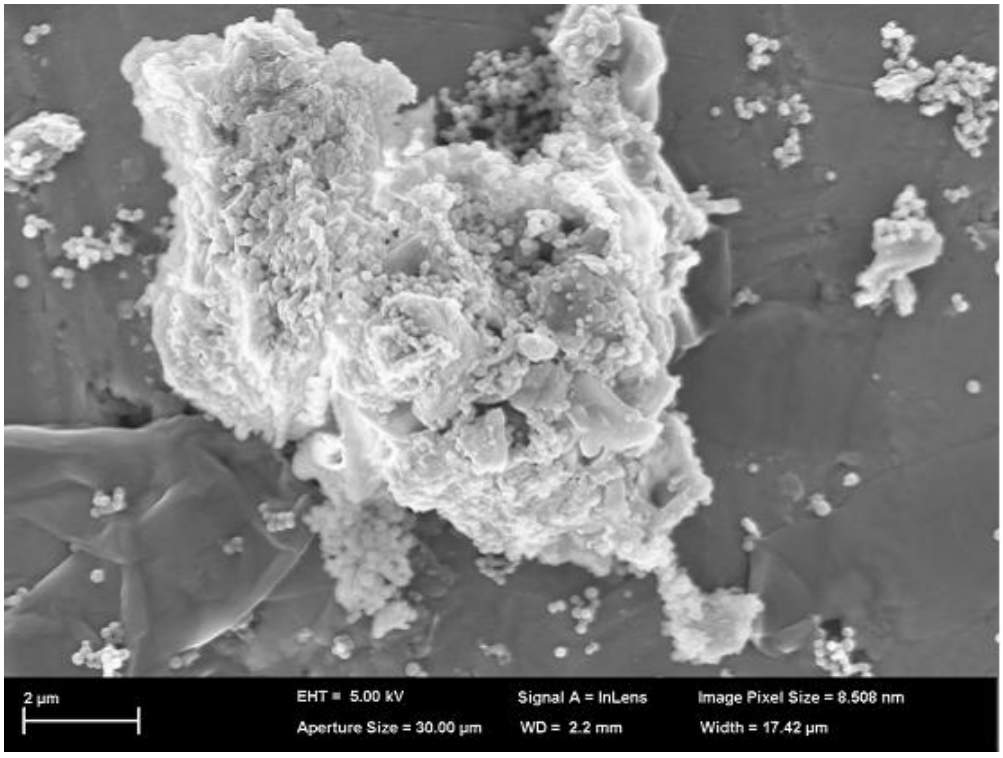

Figure 6.9 SEM image of C-g-CN (150-6h)

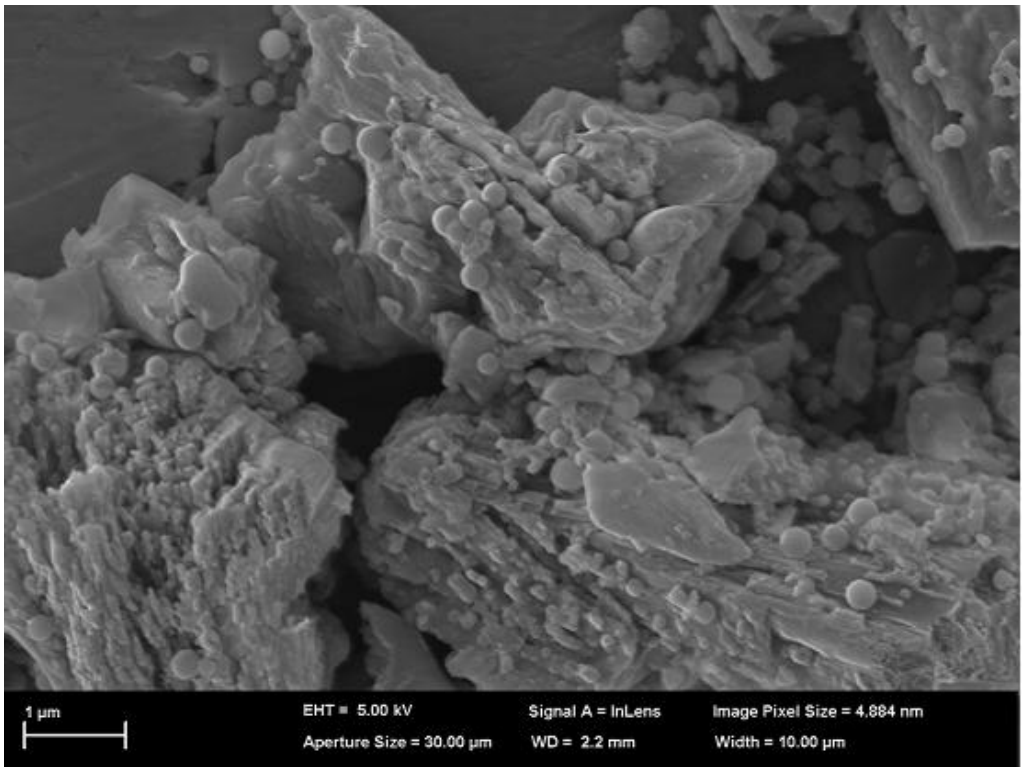

(A)

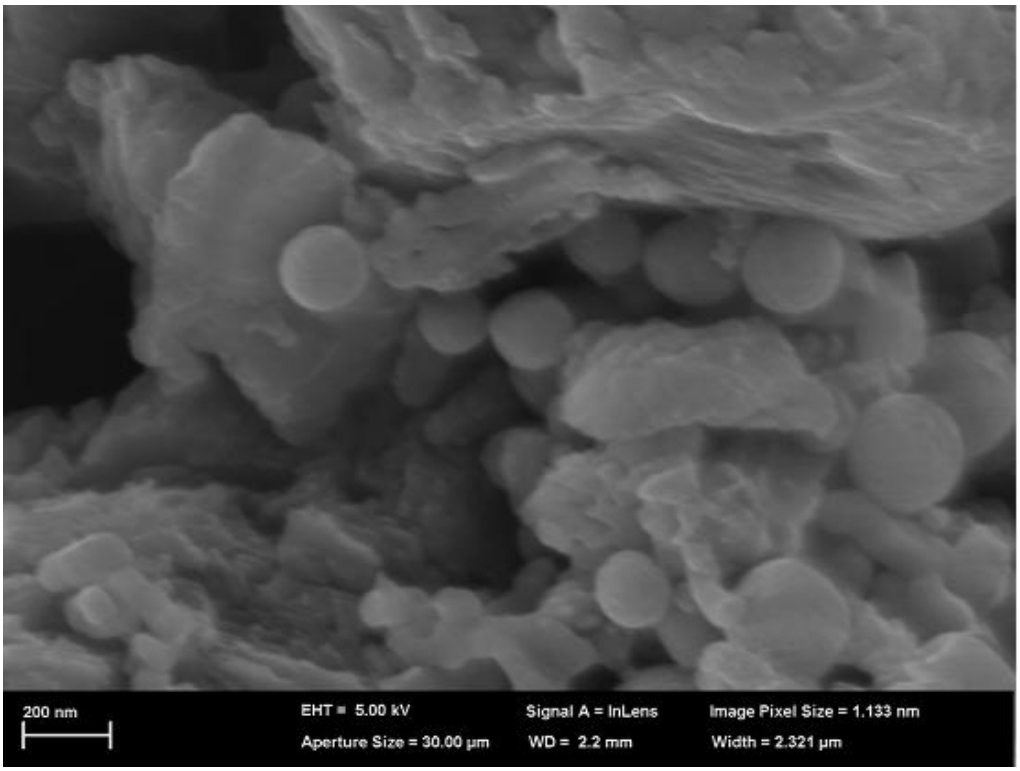

(B)

Figure 6.10 SEM images of C-g-CN (180-3h)

Figure 6.10 and 6.11 show typical microspherical morphology. The comparatively higher temperature (180^{o}C) and longer hydrothermal reaction time (6h) significantly increased the size and amount of carbon spheres.

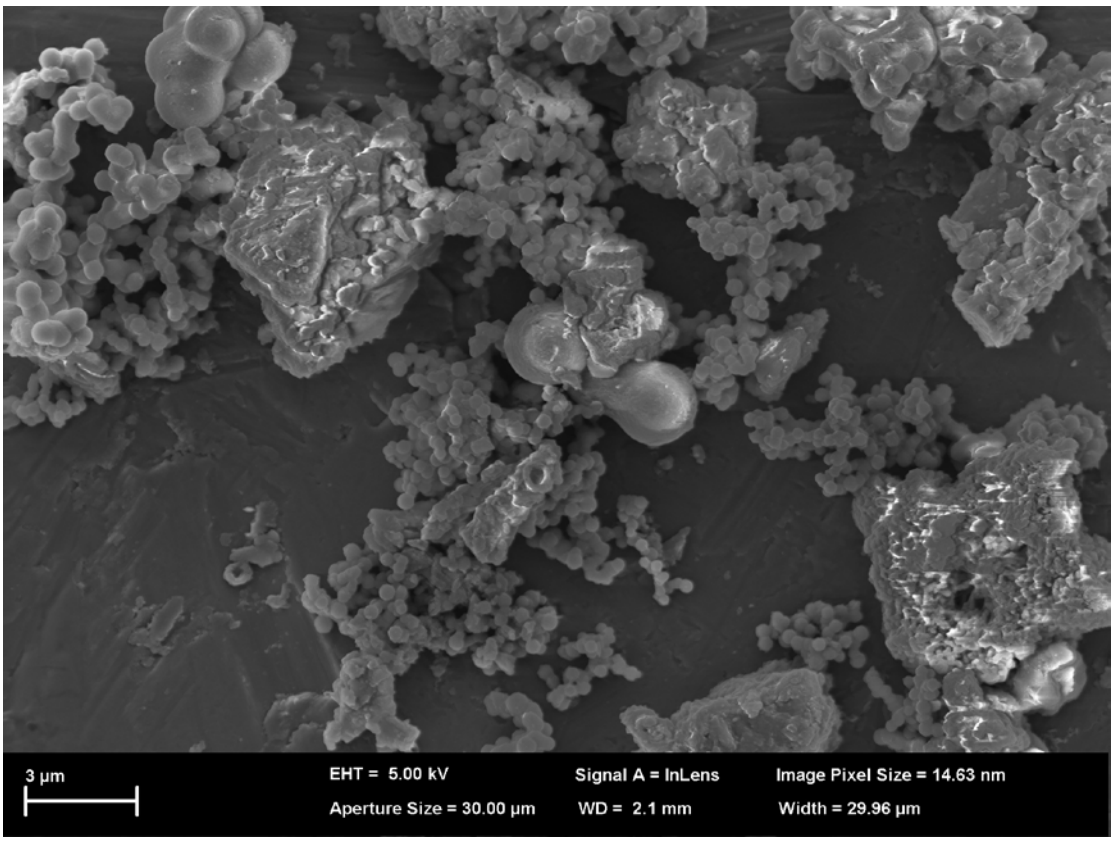

Figure 6.11 SEM image of C-g-CN (180-6h)

6.3.2. Photocatalytic activity tests

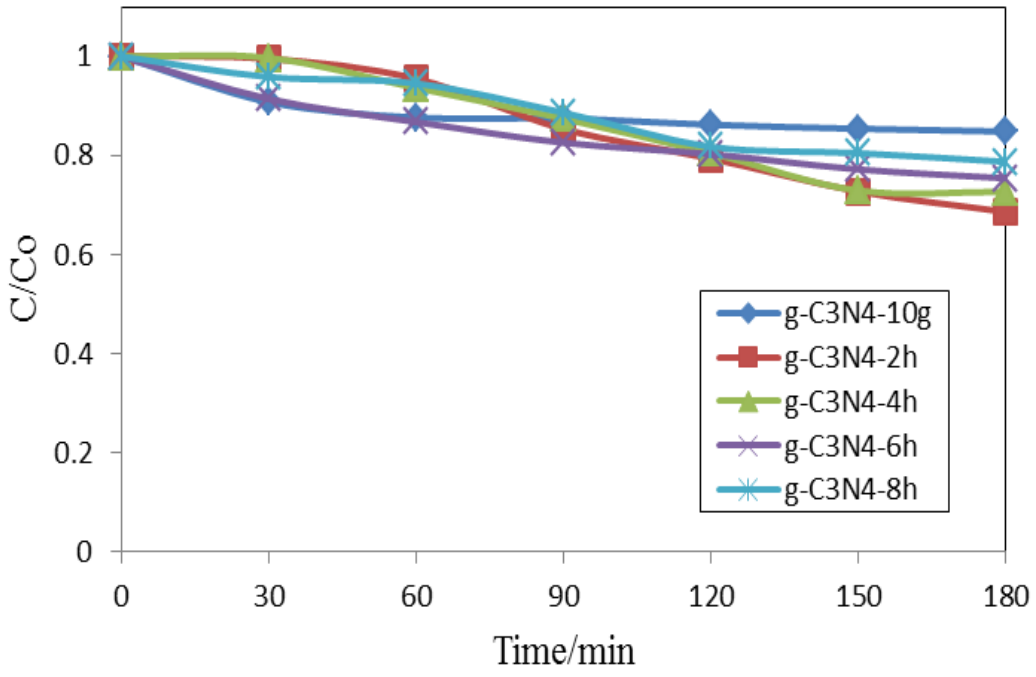

Figure 6.12 Effects of amount of melamine and calcination temperature on the activities of the photocatalysts in phenol degradation under UV-vis light irradiation

Figure 6.12 shows the change of phenol concentration dependent on reaction time under UV-vis light irradiation in the presence of various g-CN photocatalysts. It shows that the activities of g-C_3N_4 photocatalysts synthesized at low dosage of melamine (5g) were 16% higher than the g-C_3N_4 synthesized with high dosage of melamine (10g) in the same semi-closed system: a fixed volume crucible with a cover. This result indicates that the oxygen remained in the semi-closed system had positive effect on the photocatalytic activities of g-C_3N_4 catalysts. In addition, similar photocatalytic activity was observed in the presence of different g-C_3N_4 photocatalysts synthesized at different calcination time. However, the g-C_3N_4-2h catalyst showed comparatively higher activity than other photocatalysts. Similar results were reported by other studies [11, 30].

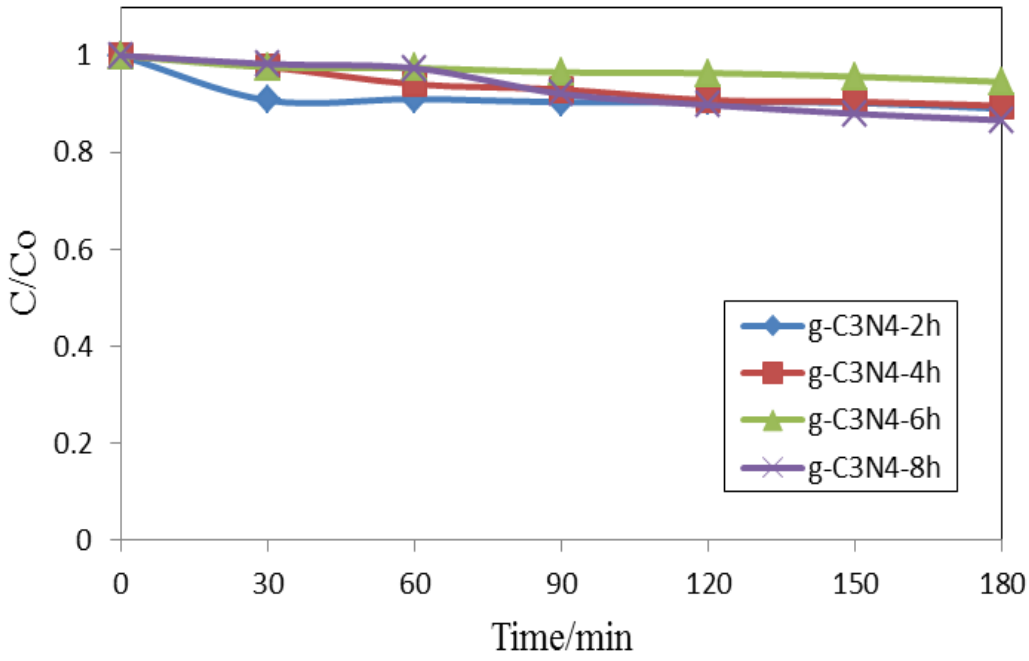

Figure 6.13 Effects of calcination temperature on the activity of various pure g-C_3N_4 photocatalysts in phenol degradation under UV light irradiation

Figure 6.13 indicates the effects of calcination time of pure g-CN photocatalysts on phenol degradation. For g-C_3N_4-2h, the decrease of phenol concentration was mainly due to the adsorption in first half hour. Therefore, the main activities of phenol degradation were activated by the visible light included in UV-vis light irradiation. Since the degradation processes were not completed within 180 min, further photocatalytic activity tests were extended to 300 min.

The mechanism of phenol photodegradation over g-CN is similar to the photocatalytic reaction using TiO_2. Generally, the two reactive oxidation species hydroxyl radicals (OH·) and superoxide (O_2· or HOO·) are formed during the photocatalytic reaction via UV-vis light irradiation. The proposed mechanism for the electron transfer in g-C_3N_4 was shown in Figure 6.14 [31].

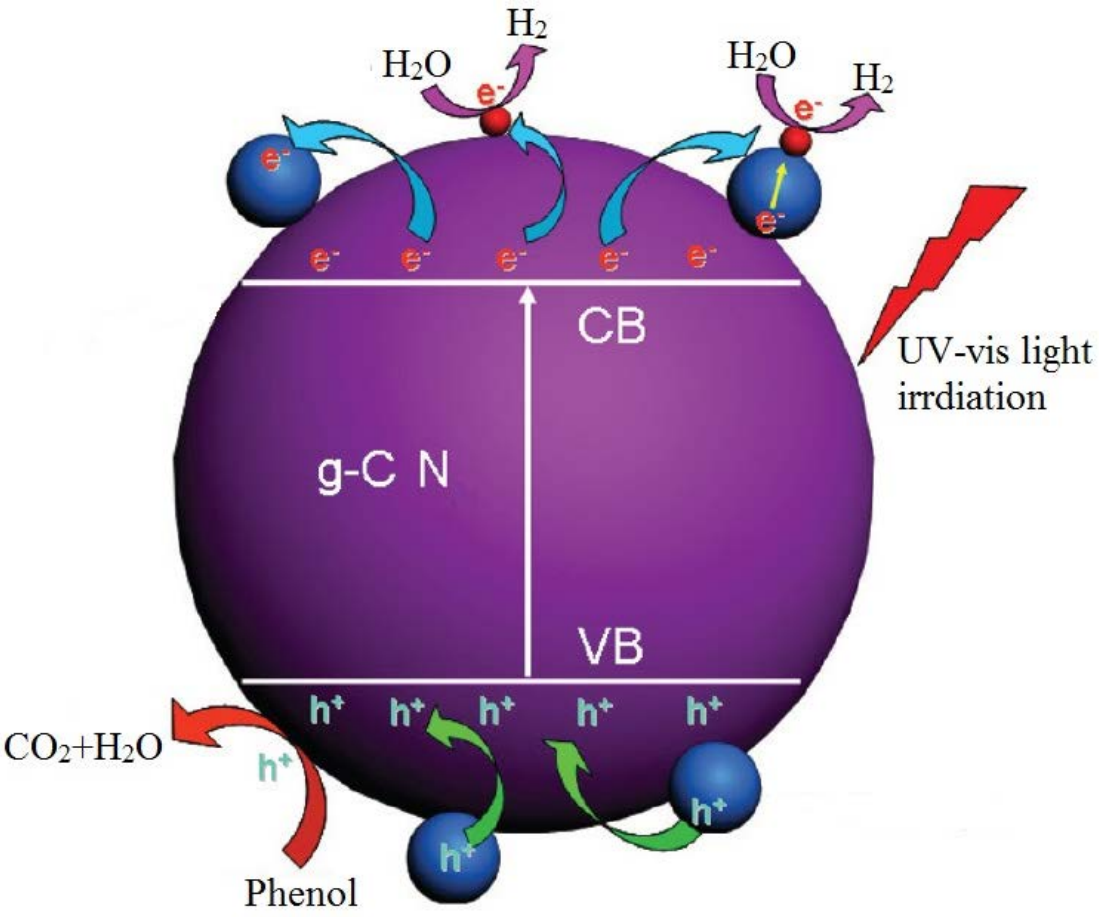

Figure 6.14 Schematic of photogenerated charge transfer in g-C_3N_4 under UV-vis light irradiation.

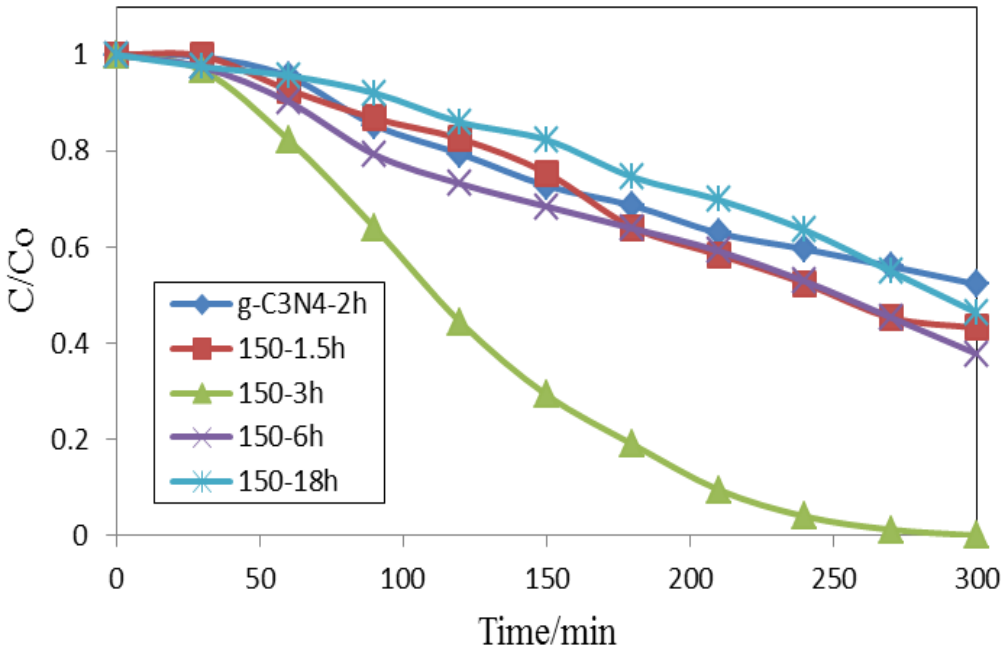

Figure 6.15 Effects of hydrothermal time on the activity of various carbon spheres modified g-C_3N_4 photocatalysts in phenol degradation under UV-vis light irradiation

In Figure 6.15, effects of hydrothermal time on the activities of various carbon spheres modified g-C_3N_4 photocatalysts in phenol degradation under UV-vis light irradiation were presented, and pure g-C_3N_4-2h catalyst was used as a reference sample. The C-g-C_3N_4: 150-3h showed the highest activity and removed all of phenol at 280 min. Therefore, 3h is the optimal reaction time of hydrothermal reaction at 150 ^oC.

In some other studies, Rhodamine B (Rh B) and methyl organe (MO) were used as model pollutants, and boron-doped g-C_3N_4 and g-C_3N_4/TiO_2 were synthesized as photocatalysts [30, 31]. They could remove all of target pollutants in 5 h, and the concentrations of pollutants used in their modes were only 4 ppm and 10 ppm. In our study, phenol was used as pollutant which was commonly known as one of the major toxic and resisted organic pollutants in air, water bodies and wastewater. Further, 200 mL, 20 ppm phenol solution was used in all of activity tests, comparing with their 30 mL and 100mL. Figure 7.16 shows the effects of hydrothermal temperature on the

activity of various C-g-C_3N_4 photocatalysts in phenol degradation under UV-vis light irradiation. The degradation rates of 150-3h and 180-3h were similar. The 150-3h decomposed 200 mL of 20 ppm phenol solution in 270 min, and 180-3h removed all of target pollutant in approximate 210 min. Therefore, 180-3h had the highest activity on phenol degradation under UV-vis light irradiation.

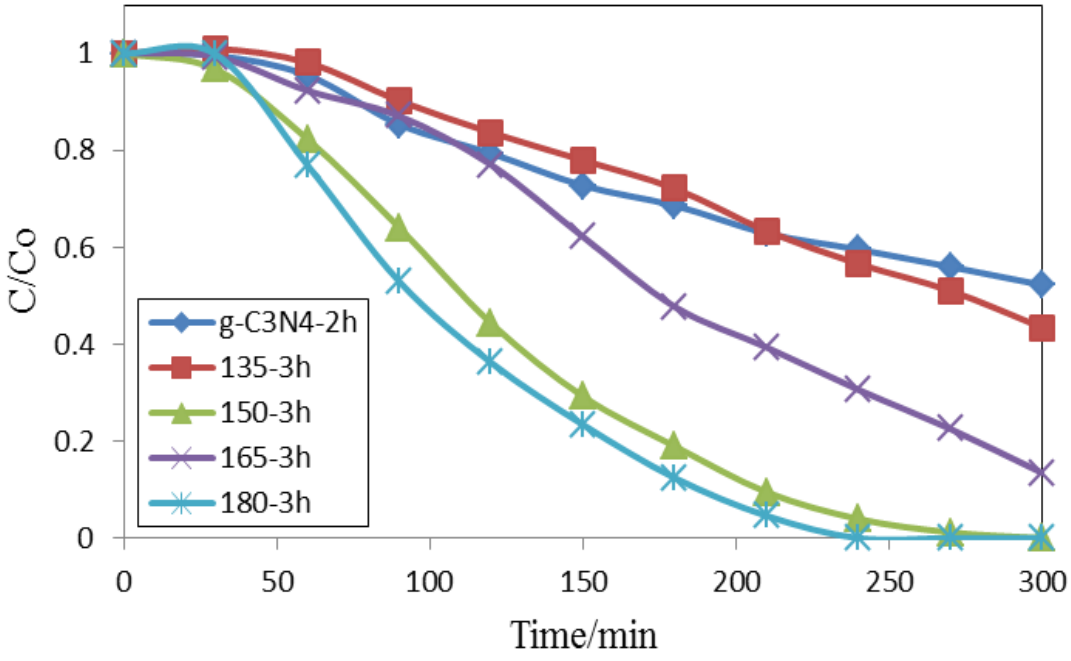

Figure 6.16 Effects of hydrothermal temperature on the activities of various carbon spheres modified g-C_3N_4 photocatalysts in phenol degradation under UV-vis light irradiation

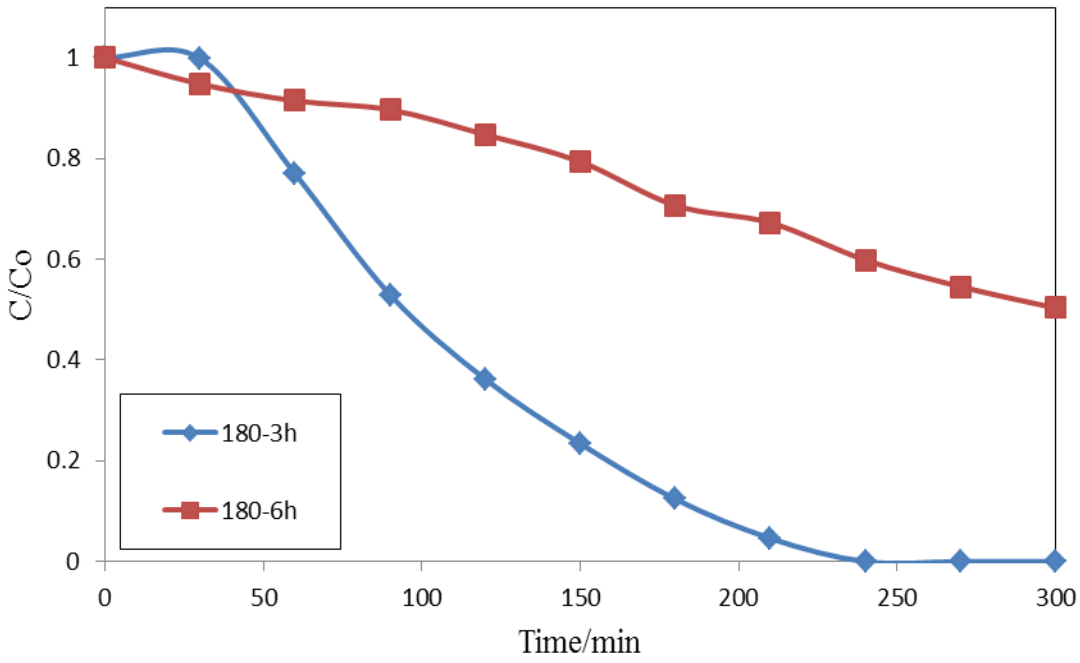

Figure 6.17 Activities of phenol degradation with 180-3h and 180-6h

Figure 6.17 shows that C-g-C_3N_4, 180-3h had a higher activity than 180-6h, indicating that the increase of the size and amount of carbon sphere (Figure 6.10 and 6.11) had negative effects on the activity of C-g-CN photocatalysts for phenol degradation. Therefore, 3 hours and 180 ^oC are the best conditions for hydrothermal reaction.

6.3.3 Adsorption performance tests

Figure 6.18 shows the adsorption of phenol on carbon spheres modified g-C_3N_4 photocatalysts. Results showed that the samples 150-3h and 180-3h presented a minor adsorption of phenol, only performing 13% and 15%, respectively at 300 min. Therefore, the decrease of phenol concentration in the catalytic tests was mainly contributed to the photodegradation of g-C_3N_4 and C-g-C_3N_4 photocatalysts.

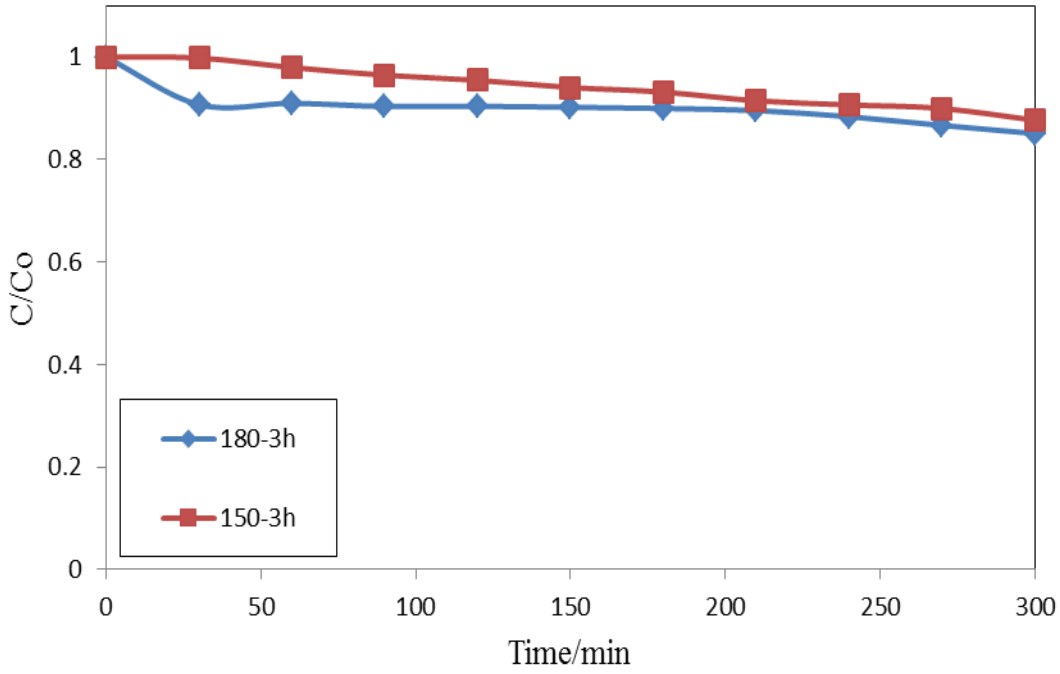

Figure 6.18 Adsorption of phenol on carbon spheres modified g-C_3N_4 photocatalysts: 150-3h and 180-3h

6.4. Conclusion

In summary, g-C_3N_4 photocatalysts were successfully synthesized by annealing malemine precursors in a simple semi-closed system in the air, and C-g-C_3N_4 photocatalysts were synthesized by a hydrothermal method. The structures and the photocatalytic properties were investigated. C-g-C_3N_4 photocatalyst (180-3h) displayed the best photocatalytic activity for phenol degradation under UV-vis light irradiation comparing with other synthesized photocatalysts.

6.5. References

1. Mantzavinos, D.; Kassinos, D.; Parsons, S.A., *Applications of advanced oxidation processes in wastewater treatment*, Water Research, 2009. **43**(16): p. 3901.

2. Simonsen, M.E.; Muff, J.; Bennedsen, LR.; Kowalski, KP.; Søgaard, EG., *Photocatalytic bleaching of p-nitrosodimethylaniline and a comparison to the performance of other AOP technologies*, Journal of Photochemistry and Photobiology A-Chemistry, 2010. **216**(2-3): p. 244–249.

3. Fujishima, A.; Zhang, X.; Tryk, D.A.; *TiO_2 photocatalysis and related surface phenomena*, Surf. Sci. Rep., 2008. **63**(12): p. 515–582.

4. Hashimoto, K.; Irie, H.; Fujishima, A., *TiO_2 photocatalysis: a historical overview and future prospects*, Jpn. J. Appl. Phys, 2005. **44**: p. 8269–8285.

5. Adewuyi, Y.G., *Sonochemistry in environmental remediation I: combinative and hybrid sonophotochemical oxidation processes for the treatment of pollutants in water*, Environ. Sci. Technol., 2005. **39**: p. 3409–3420.

6. Adewuyi, Y.G., *Sonochemistry in environmental remediation II: heterogeneous sonophotocatalytic oxidation processes for the treatment of pollutants in water*, Environ. Sci. Technol., 2005. **39**: p. 8557–8570.

7. Legrini, O.; Oliveros, E.; Braun, A.M., *Photochemical processes for water treatment*, Chem. Rev., 1983. **93**: p. 671–698.

8. Fujishima, A.; Rao, T.N.; Tryk, D., *Titanium dioxide photocatalysis*, Journal of Photochemistry and Photobiology C: Photochemistry Reviews, 2000. **1**: p. 1–21.

9. Mills, A.; LeHunte, S., *An overview of semiconductor photocatalysis*, Journal of Photochemistry and Photobiology A: Chemistry, 1997. **108**: p. 1–35.

10. Carp, O.; Huisman, C.L.; Reller, A., *Photoinduced reactivity of titanium dioxide*, Progress in Solid State Chemistry, 2004. **32**: p. 33–177.

11. Yan, S.C.; Li, Z.S.; Zou, Z.G., *Photodegradation Performance of g-C3N4 Fabricated by Directly Heating Melamine*, Langmuir, 2009. **25** (17): p. 10397–10401.

12. Neppolian, B.; Choi, H. C.; Sakthivel, S.; Arabindoo, B.; Murugesan, V., *Solar/UV-induced photocatalytic degradation of three commercial textile dyes*, Journal of Hazardous Materials, 2002, **89**(2-3): p. 303-317.

13. Comparelli, R.; Fanizza, E.; Curri, M. L.; Cozzi, P. D.; Mascolo, G.; Agostiano,A., *UV-induced photocatalytic degradation of azo dyes by organic-capped ZnO nanocrystals immobilized onto substrates*, Appl. Catal. B–Environ., 2005. **60**(1-2): p. 1-11.

14. Serpone, N.; Maruthamuthu, P.; Pichat, P.; Pelizzetti, E.; Hidaka, H., *EXPLOITING THE INTERPARTICLE ELECTRON-TRANSFER PROCESS IN THE PHOTOCATALYZED OXIDATION OF PHENOL, 2-CHLOROPHENOL AND PENTACHLOROPHENOL - CHEMICAL EVIDENCE FOR ELECTRON AND HOLE TRANSFER BETWEEN COUPLED SEMICONDUCTORS*, J. of Photochem. Photobio. A–Chem., 1995. **85**(3): p. 247-255.

15. Wang, X. C.; Maeda, K.; Thomas, A.; Takanabe, K.; Xin, G.; Carlsson J. M.; Domen, K.; Antonietti, M., *A metal-free polymeric photocatalyst for hydrogen production from water under visible light*, Nat. Mater. 2009. **8**(1): p. 76–80.

16. Xiang, Q.; Yu, J. and Jaroniec, M., *Preparation and Enhanced Visible-Light Photocatalytic H2-Production Activity of Graphene/C3N4 Composites*, J. Phys. Chem. C, 2011. **115** (15): p. 7355–7363

17. Thomas, A.; Fischer, A.; Goettmann, F.; Antonietti, M.;Mouller, J.; Schlogl, R.; Carlsson, *Graphitic carbon nitride materials: variation of structure and morphology and their use as metal-free catalysts*, J. M. J. Mater. Chem. 2008. **18**(41): p. 4893–4908.

18. Yan, S.C.; Li, Z.S.; Zou, Z.G., *Photodegradation of Rhodamine B and Methyl Orange over Boron-Doped g-C3N4 under Visible Light Irradiation*, Langmuir, 2010. **26**(6): p. 3894–3901.

19. Komatsu, T., Attempted chemical synthesis of graphite-like carbon nitride, Mater. Chem., 2001. **11**(3): p. 799–801.

20. Zhao, YC.; Yu, DL.; Yanagisawa, O.; Matsugi, K.; Tian, YJ., *Structural evolution of turbostratic carbon nitride after being treated with a pulse discharge*, Diamond Relat. Mater., 2005. **14**(10): 1700–1704.

21. Ma, H. A.; Jia, X.P.; Chen, L.X.; Zhu, P.W.; Guo, W.L.; Guo, X B.; Wang, Y.D.; Li, S.Q.; Zou, G.T.; Zhang, G.; Bex, P., *High-pressure pyrolysis study Of C3N6H6: a route to preparing bulk C3N4*, J. Phys.: Condens. Matter 2002. **14**(44): p, 11269–11273.

22. Lu, XF.; Wang, QL.; Cui, DL., *Preparation and Photocatalytic Properties of g-C3N4/TiO2 Hybrid Composite*, J. Mater. Sci. Technol., 2010. **26**(10): p. 925-930.

23. Chen, XF., Zhang, JS., Fu, XZ., Antonietti, M., and Wang, XC., *Fe-g-C3N4-Catalyzed Oxidation of Benzene to Phenol Using Hydrogen Peroxide and Visible Light*, J. Am. Chem. Soc., 2009. **131** (33): p. 11658–11659.

24. Wang, Y., Yao, J., Li, HR, Su, DS, and Antonietti, M., *Highly Selective Hydrogenation of Phenol and Derivatives over a Pd@Carbon Nitride Catalyst in Aqueous Media*, J. Am. Chem. Soc., 2011. **133**(8): p. 2362–2365.

25. Wang, CR.; Tang, KB.; Yang, Q.; Hu, JQ.; Qian, YT., *Fabrication of BiTeI submicrometer hollow spheres*, J. Mater. Chem., 2002. **12**(8): p. 2426.

26. Zheng, MB.; Cao, JM.; Chang, X.; Wang, J.; Liu, JS.; Ma, XJ., *Preparation of oxide hollow spheres by colloidal carbon spheres*, Materials Letters, 2006. **60**(24): p. 2991–2993.

27. Guo, QX.; Xie, Y.; Wang, XY.; Lv, SC.; Hou, T.; Liu, XM.; *Characterization of well-crystallized graphitic carbon nitride nanocrystallites via a benzene-thermal route at low temperatures*, Chemical Physics Letters, 2003. **380**: p. 84–87.

28. Miller, DR.; Holst, JR.; Gillan, EG., *Nitrogen-Rich Carbon Nitride Network Materials via the Thermal Decomposition of 2,5,8-Triazido-s-Heptazine*, Inorg. Chem., 2007. **46**: p. 2767-2774.

29. Sevilla, M.; Fuertes, A.B., *The production of carbon materials by hydrothermal carbonization of cellulose*, Carbon, 2009. **47**(19), p. 2281-2289.

30. Yan, SC.; Li, ZS.; Zou, ZG., *Photodegradation of Rhodamine B and Methyl Orange over Boron-Doped g-C3N4 under Visible Light Irradiation*, LANGMUIR, 2010. **26**(6): p. 3894-3901.

31. Ge, L.; Zuo, F.; Liu, JK.; Ma, Q.; Wang, C.; Sun, DZ.; Bartels, L.; Feng, PY., *Synthesis and Efficient Visible Light Photocatalytic Hydrogen Evolution of Polymeric g-C3N4 Coupled with CdS Quantum Dots*, J. Phys. Chem. C, 2012. **116**: p. 13708−13714.

7

Chapter 7: Microcarbon sphere-modified TiO_2 for the adsorption and photocatalytic degradation of phenol

Abstract

Microcarbon sphere-modified TiO_2 (C-TiO_2) photocatalysts were synthesized using D-glucose as a carbon source and P25 TiO_2 as a base material. The photocatalysts were tested for removal of phenol via photocatalytic degradation and adsorption. Photocatalytic activities of these catalysts were evaluated in liquid-phase decomposition of phenol under UV-vis light and visible light. Compared with P25 TiO_2, C-TiO_2 showed lower degradation activities for phenol degradation, but a significant enhancement in visible light photocatalytic activity. The prepared C-TiO_2 is also expected to perform an excellent pollution removal in real wastewater with complicated pollutants.

7.1. Introduction

Due to the increasing pollution and the limited resource of fresh water, wastewater treatment has become an essential technique both in Australia and other parts of the world [1]. Toxic organic chemicals such as textile dyes (azo dyes) and phenol/phenolics are the main pollutants in wastewater and the hazard of environment [2]. More than ten percents of the total organic wastes in the world are released from industry, and the resulted issues become more serious than before [3].

In order to decompose toxic organic compounds, there are several types of traditional techniques. Physical adsorption has been used to treat dyes because of its convenience, low cost and toxicity, and removal capability of the pollutants [4]. However, in adsorption process, pollutions are only transferred from fluid phase (wastewater) to solid phase (adsorbents), and then various organic pollutants still remain in wastewater and adsorbents after adsorption. Moreover, remained organic pollutions lead to the secondary pollution in both of soil and water again [5]. Although chemical oxidation technologies can decompose a variety of organics, chemical consumption, energy input and secondary pollution are the barriers of this technique [6, 7]. Due to these shortcomings of the methods (adsorption and biodegradation) and chemical oxidation, some other advanced oxidation processes (AOPs), such as photocatalysis, are considered as promising techniques for degradation of the organic compounds [7, 8]. The fundamental of photocatalysis is that this process generates powerfully oxidizing ·OH radicals, which can decompose hydrocarbons to CO_2 and H_2O, and halocarbons to the mineral acid [9].

Heterogeneous photocatalytic oxidation process is one of AOPs for degradation of organic pollutions in wastewater by employing semiconductor catalysts such as TiO_2 and ZnO [10]. TiO_2 has been widely used owing to its high photo-activity, low cost, and non-toxicity [10-12]. Moreover, TiO_2 remains stable after the repeated catalytic cycles as the most active photocatalyst under the photon energy of 300 - 390nm. Other

than these, the multifunctional properties of TiO_2 catalyst (such as chemical and thermal stability or resistance of photo-corrosion) have promoted its wide application in photocatalytic wastewater treatments [13]. Photocatalytic activity of TiO_2 depends on its micro structural and physical properties. Modification of TiO_2 surface can promote the formation of electron-hole pairs so as to increase the production of hydroxyl radicals (OH•) at the TiO_2 surface. The high concentration hydroxyl radicals facilitate the oxidation of organic molecules from surrounding [14]. Nevertheless, the barrier is that large band gap of 3.2 eV, TiO_2 can only be activated under ultraviolet (UV) irradiation, which only occupies less than 5% of the total solar irradiance at the earth's surface [15].

Intensive studies have been carried out to obtain the visible light response of TiO_2 by a variety of modification methods. For instance, Cr, Fe, Mn, and V were doped into TiO_2 in some studies to make it respond to visible light [16-19]. The photocatalytic activities of transition metals doping TiO_2 photocatalysts were proven effective, but, the thermal instability of the transition metals leads to the poor stabilities of these types of catalysts [20]. Nonmetal ions doping, such as carbon doping has been also demonstrated as an effective method for preparation of visible light responsive TiO_2 photocatalysts [21-25]. The carbon dopant has been described either as an anion which replaces oxygen in the lattice or as a cation that occupies an interstitial lattice site. The formal oxidation states of carbon dopants vary from -4 (as carbides with Ti–C bond) to +4 (as carbonates with C–O bond). During the synthesis of flame pyrolysis of Ti metal sheet [26], annealing of Ti-C powders [27, 28] and sol–gel processes [29], Ti–C bond was formed [25]. Moreover, the photo response of TiO_2 can be shifted from UV to the infrared region by a carbon doping. Besides, photocatalytic ability of carbon-doped TiO_2 could be improved by decreasing the recombination rate of photo generated electron–hole pairs by doped carbon [30]. Because commercial carbon materials (e.g. activated carbon) have ubiquitous impurity, the appropriate carbon precursors are essentially needed to synthesize carbon modified TiO_2.

In order to improve the activity of TiO_2, one promising way is to prepare nano structured material to increases the surface area of TiO_2 to directly relate to the activity. However, nanozied TiO_2 particles may be very difficult to be removed by centrifugation and filtration Thus, anchoring or embedding TiO_2 onto proper support materials is a promising method not only to avoid the loss caused by filtration, but also to obtain higher efficiency [31]. Recently, an intensive effort has been devoted to loading TiO_2 on different supports, such as TiO_2/SiO_2, TiO_2/zeolite, and TiO_2/carbon [32-35]. For example, carbon modified TiO_2, especially loading TiO_2 on activated carbon has been widely investigated. The high adsorption capability of activated carbon can enrich organic substrate around photocatalysts, promoting the pollutants transfer process and hence increasing the photocatalytic activity [30, 31, 36-38].

Recently, micro-carbon spheres have been drawn great attention owing to their high density, strength, unique spherical shape with a diameter of approximately 1 to 40 μm [39], and the potential large surface area. This study therefore aimed to investigate the synthesis of micro-carbon sphere modified TiO_2 photocatalysts and test them in photocatalytic decomposition of phenol in aqueous solution via UV-vis light. Commercial P25 TiO_2 and D-glucose were applied in synthesis.

7.2. Experimental

7.2.1. Materials

Titanium dioxide: P25 Titanium dioxide (TiO_2) (D_P=15-21 nm and S_{BET}= 55.5 m^2/g), was obtained from Degussa, Germany. It contains seventy percents of anatase and thirty percents of rutile. The titanium dioxide is the most active photocatalyst under the photon energy between 300 and 390nm, and maintains its stability after the photocatalytic reaction. TiO_2 has a Lewis-kind acid-base character, which absorbs pollutants and desorbs the intermediates and products. Nevertheless, it has a large band-gap between 3.0 and 3.2eV and also absorbs a small fraction of solar spectra corresponding to the UV region.

D-glucose: In this study, D-glucose was obtained from Sigma (99.5%). Glucose exists in several different structures, but all of these structures can be divided into two families of mirror-images (stereoisomers). Only one set of these isomers exists in nature, those derived from the "right-handed form" of glucose, denoted D-glucose. D-glucose is often referred to dextrose. The term dextrose is derived from dextrorotatory glucose. Solutions of dextrose rotate polarized light to the right. Starch and cellulose are polymers derived from the dehydration of D-glucose.

Phenol from Aldrich was used to prepare pollutant solutions.

7.2.2. Preparation of carbon sphere modified TiO_2

In a typical synthesis, 0.5 g P25 TiO_2 and 3.62 g D-glucose were dissolved in 80 mL ultrapure water, and then the mixture was stirred for 5 hours. The mixture was then transferred into a Teflon-lined autoclave (120 mL) and heated in an oven at a certain condition. After cooling to room temperature, the obtained suspension was filtered and washed by water for three times and ethanol for twice. The product was dried in an oven at 80 ^{o}C in air. Then the dried samples were annealed in nitrogen at 400 ^{o}C for 2 h at a heating rate of 5 ^{o}C/min in a tubular furnace. Later, the samples were calcined in the air at 350 ^{o}C in a crucible with a cover at heating rate of 5 ^{o}C/min for 2h.

The synthesis conditions were adjusted to optimize the photocatalytic activities. Synthesized samples in different conditions are summarized as follows.

Table 7.1 Summary of different conditions in samples synthesis

Sample ID	TiO_2 (g)	D-glucose (g)	Hydrothermal Temperature (°C)	Hydrothermal Duration (h)	Calcined temperature in nitrogen(°C)	Calcined time in nitrogen(h)	Calcined temperature in air(°C)	Calcined time in air (h)
C-Ti-1	0.5	3.62	150	1	N/A	N/A	N/A	N/A
C-Ti-2	0.5	3.62	150	1	400	2	N/A	N/A
C-Ti-3	0.5	3.62	150	1	400	2	350	2
C-Ti-4	0.5	3.62	150	3	N/A	N/A	N/A	N/A
C-Ti-5	0.5	3.62	150	3	400	2	N/A	N/A
C-Ti-6	0.5	3.62	150	3	400	2	350	2
C-Ti-7	0.5	3.62	160	3	N/A	N/A	N/A	N/A
C-Ti-8	0.5	3.62	160	3	400	2	N/A	N/A
C-Ti-9	0.5	3.62	160	3	400	2	350	2

C-Ti-10	0.5	3.62	160	5	N/A	N/A	N/A	N/A
C-Ti-11	0.5	3.62	160	5	400	2	N/A	N/A
C-Ti-12	0.5	3.62	160	5	400	2	350	2
C-Ti-13	1	3.62	150	1	400	2	350	2
C-Ti-14	1	3.62	150	3	400	2	350	2
C-Ti-15	1	3.62	160	3	400	2	350	2

7.2.3. Adsorption and photocatalysis

The aqueous oxidation of phenol was carried out in a 1 L of Pyrex double-jacket reactor. A water bath connected with a pump was used to maintain the reaction temperature at 30 ± 0.5 ^{o}C, and a magnetic stirrer was used to maintain the catalyst dispersed uniformly in reaction solutions. In a typical run, 0.1 g of catalyst (0.5 g/L) was added into 200 mL of 20 ppm phenol solution and stirred for 30 min, and took the first sample. The irradiations were supplied by a MSR 575/2 metal halide lamp (575 W, Philips). The UV intensity (315 < k < 400 nm) was measured to be 60 μW/cm^2 and the visible light intensity (k > 400 nm) was 84 μW/cm^2. At each set time interval, 1 mL solution was withdrawn by a syringe and filtered by a 0.25 μm Millipore film into a HPLC vial. The concentration of phenol was analyzed on a 380-LC HPLC (Varian, USA) with a UV detector set at k = 270 nm. A C-18 column was used to separate the organics while the mobile phase of 30% CH_3CN and 70% water was flowing through the column at a flow rate of 1.5 mL/min. The adsorption test was carried out in the same system as photocatalytic reaction except irradiations. Therefore, the adsorption was preceded in absolutely dark condition.

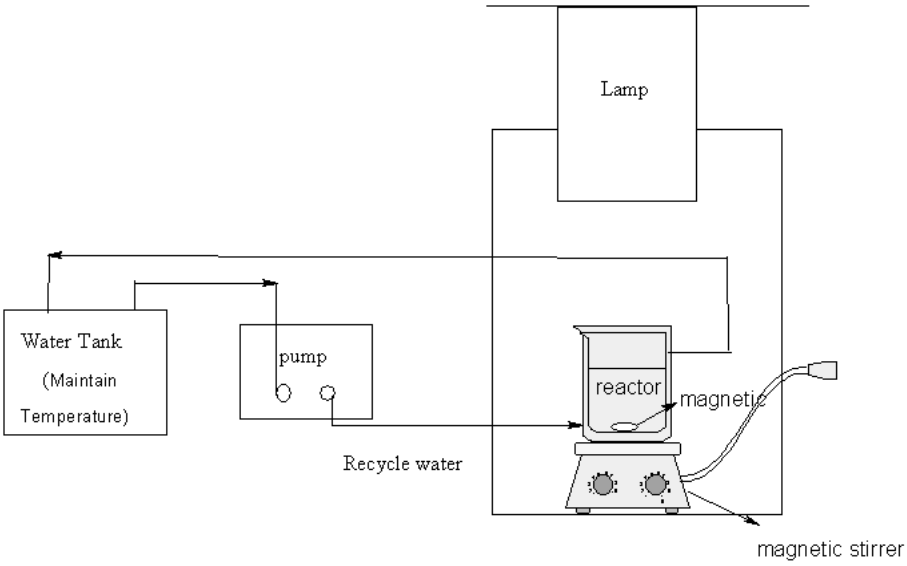

Figure 7.1 Reaction system of photocatalytic reaction

7.3. Results and discussion

To clarify the relationship between reactivity of substrates and their degradation behavior over the catalyst surface, the degree of substrate degradation was defined as C/C_0. C_0 denotes the initial concentration of substrate in solution and C denotes the equilibrium concentration of substrate in the solution after reaction with the respective catalysts at 30 ^oC. It is noted that all the samples attain the adsorption equilibrium within 30 min under this condition.

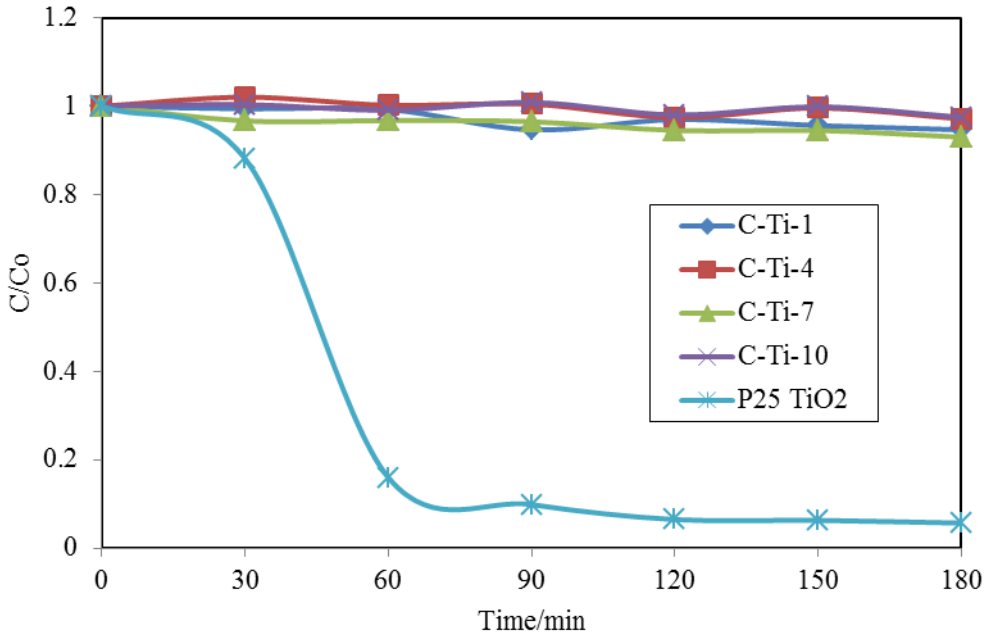

Figure 7.2 Photocatalytic degaradation of phenol by untreated microcarbon sphere modified TiO_2 catalysts and P25 TiO_2 under UV-vis light.

The photocatalytic performances of micro-carbon sphere modified TiO_2 catalysts synthesized at 150^oC, 160^oC for 1 and 3 hours, respectively, are shown in Figure 7.2. The experiments were carried out by using C-TiO_2 as catalysts to degrade 200 ml of 20 ppm of phenol under UV-vis light. It was found that P25 TiO_2 performed a better photocatalytic behavior compared with the same amount of C-TiO_2 catalysts. Synthesized C-TiO_2 catalysts did not show significant degradation. The best catalyst

was C-Ti-7 with 7% of phenol degradation in 180 min. The low degradation rates of these four synthesized photocatalysts were attributed to the carbon spheres which were produced during the hydrothermal process, and covered the surface of catalysts then caused the low photocatalytic activities in phenol degradation under the UV-vis light irradiation [27]. So, synthesized samples were then annealed in nitrogen at 400 ^{o}C for 2h at a heating rate of 5 ^{o}C/min in a tubular furnace to remove byproducts [40], and applied in further photocatalytic reactions as below.

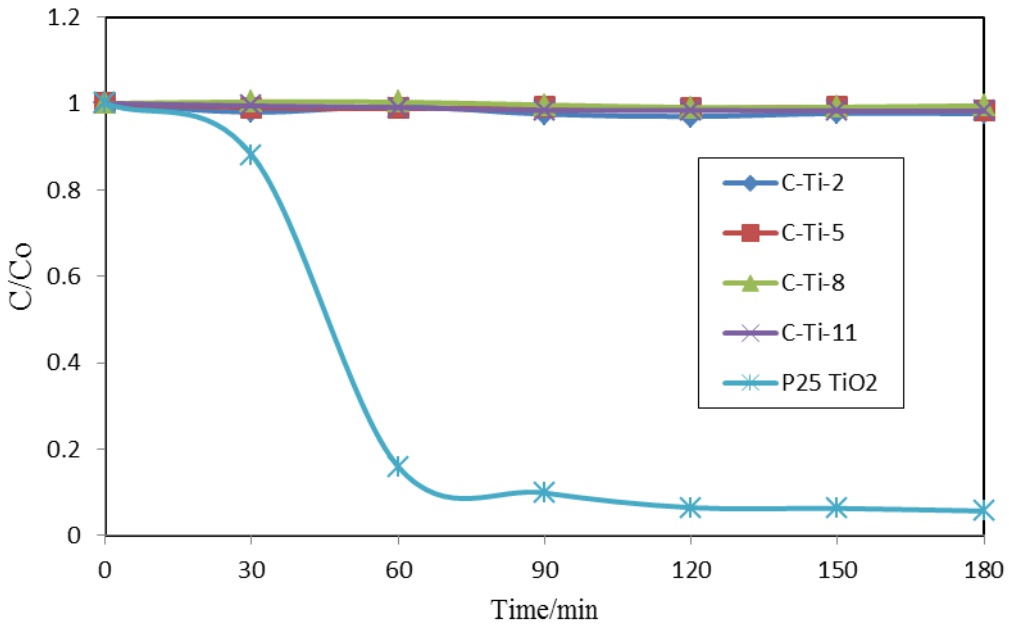

Figure 7.3 Photocatalytic degaradation of phenol by treated microcarbon sphere modified TiO_2 catalysts (400 ^{o}C, 2hr in N_2) and P25 TiO_2 via UV-vis light.

Figure 7.3 shows the photocatalytic performances of micro-carbon sphere modified TiO_2 catalysts synthesized at 150 ^{o}C, 160 ^{o}C for 1 and 3 hours, and annealed in nitrogen at 400 ^{o}C respectively. The experiments were carried out by using C-TiO_2-2 (150°C 1hr, 400°C 2hr in N_2), C-TiO_2-5 (150°C 3hr, 400°C 2hr in N_2), C-TiO_2-8 (160°C 3hr, 400°C 2hr in N_2), C-TiO_2-11 (160°C 5hr, 400°C 2hr in N_2) and P25 TiO_2 as catalysts to degrade 200 ml of 20 ppm of phenol under UV-vis light respectively. Synthesized photocatalysts treated in nitrogen did not have any

photocatalytic activity in phenol degradation. The results indicated that the removal of byproducts covered catalysts would not improve the activities of samples. Microcarbon spheres have high density, and small diameter of approximately 1 to 40 μm, so TiO_2 might be encapsulated completely by microcarbon spheres [39]. In some studies, calcination in the air showed positive effects on the photoactivity of microcarbon sphere-TiO_2 photocatalysts [27, 28]. Therefore, further treatments of reducing the ratio of micorcarbon spheres and byproducts in synthesized samples were possibly able to improve the photocatalytic activities of synthesized catalysts.

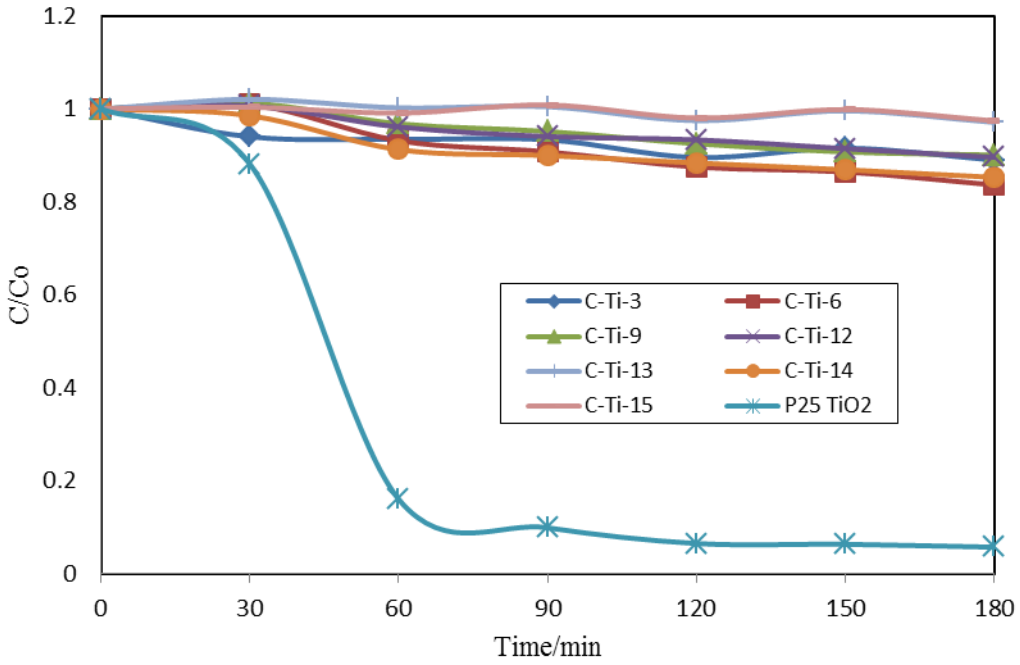

Figure 7.4 Photocatalytic degaradation of phenol by treated microcarbon sphere modified TiO_2 catalysts (400^oC, 2hr in N_2 and 350^oC, 2hr in Air) and P25 TiO_2 under UV-vis light.

The photocatalytic performances of micro-carbon sphere modified TiO_2 catalysts are showed in Figure 7.4. These samples were synthesized at 150 ^oC, 160 ^oC for 1 and 3 hours and annealed in nitrogen at 400 ^oC in a tubular furnace, then calcined in the air at 350 ^oC for 2h in a crucible with a cover at a heating rate of 5 ^oC/min respectively. The experiments were carried out by using C-TiO_2-3 (150°C 1hr, 400°C 2hr in N_2,

and 350°C 2hr in air), C-TiO_2-6 (150°C 3hr, 400°C 2hr in N_2, and 350°C 2hr in air), C-TiO_2-9 (160°C 3hr, 400°C 2hr in N_2, and 350°C 2hr in air), C-TiO_2-12 (160°C 5hr, 400°C 2hr in N_2, and 350°C 2hr in air) and P25 TiO_2 as catalysts to decompose 200 ml of 20 ppm of phenol under UV-vis light respectively. Furthermore, to improve the photocatalytic activities of synthesized catalysts, three new samples were synthesized by using 1 g P25 TiO_2 in preparation stages. They are C-TiO_2-13 (150°C 3hr, 400°C 2hr in N_2, and 350°C 2hr in air), C-TiO_2-14 (160°C 3hr, 400°C 2hr in N_2, and 350°C 2hr in air), C-TiO_2-15 (160°C 5hr, 400°C 2hr in N_2, and 350°C 2hr in air). After two stages treatments (nitrogen and air), C-TiO_2-6 and C-TiO_2-14 showed similar activities, could reach approximately 17% of phenol removal in 180 min. It was found that the increase of P25 TiO_2 used in synthesis process does not have significant effects on the photocatalytic activity of C-TiO_2 catalysts, but the calcination in the air increased the degradation rate from 3% to 17%. Similar observations were reported by other studies [27, 28].

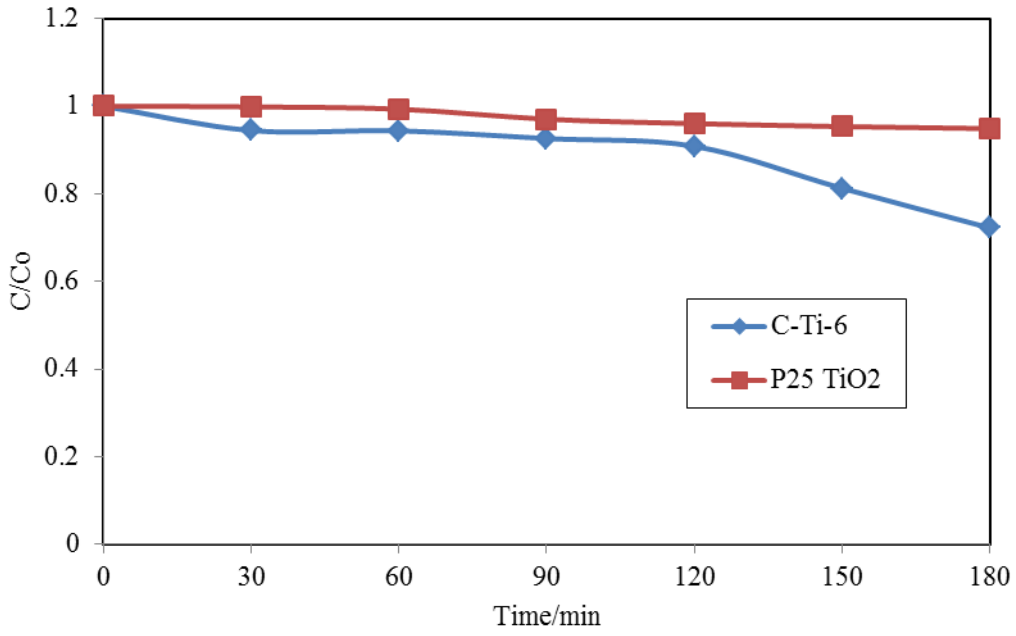

Figure 7.5 Photocatalytic degradation of phenol by C-Ti-6 and P25 TiO_2 under visible light.

Figure 7.5 shows the performances of P25 TiO_2 and C-Ti-6 (150°C 3hr, 400°C 2hr in N_2, and 350°C 2hr in air) in photocatalytic degradation of phenol under visible light. The C-Ti-6 would increase the degradation rate of phenol under visible light, and 30% of phenol degradation was achieved in 180 min. On the other hand, P25 TiO_2 hardly showed the efficiency of phenol degradation in visible-light system. These experiments proved that P25 TiO_2 cannot be activated by visible light due to its large band. Further, after two treatments steps (nitrogen and air), synthesized microcarbon sphere modified catalysts showed a moderate photocatalytic activity for phenol degradation under visible light. In Lv et al.'s study, WO_3/TiO_2 carbon spheres photocatalysts had a photocatalytic activity in degradation of methylene blue (MB), but showed much lower degradation rate in the visible light in comparison to the UV photoactivity [41]. But in this study, results in Figure 5.4 and 5.5 indicated an opposite situation. The photoactivity of C-Ti catalysts performed a higher degradation rate under the visible light (30%) comparing with the tests under UV-vis light irradiation (17%). According to the studies by Saepurahman et al. [26, 42, 43], the optimal synthesis conditions of TiO_2-based photocatalysts with other preparation techniques (sol–gel method [29], and flame-made method [26]) are not same, and the apparent rate constant of organic degradation could be improved by the procedure of preparation such as catalyst loading, optical absorption, initial pH, light wavelength, and calcination temperature [26, 42, 43]. For this microcarbon sphere-modified TiO_2 photocatalyst (C-Ti-6), calcination in N_2 and air phases improved the visible light response ability of TiO_2 based photocatalyst significantly. It showed that microcabon sphere is a positive support material to modify commercial TiO_2 photocatalyst for degradation of organic compounds in aqueous phase under visible light. The micro-carbon spheres functioned for absorption in the visible light region, and acted as a photosensitizer which could be excited to inject electrons into the conduction of band of TiO_2. Yang et al. indicated that in C-Ti system, surface-adsorbed oxygen molecules could be transferred by the electrons, and the electrons formed superoxide anions, and then further transformed to OH• for degradation of organics [22].

Meanwhile, in other studies, precursors of TiO_2 were commonly used to synthesize microcarbon sphere-TiO_2 photocatalysts which showed high activity in degradation of organic compounds, such as phenol and methylene blue [27, 28, 44]. Although there is not comparatively high degradation rate of phenol by using synthesized photocatalysts, the synthesis method investigated in this study simplified the procedures and avoided employing hazardous materials, such as $(NH_4)_2SO_4$ and HCl [27], HNO_3[37], and hydrofluoric acid [44]. Moreover, comparing pure commercial TiO_2, microcarbon sphere-modified TiO_2 photocatalyst can still be considered as a "green catalyst" with development potential in photodegradation of organic pollutants by employing solar energy which is free and environmentally friendly.

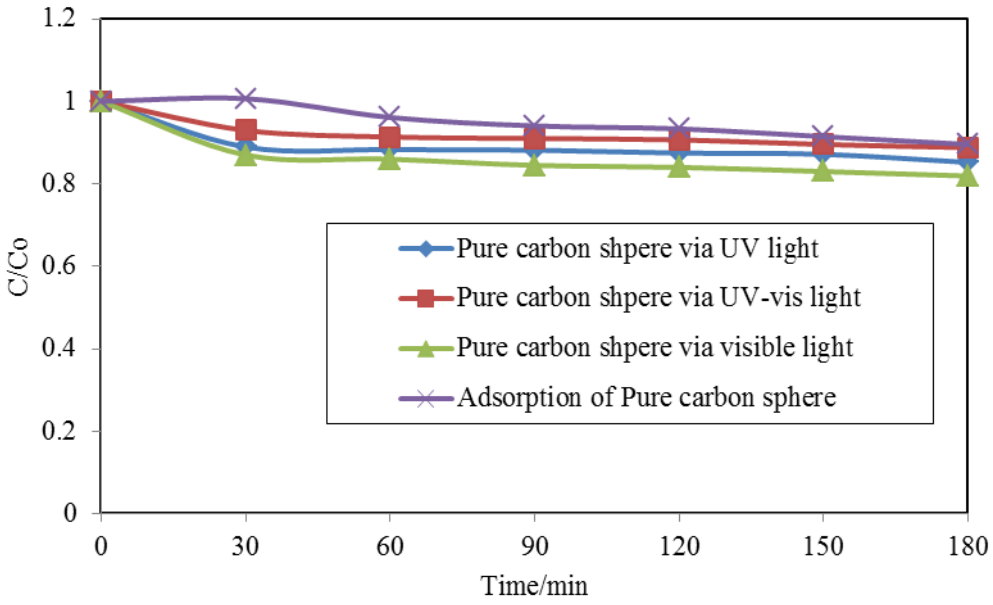

Figure 7.6 Removal of phenol with pure micorcarbon sphere and adsorption study of C-Ti-6

Figure 7.6 shows the performances of pure microcarbon sphere for removal of phenol. It proved that microcarbon sphere did not have any photocatalytic activity, but achieved 15% of adsorption of phenol in 180 min, and 15.5% of phenol was removed by the adsorption of C-Ti-6. These results indicated that carbon spheres and microcarbon sphere modified-TiO_2 was not a suitable adsorbent for phenol. However,

Qian et al. reported carbon sphere-TiO_2 nano-catalysts posed much higher adsorption capacity for Cr(VI) than pure carbon sphere and TiO_2 [45]. For instance, the adsorption capacity of the TiO_2- microspheres is 18.1 mg/g for the initial 40.0 ppm concentration of Cr (VI), while Degussa P25 and pure carbon microspheres can only achieve 5.0 and 4.5 mg/g in the same conditions, respectively [45]. It indicated that microcarbon sphere modified-TiO_2 photocatalysts obtained in this study may have adsorption activity for metal ions in wastewater. Further, in multi-compounds (organics, inorganics, heavy metals and et al.) wastewater system, microcarbon sphere modified-TiO_2 photocatalysts are possibly able to perform good pollutants removal due to the abilities of photodegradation of organics and adsorption of metal ions, and this characteristic will be tested in future study.

7.4. Conclusions

Microcarbon sphere modified-TiO_2 photocatalysts were synthesized via a hydrothermal method using D-glucose as a carbon source and commercial P25 TiO_2 powder as a base material. The byproducts and carbon spheres were removed by calcination in N_2 and the air, respectively. The results indicated that the use of apposite calcination conditions can improve the photocatalytic activity of the material. C-Ti-6 showed positive photocatalytic activity in removal of phenol under visible light in comparison with P25 TiO_2.

In the future study, i) microcarbon sphere modified-TiO_2 catalysts will be tested for adsorption of metal ions to extend their application in wastewater treatment; ii) different calcination conditions, such as temperature and time, in the air are supposed to be studied; iii) though employing the precursor of TiO_2 in synthesis of microcarbon sphere modified-TiO_2 catalysts breaches the notion of “green chemistry”, the appropriate selection of precursor and synthesis method are a promising way to improve the photocatalytic activity of C-Ti catalysts under the solar light significantly.

7.7. References

1. Ahmed, S., et al., *Advances in Heterogeneous Photocatalytic Degradation of Phenols and Dyes in Wastewater: A Review.* Water Air and Soil Pollution, 2011. **215**(1-4): p. 3-29.

2. Wongkalasin, P., S. Chavadej, and T. Sreethawong, *Photocatalytic degradation of mixed azo dyes in aqueous wastewater using mesoporous-assembled TiO2 nanocrystal synthesized by a modified sol-gel process.* Colloids and Surfaces a-Physicochemical and Engineering Aspects, 2011. **384**(1-3): p. 519-528.

3. Houas, A., et al., *Photocatalytic degradation pathway of methylene blue in water.* Applied Catalysis B-Environmental, 2001. **31**(2): p. 145-157.

4. Bhatnagar, A. and M. Sillanpaa, *Utilization of agro-industrial and municipal waste materials as potential adsorbents for water treatment-A review.* Chemical Engineering Journal, 2010. **157**(2-3): p. 277-296.

5. Konstantinou, I.K. and T.A. Albanis, *TiO2-assisted photocatalytic degradation of azo dyes in aqueous solution: kinetic and mechanistic investigations - A review.* Applied Catalysis B-Environmental, 2004. **49**(1): p. 1-14.

6. Slokar, Y.M. and A.M. Le Marechal, *Methods of decoloration of textile wastewaters.* Dyes and Pigments, 1998. **37**(4): p. 335-356.

7. Wang, H., et al., *Analysis of TiO2 photocatalysis in a pulsed discharge system for phenol degradation.* Journal of Electrostatics, 2009. **67**(6): p. 886-889.

8. Butterfield, I.M., et al., *Applied studies on immobilized titanium dioxide films as catalysts for the photoelectrochemical detoxification of water.* Journal of Applied Electrochemistry, 1997. **27**(4): p. 385-395.

9. Hu, C., Y.Z. Wang, and H.X. Tang, *Destruction of phenol aqueous solution by photocatalysis or direct photolysis.* Chemosphere, 2000. **41**(8): p. 1205-1209.

10. Linsebigler, A.L., G.Q. Lu, and J.T. Yates, *PHOTOCATALYSIS ON TIO2 SURFACES - PRINCIPLES, MECHANISMS, AND SELECTED RESULTS.* Chemical Reviews, 1995. **95**(3): p. 735-758.

11. Hoffmann, M.R., et al., *ENVIRONMENTAL APPLICATIONS OF SEMICONDUCTOR PHOTOCATALYSIS.* Chemical Reviews, 1995. **95**(1): p. 69-96.

12. Zahraa, O., et al., *Treatment of wastewater dyeing agent by photocatalytic process in solar reactor.* International Journal of Photoenergy, 2006.

13. Chong, M.N., et al., *Recent developments in photocatalytic water treatment technology: A review.* Water Research, 2010. **44**(10): p. 2997-3027.

14. de la Cruz Romero, D., et al., *Synthesis and characterization of TiO2 doping with rare earths by sol-gel method: photocatalytic activity for phenol degradation.* Journal of Sol-Gel Science and Technology, 2010. **56**(3): p. 219-226.

15. Lin, X., et al., *Carbon-doped mesoporous TiO2 film and its photocatalytic activity.* Microporous and Mesoporous Materials, 2011. **142**(1): p. 276-281.

16. Wantala, K., et al., *Calcination temperature effect on solvothermal Fe-TiO2 and its performance under visible light irradiation.* Journal of the Taiwan Institute of Chemical Engineers, 2010. **41**(5): p. 612-616.

17. Wang, C., H. Shi, and Y. Li, *Synthesis and characterization of natural zeolite supported Cr-doped TiO2 photocatalysts.* Applied Surface Science, 2012. **258**(10): p. 4328-4333.

18. Papadimitriou, V.C., et al., *Determination of photo-catalytic activity of un-doped and Mn-doped TiO2 anatase powders on acetaldehyde under UV and visible light.* Thin Solid Films, 2011. **520**(4): p. 1195-1201.

19. Liu, B., et al., *Low temperature fabrication of V-doped TiO2 nanoparticles, structure and photocatalytic studies.* Journal of Hazardous Materials, 2009. **169**(1-3): p. 1112-1118.

20. Ren, W., et al., *Low temperature preparation and visible light photocatalytic activity of mesoporous carbon-doped crystalline TiO2.* Applied Catalysis B-Environmental, 2007. **69**(3-4): p. 138-144.

21. Wang, D., et al., *Highly efficient visible light TiO2 photocatalyst prepared by sol–gel method at temperatures lower than 300 °C.* Journal of Hazardous Materials, 2011. **192**(1): p. 150-159

22. Yang, X., et al., *Synthesis of visible-light-active TiO2-based photocatalysts by carbon and nitrogen doping.* Journal of Catalysis, 2008. **260**(1): p. 128-133.

23. Liu, S. and X. Chen, *A visible light response TiO2 photocatalyst realized by cationic S-doping and its application for phenol degradation.* Journal of Hazardous Materials, 2008. **152**(1): p. 48-55.

24. Hamal, D.B. and K.J. Klabunde, *Synthesis, characterization, and visible light activity of new nanoparticle photocatalysts based on silver, carbon, and sulfur-doped TiO2.* Journal of Colloid and Interface Science, 2007. **311**(2): p. 514-522.

25. Park, Y., et al., *Carbon-doped TiO2 photocatalyst synthesized without using an external carbon precursor and the visible light activity.* Applied Catalysis B: Environmental, 2009. **91**(1–2): p. 355-361.

26. Akurati, K.K., et al., *Flame-made WO3/TiO2 nanoparticles: Relation between surface acidity, structure and photocatalytic activity.* Applied Catalysis B-Environmental, 2008. **79**(1-2): p. 53-62.

27. Zhang, Q., W. Li, and S. Liu, *Controlled fabrication of nanosized TiO2 hollow sphere particles via acid catalytic hydrolysis/hydrothermal treatment.* Powder Technology, 2011. **212**(1): p. 145-150.

28. Wang, C., et al., *Preparation, characterization and photocatalytic activity of the neodymium-doped TiO2 hollow spheres.* Applied Surface Science, 2010. **257**(1): p. 227-231.

29. Li, X., et al., *Layer-by-layer synthesis of hollow spherical CeO2 templated by carbon spheres.* Journal of Porous Materials, 2010. **17**(3): p. 297-303.

30. Xu, J., et al., *Synthesis of fluorine-doped titania-coated activated carbon under low temperature with high photocatalytic activity under visible light.* Journal of Physics and Chemistry of Solids, 2008. **69**(10): p. 2366-2370.

31. Carpio, E., et al., *Photocatalytic degradation of phenol using TiO2 nanocrystals supported on activated carbon.* Journal of Molecular Catalysis a-Chemical, 2005. **228**(1-2): p. 293-298.

32. Chuan, X.Y., M. Hirano, and M. Inagaki, *Preparation and photocatalytic performance of anatase-mounted natural porous silica, pumice, by hydrolysis under hydrothermal conditions.* Applied Catalysis B-Environmental, 2004. **51**(4): p. 255-260.

33. Ding, Z., et al., *Novel silica gel supported TiO(2) photocatalyst synthesized by CVD method.* Langmuir, 2000. **16**(15): p. 6216-6222.

34. Panayotov, D., P. Kondratyuk, and J.T. Yates, *Photooxidation of a mustard gas simulant over TiO2-SiO2 mixed-oxide photocatalyst: Site poisoning by oxidation products and reactivation.* Langmuir, 2004. **20**(9): p. 3674-3678.

35. Wu, B., R. Yuan, and X. Fu, *Structural characterization and photocatalytic activity of hollow binary ZrO2/TiO2 oxide fibers.* Journal of Solid State Chemistry, 2009. **182**(3): p. 560-565.

36. Gao, B., et al., *Adsorption-photocatalytic degradation of Acid Red 88 by supported TiO2: Effect of activated carbon support and aqueous anions.* Chemical Engineering Journal, 2011. **171**(3): p. 1098-1107.

37. Li, Y., et al., *Preparation and photocatalytic activity of TiO2-carbon surface composites by supercritical pretreatment and sol-gel process.* Catalysis Communications, 2008. **9**(7): p. 1583-1587.

38. Li, Y., et al., *The effects of activated carbon supports on the structure and properties of TiO2 nanoparticles prepared by a sol-gel method.* Applied Surface Science, 2007. **253**(23): p. 9254-9258.

39. Mi, Y., et al., *Synthesis of carbon micro-spheres by a glucose hydrothermal method.* Materials Letters, 2008. **62**(8-9): p. 1194-1196.

40. Sun, H., et al., *Nano-Fe-0 Encapsulated in Microcarbon Spheres: Synthesis, Characterization, and Environmental Applications.* Acs Applied Materials & Interfaces, 2012. **4**(11): p. 6235-6241.

41. Lv, K., et al., *Synthesis and photo-degradation application of WO3/TiO2 hollow spheres.* Journal of Hazardous Materials, 2011. **189**(1-2): p. 329-335.

42. Saepurahman, M.A. Abdullah, and F.K. Chong, *Dual-effects of adsorption and photodegradation of methylene blue by tungsten-loaded titanium dioxide.* Chemical Engineering Journal, 2010. **158**(3): p. 418-425.

43. Saepurahman, M.A. Abdullah, and F.K. Chong, *Preparation and characterization of tungsten-loaded titanium dioxide photocatalyst for enhanced dye degradation.* Journal of hazardous materials, 2010. **176**(1-3): p. 451-8.

44. Liu, L., et al., *Synthesis of sandwich-like TiO2@C composite hollow spheres with high rate capability and stability for lithium-ion batteries.* Journal of Power Sources, 2013. **221**: p. 141-148.

45. Qian, H., et al., *Electrostatic self-assembly of TiO2 nanoparticles onto carbon spheres with enhanced adsorption capability for Cr(VI).* Materials Letters, 2012. **68**: p. 174-177.

8

Chapter 8: Conclusions and Future Work

8.1. Concluding comments

The major objective of this research: to synthesize novel photocatalysts being capable to degrade organics in aqueous phase at room temperature and to investigate "green cobalt based catalysts" for degradation of organic pollutants via advanced oxidation processes, was successfully achieved as per the scheduled timeline. Various types of catalysts were synthesized with hydrothermal carbonization method or wet impregnation method, and used for degradation of phenol in aqueous phase with UV-vis and visible light irradiation. Titanates: $ZnTiO_3$, $FeTiO_3$ and $Bi_4Ti_3O_{12}$ were modified by coating cobalt (Co) to prepare photocatalysts. Microcarbon spheres were also synthesized by hydrothermal method, and used to support TiO_2 (C-TiO_2), nanoscaled zerovalent iron (nano-Fe^0@CS), cobalt (micro-CS@Co) and graphitic carbon nitride (C-g-CN). All of these catalyst materials were tested for phenol degradation. Some of these synthesized catalysts were also examined for activating peroxymonosulfate (PMS, Oxone) for the decomposition of phenol. The major outcomes of this research thesis are outlined as below.

8.2. Photocatalytic activities of titanate supported cobalt catalysts

$ZnTiO_3$ (Zn), $FeTiO_3$ (Fe) and $Bi_4Ti_3O_{12}$ (Bi), were employed to prepare supported cobalt catalysts. The supported cobalt catalysts were prepared by a wet impregnation method, and used for photocatalytic and photocatalytic oxidation of phenol with peroxymonosulfate (PMS) or peroxydisulfate (PDS) under visible light irradiations.

Cobalt supported on titanates, $ZnTiO_3$, $FeTiO_3$ and $Bi_4Ti_3O_{12}$, were proven as efficient catalysts for photochemical oxidation of phenol by activation of PMS and PDS. The cobalt was suggested to be in the form of Co_3O_4, which would strongly influence the photocatalysis and photochemical behaviours from activation of sulphate oxidants of PMS and PDS. Co_3O_4 decreased the photocatalytic activity of $ZnTiO_3$ and $Bi_4Ti_3O_{12}$, but enhanced the activity of $FeTiO_3$. Generally, loading of Co_3O_4 would promote the photochemical efficiency in phenol removal by activation

of PMS, in which $Bi_4Ti_3O_{12}$ supported catalysts showed the best activities. Although the efficiencies of the titanate supported Co in activation of PDS was not as high as PMS, $Bi_4Ti_3O_{12}$ supported catalysts still provided the best activity. The stability of Co(5%)/Zn with PMS was further investigated and it was found that the activity remained at 85.4% phenol degradation in the fourth run.

8.3. Oxidative activities of microcarbon sphere supported nanoscaled zero valent iron catalysts

Nanoscaled zero valent iron (ZVI) encapsulated in carbon spheres (nano-Fe^0@CS) were fabricated via a hydrothermal carbonization method, using glucose and iron(III) nitrate as precursors. The structure of Fe^0@CS consisted of carbon spheres (6−8 μm) composed of fine carbon particles (50−200 nm) encapsulating nanosized ZVI (5−10 nm). The iron/carbon hybrids annealed at 550 °C showed a porous structure with high specific surface area and pore volume. The carbon facilitated a good Fe dispersion by an in situ reduction and increased the stability of nanoscaled ZVI. Fe^0@CS showed an efficient activity in producing oxidative radicals from PMS, thus leading to a superior performance in degradation of phenol to homogeneous iron/PMS and cobalt oxide/PMS. The higher activity of Fe^0@CS was attributed to the nature of ZVI and the unique structure. The core of the design was to fabricate a porous structure for attracting substrates, and to controllably release Fe ions to avoid the quenching of active radicals.

8.4. Oxidative activities of microcarbon sphere supported cobalt catalysts

Cobalt nitrate and glucose were employed to prepare microcarbon sphere supported cobalt catalysts (micro-CS@Co) via a hydrothermal carbonization method for chemical oxidation of phenol with peroxymonosulfate (PMS, oxone). New synthesized catalysts were proven having high activity from chemical oxidation of phenol by activation of PMS. Co_3O_4 crystallites were found on the surface of microcarbon. Microcarbon sphere supported cobalt catalysts exhibited high activity

for activation of PMS to produce sulphate radicals for oxidation of phenol. Several factors such as temperature, dosages of catalyst or PMS influenced the degradation of phenol. Although fresh micro-CS@Co, 400 ^{o}C showed the greatest activity, the micro-CS@Co, 500^{o}C catalyst demonstrated as the most stable as well as environmentally friendly catalyst by the tests of multiple chemical oxidation experiments.

8.5. Photocatalytic activities of microcarbon sphere-modified graphitic carbon nitride catalysts

The graphitic carbon nitride (g-C_3N_4) was synthesized by directly heating melamine at 500 ^{o}C at a heating rate of 15 ^{o}C/min for 2 h, and microcarbon sphere modified graphitic carbon nitride (C-g- C_3N_4) composite photocatalyst was synthesized by treating g- C_3N_4 in D-glucose solution using a hydrothermal route at various temperatures and reaction times. The sample synthesized by the hydrothermal method at 180 ^{o}C for 3 hours showed the highest activity on phenol degradation under UV-vis light irradiation.

8.6. Photocatalytic activities of microcarbon sphere-modified TiO_2

Microcarbon sphere-modified TiO_2 (C-TiO_2) photocatalysts were synthesized using D-glucose as a carbon source and P25 TiO_2 as a base material via hydrothermal method. The byproducts and carbon templates were removed by calcination in N_2 and the air, respectively. The synthesis route can be defined as environmental green chemical method. The results indicate that the use of apposite calcination conditions can improve the photocatalytic activity of the material. C-Ti-6 showed better photocatalytic activity in removal of phenol under visible light in comparison with P25 TiO_2.

8.7. Recommendations for future work

This research was focused on the catalytic degradation of phenol in aqueous phase.

The results of this study showed that phenol can be successfully oxidized into byproducts using various complex catalysts under UV-vis and visible light irradiation or employing peroxymonosulfate (PMS) or peroxydisulfate (PDS) as oxidants. However, in view of the urgent need for more comprehensive solutions of removal of organic compounds in wastewater, the recommendations for future work are as follows:

(1) Unexpected toxic byproducts and intermediates are the main reasons what cause the secondary pollution in wastewater treatment processes. Previous studies indicated that parts of byproducts or target organic compounds could be adsorbed by catalysts. Therefore, detailed testing route is highly required to be investigated to determine both the byproducts and intermediates and their adsorption on the catalyst surface.

(2) Comparing with P25 TiO_2, newly synthesized micro-carbon spheres modified TiO_2 photocatalyst has showed better photocatalytic activity in phenol degradation with visible light irradiation. However, synthesizing TiO_2 by employing suitable precursor to take place of commercial P25 TiO_2 in the preparation of C-TiO_2 photocatalysts would be a possibility to further improve the activity of C-TiO_2 photocatalysts.

(3) Micro-carbon sphere materials have been synthesized successfully by a glucose hydrothermal method, and proven that these materials could enhance the stability of catalysts significantly due to their high-density, high-strength and unique spherical shape with a diameter of approximately 1 to 40μm. However, the influences contributed by micro-carbon sphere materials could be positive or negative due to the parameters of hydrothermal reaction. So, it is also high required to investigate the appropriate reaction pathway to dominate the characteristics, particle sizes, pore sizes, surface area and structures of micro-carbon sphere materials for improvement of their adsorption capacity and applications as support materials for more types of

catalysts.

(4) Our investigations showed that almost all of the newly synthesized catalysts were quite stable in multiple repeating tests. But, we suggest that detailed investigations of the surface of the used materials are still required to identify the root cause of the light reduction in phenol degradation reactions. Although SEM did not show any structure of micro-carbon spheres in the analysis of one newly C-g-C_3N_4 material, the activity of this catalyst was still better than some other materials. So some surface investigations are required to identify the reason.

(5) Graphitic carbon nitride materials were synthesized by heating the low-cost melamine, and showed photocatalytic activities. This unique material has been increasing great interest in photocatalysis technology applications. The preliminary results indicate that g-C_3N_4 would be another possible photocatalyst materilas that can work with visible light irradiation to degrade phenol in water. We suggest that co-catalyst, grapheme-catalyst, TiO_2-catalyst would enhance the photocatalytic properties of g-C_3N_4. Moreover, using g-C_3N_4 or modified g-C_3N_4 materials to activate peroxymonosulfate or peroxydisulfate for oxidation of organic pollutants could be one potential possibility.